# Reconstructing the thermal history of the Morondava Basin, Madagascar during Gondwana breakup: A detrital zircon (U-Th)/He and U-Pb study

**Willem Martijn Schetselaar**

A thesis submitted to the University of Ottawa
in partial fulfillment of the requirements for the M.Sc. degree in Earth Science

Faculty of Science
University of Ottawa

**Abstract**

The Morondava Basin is one of three Phanerozoic rift basins bordering the western coast of Madagascar. Sediments were first deposited in this basin during the initial stages of breakup of Gondwana in the Permian, sourced from the adjacent Precambrian basement terranes. Gondwana breakup resulted in several stages of subsidence, tilting, and uplift of Madagascar, the thermal history of which is recorded within the strata of the Morondava Basin. We have applied U-Pb detrital zircon techniques to investigating the sedimentation and transport patterns of Jurassic and Cretaceous strata. In order to reconstruct the thermal history of the Morondava Basin throughout the stages of rift basin development we have applied modelling of (U-Th)/He thermochronology data. Our models show a protracted cooling history influenced by multiple stages of uplift and subsidence occurring differentially across the basin. A furthered understanding of the Morondava Basin with respect to its development during Gondwana breakup has implications for oil exploration in the region.

**Résumé**

Le bassin de Morondava est l'un des trois bassins de rift phanérozoïques qui bordent la côte occidentale de Madagascar. Les sédiments se sont déposés pour la première fois dans ce bassin pendant les premières étapes de la rupture du Gondwana au Permien, en provenance des terranes du socle précambrien adjacent. La rupture du Gondwana a entraîné plusieurs étapes de subsidence, de basculement et de soulèvement de Madagascar, dont l'histoire thermique est enregistrée dans les strates du bassin de Morondava. Nous avons appliqué les techniques de zircon détritique U-Pb pour étudier les schémas de sédimentation et de transport des strates du Jurassique et du Crétacé. Afin de reconstruire l'histoire thermique du bassin de Morondava à travers les étapes du développement du bassin rift, nous avons appliqué la modélisation des données thermochronologiques (U-Th)/He. Nos modèles montrent une histoire prolongée de refroidissement influencée par de multiples étapes de soulèvement et de subsidence se produisant de manière différentielle dans le bassin. Une meilleure compréhension du bassin de Morondava en ce qui concerne son développement pendant la rupture du Gondwana a des implications pour l'exploration pétrolière dans la région.

**Acknowledgments**

First and foremost, I'd like to extend my deepest appreciation to my supervisor, Dr. David Schneider for giving me the opportunity to work on this project and presenting my work at conferences. I am thankful for your kind and supportive supervision especially during a personally difficult last two years during the COVID-19 pandemic.

Additionally, special thanks go to Dr. Gabor Tari at OMV Austria, for providing samples and background knowledge on the Morondava Basin. I will always remember my time working with you in Vienna fondly.

Many thanks to Dr. Jon O'Neil and Dr. Jeremy Powell for serving on my defence committee, and for Dr. Powell for sharing his wisdom using HeFTy. Your insightful comments and feedback have been essential to the improvement of the manuscript.

I would like to recognize the OMNIS for their support in this project; and the Malagasy field team for collection and accurate description and cataloguing of samples.

I am also grateful for the work of the many people and labs who helped me during data collection and analysis. Thank you to Dr. James Metcalf and the rest of the staff at the TRaIL lab in Boulder Colorado for (U-Th)/He analysis. Thank you to Dr. Renelle Dubosq and Glenn Poirier for their assistance in imaging of zircon at the University of Ottawa SEM lab. Thank you to Samuel Morfin at the University of Ottawa ICP-MS lab for his help in conducting zircon U-Pb analysis.

And finally, to my parents, Ernst and Marja. Thank you for the unconditional emotional and moral support throughout the entire process. Words cannot encompass my gratitude to you both. Thank you. Dankjewel - Tijnie.

**Table of Contents**

**List of Figures**

**Figure 7:** Zircon (U-Th)/He date-eU relationships of the Cretaceous and Jurassic samples from the Morondava Basin, Madagascar. Samples are grouped by stratigraphic age (Cretaceous, Jurassic) and transect (North = northern transect; South = southern transect). One outlier at (2675 ppm, 7.73 Ma) for sample 34/1 is excluded for analysis and visualization.

**Figure 8:** North Transect – Jurassic samples: (I) inverse models with the range of "acceptable" path solutions in dark grey envelope, "good" path solutions in light grey and best-fit thermal history in black (BF). Selected forward models (A, B, C) based on best-fit path and observed trends in inverse paths. (II) Post-depositional t-T paths based on forward models A, B, C. Grey box represents the ZHe partial rentention zone. (III) Forward models of the expected ZHe date-eU response for (BF) best-fit thermal history, (A) simplified best-fit thermal history, (B) similar to A but with tertiary heating and rapid cooling, (C) similar to B but with rapid pre-depositional cooling at ca. 500 Ma. Black line represents the cooling path of the average (63 μm) grain-size within the sample, grey envelope represents the range of cooling paths between the maximum (73 μm) and minimum (51 μm) grain-size within the sample. Orange (41/1) and grey (01/2), bolded points represent grains used in inverse modelling.

**Figure 9:** South transect – Jurassic samples: (I) inverse models with the range of "acceptable" path solutions in dark grey envelope, "good" path solutions in light grey and best-fit thermal history in black (BF). Selected forward models (A, B, C) based on best-fit path and observed trends in inverse paths. (II) Post-depositional t-T paths based on forward models A, B, C. Grey box represents the ZHe partial rentention zone. (III) Forward models of the expected ZHe date-eU response for (BF) best-fit thermal history based on results for the north transect, (A) simplified best-fit thermal history, (B) simplified best-fit thermal history for south transect with Tertiary heating, (C) similar to B but with rapid pre-depositional cooling at ca. 500 Ma. Black line represents the cooling path of the average (57 μm) grain-size within the sample, grey envelope represents the range of cooling paths between the maximum (92 μm) and minimum (39 μm) grain-size within the sample. Orange points (40/3) and grey points (39/3), bolded points represent grains used in inverse modelling.

**Figure 10:** North transect – Cretaceous samples: (I) inverse models with the range of "acceptable" path solutions in dark grey envelope, "good" path solutions in light grey and best-fit thermal history in black (BF). Selected forward models (A, B, C) based on best-fit path

and observed trends in inverse paths. (II) Post-depositional t-T paths based on forward models A, B, C. Grey box represents the ZHe partial rentention zone. (III) Forward models of the expected ZHe date-eU response for (BF) best-fit thermal history, (A) simplified best-fit thermal history, (B) similar to A but with heating and cooling in the Middle Jurassic to test sediment recycling scenario, (C) similar to A but with higher temperature in Late Cretaceous and uninterrupted cooling in the Tertiary. Black line represents the cooling path of the average (59 μm) grain-size within the sample, grey envelope represents the range of cooling paths between the maximum (73 μm) and minimum (48 μm) grain-size within the sample. Orange points (17/1) and grey points (09/2), bolded points represent grains used in inverse modelling.

**Figure 11:** South transect – Cretaceous samples: (I) inverse models with the range of "acceptable" path solutions in dark grey envelope, "good" path solutions in light grey and best-fit thermal history in black (BF). Selected forward models (A, B, C) based on best-fit path and observed trends in inverse paths. (II) Post-depositional t-T paths based on forward models A, B, C. Grey box represents the ZHe partial rentention zone. (III) Forward models of the expected ZHe date-eU response for (BF) best-fit thermal history, (BF2) best-fit thermal history testing sediment recycling scenario, (A) simplified best-fit thermal history, (B) simplified best-fit sediment recycling scenario thermal history. Black line represents the cooling path of the average (68 μm) grain-size within the sample, grey envelope represents the range of cooling paths between the maximum (80 μm) and minimum (59 μm) grain-size within the sample. Orange points (34/1) and grey points (31/1), bolded points represent the grains used in inverse modelling.

**Figure 12:** Morondava Basin reconstruction based on detrital zircon (U-Th)/He thermochronology. Black circles mark approximate position of samples taken in this study. Cross-section based on the same transect examined in figure 4. Figure is not true to vertical scale. Red arrows indicate heating, green arrows indicate cooling with size indicating the relative magnitude of heating/cooling event. Equal sign denotes models show uncertainty or no significant thermal event occurring.

**List of Tables**

**List of Abbreviations**

U-Pb – uranium-lead

(U-Th)/He – (uranium-thorium)/helium

FT – fission track

Ma – Mega-annum (one million years)

Ga – Giga-annum (one billion years)

Myr – million years

nm – nanometre

µm – micrometer

mm – millimetre

cm – centimetre

m – metre

km – kilometre

J – Joules

℃ - degrees Celsius

LA ICP-MS – laser ablation inductively coupled plasma – mass spectrometry

PRZ – partial retention zone

eU – effective uranium

ESR – equivalent spherical radius

ppm – parts per million

MDS – multidimensional scaling

ZRDAAM – zircon radiation damage accumulation and annealing model

t-T – temperature-time

K-S – Kolmogorov-Smirnov

BF – best fit

**Extended Abstract**

Formation of the Phanerozoic basins of Madagascar coincided with the initial stages of Permian break-up of Gondwana. The sources of the sediments in these basins are from the seven major Precambrian terranes that border them. The tectonic history of rifting, drifting, and uplift of the Madagascan terrane over the last 300 million years is recorded within the sedimentary strata that comprise the Morondava Basin, the largest of these basins located along the west coast. In this study, we have applied detrital zircon U-Pb geochronology and (U-Th)/He low-temperature thermochronology to resolve the sedimentation patterns and thermal history of the basin as Madagascar separated from Africa and subsequently India. Nine coarse-grained siliciclastic samples were taken along two transects parallel to the Morondava River in the central basin. Four samples are taken from the Permo-Triassic failed rift basin, whilst five samples were taken from post-Jurassic passive margin sequences separated by the crustal-scale Illovo Fault. Detrital zircon U-Pb age distributions include common Neoarchean and Neoproterozoic populations which suggests input from the basement terranes of the Madagascan central highlands (Antananarivo domain). A subset of samples contains a Paleo- to Mesoarchean population linked to the metasedimentary Anosyen domain and a Cambrian population associated with metamorphic zircon formed during the Pan-African Orogeny linked to the southwestern basement terranes. Spatial variations within the detrital zircon U-Pb age populations indicate two distinct sedimentation patterns separating the north and south parts of the basin and a likely post-Jurassic sediment recycling history within the Morondava Basin. Zircon (U-Th)/He ages range from 503 ± 17 Ma to 40 ± 1 Ma with effective uranium (eU) values ranging from 35 to 1760 ppm, which exhibit a strong negative eU-age relationship and indicate partial resetting of zircon throughout the basin. We present inverse and forward thermal history models for samples deposited prior to and subsequent to successful rifting using the zircon radiation damage and annealing model to produce a thermal history model for the basin. Thermal history modelling reveals separate thermal histories for sediments deposited on either side of the Illovo Fault. Cooling to the west of the fault coincident with heating to the west of the Illovo fault suggests reactivation of the crustal scale structure and the development of a rift flank in the Permo-Triassic failed rift. Final cooling occurred in the last 40 Myr but is poorly constrained. Different rates of cooling on either side of the Illovo Fault may indicate re-activation and an explanation for the presence of a structural high along the east flank of the fault.

## 1.0 Introduction

The island of Madagascar was centrally located in Gondwana prior to the Jurassic break-up of the supercontinent, surrounded by modern-day Tanzania, India, and Antarctica (**Fig. 1**). The break-up of the supercontinent led to the development of several sedimentary basins along the coast of the island. The largest basin, Morondava Basin, is positioned along the west coast of the island in the Mozambique Channel and hosts the onshore Tsimiroro and Bemolanga oil fields in Permo-Triassic strata. The basin has been the subject of several drilling programs and structural investigations to investigate the source potential of younger strata, such as the Isalo and Sakoa Groups (Clark, 1998). Thermal maturity studies of Permo-Triassic sedimentary sequences in the basin indicate they are a poor source for oil, though there may be some gas potential (Ramanampisoa & Radke, 1992). Analysis of Jurassic and Cretaceous sediments in the northern Mahajanga Basin are supportive for moderate levels of thermal evolution yet structural complexities within the basins have resulted in inconsistent hydrocarbon generation.

The sedimentary and thermal evolution of the Morondava Basin was broadly influenced by three major events (e.g., Geiger et al., 2004): 1) the formation of a continental failed Permo-Triassic rift, 2) successful rifting initiated in the Middle Jurassic as Madagascar began to separate from Africa, and 3) Late-Cretaceous break-up from India followed by Miocene break-up from Antarctica. A large fault system stretching N-S through the entire basin, the Illovo (also named Bemaraha in north Morondava), lies approximately on the boundary between the two rift systems and may play a central role in accommodating the structural evolution of the region. Since its separation from eastern Africa in Jurassic times, the western margin of Madagascar has occupied a passive tectonic setting and has been relatively stable. This study focuses on sedimentary rocks deposited both before and after the successful break-up of Gondwana to investigate the structural and thermal events at all stages of break-up.

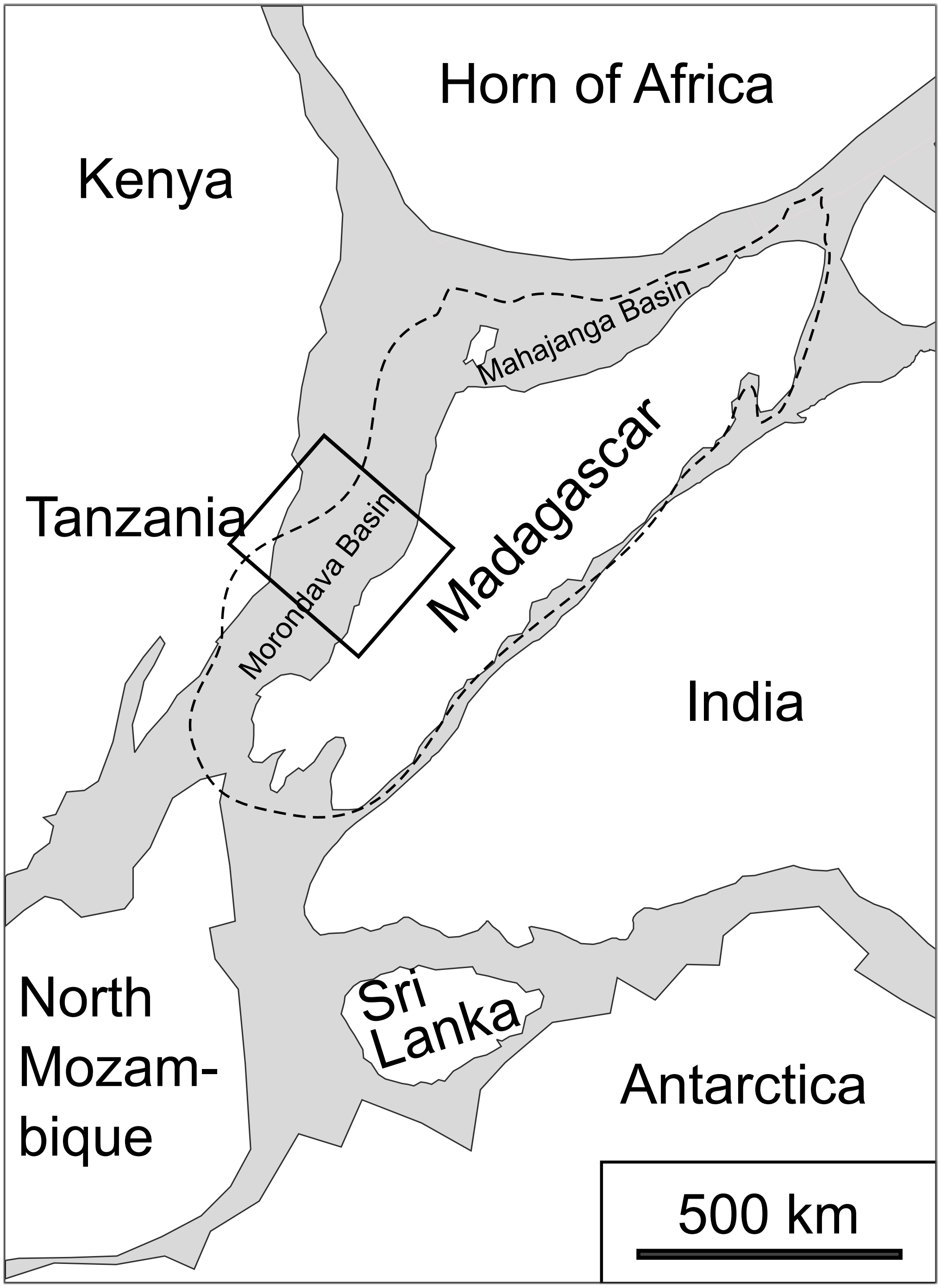


*Figure 1: Position of Madagascar within Gondwana at 200 Ma based on observations of ocean-floor topography by Reeves et al. (2002). Precambrian crustal fragments which still exist today are shown in white, whilst original continental rocks lost to rifting are shown in grey. Dotted line represents the present-day extent of Madagascar. Black box represents the study area, with relevant sedimentary basins indicated.*

Previous thermochronological studies have focused on assessing the effects of Permo-Triassic rifting of the Morondava Basin and the adjacent crystalline basement using low-temperature thermochronometry techniques such as apatite and titanite fission track dating (Emmel et al., 2004; Emmel, Geiger, et al., 2006; Emmel, Jacobs, et al., 2006; Giese et al., 2012; Seward et al., 2004), and apatite and zircon (U-Th)/He dating (Stephenson et al., 2021). These studies focus on Madagascar-scale uplift and exhumation of Madagascar during break-up of Gondwana. Herein, we present detrital zircon (U-Th)/He and U-Pb data from Jurassic and Cretaceous strata in an attempt to better understand the thermal influence of the three major tectonic events on the basin as they relate to burial, exhumation, and other thermal events since the break-up of Gondwana pertaining directly to the Morondava Basin. We apply U-Pb geochronology techniques to establishing a simple sediment-source relationship between the various basement terranes of Madagascar and the Morondava Basin; detrital zircon U-Pb data are also used to identify general sedimentation patterns and possible sediment recycling within the basin, which may have implications for the zircon thermochronology data. The (U-Th)/He data are used to evaluate plausible temperature-time models of the basin to quantify the timing and magnitude of the heating and cooling episodes that may be recorded in the basin. We employ inverse and forward thermal history modelling strategies to investigate the thermal history of the basin as it experienced several stages of faulting, tilting, subsidence and exhumation. The results and discussion in this paper aim to help resolve the magnitude and timing of these stages as the Morondava Basin developed from a failed rift into a passive margin and could further be applied to better understanding the hydrocarbon potential of the basin.

## 2.0 Geologic history

The geology of Madagascar can be subdivided into two major tectonic domains: 1) the Eastern and Central Highlands defined by Precambrian and early Paleozoic crystalline basement that was amalgamated during the Pan-African Orogeny, and 2) the Carboniferous to Quaternary sedimentary basins stretching along the western coast, and include from north to south: the Antsiranana, Mahajanga, and Morondava basins. The Precambrian basement (**Fig. 2**) can be further subdivided into five terranes (Andriampenomanana et al., 2017), from oldest to youngest: the Antongil-Masora Craton (Paleoarchean-Mesoarchean), Antananarivo (Neoarchean), Anosyen-Androyen (Paleoproterozoic), Ikalamavony (Mesoproterozoic), and Vohibory-Bemarivo terranes (Neoproterozoic). These terranes are composed primarily of ortho- and paragneisses and granitoids (Seward et al., 2004). The basement was extensively reworked during the Neoproterozoic-late Paleozoic Pan-African Orogeny, imparting a medium to high grade metamorphic overprint and thus resetting most geochronological systems (Emmel et al., 2006). Opening of the Mozambique Channel during the breakup of Gondwana resulted in several stages of basin-sag and uplift and the creation of the three basins on the western margin of the island (Emmel et al., 2008). The basement terranes defined the rift-flanks during breakup-related uplift and supplied sediments into the basins. Below we discuss the characteristics of the Precambrian blocks and the tectonostratigraphic development of the Morondava Basin, which is the focus of this study.

## 2.1 Madagascar terranes

### 2.1.1 Antananarivo

The Antananarivo Domain is the largest of the Precambrian basement terranes underlying most of central and northern Madagascar (**Fig. 2**). The Antananarivo Domain (sensu lato) is

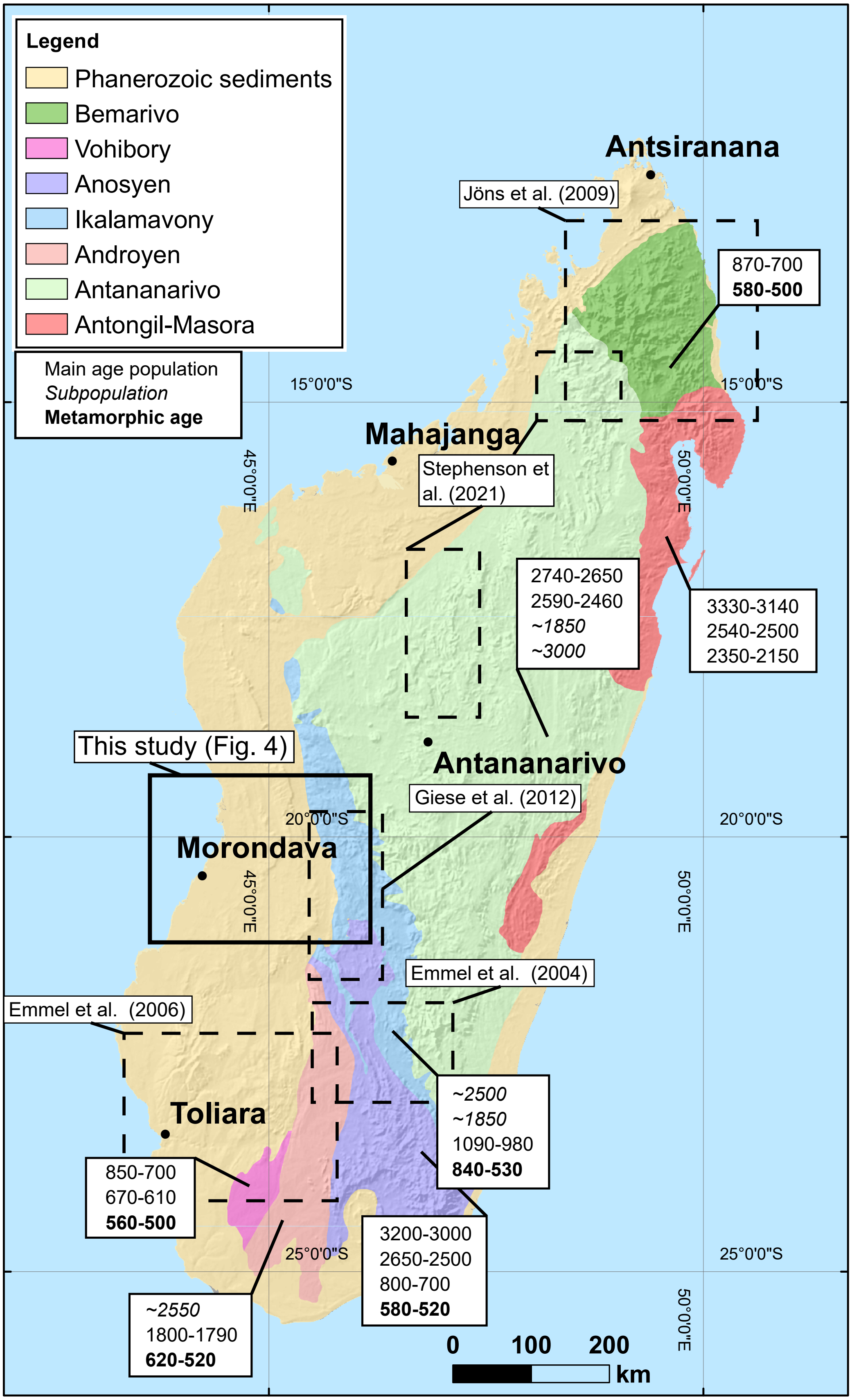


*Figure 2: A map of the major crystalline basement terranes of Madagascar and adjacent basins (modified after Boger et al., 2019). The map also includes the dominant zircon U-Pb age populations found within each terrane (Archibald et al., 2015; Boger et al., 2014; Collins et al., 2003; Kroener, 2000; Tucker et al., 2011). Subpopulations are listed in italics and metamorphic zircon ages are listed in bold. Study area outlined by black box, presented in figure 4.*

comprised of structurally lower paragneiss of the Sofia and Vondrozo groups, which are together within the Antananarivo Complex (sensu stricto; Boger et al., 2019). Structurally above the Antananarivo Complex are three north-south trending belts of interlayered mafic gneiss and schist of the Tsaratanana Complex. The Antananarivo and Tsaratanana complexes are intruded by Neoarchean-Paleoproterozoic Betsiboka suite granites, and experienced granulite to amphibolite facies metamorphism (Boger et al., 2015). Published zircon U-Pb crystallization ages for the Antananarivo and Tsaratanana complexes range between 2740 and 2650 Ma (Ichiki et al., 2015; Kabete et al., 2006). The intruding Betsiboka suite has zircon U-Pb ages ranging from 2590-2460 Ma (Ashwal & Tucker, 1999; Kabete et al., 2006; Kroener, 2000).

Overlying the Antananarivo Domain are several variably metamorphosed and deformed metasedimentary groups. The Paleoproterozoic (1800-1650 Ma) Itremo Group, bordering the Ikalamavony Domain on the southwestern edge of the Antananarivo Domain, has been the subject of several detrital zircon provenance studies (i.e., Armistead et al., 2021). The Itremo is comprised of stratified quartzite, mica schist, and dolomitic marble metamorphosed to greenschist facies conditions, or amphibolite facies for structurally lower units. Quartzites from this assemblage record a wide range of detrital zircon U-Pb ages with major age modes at 2500 and 1850 Ma, and minor proportions of 2200-1900 Ma, 800 Ma, and 2900+ Ma (**Fig. 3**; Boger et al., 2014; Fitzsimons & Hulscher, 2005). The somewhat older (2200-1800 Ma) Ampasary-Manapotsy Group, bordering the Antongil-Masora Domain, is comprised of quartzite, schist, and gneiss. The Ampasary-Manapotsy Group has a detrital zircon signature similar to the Itremo, although with a significantly greater proportion of Paleo-Mesoarchean zircon (Archibald et al., 2015; Boger et al., 2014). The remaining two groups overlying the Antananarivo are the Maha and Ambatolampy groups with similar ages and lithologies to the Itremo Group (Collins et al., 2012).

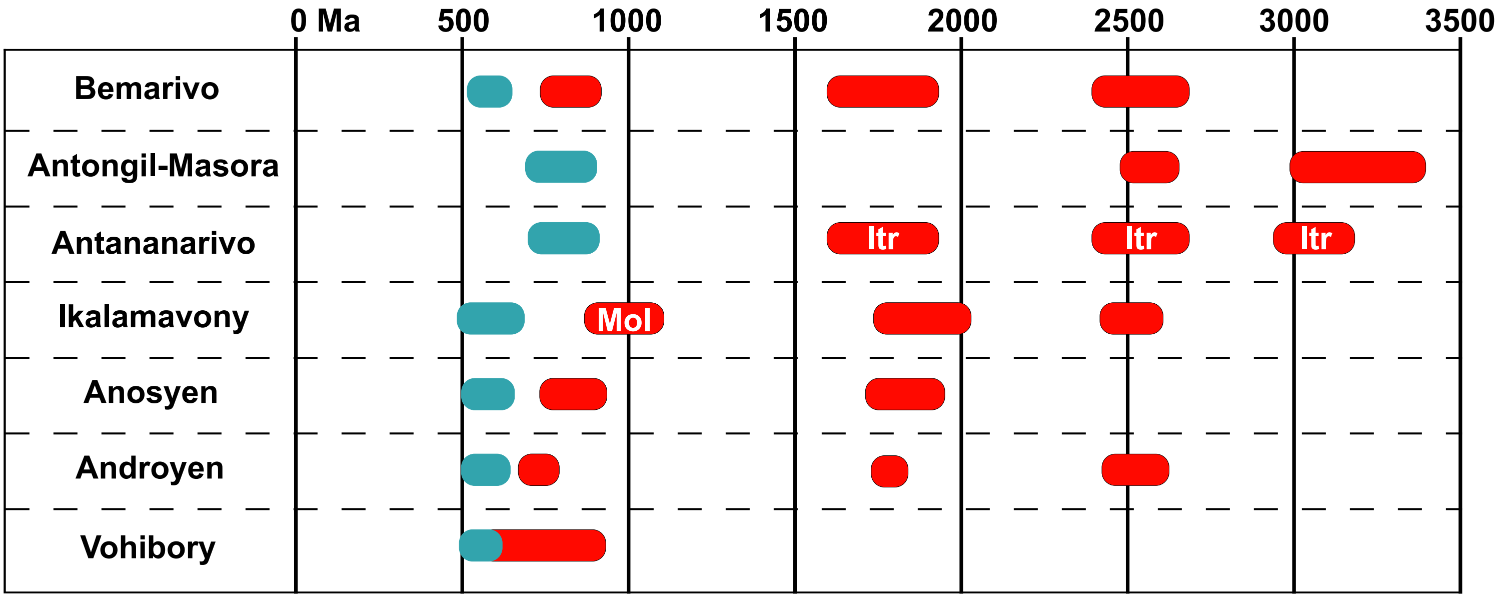


*Figure 3: Simplified distribution of U-Pb zircon age populations present in basement terranes of Madagascar. U-Pb age populations associated with localized metasedimentary sequences are highlighted. Itr: Itremo Group, Mol: Molo group. Light blue are ages associated with final metamorphic overprint and magmatism due to accretion of terranes. See text for references.*

The Archean Antananarivo basement and its overlying metasedimentary groups are intruded by Cryogenian (820-750 Ma) and Edicarian (560-530 Ma) batholiths and stocks. The Imorona-Itsindro Suite (820-760 Ma) formed intermediate to felsic intrusions throughout several domains in Madagascar as a product of continental magmatism during pre-Gondwana subduction. The Maevarano-Ambalavao Suite forms a series of post-tectonic plutons, stocks, and dykes throughout the Antananarivo and Bemarivo domains (Archibald et al., 2015; Handke et al., 1999; Kroener, 2000; Tucker et al., 2011).

2.1.2 Antongil-Masora

The Antongil and Masora domains are the oldest domains on Madagascar exposed along the northeastern and eastern coast of the island, respectively, linked to the south Indian Dharwar Craton (**Fig. 3**; Fitzsimons & Hulscher, 2005). Although the two domains are separated geographically, they are correlated by 3330-3140 Ma paragneiss-hosted migmatitic orthogneisses: Nosy Boraha in the Antongil, and Befody in the Masora. Magmatic activity recorded only in the Antongil occurs at 2540-2500 Ma synchronous with high-temperature metamorphism (Fig. 2), and again at 2350 Ma and 2150 Ma. Overlying the Antongil is a series of metavolcanic schists and quartzite of the Andrarona Group with detrital zircon U-Pb ages between 2800 Ma and 1800 Ma with a major mode at 1850 Ma (Bauer et al., 2011). In contrast, the Masora Group is overlain by pelitic schist and amphibolite of the Maha Group. Detrital zircon U-Pb ages from the Maha Group range from 3100 Ma to 1670 Ma, also with a major mode at 1850 Ma (De Waele et al., 2011). Intrusion of the Imorona-Itsindro Suite found in the Antananarivo Domain similarly occurred in the Masora Domain, although not in the Antongil Domain (Ashwal & Tucker, 1999; Tucker et al., 2011).

### 2.1.3 Ikalamavony

The Ikalamavony forms a narrow (50-200 km) domain trending along the southwestern border of the Antananarivo Domain and is thrust over the Itremo Group (**Fig. 2**). The largest component of the Ikalamavony Domain (sensu lato) is a thick package of quartzite intercalated with formations of feldspathic leucogneiss, amphibolite and thin packages of calcite marble and calc-silicate gneiss named the Ikalamavony Group (sensu stricto). Other rocks found within the Ikalamavony (sensu lato) are minor quartz-rich metasedimentary rocks of the Molo Group, small outliers of the Itremo Group (see above), and several intrusions. The Ikalamavony Domain was metamorphosed to upper amphibolite or lower granulite facies (Boger et al., 2019).

Detrital zircon from the Ikalamavony Group have been U-Pb dated at 1070-1010 Ma and possess ca. 1000 Ma metamorphic rims (Tucker et al., 2011). The Molo Group is generally younger than the Ikalamavony Group with zircon ages of ca. 1030 Ma, and with small sub-populations of zircon dates between 840 and 530 Ma (Cox et al., 2004; Fitzsimons & Hulscher, 2005). Itremo Group age populations as described above are also present with dates of 2500-1800 Ma and a major mode at 1850 Ma. The Ikalamavony Domain is intruded by Imorona-Itsindro and Ambalavao felsic and intermediate intrusive rocks also found in the Antananarivo Domain.

### 2.1.4 Bemarivo

The Bemarivo Domain forms the northernmost Precambrian terrane on Madagascar bordering both the Antongil and Antananarivo domains. Thomas et al. (2009) suggested that the Bemarivo represents a Cryogenian magmatic arc accreted to the Antananarivo Domain at 570-520 Ma. Alternatively Boger et al. (2014) suggest that the Bemarivo represents a back-arc basin formed behind a continental magmatic arc. The Bemarivo is comprised of a mix of schist, quartzite, and paragneiss Paleoproterozoic in age intruded by Neoproterozoic intermediate to felsic intrusive rocks. The southern sedimentary units have Itremo-like detrital zircon U-Pb ages (2500-1800 Ma with a major mode at 1850 Ma; **Fig. 3**). Older sedimentary units are found in the north with detrital zircon U-Pb ages between 3400-2400 Ma with a major age mode at 2500 Ma (Thomas et al., 2009). The volcanogenic Milanoa Group contains a unimodal zircon U-Pb age population of 750 Ma. The entire Bemarivo Domain underwent metamorphism and magmatism at 580-520 Ma, associated with accretion to the Antananarivo Domain following the suggestion of Thomas et al. (2009).

#### 2.1.5 Anosyen

The Anosyen Domain lies to the east of the Androyen and Vohibory domains and is comprised of the volcanic Horombe Group and the sedimentary Iakora Group. The Iakora Group is comprised of pelitic and calc-silicate gneisses with minor quartzite and marble thought to be Cryogenian (740 Ma; Tucker et al., 2011; Boger et al., 2014). Detrital zircon age signatures from the Iakora are similar to those found in the Itremo Group covering the Ikalamavony and Antananarivo domains (2500-1800 Ma with a major mode at 1850 Ma; Collins et al., 2012; Boger et al., 2014). The Horombe Group is comprised of volcanic quartzofeldspathic gneisses formed concurrently, and intercalated, with the Iakora. The youngest detrital zircon U-Pb ages found in one of the formations of the Horombe range from 580 Ma to 545 Ma with discordant grains providing an upper intercept at 1840 Ma (Muller, 2000). This upper intercept has been interpreted to suggest a Paleoproterozoic depositional age for the Horombe, whilst the younger 580 Ma to 545 Ma represents a metamorphic overprint (Tucker et al., 2011). The metamorphic history of the Anosyen records a single event at granulite facies conditions at 545 Ma and was accompanied by Ambalavao suite intrusions ranging between 545 and 510 Ma (Boger et al., 2014; Kroener, 2000; Paquette et al., 1994)

2.1.6 Androyen

The Androyen lies between the Anosyen and Vohibory domains. In previous studies the Androyen was further subdivided into the Graphite and Androyen systems, however for the purposes of our study they can be considered contiguous. The Androyen is comprised of the Mangoky and Imaloto groups. The Mangoky Group includes psammitic and pelitic paragneiss, with abundant graphite and sillimanite in certain localities, intercalated with intermediate to mafic paragneiss. Paragneiss from the north of the domain has yielded three distinct age populations (**Fig. 3**): 1) A Neoarchean age (2550 Ma) thought to reflect the presence of xenocrystic zircon, sourced from Neoarchean basement rocks. 2) A well-constrained mode at 1795 Ma is thought to reflect the depositional age of the protolith of this formation. 3) A wider set of zircon U-Pb ages range from 620 to 520 Ma likely reflects zircon growth during separate metamorphic events. The first stage of metamorphism occurred between 620 Ma and 600 Ma and can be associated with peak metamorphism in the Vohibory Domain to the southwest. A second stage of metamorphism occurred between 570 Ma and 530 Ma which is associated with the accretion of the Anosyen and Ikalamavony to the northeast. Although previous studies (i.e., Besairie, 1964) found difficulty in differentiating the Androyen and Anosyen domains, the presence of both stages of metamorphism can be used to differentiate between the two domains (with only one stage in the Anosyen). The Androyen Domain is intruded by the Ambalavao-Maevarano Suite also observed in the Antananarivo and Ikalamavony domains.

2.1.7 Vohibory

The Vohibory is the most southwestern domain in Madagascar, and the last terrane to be accreted to Madagascar during collision with east Africa. The Vohibory is comprised of a series of mafic and felsic gneiss of the Mahafaly, Gogogogo, and Marosavoa groups intercalated with metasedimentary Linta Group. The mafic rocks of the Mahafaly are interpreted to be a mix of mid-ocean, back-arc and island arc basalts and volcanoclastic sediments. Detrital zircon U-Pb ages in the Mahafaly range between 850 and 570 Ma with a group of metamorphic zircon dated at 610 Ma. These rocks are intercalated with metasedimentary paragneiss, calc-silicate and marbles of the Linta Group. The Linta Group possesses zircon dated between 910 and 750 Ma with a major mode at 850 Ma. The zircons found in the Linta Group also contain neoblastic zircon and zircon with metamorphic rims dated at 620 Ma. Peak metamorphism in the Vohibory occurred between 630-600 Ma (Fig. 2), in contrast to the rest of Madagascar, this age is reflected in the detrital zircon populations of the Mahafaly and Linta groups.

### 2.2 Morondava Basin

One of the three major sedimentary basins of Madagascar, the Morondava Basin, is primarily comprised of fluvial and marine sedimentary rocks ranging in age from Permian in the east to Eocene in the west. Sediment thicknesses within the basin reach up to 10 km in the south, thinning towards the north (**Fig. 4**; Razafimbelo, 1987). The Mahajanga and Ambilobe basins to the north of the Morondava along the northwestern coast of the island formed contemporaneously to the Morondava Basin, but have seen significantly less investigation by the energy industry. The total succession of most of the modern sedimentology and stratigraphic naming conventions are based on the work of Besairie (1972); adjustments to the terminology and identification of sedimentological units have been made over the past 50 years (Luger et al., 1994).

Formation of the Morondava Basin was initiated in the late Carboniferous by crustal extension along the margins of east Gondwana (Madagascar, India, Antarctica) and west Gondwana (Africa, Arabia, South America). The initial stage of pre-breakup crustal extension led

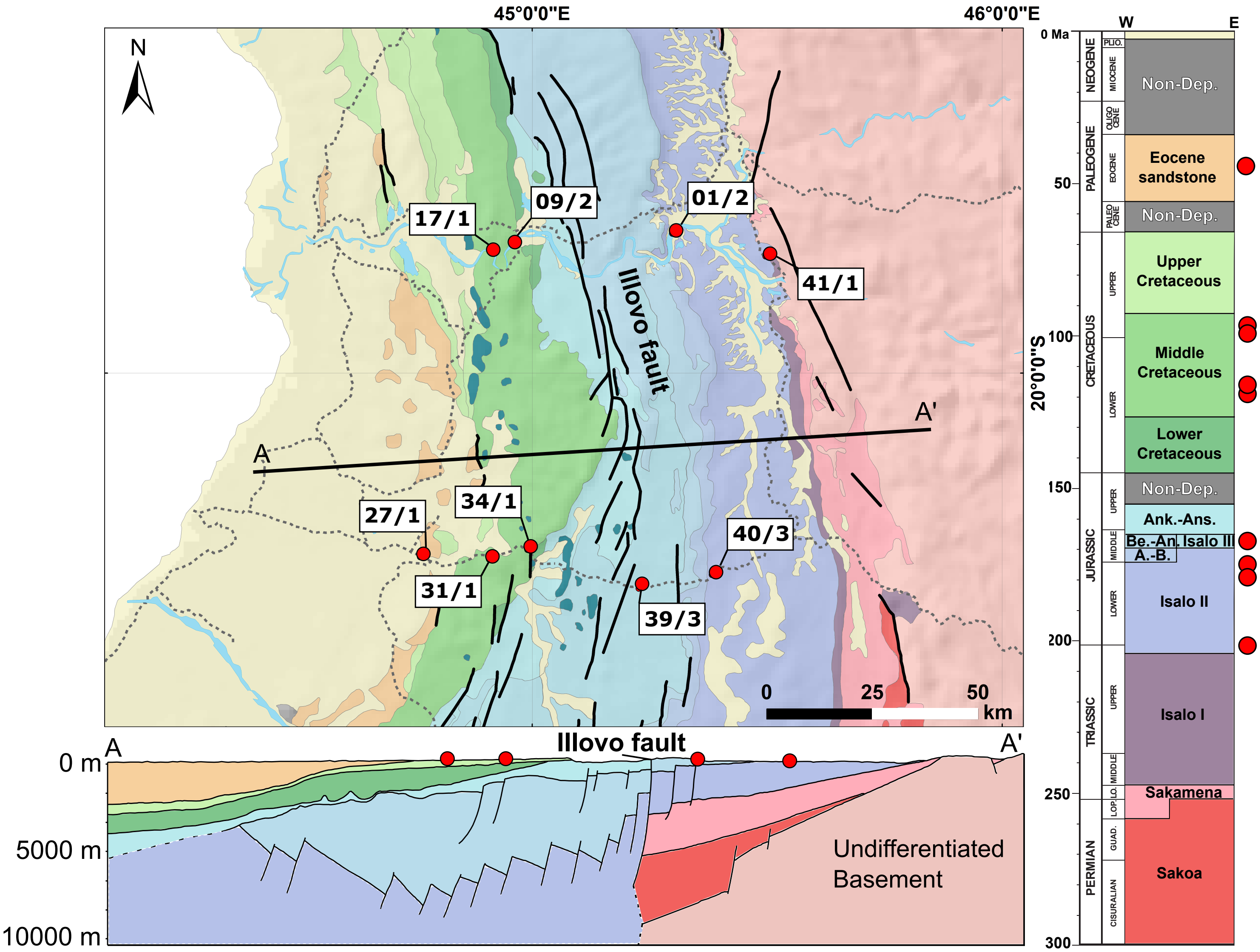


*Figure 4: Geologic map, stratigraphic section, and seismic interpretation of the Morondava Basin. Sample locations and their relative geographic and stratigraphic position are marked with red dots. Major faults are marked in black. Map after (Besairie, 1969; Giese et al., 2012; Roig et al., 2012). Stratigraphic column after Giese et al. (2012) and Geiger et al. (2004). Seismic interpretation after unpublished Amoco report (1986). Abbreviations: A.-B.: Andafia/Beronono; Be.-An.:Bemaraha/ Ankarana; Ank.-Ans.: Ankilizato/Ansalova.*

to the development of a failed rift, depositing a fluvial succession of three units: the Sakoa Group, the Sakamena Group, and the lower part of the Isalo Formation (as identified by Besairie, 1972) formed in a series of half-grabens (Schandelmeier et al., 2004). These units comprise the Karoo Supergroup, elsewhere exposed on the eastern margin of Africa. The oldest unit of the basin residing structurally above the crystalline basement, the early Permian Sakoa succession, is exposed along the eastern contact with the basement and is comprised primarily of sandstones, shales, coals deposited in braided river and swamp environments in a series of pull-apart basin developed along NNE-SSW trending strike-slip faults (Clark, 1998; Coffin & Rabinowitz, 1988). Renewed rifting in the middle to late Permian resulted in the reactivation half-grabens and brief establishment of marine conditions and the deposition of shallow marine limestones. Further extension resulted in the tilting and uplift of individual fault blocks and the deposition of conglomerates, sandstones, shales in fluviatile, deltaic, and marginal marine environments. Together, these limestones and marginal marine clastic assemblages form the Lower Sakamena Formation (Clark, 1998; Wescott & Diggens, 1998). This was followed by a period of non-deposition as the horsts were uplifted possibly due to crustal thinning and upwelling of hot mantle material beneath the rift, cutting off sediment supply to the grabens (Moucha & Forte, 2011).

Marine transgression in the Early Triassic deposited a thick package of shales rich in organic matter, which progressively becomes less organic-rich towards the top as the waters turned more brackish to lacustrine (Pique, 1999; Wescott & Diggens, 1998). The progradation of fluvial deltas into the Middle Triassic deposited a package of cross-laminated and cross-bedded sandstones thought to have been deposited in delta-front, mouth bar and fluvial channel environments (Clark, 1998; Coffin & Rabinowitz, 1988). In the Late Triassic a period of uplift resulted in widespread erosion and the development of an angular unconformity overlain by cross-bedded sandstones and gravels of the Isalo that were deposited in fluvial channels. The Isalo forms a package of sediment up to 6 km in thickness in places, likely due to an extended phase of basin sag (Coffin & Rabinowitz, 1988). This is evinced by the deposition of a package of sediment of uniform thickness over a wide area, in places overstepping unto the Sakamena and the basement (Razafimbelo, 1987).

A new rift developed to the west of the failed Permo-Triassic rift at the end of the Early Jurassic, eventually leading to separation of Madagascar from Africa (Geiger et al., 2004; Geiger & Schweigert, 2006). Extension resulted in the dissection of Isalo sandstones into a series of fault blocks that progressively rotated throughout the upper Jurassic to form several half-grabens (Clark, 1998). With this, marine conditions were re-established and a thick package of organic-rich shales and argillaceous limestones were deposited as the Andafia Formation. Towards the top of the Andafia is a series of bioturbated and cross-bedded sandstones, named the Isalo III, differentiated by mixed facies of sandstone and marls deposited in deltaic or coastal-barrier/lagoon complexes (Clark, 1998).

As Madagascar, still attached to the Indian subcontinent, began to drift away from Africa the Morondava Basin developed into a passive margin during the Middle Jurassic. In the mid-latitudes, subsidence of the basin resulted in the development of a carbonate platform on top of the half-grabens. Two types of environments are observed in the sediments deposited during this event: coastal barrier-lagoon complexes, and slope and basin-plain deposits. The lagoon deposits comprise primarily light-grey mudstones and oolitic grainstones whilst the slope and basin-plain deposits are organic-rich laminated mudstones, together defining the Bemaraha Limestone (Geiger et al., 2004). Despite widespread carbonate deposition, the Middle Jurassic was marked by a series of transgressions and the deposition of marine shales onlapping the Bemaraha limestone.

Deposition of shales as well as coastal and deltaic sandstones occurred during this time. Most of these shales and sandstones remain preserved only in the northern part of the basin, with only localized outcrops of sandstones observable at surface in the southern basin. The Illovo Fault was likely active during the Middle Jurassic, inferred by apparent thickening of Middle Jurassic sequences towards the fault (**Fig. 4**, Clark, 1998). The presence of a structural high to the east of the Illovo fault is currently debated.

As the passive margin continued to subside during the Cretaceous, three to four cycles of sedimentation occurred coinciding with changes in eustatic sea level: the Valanginian-early Aptian, late Aptian-early Turonian, and late Turonian-Maastrichtian. Sediment packages corresponding to each of these periods consist of shale sequences overlain by sandstone (Tsiandava and Anakarafantsika sandstones) and an upper unit of shales, described as Aptian-Albian Shales in the literature (Besairie, 1972). Shales were deposited in open marine environments, whilst the sandstones were deposited at the end of each high-stand in deltaic and coastal environments.

Separation of Madagascar from the Indian subcontinent resulted in uplift of the Central Highlands to the east and overall tilting of Madagascar to the west. During uplift, some of the previously deposited sediments were eroded along the eastern edges of the basin. The crustal-scale separation was also associated with extensive volcanism coincident with activity of the Marion hot spot (Torsvik et al., 1998), which likely resulted in the formation of Turonian basaltic sills found throughout the basin. Tilting continued to progress through into the Tertiary as Madagascar began to drift away from Antarctica. Several units of Mio-Pliocene sandstone and shale were deposited on the western margins of the basin together with the Katsepe and Mahabibo Limestones. These units are exposed as small outcrops of both siliciclastic and carbonate sedimentary rocks along the coast of the island as coastal barrier-lagoon complexes.

## 2.3 Previous thermochronology

Most of the previously published thermochronology involves apatite and zircon fission track (FT) analysis focuses on the crystalline basement terranes and the Karoo sedimentary rocks deposited in the Permo-Triassic failed rift system of the Morondava Basin (**Fig. 2**). Seward et al. (2004) provides a summary of the earliest published FT data from Madagascar covering a wide extent of the Malagasy Precambrian basement. Apparent apatite and zircon FT ages range from 431 ± 46 Ma to 68 ± 8 Ma and 452 ± 64 Ma to 238 ± 46 Ma, respectively. Seward et al. (2004) discuss the thermochronological division of Madagascar as three domains from north to south and notable east-west variations in each of these domains. Samples from the western margin of the basement, bordering the basin, experienced Paleozoic cooling interpreted to have occurred subsequent to intracontinental rifting due to relaxation of the geotherm. The samples then experienced a period of heating, likely associated with Mesozoic burial. Consistent with Permo-Triassic to Jurassic sedimentation progressively on-lapping the basement, FT ages decrease from west to east in the northern and southern regions. In contrast, the eastern central domain underwent consistent, slow cooling from the Devonian onwards with estimated exhumation rates on the order of 1-5 m/Myr. The lack of apparent heating indicates that the margins of this region may represent the maximum extent of the Morondava and Mahajanga basins.

Emmel et al. (2004, 2006) studied the south-central basement of Madagascar to investigate the thermal history since the Cambrian. Apatite FT ages range between 460 ± 21 and 79 ± 5 Ma. Based on the data, the authors suggest that final cooling after the assembly of Gondwana lasted until the Early Ordovician (ca. 500 Ma). This was followed by ca. 150 Myr of protracted cooling attributed to isostatic compensation after denudation of the Pan-African Orogen. Rapid cooling in the Carboniferous is suggested to have occurred as the structural architecture of the Morondava

Basin developed, with denudation rates at the western paleo-margin of the basement estimated up to 100-200 m/Myr. This is followed by heating associated with the deposition of a ~4.5 km thick package of Permo-Triassic sediments in the basin. Based on reheating of the westernmost samples of their study during the Late Permian-Early Triassic, the authors suggest that the Morondava Basin reached its maximum extent at this time, roughly during the deposition of the Sakamena Group. The authors found no significant thermal effects of the Jurassic break-up of Gondwana. However, apatite FT data from southern Madagascar suggests a thermal overprint occurred in the Late Cretaceous and Cenozoic which is attributed to heating related to magmatism associated with Turonian-aged dykes.

Further investigation by Emmel et al. (2006) focused on Middle Jurassic strata of the Morondava Basin. The apparent detrital apatite FT data in this study range between 428 ± 31 Ma and 233 ± 18 Ma, significantly older than the depositional age of the rocks. Since the apatite were not fully reset after deposition, they reflect the pre-depositional thermal history and exclude the possibility of significant post-depositional heating to temperatures >60°C. Decreasing detrital apatite FT ages towards the bottom of the profile are proposed as evidence for burial of Karroo-sediments in these Middle Jurassic strata as a result of westward rift migration prior to breakup of Gondwana. Comparison of basement and basin FT ages together with paleocurrent measurements and apatite morphology are used as evidence for short-distance sediment transport from east to west with minimal along-shore transport.

Emmel et al. (2008) presents a geo- and thermochronometer study on the Vohibory basement terrane to construct a detailed thermal history of that region. The main metamorphism associated with the closure of the Neo-Mozambique ocean and accretion of the Vohibory terrane to the rest of Madagascar is thought to have occurred between 640 and 610 Ma. Extension started in the late Carboniferous/early Permian with cooling at rates of ~5°C/Myr. The central and western parts of the Vohibory terrane experienced heating during the late Permian/Early Triassic as Sakoa and Sakamena sediments were deposited, whilst the eastern flank of the Vohibory already began to exhume. The authors suggest this east-west pattern in burial and exhumation is indicative of sediment transport from the eastern flank into the central basin. Deposition of Triassic/Jurassic Isalo group in the center of the terrane resulted in heating to temperatures in >110°C. The timing of exhumation of the Vohibory during basin development is used as evidence to invoke the transport of sediments from continental sediments and Vohibory basement into the Morondava during the Early to Middle Jurassic.

Jöns et al. (2009) investigated the cooling history within the northernmost Bemarivo basement domain also using a multi-geochronometer approach. Titanite and apatite FT ages range between 318 ± 35 Ma and 157 ± 9 Ma and records cooling subsequent to Gondwana amalgamation; the oldest apatite FT ages were located at the margin with the Mahajanga Basin. The Bemarivo basement cooled through shallow crustal temperatures due to rifting and development of a passive margin during the Permian to Early Jurassic, which is contemporaneous to Karoo deposition in the adjacent basins. The thermochronology do not record major thermal effects from the breakup of Gondwana or separation of Madagascar from the Indian subcontinent. Final cooling to surface temperatures commenced in the early Miocene.

Giese et al. (2012) applied apatite FT thermochronometry to twelve samples along the present-day margin between the crystalline basement and the Morondava Basin, interpreted to be the rift shoulder at the time of the Permo-Triassic failed rift. Seven samples from the basement yield apparent apatite FT ages between 332 ± 50 Ma and 217 ± 29 Ma, five samples from Karoo sedimentary rocks yield ages between 260 ± 36 Ma and 94 ± 20 Ma. Basement samples are thought to have been at or near the surface during Sakamena and Isalo group deposition. These samples are partially reset, with one basement apatite FT age younger than deposition of nearby sedimentary rocks. Thermal history modelling was applied to both sets of samples and suggest maximum temperatures were reached in the Early to middle Cretaceous, consistent with post-depositional thermal overprinting of the Sakamena and Isalo groups to temperatures of up to 90-100°C. Final cooling of the samples appears to have occurred in three stages, each related to exhumation: 1) Early Cretaceous (120 Ma), 2) Late Cretaceous (80-90 Ma), and Eocene (40-50 Ma). The Early Cretaceous stage is thought to have occurred during separation of Madagascar from India; the Late Cretaceous event coincides with break-up between Madagascar and the Indian subcontinent. The authors suggest that the Eocene event is related to a change in plate motion at ca. 43 Ma (Reeves and de Wit, 2000).

Stephenson et al. (2021) present a compilation of published apatite FT data in addition to eighteen new basement apatite FT and apatite (U-Th)/He ages. Apatite FT ages range between 280 ± 20 Ma and 111 ± 20 Ma, whilst single grain apatite (U-Th)/He ages on a subset of the samples range from 586 Ma to 10 Ma (errors not reported). Inverse modelling of the combination of these datasets was used to resolve a regional thermal history of Madagascar. Despite the wide dispersal of the data, the authors found that they were successful in resolving the Neogene/Paleogene and Cretaceous episodes of cooling. Older episodes of heating and cooling were poorly constrained. The authors invoke two episodes of cooling: the first occurring between 275 and 200 Ma, the second occurring between 30 Ma and present day, thought to be broadly consistent with the thermal histories calculated by Seward et al. (2004) and Giese et al. (2012). Through independent observations, the authors conclude that this final stage of exhumation is the result of regional uplift due to a thermal anomaly beneath a thinned plate.

## 3.0 Methodology

### 3.1 Sampling strategy and sample preparation

Samples were collected in the Morondava Basin during the summer of 2017 by a field team organized by OMV along two east-west traverses. The northern traverse was taken by boat along the Mania River, whereas the southern traverse was taken by road from Morondava to Malaimbady (**Table 1**; **Fig. 4**). The samples selected for this study were primarily coarse-grained siliciclastic sedimentary rocks ranging from Triassic to Eocene in age. Representative samples were selected from each of the major stratigraphic units within the Morondava Basin. In order to allow for correlation across the field area, the sampling strategy included taking samples from similar formations in both the northern and southern traverse where possible. In an effort to characterize the samples, we have accessed archival material from OMV including field observations, X-ray diffraction analysis, and industry reports to build an understanding of the field relations and petrology of the lithologies within the basin.

In preparation for geochronologic analyses, sample preparation was completed using standard procedures for heavy mineral separation. Rock samples were cleaned with a wire brushed to remove any possible surface contamination. Samples were crushed with a jaw crusher and passed through a series of sieves in order to separate the material into >250 µm, 63-250 µm and <63 µm size fractions. The 63-250 µm size fraction was then repeatedly washed with water and ethanol, decanting any fine particles between washes, and then dried overnight at room temperature. Mineral separation using methylene iodide (diluted to a specific gravity of 3.0 g/cm$^3$) was conducted on the 63-250 µm size fraction in order to isolate dense minerals including white mica, apatite, and zircon from the less dense fraction which consisted primarily quartz and

**Table 1. List of samples from the Morondava Basin, Madagascar, used for geochronology**

| Sample | Coordinates | Age | Formation | Description |
|---|---|---|---|---|
| 01/2 | 19°42'10,2"S, 45°17'54,0"E | Jurassic | Isalo II | Yellow-beige fine to medium grained sandstone with fine laminations |
| 09/2 | 19°43'32,53"S , 44°57'38,48"E | Cretaceous | N/A | Orange-brown fine to coarse grained massive sandstone, very friable |
| 17/1 | 19°44'22,72"S , 44°55'14,56"E | Cretaceous | N/A | Yellow-brown fine to medium grained massive sandstone, poorly cemented |
| 27/1 | 20°23'29,20''S , 44°45'41,33''E | Eocene | N/A | Light brown fine to medium grained sandstone with some lithic fragments |
| 31/1 | 20°23'45,17''S , 44°54'29,72''E | Cretaceous | N/A | Pale brown to light grey medium to very coarse grained sandstone, very friable |
| 34/1 | 20°22'31,89''S , 44°59'24,26''E | Cretaceous | N/A | Light brown fine to medium grained sandstone, very friable with some lithic fragments |
| 39/3 | 20°27'30,3"S , 45°13'36,8"E | Jurassic | Isalo III | Beige to light grey fine to medium grained laminated sandstone, loosely cemented |
| 40/3 | 20°25'43,3"S , 45°22'57,3"E | Jurassic | Isalo II | Reddish-brown massive sandstone with several granule to pebble sized clasts |
| 41/1 | 19°45'05,7"S , 45°29'48,6"E | Jurassic | Isalo II | Light brown, fine to coarse grained sandstone |

feldspars. In order to complete both (U-Th)/He and U-Pb analyses on zircon from each sample, 150-200 zircon per sample were picked using a binocular stereoscope under reflected light.

### 3.2 Detrital zircon U-Pb geochronology

One of the most commonly applied techniques for sedimentary basin analysis is detrital zircon U-Pb geochronology for sediment source tracing, depositional pattern analysis and in some cases for determining a maximum depositional age for strata (i.e. Nemchin & Cawood, 2005). The suitably of zircon lies in its resistance to chemical and physical weathering, its high closure temperature to the diffusion of Pb, and its abundance in the sedimentary record (Garzanti et al., 2009). Due to its high closure temperature of Pb, zircon dates commonly record the initial time of crystallization by metamorphic or igneous processes. Moreover, the robustness of zircon allows for the U-Pb record to be preserved through initial crystallization through multiple cycles of burial, unroofing and deposition. Abundance of zircon within the sedimentary record allows for obtaining sufficient grains to build a representative U-Pb age spectrum from a relatively small amount of sample material. Together, these factors make U-Pb detrital zircon analysis ideal for investigations into depositional patterns and identification of sediment source terranes provided that there is an existing framework of the various U-Pb age populations within the possible sediment source terranes.

Zircon for laser ablation inductively coupled plasma mass spectrometry (LA-ICP-MS) U-Pb analysis were selected to avoid biasing the samples. Broken or fractured zircon grains, grains exhibiting extensive radiation damage, and grains with inclusions were not excluded from analysis. A JEOL 6610LV Scanning Electron Microscope (SEM; University of Ottawa, Canada) was used to characterize the zircon and to identify the internal structure of the mineral or rim overgrowths on the zircon using cathodoluminescence imaging. A Resonetics M-50 193 nm ArF Excimer laser ablation system coupled to an Agilent 7700x quadrupole ICP-MS system (University of Ottawa, Canada) was utilized for the zircon U-Pb analyses, following the protocol of McFarlane & Luo (2012) and the common Pb correction of Andersen et al. (2002). Single spot analyses were completed with the laser operated at a repetition rate of 6 Hz, spot size of 32 μm, and pulse energy of 4.72 J/cm$^2$. Reference material 91500 zircon (U-Pb: 1065.4 ± 0.3 Ma; Wiedenbeck et al., 1995) was analyzed as a standard under the same conditions as the unknowns. A secondary standard, Plešovice zircon (U-Pb: 337.1 ± 0.4 Ma; Sláma et al., 2008), was also used to correct for analytical drift. All data was reduced and drift corrected using Glitter v4.4.4, with reference material uncertainty calibrated to 1%. The final corrected data were plotted using IsoplotR (Vermeesch, 2018). For all results, $^{206}$Pb/$^{238}$U ages are reported for ages <1 Ga and $^{207}$Pb/$^{206}$Pb ages are reported for ages of >1 Ga, and only the results that were <10% discordant were considered. This is a generous cut off but designed to reduce bias in the dataset (cf. Gehrels, 2011). A <20% discordance cut-off did not result in a discernable change in the zircon age distribution, indicating that a 10% discordance cut-off does not restrict the dataset in capturing the widest range of zircon populations.

### 3.3 Detrital zircon (U-Th)/He thermochronology

The popularity of (U-Th)/He thermochronology has increased drastically over the last decade, and with good reason (Guenthner et al., 2015; Powell et al., 2016; Tian et al., 2012). Within a sedimentary basin, this technique is able to reveal the thermal evolution of individual strata, and with sufficient understanding of the local structural geology, a tectonic history of burial, uplift, and tilting can be unveiled. Principally $^{238}$U, $^{235}$U, and $^{232}$Th within zircon undergo radioactive decay thereby emitting an alpha-particle ($^4$He). The $^4$He emitted during alpha decay may be retained within, diffuse out of, or ejected from the zircon crystal lattice depending on thermal conditions, grain size, and radiation damage of the zircon. Analyses of the relative proportion of the parent and daughter isotopes produce a date, reflecting the nominal closure temperature at which the grain passed through a particular temperature range or isotherm. For example, experiments indicate that zircon with widths 40-100 mm and cooling at a rate of 10°C/Myr record a date that corresponds to a closure temperature of ~185℃ (Reiners et al., 2002, 2004).

The retentiveness of $^4$He in zircon varies additionally depending on the rock's residence time in the helium partial retention zone (PRZ) between 200℃ and 130℃ where protracted cooling through the PRZ results in apparent cooling ages. A zircon, initially at the surface, that is heated to temperatures in excess of the PRZ will release the $^4$He contained within its crystal lattice, thereby completely resetting the clock of the (U-Th)/He system. If a grain in a rock is buried to within the PRZ, but does not exceed the PRZ temperature, it is considered to be partially reset, complicating the idealized concept of a simple cooling age-closure temperature relationship. In partially reset grains, radiogenic helium from two or more cooling events may be retained within the crystal lattice, providing a mixed (U-Th)/He date, and a meaningless apparent age. In sedimentary basins, repeated burial-unroofing cycles and variations in zircon grain size and pre-depositional history can make it difficult to understand how multiple thermal events may affect the final cooling date recorded within the zircon (U-Th)/He system.

Further complications to apparent cooling dates arise when considering zircon's degree of radiation damage where the damage zones can either be traps or fast-diffusion pathways for $^4$He. At relatively low temperatures (<300°C) the radioactive decay of U and Th within the zircon results in the accumulation of radiation damage in the crystal lattice. Since higher concentrations of U and Th within a zircon lead to more accumulation of radiation damage, effective uranium (eU

= [U]+0.235•[Th]) is calculated for each zircon and commonly used as a proxy for radiation damage. The relationship between the accumulation and annealing of radiation damage in zircon as a function of temperature and eU was previously poorly understood. Through work in the last decade (Guenthner et al., 2013; Powell et al., 2016) we have begun to understand that low amounts of radiation damage initially decrease helium diffusivity (a positive date-eU relationship) resulting in apparent older dates. However, as radiation damage increases, damaged zones within the crystal lattice connect which drastically increase the diffusivity of helium within zircon (a negative date/eU relationship) leading to apparent younger dates. Zircon exposed to temperatures in excess of ~310-223℃, which is well beyond the PRZ, progressively anneal the radiation damage that has accumulated. Once suitable samples are identified which follow the predicted behaviour of $^{4}$He diffusion, numerical modeling is required to produce plausible thermal histories from a set of zircon grains that have experienced a protracted cooling history in the PRZ and/or multiple thermal events that result in the accumulation/annealing of radiation damage. To this end, thermal histories of the Morondava Basin zircon (U-Th)/He data are calculated with the zircon damage and annealing model (ZRDAAM) of Guenthner et al. (2013). In the thermal history models that are calculated using this model, each zircon grain from a sample essentially becomes a separate thermochronometer with varying diffusivity (and therefore sensitivity to thermal events) dependent on the radiation damage and size of each respective zircon grain.

After mineral separation and selection, the analytical portion of the low-temperature geochronological experiments was conducted at the Thermochronology Research and Instrumentation Laboratory (TRaIL) (U-Th)/He facility at the University of Colorado (Boulder, USA). Individual mineral grains are handpicked using a Leica M165 binocular microscope equipped with a calibrated digital camera and capable of both reflected and transmitted, polarized light. The grains were screened for quality, including crystal shape and the presence of inclusions. Within each sample zircon were selected to have varying clarity in order to capture a wide range of eU values (as a proxy for radiation damage). The dimensions of the crystals are measured and converted to the radius of a sphere with an equivalent alpha ejection correction as the grain (Rs) as this value is more readily incorporated into the equations that govern the diffusion of He throughout the grain; from this point forward in the paper references to grain size are measurements of Rs. After characterization, grains are placed into small Nb tubes that are then crimped on both ends. This Nb packet is then loaded into an ASI Alphachron He extraction and measurement line. The packet is placed in the UHV extraction line (~$3x10^{-8}$ torr) and heated with a diode laser to ~800-1100°C for 5 to 10 minutes to extract the radiogenic $^{4}$He. The degassed $^{4}$He is then spiked with approximately 13 ncc of pure $^{3}$He, cleaned via interaction with two SAES getters, and analyzed on a Balzers PrismaPlus QME 220 quadrupole mass spectrometer. Degassed grains are then removed from the line, and taken to a Class 10 clean lab for dissolution. Zircon are dissolved using Parr large-capacity dissolution vessels in a multi-step acid-vapor dissolution process. Grains (including the Nb tube) are placed in Ludwig-style Savillex vials, spiked with a $^{235}$U-$^{230}$Th tracer, and mixed with 200 µl of Optima grade HF. The vials are then capped, stacked in a 125 mL Teflon liner, placed in a Parr dissolution vessel, and baked at 220°C for 72 h. After cooling, the vials are uncapped and dried down on a 90°C hot plate until dry. The vials then undergo a second round of acid-vapor dissolution, this time with 200 µl of Optima grade HCl in each vial that is baked at 200°C for 24 h. Vials are then dried down a second time on a hot plate. Once dry, 200 µl of a 7:1 $HNO_3$:HF mixture is added to each vial, the vial is capped, and cooked on the hot plate at 90°C for 4 h. Once the minerals are dissolved, they are diluted with 1 to 3 mL of doubly-deionized water, and taken to the ICP-MS lab for analysis. Mineral standards of

Durango apatite (31.5 Ma) and Fish Canyon Tuff zircon (28.2 Ma) are routinely analyzed (degassed and dissolved) in conjunction with the samples with each run to ensure data integrity. Sample solutions, along with standards and blanks, are analyzed for U, Th, and Sm content using a Thermo Element 2 magnetic sector mass spectrometer. Once the U, Th, and Sm contents have been measured, He dates and all associated data are calculated on a custom spreadsheet made by TRaIL staff.

## 4.0 Results

### 4.1 U-Pb detrital zircon geochronology

Reflected light microscopy and SEM imaging was used to characterize zircon grains from the Morondava Basin (**Figure SI1**). Zircon grains varied in size from ~50 μm to ~200 μm in length and a significant subset of the zircon population is fractured, including broken grain terminations. A wide range of zircon morphologies are observed within the samples, ranging from subrounded prismatic grains, to well-rounded near-spherical grains. Zircon grain clarity was widely varied amongst all samples from clear with few inclusions and fractures to low clarity with an abundance of fractures and solid inclusions up to 10 μm in diameter. No distinguishable variance in these characteristics was observed between samples. In almost all grains large fractures and inclusions could be avoided during laser ablation. In the case where an inclusion or large fracture could not be avoided, a note was made.

A total of 1260 LA-ICP-MS analyses were made on detrital zircon from nine samples of the Morondava Basin (**Table 1, Table SI1**), of which three measurements were on apparent metamorphic rims noted during characterization. A total of 903 analyses yielded concordant U-Pb dates (<10% discordant cut-off). The largest number of concordant dates within a sample is 130 (sample 27/1), the smallest number of concordant dates is 65 (sample 39/3). Across all samples, the oldest concordant age is 3486 ± 134 Ma, and the youngest concordant age is 466 ± 16 Ma. All U-Pb dates are at least 200 Myr older than the depositional age of their respective sedimentary sequences. Therefore, these ages are not suitable for determining a maximum depositional age for any of the sedimentary sequences. Five major age populations can be identified within the total dataset (**Fig. 5**): 1) Neoproterozoic-Cambrian (480-620 Ma), 2) Neoproterozoic (700-850 Ma), 3) Mesoproterozoic (900-1100 Ma), 4) Paleoproterozoic (1650-1900 Ma), and 5) Paleoproterozoic-Neoarchean (2350-2650 Ma). In addition, a small population of Mesoarchean to Paleoarchean (3000-3500 Ma) grains is present. A single grain in sample 39/3 with an age of 1405 ± 61 cannot readily be placed within any particular population.

Jurassic Isalo II samples 01/2 and 41/1, both taken from the northern transect in the east of the study area, have Neoproterozoic and Paleoproterozoic-Neoarchean age populations, with the former defining the primary age population. Zircon U-Pb dates which fall outside of these primary populations are limited to only a few grains. Cross-correlation results (**Table 2**) confirm that samples 01/2 and 41/1 share similar detrital zircon signatures, whilst also being the most distinct from all other samples. We present a multidimensional scaling (MDS) model (**Fig. 6**), whereby we apply a technique similar to principal component analysis to the probability density plots (PDP) of all of our detrital zircon age populations. The MDS model is a visual representation of dissimilarities within the dataset, where each principal component is plotted along an axis and data that are more similar plot closer together (Vermeesch, 2013). In the example of samples 01/2 and 41/1, these two samples plot close together on both x-axis and the y-axis and can therefore be found to have similar detrital zircon distributions.

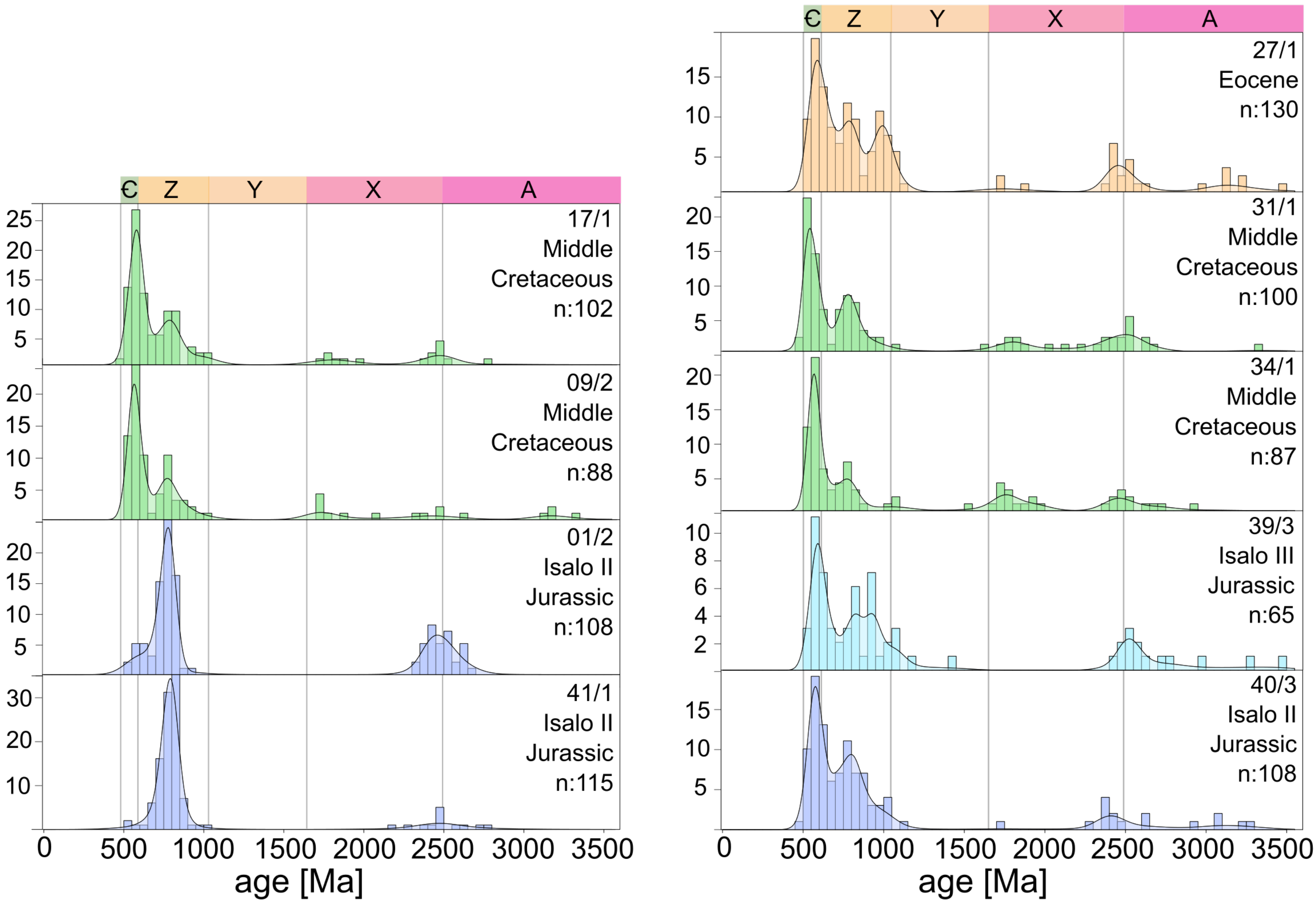


*Figure 5: U-Pb detrital zircon kernel density estimations of <10% discordant U-Pb data Columns left (northern transect) and right (southern transect) are presented in stratigraphic order. Abbreviations: Є: Cambrian; Z: Neoproterozoic; Y: Mesoproterozoic; X: Paleoproterozoic; A: Archean.*

**Table 2. Cross-correlation table of zircon U-Pb age data from Morondava Basin, Madagascar†**

| | 01/2 | 09/2 | 17/1 | 27/1 | 31/1 | 34/1 | 39/3 | 40/3 | 41/1 |
|---|---|---|---|---|---|---|---|---|---|
| **01/2** | 1 | 0.199 | 0.2345 | 0.3248 | 0.2769 | 0.1717 | 0.256 | 0.3487 | 0.8701 |
| **09/2** | 0.199 | 1 | 0.9022 | 0.6836 | 0.7528 | 0.9432 | 0.6654 | 0.8482 | 0.1198 |
| **17/1** | 0.2345 | 0.9022 | 1 | 0.8053 | 0.7246 | 0.9079 | 0.7894 | 0.9195 | 0.1475 |
| **27/1** | 0.3248 | 0.6836 | 0.8053 | 1 | 0.5738 | 0.6708 | 0.8883 | 0.8778 | 0.2434 |
| **31/1** | 0.2769 | 0.7528 | 0.7246 | 0.5738 | 1 | 0.7081 | 0.5442 | 0.7046 | 0.1966 |
| **34/1** | 0.1717 | 0.9432 | 0.9079 | 0.6708 | 0.7081 | 1 | 0.6497 | 0.8313 | 0.0837 |
| **39/3** | 0.256 | 0.6654 | 0.7894 | 0.8883 | 0.5442 | 0.6497 | 1 | 0.8589 | 0.1964 |
| **40/3** | 0.3487 | 0.8482 | 0.9195 | 0.8778 | 0.7046 | 0.8313 | 0.8589 | 1 | 0.2835 |
| **41/1** | 0.8701 | 0.1198 | 0.1475 | 0.2434 | 0.1966 | 0.0837 | 0.1964 | 0.2835 | 1 |

†U-Pb data are <10% discordant; darker shade indicates higher cross-correlation coefficient

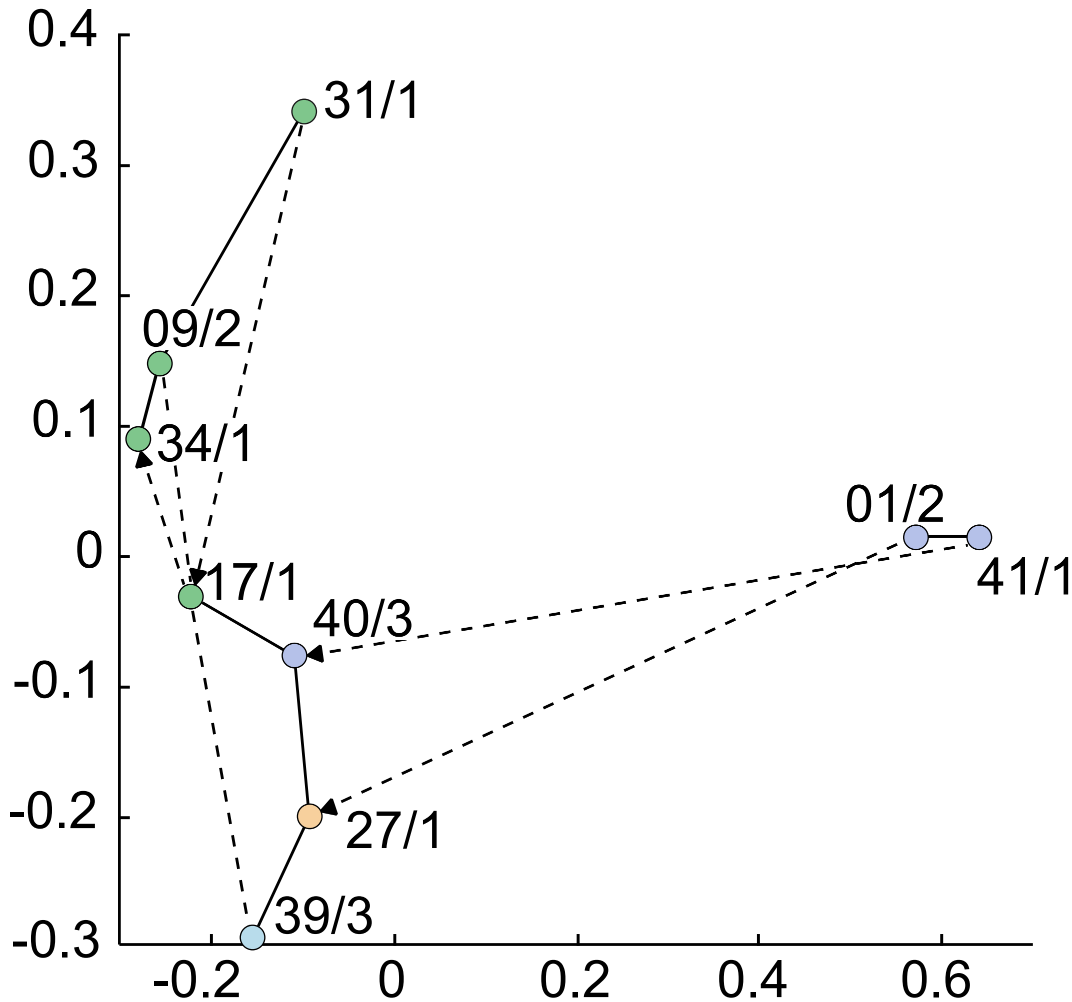


*Figure 6: Two-dimensional multidimensional scaling (MDS) model of <10% discordant U-Pb data. Data are plotted at 2s using a probability density plot (PDP) cross-correlation for a basis of comparison (metric squared stress criterion). Solid lines mark the closest neighbours, dotted lines mark the second closest neighbours.*

Sample 39/3, a sandstone from Jurassic Isalo III, and sample 40/3, a sandstone from Jurassic Isalo II, have distinct populations that are defined by a Neoproterozoic-Cambrian, Neoproterozoic, and Paleoproterozoic-Neoarchean populations. These samples are differentiated from the remaining samples that also share these populations by the absence of U-Pb dates ranging between 1500 and 2200 Ma (**Fig. 5**). Both samples have five to ten grains which lie within the Mesoproterozoic population and five grains that are Mesoarchean to Paleoarchean in age.

Middle Cretaceous samples 09/2, 17/1, 34/1, 31/1 and Tertiary sample 27/1 taken from higher stratigraphic levels area have similar detrital zircon age distributions. The largest population within these samples is Neoproterozoic-Cambrian, followed by a Neoproterozoic population. The remaining Paleoproterozoic and Paleoproterozoic-Neoarchean populations consist of five to ten grains each. The Tertiary sample, 27/1, is the only sample within the dataset that has a significant population of Mesoproterozoic grains. Samples 09/2 (Mid-Cretaceous) and 27/1 (Tertiary) each have a small population of Mesoarchean to Paleoarchean zircon grains. Cross-correlation and MDS models (**Fig. 6**) confirm that all samples from the southern transect and the Cretaceous samples from the northern transect may be correlated. Cross-correlation values range between 0.80 and 0.90 for most of these samples indicating that they are highly correlated. A broad first-order interpretation suggests that these very comparable detrital zircon age populations indicate similar sediment sources present within the samples.

### 4.2 U-Pb detrital zircon geochronology discussion

A good understanding of the U-Pb detrital zircon geochronology is essential for the (U-Th)/He thermal history modelling strategy applied in this study. Therefore, we have elected to discuss the sediment tracing component of the U-Pb geochronology results below rather than in the discussion section; a synthesis of the detrital zircon U-Pb and (U-Th)/He data will follow.

First to consider in a sediment tracing study is the likely transport distance of the bulk of the sediments. The immature texture and composition of the samples taken across the basin would suggest minimal sediment transport and proximal sediment source terranes. Zircon morphologies varied greatly but included euhedral, prismatic crystals suggesting short transportation distances, whilst rounded, anhedral grains result from large transportation distances. This may indicate that sediments were derived from a mixture of proximal and distant terranes, or some grains within the sample experienced sediment recycling prior to deposition in the basin. Previous analysis of apatite morphology in the basin can be interpreted as minimal transport of the detritus (Emmel et al., 2006). The lower resistivity of apatite to chemical and physical weathering when compared to zircon suggests that overall, the final stage of sedimentation occurred over short transportation distances.

The separation of the Morondava Basin samples into two distinct detrital zircon age distributions gives some insight into the depositional patterns and sediment sourcing within the basin. The major detrital age peaks of 600-800 Ma and 1800-2500 Ma found in the northern part of the study area (samples 41/1, 01/2) is indicative of sediments derived from the Tsaratanana (2650-2740 Ma) and Antananarivo (2460-2590 Ma) complexes found within the Antananarivo Domain, together with sediments derived from the Neoproterozoic (ca. 800 Ma) and Late Proterozoic (ca. 600 Ma) magmatic rocks intruding the Antananarivo complex. Notably, evidence for sediments traced to the Itremo Group, located directly to the east of the study area, appear to be absent from the sequences found in this part of the basin. Consequently, this indicates a proximal source of sediments for the north part of the study area, consistent with accessory mineral morphology. Other nearby basement terranes such as the Ikalamavony and Anosyen are unlikely candidates due to the lack of Archean (3000 Ma+) and Late Paleoproterozoic (ca. 1800 Ma) dates, respectively. The paucity of Late Neoproterozoic zircon dates indicates that the Ikalamavony, which presently borders the Morondava Basin along its eastern margin, may not have been fully exposed in the Jurassic. We posit that at the time of Jurassic deposition the currently exposed Ikalamavony may have been largely covered by Permo-Triassic sediments.

The remaining Jurassic, Cretaceous, and Tertiary samples in this study have detrital zircon age distributions differentiated from the previous two samples by a greater proportion of Neoproterozoic to Cambrian (ca. 500-600 Ma) zircon, a small population of Paleoproterozoic (ca. 1800 Ma) zircon, and a small number of Neoarchean to Mesoarchean zircon (3000 Ma+). The large proportion of Neoproterozoic-Cambrian dates are likely from metamorphic zircon derived from the Vohibory, Androyen, and Anosyen terranes, which all experienced extensive Neoproterozoic metamorphism during collision with East Africa (Boger et al., 2014). Uplift of the Vohibory terrane during the Early to Middle Jurassic further suggests that the Vohibory supplied sediment to the Morondava Basin at this time (Emmel et al., 2008). Though, the lack of Vohibory-like detrital zircon dates in the northern basin indicate localized sedimentation. Archean zircon are relatively rare in the terranes of Madagascar, found only in the Antongil and Masora terranes, where 2500-3500 Ma zircon are abundant and the Itremo Group, in turn likely derived from the Antongil-Masora Terrane (Armistead et al., 2021). Archean zircon within the Itremo Group make up a very small proportion of the total zircon load but can nonetheless be used for sediment tracing (Boger et al., 2014, Fitzsimons and Hulscher, 2005). The Itremo Group is the more likely candidate as a source terrane for the Morondava Basin due to its proximity and similar low proportion of Archean zircon.

The apparent differences in sediment sources between the north and south transect of the Jurassic samples is likely due to the >50 km distance between the samples. Previous research by Delaunay (2018) and Stephenson et al. (2021) has proposed that sediment was fed to the basin by a fluvial system similar to the modern east-west Morondava and Mahajanga rivers. Thus, it is not improbable that the northern Jurassic samples may have been sourced from the Antananarivo, whilst the southern Jurassic sediments of the basin were derived from the southern domains such as the Vohibory, Androyen, and Anosyen along similar directions as modern-day sediment transport.

Interpretation of source regions for the Cretaceous and Tertiary sedimentary rocks in the Morondava Basin is more complex since they were deposited on a passive margin. Sediments were likely transported over longer distances, and thus came from a wider geographical area. Whereas sediments deposited in a fluvial system can be assumed to have been derived from within the watershed, sediments deposited under marine conditions may experience along-shore transport. Similarities between the detrital zircon age populations of the Cretaceous and Tertiary and the detrital zircon age populations of Jurassic samples 39/3 and 40/1 may indicate similar source regions between these samples. Alternatively, or in addition, to basement source terranes, the sediments may be derived from previously deposited Jurassic sedimentary units. The possibility of sediment recycling from the Permo-Triassic rift basin into the Jurassic rift basin has previously been proposed by Emmel et al. (2006). The authors describe an inverted apatite FT stratigraphy, whereby older Karoo apatite FT ages are found on top in the younger Jurassic stratigraphy. The intersample similarities of detrital zircon U-Pb ages observed in our data within the Jurassic basin would suggest extensive mixing of sediment. Were the samples within the Jurassic basin derived from more singular sediment sources, we would expect more similarities between adjacent samples.

### 4.3 Zircon (U-Th)/He thermochronology

Grains selected for zircon (U-Th)/He (ZHe) thermochronology were intact, prismatic crystals in order to reflect an accurate ESR measurement and therefore better model the diffusion of He in each grain. Zircon were visually selected prior to (U-Th)/He analysis to include varying degrees of metamictization, thereby using metamictization as a proxy for the potential eU content of individual grains. The degree of metamictization was estimated by the colour and clarity of individual zircon, where brown to dark grey zircon with low clarity were estimated to have more radiation damage. This proves to be essential during numerical modeling with the zircon radiation damage accumulation and annealing model, where a wide distribution of ages and eU content will allow us to investigate thermal paths from a sample's entire history (Guenthner et al., 2013).

A total of 74 (U-Th)/He dates from nine samples (8-9 grains per sample) were collected (**Table 3**) with date-eU plots for eight of the samples shown in **Figure 7**. Models and date-eU plots are not presented for sample 27/1, which will be covered in the discussion section. The oldest ZHe single grain age within each sample is significantly older than their respective depositional age, which leads us to conclude that the system has only been partially reset. The ZHe dates range from 7.7 ± 0.2 Ma to 485.0 ± 12.7 Ma. Within individual samples, the ZHe dates have a maximum dispersion of 464 Myr (sample 09/2) and a minimum dispersion of 73 Myr (sample 41/1). The eU concentrations range from 35 ppm to 2675 ppm, with most samples having eU values from ~100 to >1000 ppm. The exceptions are sample 41/1 with eU values of 35 to 355 ppm and sample 27/1 with a range from 63 to 760 ppm (**Table 3**). Further, sample 41/1 produced ZHe dates older than

**Table 3. Single-grain zircon (U-Th)/He data from the Morondava Basin, Madagascar**

| Full Sample Name | length 1 (mm)[a] | width 1 (mm)[b] | length 2 (mm)[a] | width 2 (mm)[b] | Geometry[c] | Mineral[d] | Np[e] | Dim Mass (mg)[f] | rs (mm)[g] | $^{4}$He (nmol/g)[h] | ±[i] | U (ppm)[h] | ±[i] | Th (ppm)[h] | ±[i] | Sm (ppm)[h] | ±[i] | eU[j] | ±[k] | $^{4}$He (ncc)[l] | ±[m] | U (ng)[n] | ±[m] | Th (ng)[o] | ±[m] | Th/U[q] | Raw Date lt (Ma)[r] | ±[s] | Ft[t] | Corrected Date (lt) (Ma)[u] | Analytic Unc. (Ma) 2σ[v] | Full Sample Name |
|---|---|---|---|---|---|---|---|---|---|---|---|---|---|---|---|---|---|---|---|---|---|---|---|---|---|---|---|---|---|---|---|---|
| 01/2_z01 | 324.7 | 79.9 | 325.5 | 108.4 | t | z | 2 | 10.52 | 62.8 | 289.2 | 1.2 | 116.6 | 1.3 | 139.6 | 3.2 | 0.0 | 0.0 | 149.7 | 22.5 | 68.153 | 0.287 | 1.226 | 0.014 | 1.467 | 0.033 | 1.197 | 348.8 | 3.7 | 0.808 | 428.8 | 9.3 | 01/2_z01 |
| 01/2_z02 | 265.8 | 101.5 | 266.9 | 56.5 | t | z | 2 | 5.54 | 49.1 | 153.8 | 0.6 | 119.9 | 1.9 | 184.1 | 1.8 | 0.0 | 0.0 | 163.6 | 24.5 | 19.093 | 0.080 | 0.664 | 0.011 | 1.020 | 0.010 | 1.536 | 172.3 | 2.1 | 0.754 | 227.5 | 5.5 | 01/2_z02 |
| 01/2_z03 | 245.1 | 99.2 | 239.7 | 102.9 | t | z | 2 | 8.31 | 64.5 | 166.4 | 0.6 | 84.9 | 1.1 | 51.2 | 0.6 | 0.0 | 0.0 | 97.1 | 14.6 | 30.991 | 0.109 | 0.706 | 0.009 | 0.425 | 0.005 | 0.602 | 309.9 | 3.5 | 0.816 | 377.7 | 8.6 | 01/2_z03 |
| 01/2_z04 | 281.4 | 124.5 | 278.2 | 95.7 | t | z | 2 | 11.36 | 69.6 | 383.7 | 1.9 | 150.5 | 1.5 | 181.3 | 18.9 | 0.0 | 0.0 | 193.5 | 29.0 | 97.667 | 0.482 | 1.708 | 0.017 | 2.058 | 0.214 | 1.205 | 357.8 | 8.9 | 0.826 | 430.4 | 21.5 | 01/2_z04 |
| 01/2_z05 | 276.2 | 108.4 | 278.3 | 76.2 | t | z | 2 | 8.20 | 59.6 | 123.9 | 0.4 | 54.0 | 1.3 | 103.1 | 1.6 | 0.0 | 0.0 | 78.5 | 11.8 | 22.762 | 0.081 | 0.443 | 0.010 | 0.845 | 0.013 | 1.908 | 286.9 | 4.8 | 0.795 | 358.8 | 12.0 | 01/2_z05 |
| 01/2_z06 | 215.1 | 87.2 | 218.5 | 68.7 | t | z | 2 | 4.57 | 51.0 | 928.5 | 2.7 | 641.6 | 9.1 | 389.8 | 8.6 | 0.0 | 0.0 | 734.2 | 110.1 | 95.078 | 0.278 | 2.931 | 0.041 | 1.781 | 0.040 | 0.608 | 230.2 | 2.9 | 0.768 | 298.2 | 7.6 | 01/2_z06 |
| 01/2_z07 | 248.3 | 100.8 | 247.2 | 93.4 | t | z | 2 | 8.01 | 62.6 | 1014.3 | 4.2 | 1175.9 | 21.6 | 2458.8 | 79.3 | 0.0 | 0.0 | 1759.9 | 264.0 | 182.053 | 0.759 | 9.417 | 0.173 | 19.689 | 0.635 | 2.091 | 106.2 | 1.8 | 0.804 | 131.8 | 4.4 | 01/2_z07 |
| 01/2_z08 | 287.3 | 116.5 | 288.8 | 108.4 | t | z | 2 | 12.51 | 72.5 | 1144.6 | 5.2 | 1084.4 | 12.0 | 659.8 | 49.3 | 0.0 | 0.0 | 1241.1 | 186.2 | 320.870 | 1.465 | 13.562 | 0.150 | 8.252 | 0.616 | 0.608 | 168.8 | 2.4 | 0.836 | 201.4 | 5.7 | 01/2_z08 |
| 09/2_z01 | 222.7 | 77.4 | 221.8 | 76.5 | t | z | 2 | 4.71 | 51.5 | 228.1 | 1.0 | 126.0 | 2.8 | 59.9 | 1.0 | 0.0 | 0.0 | 140.2 | 21.0 | 24.068 | 0.103 | 0.593 | 0.013 | 0.282 | 0.005 | 0.475 | 294.4 | 5.9 | 0.771 | 379.1 | 15.4 | 09/2_z01 |
| 09/2_z02 | 258.5 | 97.8 | 259.6 | 87.9 | t | z | 2 | 7.87 | 61.1 | 329.8 | 1.4 | 156.8 | 1.7 | 138.1 | 2.4 | 0.0 | 0.0 | 189.6 | 28.4 | 58.201 | 0.253 | 1.235 | 0.014 | 1.087 | 0.019 | 0.880 | 314.6 | 3.3 | 0.804 | 388.8 | 8.2 | 09/2_z02 |
| 09/2_z03 | 344.1 | 90.6 | 347.1 | 84.7 | t | z | 2 | 10.24 | 61.0 | 205.4 | 0.9 | 85.6 | 1.3 | 67.1 | 2.2 | 0.0 | 0.0 | 101.6 | 15.2 | 47.166 | 0.195 | 0.877 | 0.013 | 0.687 | 0.022 | 0.783 | 364.2 | 5.0 | 0.804 | 449.5 | 12.5 | 09/2_z03 |
| 09/2_z04 | 284.9 | 113.9 | 286.8 | 108.0 | t | z | 2 | 12.12 | 71.8 | 665.3 | 3.4 | 549.9 | 6.9 | 179.1 | 41.7 | 0.0 | 0.0 | 592.4 | 88.9 | 180.696 | 0.934 | 6.663 | 0.083 | 2.170 | 0.506 | 0.326 | 204.8 | 4.3 | 0.835 | 244.2 | 10.3 | 09/2_z04 |
| 09/2_z05 | 264.9 | 104.3 | 259.8 | 112.3 | t | z | 2 | 10.35 | 69.1 | 1380.6 | 7.0 | 533.7 | 6.6 | 227.5 | 31.3 | 0.0 | 0.0 | 587.7 | 88.2 | 320.313 | 1.615 | 5.524 | 0.068 | 2.355 | 0.324 | 0.426 | 420.1 | 7.3 | 0.829 | 503.2 | 17.7 | 09/2_z05 |
| 09/2_z06 | 218.7 | 92.8 | 215.3 | 86.4 | t | z | 2 | 5.86 | 57.6 | 1134.1 | 4.9 | 632.6 | 10.8 | 96.7 | 12.1 | 0.0 | 0.0 | 655.5 | 98.3 | 148.976 | 0.648 | 3.707 | 0.063 | 0.567 | 0.071 | 0.153 | 312.1 | 5.3 | 0.796 | 389.1 | 13.4 | 09/2_z06 |
| 09/2_z07 | 222.5 | 90.6 | 227.5 | 93.5 | t | z | 2 | 6.45 | 59.12 | 197.0 | 1.3 | 932.1 | 18.2 | 947.0 | 33.7 | 0.00 | 0.00 | 1157.0 | 173.6 | 28.452 | 0.188 | 6.0074 | 0.117 | 6.1036 | 0.217 | 1.016 | 31.5 | 0.6 | 0.797 | 39.5 | 1.4 | 09/2_z07 |
| 09/2_z08 | 284.6 | 123.4 | 284.9 | 106.7 | t | z | 2 | 12.71 | 73.36 | 1206.8 | 6.8 | 791.3 | 8.8 | 184.8 | 4.2 | 0.00 | 0.00 | 835.2 | 125.3 | 343.817 | 1.951 | 10.0591 | 0.112 | 2.3493 | 0.054 | 0.234 | 262.0 | 3.1 | 0.839 | 310.7 | 7.4 | 09/2_z08 |
| 17/1_z01 | 266.8 | 107.9 | 268.9 | 67.9 | t | z | 2 | 6.99 | 55.80 | 340.3 | 1.7 | 215.2 | 4.2 | 58.6 | 0.9 | 0.00 | 0.00 | 229.1 | 34.4 | 53.351 | 0.259 | 1.5052 | 0.029 | 0.4096 | 0.006 | 0.272 | 269.2 | 4.9 | 0.789 | 338.9 | 12.4 | 17/1_z01 |
| 17/1_z02 | 170.4 | 71.4 | 172.2 | 81.5 | t | z | 2 | 3.25 | 48.22 | 209.8 | 1.2 | 102.9 | 1.7 | 82.0 | 0.4 | 0.00 | 0.00 | 122.4 | 18.4 | 15.282 | 0.085 | 0.3345 | 0.006 | 0.2666 | 0.001 | 0.797 | 310.0 | 4.6 | 0.753 | 408.1 | 12.2 | 17/1_z02 |
| 17/1_z03 | 227.3 | 86.6 | 224.4 | 62.5 | t | z | 2 | 4.39 | 48.93 | 104.8 | 0.6 | 56.4 | 1.3 | 40.2 | 1.1 | 0.00 | 0.00 | 66.0 | 9.9 | 10.318 | 0.059 | 0.2481 | 0.006 | 0.1765 | 0.005 | 0.712 | 287.7 | 5.8 | 0.757 | 376.9 | 15.3 | 17/1_z03 |
| 17/1_z04 | 191.5 | 79.7 | 194.3 | 90.5 | t | z | 2 | 4.56 | 53.72 | 609.9 | 1.9 | 308.2 | 3.9 | 97.1 | 1.4 | 0.00 | 0.00 | 331.2 | 49.7 | 62.336 | 0.194 | 1.4051 | 0.018 | 0.4430 | 0.006 | 0.315 | 331.8 | 4.0 | 0.781 | 421.4 | 10.2 | 17/1_z04 |
| 17/1_z05 | 249.0 | 91.6 | 247.1 | 80.8 | t | z | 2 | 6.55 | 57.21 | 387.9 | 1.4 | 197.2 | 2.0 | 106.9 | 4.9 | 0.00 | 0.00 | 222.6 | 33.4 | 56.950 | 0.212 | 1.2920 | 0.013 | 0.7004 | 0.032 | 0.542 | 314.8 | 3.4 | 0.793 | 394.2 | 8.6 | 17/1_z05 |
| 17/1_z06 | 231.2 | 76.5 | 235.3 | 86.7 | t | z | 2 | 5.51 | 54.26 | 1138.7 | 5.0 | 823.7 | 8.5 | 201.1 | 2.3 | 0.00 | 0.00 | 871.4 | 130.7 | 140.621 | 0.623 | 4.5382 | 0.047 | 1.1079 | 0.013 | 0.244 | 237.5 | 2.5 | 0.784 | 301.3 | 6.4 | 17/1_z06 |
| 17/1_z07 | 223.0 | 87.7 | 220.9 | 78.0 | t | z | 2 | 5.30 | 54.43 | 842.1 | 4.4 | 1581.3 | 29.9 | 191.3 | 10.7 | 0.00 | 0.00 | 1626.8 | 244.0 | 99.966 | 0.524 | 8.3758 | 0.159 | 1.0135 | 0.057 | 0.121 | 95.3 | 1.8 | 0.785 | 121.1 | 4.5 | 17/1_z07 |
| 17/1_z08 | 262.5 | 101.4 | 265.5 | 100.1 | t | z | 2 | 9.29 | 65.70 | 1129.2 | 5.9 | 873.4 | 16.4 | 124.1 | 2.2 | 0.00 | 0.00 | 902.8 | 135.4 | 235.119 | 1.222 | 8.1135 | 0.152 | 1.1529 | 0.021 | 0.142 | 227.4 | 4.2 | 0.821 | 275.6 | 10.2 | 17/1_z08 |
| 27/1_z01 | 183.3 | 74.8 | 187.6 | 77.3 | t | z | 2 | 3.62 | 49.19 | 1161.8 | 6.5 | 526.8 | 5.8 | 381.1 | 5.6 | 0.00 | 0.00 | 617.3 | 92.6 | 94.331 | 0.530 | 1.9083 | 0.021 | 1.3804 | 0.020 | 0.723 | 339.5 | 3.7 | 0.759 | 443.6 | 9.8 | 27/1_z01 |
| 27/1_z02 | 346.1 | 106.1 | 345.4 | 94.7 | t | z | 2 | 13.02 | 68.26 | 67.1 | 0.3 | 53.9 | 0.8 | 38.2 | 1.6 | 0.00 | 0.00 | 62.9 | 9.4 | 19.570 | 0.085 | 0.7013 | 0.010 | 0.4969 | 0.021 | 0.709 | 194.7 | 2.8 | 0.825 | 235.1 | 6.8 | 27/1_z02 |
| 27/1_z03 | 304.6 | 101.9 | 298.1 | 89.1 | t | z | 2 | 10.02 | 64.06 | 300.7 | 1.3 | 151.3 | 1.9 | 132.2 | 0.9 | 0.00 | 0.00 | 182.7 | 27.4 | 67.546 | 0.302 | 1.5161 | 0.019 | 1.3252 | 0.009 | 0.874 | 298.2 | 3.3 | 0.813 | 364.6 | 8.2 | 27/1_z03 |
| 27/1_z04 | 314.9 | 99.0 | 293.1 | 76.9 | t | z | 2 | 8.65 | 59.32 | 617.5 | 2.5 | 397.2 | 4.2 | 187.2 | 0.6 | 0.00 | 0.00 | 441.7 | 66.3 | 119.697 | 0.493 | 3.4355 | 0.036 | 1.6187 | 0.005 | 0.471 | 253.9 | 2.6 | 0.800 | 315.4 | 6.4 | 27/1_z04 |
| 27/1_z05 | 385.8 | 153.2 | 383.3 | 151.0 | t | z | 2 | 30.46 | 97.03 | 186.0 | 1.0 | 159.1 | 1.5 | 135.9 | 0.9 | 0.00 | 0.00 | 191.4 | 28.7 | 126.987 | 0.678 | 4.8464 | 0.047 | 4.1391 | 0.027 | 0.854 | 177.8 | 1.7 | 0.876 | 202.5 | 3.9 | 27/1_z05 |
| 27/1_z06 | 361.0 | 165.9 | 354.0 | 96.6 | t | z | 2 | 19.50 | 78.66 | 213.0 | 0.7 | 98.4 | 1.1 | 62.0 | 0.5 | 0.00 | 0.00 | 113.2 | 17.0 | 93.110 | 0.320 | 1.9200 | 0.022 | 1.2091 | 0.009 | 0.630 | 339.4 | 3.4 | 0.848 | 398.0 | 8.0 | 27/1_z06 |
| 27/1_z07 | 258.3 | 109.0 | 247.3 | 104.6 | t | z | 2 | 9.63 | 67.81 | 528.3 | 2.4 | 469.2 | 5.4 | 298.9 | 6.1 | 0.00 | 0.00 | 540.1 | 81.0 | 113.990 | 0.523 | 4.5161 | 0.052 | 2.8771 | 0.058 | 0.637 | 178.9 | 2.0 | 0.824 | 216.3 | 4.8 | 27/1_z07 |
| 27/1_z08 | 247.8 | 106.1 | 245.1 | 106.2 | t | z | 2 | 9.20 | 66.92 | 370.7 | 2.3 | 531.2 | 7.9 | 963.7 | 6.4 | 0.00 | 0.00 | 760.1 | 114.0 | 76.481 | 0.467 | 4.8899 | 0.073 | 8.8710 | 0.059 | 1.814 | 90.0 | 1.1 | 0.818 | 109.9 | 2.6 | 27/1_z08 |
| 31/1_z01 | 205.5 | 76.2 | 203.1 | 63.0 | t | z | 2 | 3.51 | 46.4 | 627.3 | 3.4 | 334.4 | 3.8 | 196.1 | 3.4 | 0.0 | 0.0 | 381.0 | 57.1 | 49.416 | 0.265 | 1.175 | 0.013 | 0.689 | 0.012 | 0.587 | 298.0 | 3.4 | 0.746 | 396.3 | 9.0 | 31/1_z01 |
| 31/1_z02 | 302.8 | 116.4 | 295.1 | 119.0 | t | z | 2 | 14.20 | 75.9 | 173.9 | 0.9 | 72.1 | 0.9 | 13.5 | 0.2 | 0.0 | 0.0 | 75.3 | 11.3 | 55.354 | 0.300 | 1.024 | 0.013 | 0.192 | 0.002 | 0.188 | 412.6 | 5.4 | 0.845 | 485.0 | 12.7 | 31/1_z02 |
| 31/1_z03 | 276.8 | 98.5 | 271.2 | 67.4 | t | z | 2 | 6.68 | 54.4 | 571.2 | 1.6 | 247.5 | 5.2 | 198.0 | 2.3 | 0.0 | 0.0 | 294.5 | 44.2 | 85.495 | 0.242 | 1.652 | 0.035 | 1.322 | 0.015 | 0.800 | 349.7 | 6.2 | 0.781 | 444.2 | 15.7 | 31/1_z03 |
| 31/1_z04 | 387.5 | 126.9 | 379.7 | 116.6 | t | z | 2 | 23.60 | 81.2 | 517.1 | 2.5 | 181.5 | 2.6 | 263.3 | 5.7 | 0.0 | 0.0 | 244.0 | 36.6 | 273.462 | 1.329 | 4.282 | 0.061 | 6.214 | 0.135 | 1.451 | 381.9 | 4.8 | 0.850 | 446.8 | 11.3 | 31/1_z04 |
| 31/1_z05 | 238.0 | 97.1 | 231.9 | 92.1 | t | z | 2 | 7.15 | 61.0 | 554.2 | 2.5 | 298.9 | 5.3 | 136.7 | 2.0 | 0.0 | 0.0 | 331.4 | 49.7 | 88.768 | 0.394 | 2.136 | 0.038 | 0.977 | 0.014 | 0.457 | 302.4 | 4.9 | 0.806 | 372.9 | 12.3 | 31/1_z05 |
| 31/1_z06 | 284.8 | 106.2 | 288.2 | 92.9 | t | z | 2 | 10.08 | 65.8 | 1037.9 | 4.3 | 638.2 | 6.6 | 217.0 | 4.3 | 0.0 | 0.0 | 689.7 | 103.5 | 234.590 | 0.965 | 6.436 | 0.066 | 2.188 | 0.043 | 0.340 | 272.7 | 2.8 | 0.820 | 330.6 | 6.8 | 31/1_z06 |
| 31/1_z07 | 193.9 | 100.4 | 195.7 | 99.0 | t | z | 2 | 5.93 | 60.2 | 1213.6 | 6.0 | 1125.2 | 14.6 | 297.6 | 25.0 | 0.0 | 0.0 | 1195.9 | 179.4 | 161.332 | 0.791 | 6.674 | 0.087 | 1.765 | 0.148 | 0.265 | 185.3 | 2.6 | 0.805 | 229.4 | 6.3 | 31/1_z07 |
| 31/1_z08 | 262.0 | 98.9 | 261.4 | 89.8 | t | z | 2 | 8.20 | 62.18 | 915.8 | 3.6 | 697.3 | 7.0 | 175.7 | 1.4 | 0.00 | 0.00 | 739.1 | 110.9 | 168.396 | 0.665 | 5.7206 | 0.057 | 1.4415 | 0.011 | 0.252 | 225.4 | 2.3 | 0.811 | 276.8 | 5.6 | 31/1_z08 |
| 34/1_z01 | 312.2 | 117.9 | 311.2 | 115.4 | t | z | 2 | 14.80 | 75.63 | 299.9 | 1.5 | 153.4 | 2.5 | 299.5 | 7.3 | 0.00 | 0.00 | 224.5 | 33.7 | 99.494 | 0.508 | 2.2700 | 0.038 | 4.4331 | 0.107 | 1.953 | 243.7 | 3.5 | 0.838 | 289.8 | 8.3 | 34/1_z01 |
| 34/1_z02 | 281.9 | 98.7 | 275.3 | 77.7 | t | z | 2 | 7.80 | 58.76 | 293.2 | 1.4 | 174.6 | 2.3 | 105.2 | 10.9 | 0.00 | 0.00 | 199.6 | 29.9 | 51.293 | 0.250 | 1.3627 | 0.018 | 0.8210 | 0.085 | 0.602 | 266.6 | 4.7 | 0.798 | 332.3 | 11.9 | 34/1_z02 |
| 34/1_z03 | 282.0 | 111.9 | 278.8 | 95.1 | t | z | 2 | 10.44 | 67.30 | 640.8 | 3.4 | 348.4 | 4.0 | 223.3 | 3.1 | 0.00 | 0.00 | 401.4 | 60.2 | 149.892 | 0.790 | 3.6357 | 0.041 | 2.3308 | 0.033 | 0.641 | 289.2 | 3.2 | 0.823 | 349.5 | 7.8 | 34/1_z03 |
| 34/1_z04 | 284.8 | 107.6 | 261.6 | 103.7 | t | z | 2 | 10.52 | 68.30 | 571.6 | 3.0 | 263.6 | 2.2 | 401.7 | 5.3 | 0.00 | 0.00 | 359.0 | 53.9 | 134.779 | 0.714 | 2.7733 | 0.023 | 4.2261 | 0.056 | 1.524 | 289.2 | 2.5 | 0.822 | 350.0 | 6.1 | 34/1_z04 |
| 34/1_z05 | 296.6 | 104.1 | 281.1 | 96.2 | t | z | 2 | 10.34 | 66.35 | 818.0 | 2.5 | 521.9 | 5.8 | 260.2 | 4.0 | 0.00 | 0.00 | 583.7 | 87.6 | 189.528 | 0.582 | 5.3946 | 0.060 | 2.6897 | 0.041 | 0.499 | 254.5 | 2.6 | 0.821 | 308.5 | 6.4 | 34/1_z05 |
| 34/1_z06 | 273.9 | 94.3 | 266.1 | 88.2 | t | z | 2 | 8.09 | 60.97 | 994.9 | 3.4 | 835.0 | 12.9 | 304.1 | 15.8 | 0.00 | 0.00 | 907.2 | 136.1 | 180.338 | 0.623 | 6.7525 | 0.104 | 2.4593 | 0.127 | 0.364 | 200.1 | 3.0 | 0.806 | 247.1 | 7.4 | 34/1_z06 |
| 34/1_z07 | 324.6 | 145.8 | 309.6 | 101.5 | t | z | 2 | 15.93 | 76.60 | 93.7 | 0.3 | 1949.2 | 29.2 | 3056.6 | 16.0 | 0.00 | 0.00 | 2675.2 | 401.3 | 33.449 | 0.121 | 31.0449 | 0.465 | 48.6811 | 0.255 | 1.568 | 6.5 | 0.1 | 0.841 | 7.7 | 0.2 | 34/1_z07 |
| 34/1_z08 | 285.9 | 125.6 | 293.2 | 131.3 | t | z | 2 | 15.63 | 80.17 | 525.8 | 1.1 | 1463.8 | 20.6 | 625.5 | 4.3 | 0.00 | 0.00 | 1612.4 | 241.9 | 184.257 | 0.398 | 22.8857 | 0.322 | 9.7793 | 0.067 | 0.427 | 60.2 | 0.8 | 0.852 | 70.6 | 1.8 | 34/1_z08 |
| 39-3_z01 | 314.5 | 82.4 | 315.1 | 58.0 | t | z | 2 | 5.92 | 46.45 | 80.2 | 0.5 | 41.2 | 1.1 | 15.7 | 0.3 | n.m. | n.m. | 44.9 | 6.7 | 10.633 | 0.073 | 0.2438 | 0.007 | 0.0928 | 0.002 | 0.380 | 321.9 | 8.2 | 0.757 | 421.3 | 21.6 | 39-3_z01 |
| 39-3_z02 | 287.8 | 80.0 | 289.9 | 79.5 | t | z | 2 | 6.97 | 53.10 | 139.2 | 0.7 | 58.0 | 0.6 | 51.0 | 2.0 | n.m. | n.m. | 70.0 | 10.5 | 21.753 | 0.111 | 0.4045 | 0.004 | 0.3556 | 0.014 | 0.879 | 357.7 | 4.2 | 0.783 | 453.0 | 10.8 | 39-3_z02 |
| 39-3_z03 | 274.5 | 78.6 | 278.8 | 64.2 | t | z | 2 | 5.36 | 47.46 | 529.8 | 2.3 | 227.2 | 5.9 | 289.2 | 6.1 | n.m. | n.m. | 295.2 | 44.3 | 63.667 | 0.272 | 1.2182 | 0.032 | 1.5509 | 0.033 | 1.273 | 324.0 | 6.7 | 0.756 | 424.8 | 17.6 | 39-3_z03 |
| 39-3_z04 | 204.7 | 73.0 | 211.3 | 75.0 | t | z | 2 | 4.04 | 47.25 | 794.9 | 2.8 | 505.7 | 13.6 | 169.1 | 3.8 | n.m. | n.m. | 545.4 | 81.8 | 71.969 | 0.256 | 2.0426 | 0.055 | 0.6831 | 0.015 | 0.334 | 264.1 | 6.4 | 0.762 | 344.0 | 17.0 | 39-3_z04 |
| 39-3_z05 | 198.3 | 68.5 | 201.2 | 52.3 | t | z | 2 | 2.64 | 38.93 | 849.4 | 4.3 | 1040.7 | 16.3 | 221.9 | 18.2 | n.m. | n.m. | 1092.8 | 163.9 | 50.314 | 0.254 | 2.7504 | 0.043 | 0.5865 | 0.048 | 0.213 | 142.4 | 2.2 | 0.715 | 198.0 | 6.3 | 39-3_z05 |
| 39-3_z06 | 169.9 | 59.5 | 164.7 | 58.5 | t | z | 2 | 2.07 | 37.74 | 773.8 | 4.9 | 762.9 | 9.9 | 196.1 | 3.9 | n.m. | n.m. | 809.0 | 121.4 | 35.920 | 0.227 | 1.5801 | 0.020 | 0.4061 | 0.008 | 0.257 | 174.7 | 2.4 | 0.707 | 245.5 | 6.7 | 39-3_z06 |
| 39-3_z07 | 229.3 | 80.5 | 228.9 | 85.7 | t | z | 2 | 5.57 | 52.82 | 784.5 | 3.6 | 425.4 | 7.2 | 359.7 | 2.0 | n.m. | n.m. | 509.9 | 76.5 | 97.956 | 0.452 | 2.3697 | 0.040 | 2.0040 | 0.011 | 0.846 | 278.6 | 4.0 | 0.782 | 353.8 | 10.3 | 39-3_z07 |
| 39-3_z08 | 267.7 | 81.1 | 265.4 | 89.9 | t | z | 2 | 7.10 | 55.49 | 508.4 | 2.3 | 1423.5 | 36.7 | 205.9 | 5.4 | n.m. | n.m. | 1471.9 | 220.8 | 80.891 | 0.361 | 10.1060 | 0.261 | 1.4618 | 0.038 | 0.145 | 63.7 | 1.6 | 0.797 | 79.9 | 4.0 | 39-3_z08 |
| 39/3_z09 | 224.2 | 99.9 | 225.0 | 107.9 | t | z | 2 | 7.78 | 64.3 | 151.3 | 0.4 | 640.6 | 11.9 | 729.7 | 12.1 | 0.0 | 0.0 | 813.9 | 122.1 | 26.389 | 0.069 | 4.985 | 0.093 | 5.678 | 0.095 | 1.139 | 34.4 | 0.5 | 0.813 | 42.3 | 1.3 | 39/3_z09 |
| 40/3_z01 | 404.4 | 158.0 | 381.2 | 101.8 | t | z | 2 | 22.51 | 81.7 | 795.6 | 3.0 | 330.1 | 4.0 | 280.3 | 2.4 | 0.0 | 0.0 | 396.7 | 59.5 | 401.498 | 1.528 | 7.432 | 0.091 | 6.310 | 0.054 | 0.849 | 361.3 | 3.8 | 0.853 | 421.3 | 9.0 | 40/3_z01 |
| 40/3_z02 | 240.5 | 81.5 | 246.2 | 73.8 | t | z | 2 | 5.35 | 52.5 | 203.9 | 0.9 | 85.9 | 1.7 | 80.6 | 1.5 | 0.0 | 0.0 | 105.1 | 15.8 | 24.471 | 0.103 | 0.460 | 0.009 | 0.432 | 0.008 | 0.938 | 350.0 | 5.8 | 0.772 | 449.4 | 15.1 | 40/3_z02 |
| 40/3_z03 | 229.5 | 88.1 | 233.6 | 85.4 | t | z | 2 | 6.08 | 57.0 | 533.3 | 2.1 | 328.1 | 5.3 | 171.5 | 33.8 | 0.0 | 0.0 | 368.8 | 55.3 | 72.645 | 0.290 | 1.994 | 0.032 | 1.042 | 0.205 | 0.523 | 262.5 | 6.9 | 0.792 | 329.4 | 17.4 | 40/3_z03 |
| 40/3_z04 | 235.6 | 80.3 | 234.6 | 91.8 | t | z | 2 | 6.08 | 56.5 | 775.0 | 1.9 | 303.5 | 3.8 | 292.2 | 2.2 | 0.0 | 0.0 | 372.9 | 55.9 | 105.682 | 0.260 | 1.847 | 0.023 | 1.778 | 0.013 | 0.963 | 374.1 | 3.8 | 0.788 | 471.0 | 9.7 | 40/3_z04 |
| 40/3_z05 | 327.5 | 98.2 | 327.8 | 89.3 | t | z | 2 | 10.81 | 64.1 | 823.4 | 3.3 | 397.1 | 7.0 | 197.5 | 11.4 | 0.0 | 0.0 | 444.0 | 66.6 | 199.420 | 0.807 | 4.291 | 0.076 | 2.134 | 0.123 | 0.497 | 334.4 | 5.7 | 0.815 | 407.6 | 14.1 | 40/3_z05 |
| 40/3_z06 | 246.9 | 73.7 | 253.0 | 68.5 | t | z | 2 | 4.75 | 49.2 | 1306.6 | 6.9 | 701.8 | 9.6 | 335.1 | 35.0 | 0.0 | 0.0 | 781.4 | 117.2 | 139.209 | 0.737 | 3.336 | 0.045 | 1.593 | 0.166 | 0.477 | 302.3 | 5.1 | 0.760 | 394.6 | 13.5 | 40/3_z06 |
| 40/3_z07 | 397.4 | 150.4 | 385.8 | 132.9 | t | z | 2 | 27.58 | 92.0 | 1339.2 | 2.0 | 966.6 | 12.5 | 331.3 | 2.5 | 0.0 | 0.0 | 1045.3 | 156.8 | 827.995 | 1.232 | 26.663 | 0.346 | 9.138 | 0.069 | 0.343 | 233.0 | 2.7 | 0.871 | 266.6 | 6.3 | 40/3_z07 |
| 40/3_z08 | 241.9 | 89.5 | 239.6 | 105.1 | t | z | 2 | 7.68 | 62.3 | 760.7 | 2.0 | 930.8 | 11.6 | 290.1 | 2.7 | 0.0 | 0.0 | 999.7 | 150.0 | 130.873 | 0.338 | 7.145 | 0.089 | 2.227 | 0.021 | 0.312 | 139.5 | 1.6 | 0.811 | 171.6 | 4.0 | 40/3_z08 |
| 40/3_z09 | 271.7 | 112.9 | 271.8 | 104.5 | t | z | 2 | 10.93 | 69.7 | 983.6 | 2.8 | 630.4 | 7.3 | 584.7 | 79.8 | 0.0 | 0.0 | 769.3 | 115.4 | 240.896 | 0.693 | 6.888 | 0.080 | 6.388 | 0.872 | 0.927 | 232.9 | 6.2 | 0.828 | 280.3 | 14.9 | 40/3_z09 |
| 41/1_z01 | 222.3 | 75.8 | 218.6 | 88.6 | t | z | 2 | 5.16 | 53.8 | 275.5 | 1.8 | 117.0 | 1.3 | 64.0 | 0.9 | 0.0 | 0.0 | 132.2 | 19.8 | 31.883 | 0.206 | 0.604 | 0.007 | 0.330 | 0.005 | 0.547 | 374.6 | 4.4 | 0.780 | 476.0 | 11.4 | 41/1_z01 |
| 41/1_z02 | 503.4 | 179.1 | 514.7 | 146.7 | t | z | 2 | 48.78 | 106.7 | 68.8 | 0.4 | 26.1 | 0.4 | 35.9 | 0.4 | 0.0 | 0.0 | 34.6 | 5.2 | 75.220 | 0.385 | 1.274 | 0.017 | 1.751 | 0.019 | 1.375 | 358.5 | 4.1 | 0.886 | 403.1 | 9.3 | 41/1_z02 |
| 41/1_z03 | 359.5 | 91.4 | 364.5 | 72.7 | t | z | 2 | 9.47 | 57.2 | 324.4 | 2.3 | 130.9 | 1.6 | 122.2 | 1.0 | 0.0 | 0.0 | 159.9 | 24.0 | 68.856 | 0.487 | 1.239 | 0.015 | 1.158 | 0.009 | 0.934 | 365.5 | 4.4 | 0.791 | 458.5 | 11.1 | 41/1_z03 |
| 41/1_z04 | 363.2 | 159.3 | 364.8 | 127.5 | t | z | 2 | 25.22 | 90.5 | 315.7 | 1.0 | 123.7 | 1.8 | 88.2 | 1.7 | 0.0 | 0.0 | 144.6 | 21.7 | 178.497 | 0.566 | 3.120 | 0.045 | 2.225 | 0.044 | 0.713 | 391.9 | 4.9 | 0.868 | 449.3 | 11.4 | 41/1_z04 |
| 41/1_z05 | 316.7 | 114.6 | 315.3 | 96.6 | t | z | 2 | 12.61 | 69.9 | 369.6 | 1.4 | 161.1 | 1.8 | 52.9 | 0.5 | 0.0 | 0.0 | 173.7 | 26.1 | 104.491 | 0.390 | 2.033 | 0.023 | 0.667 | 0.006 | 0.328 | 381.6 | 4.2 | 0.831 | 456.1 | 10.1 | 41/1_z05 |
| 41/1_z06 | 311.3 | 128.1 | 329.6 | 125.0 | t | z | 2 | 17.58 | 81.1 | 174.7 | 0.9 | 70.1 | 0.8 | 61.0 | 0.7 | 0.0 | 0.0 | 84.6 | 12.7 | 68.821 | 0.362 | 1.233 | 0.014 | 1.073 | 0.013 | 0.870 | 371.5 | 3.9 | 0.852 | 433.7 | 9.2 | 41/1_z06 |
| 41/1_z07 | 396.3 | 147.5 | 395.8 | 136.8 | t | z | 2 | 28.26 | 92.6 | 434.9 | 0.9 | 187.2 | 2.2 | 98.7 | 0.9 | 0.0 | 0.0 | 210.7 | 31.6 | 275.413 | 0.556 | 5.291 | 0.062 | 2.789 | 0.026 | 0.527 | 371.0 | 3.8 | 0.872 | 423.7 | 8.8 | 41/1_z07 |
| 41/1_z08 | 264.1 | 138.6 | 273.2 | 139.4 | t | z | 2 | 15.81 | 82.7 | 689.0 | 2.4 | 305.2 | 3.2 | 207.9 | 3.0 | 0.0 | 0.0 | 354.6 | 53.2 | 244.168 | 0.848 | 4.826 | 0.050 | 3.287 | 0.047 | 0.681 | 350.1 | 3.4 | 0.856 | 407.2 | 7.8 | 41/1_z08 |

a - Length of zircon
b - Width of zircon
c - Geometry of
d - Mineral analyzed, z = zircon.
e - Number of grain terminations.
f - Mass of the crystal estimated from measured grain dimensions, volume assuming the geometry, and volume equations and mineral densities laid out in Ketcham et al. (2011).
g - Radius of a sphere with an equivalent alpha ejection correction as the grain, calculated using equation A6 in Cooperdock et al. (2019).
h - Concentrations of He, U, Th and Sm computed from their absolute amounts and the estimated dimensional mass reported.
i - 2s propagated analytical uncertainty on the U, Th, Sm, and He measurements.
j - effective uranium concentration. Calculated as U + 0.2375*Th.
k - Uncertainty on eU is estimated at 15% of the eU value.
l - Blank-corrected $^{4}$He.

m - Uncertainties on $^{4}$He, U, Th, and Sm are reported at 2s and include the propagated uncertainties on the measurements of the sample, blank, spike, and standard.
n - Total blank-corrected ng of $^{238}$U and $^{235}$U. Total amount of $^{238}$U is measured, $^{235}$U is calculated assuming $^{235}U = {}^{238}U/137.818$.
o - Total blank-corrected ng of $^{232}$Th.
p - Total blank-corrected ng of $^{147}$Sm. Not measured.
q - Ratio of Th to U, calculated from amounts measured in ng.
r - Uncorrected date is calculated iteratively using the 4He production equation defined as equation 1 in Wolf et al. (1998) and assuming secular equilibrium.
s - 2s propagated analytical uncertainty on the U, Th, Sm, and He measurements.
t - The combined alpha-ejection correction for the crystal calculated from the isotope specific $F_T$ corrections, the proportion of U and Th contributing to $^{4}$He production, and
u - The corrected date is calculated iteratively using the absolute values of He, U, Th, and Sm, the isotope specific $F^T$ corrections, and equation 34 in Ketcham et al. (2011) ass
v - 2s propagated analytical uncertainty on the U, Th, Sm, and He measurements.
Fish Canyon tuff zircons run in conjunction with these grains yield a date of 28.7 ± 2.4 Ma (1s)

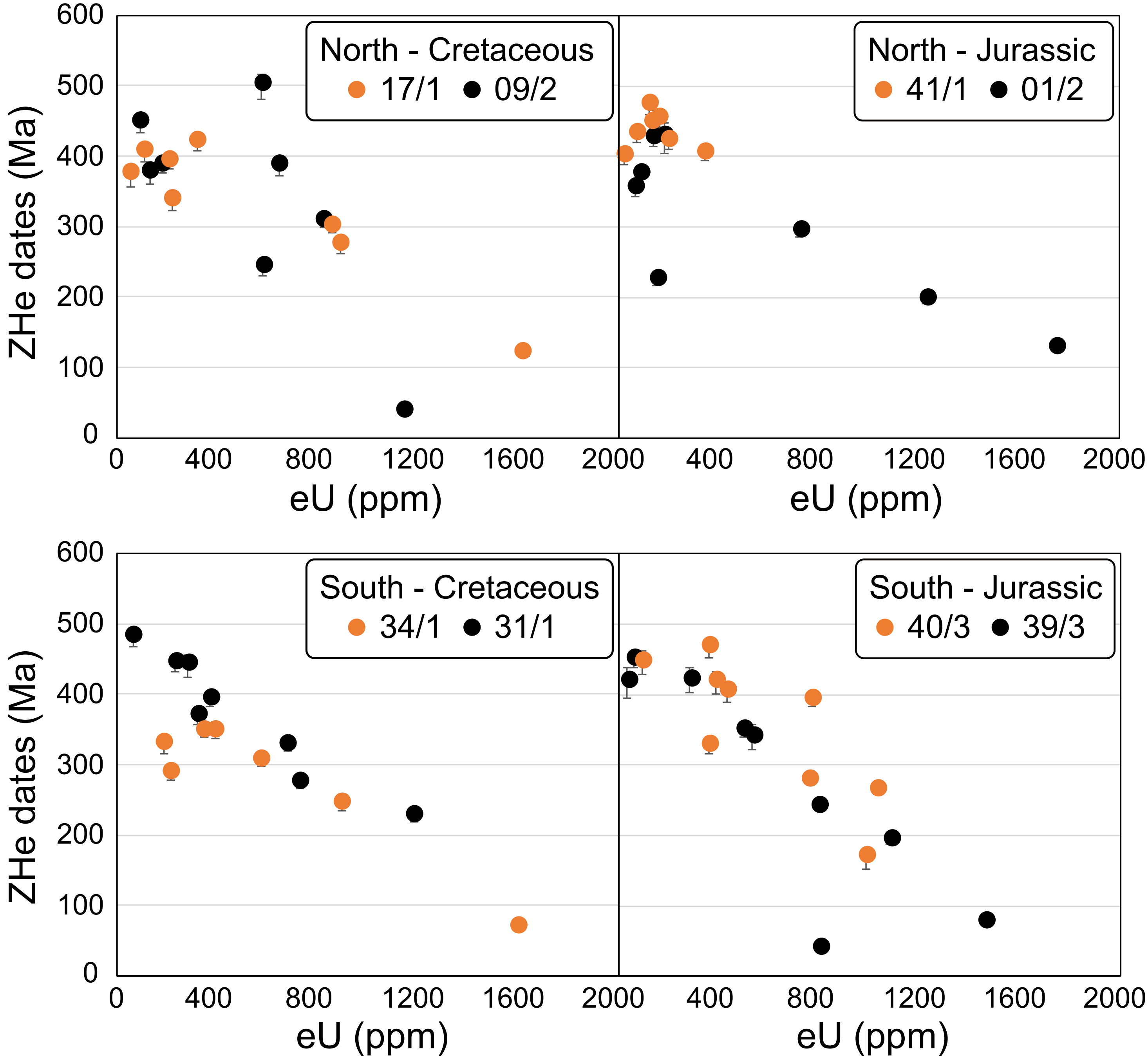


*Figure 7: Zircon (U-Th)/He date-eU relationships of the Cretaceous and Jurassic samples from the Morondava Basin, Madagascar. Samples are group by stratigraphic age (Cretaceous, Jurassic) and transect (North = northern transect, South = southern transect). One outlier at (2675 ppm, 7.73 Ma) for sample 34/1 is excluded for analysis and visualization.*

the depositional age within a narrow limit of eU values, from 400 to 480 Ma. The narrow distribution of values, isolated to the time before deposition, does not likely possess sufficient information to reliably capture the post-depositional thermal history of this sample. The most notable outlier in the dataset (sample 34/1, at 7.7 Ma and 2675 ppm eU) was not further considered due to its high eU value and very young ZHe date, indicating an extremely diffusive grain which is likely leaking He at near-surface temperatures.

Most of the (U-Th)/He data from the Jurassic and Cretaceous samples from both northern and southern transect exhibit a strong, predictable negative date-eU relationship. The presence of negative date-eU relationships throughout the dataset is indicative of conditions of protracted cooling histories with moderate alpha dose damage. Some of the samples (i.e., 01/2, 41/1, 34/1) initially show weak positive relationships at low eU values (and therefore low alpha doses, <300 ppm eU). A range of eU values, including positive date-eU to negative date-eU trends, is favourable and suggestive of samples that captured the rock's thermal history from pre-deposition to post-deposition. Below we capitalize on these aspects of the data with inverse and forward numerical modelling techniques.

## 5.0 Thermal history modelling

### 5.1 Modelling approach

A first-order observation in the ZHe data evince protracted cooling history that occurred at temperatures cooler than the upper limit of the ZHe partial retention zone. Therefore, a combined forward and inverse modelling approach has been applied using the ZRDAAM (Guenthner et al., 2013) via the thermal history modelling program HeFTy (Ketcham, 2005). Inverse modelling is capable of rapidly evaluating a large number of plausible thermal histories relative to the empirical data with minor input from the user. Due to the apparent partial resetting of ZHe dates, uncertainty exists regarding the rock's thermal history, as the zircon still preserve some memory of the pre-depositional thermal history. Whereas usually, in the case of full resetting, one can assume that the recorded thermal history is identical for zircon grains within a sample, this is not possible in the case of partial resetting. In this case, individual zircon grains within a sample may record different pre-depositional thermal histories as they were derived from discrete source terranes and possess unique radiation damage. Forward modelling is applied in addition to inverse modelling to better understand the pre-depositional history reflected in the date-eU trends of the data (**Fig. 7**). Due to the geographical separation (~100 km) between the north and the south transects, the Jurassic and Cretaceous samples from each transect are evaluated separately. This has been done, in part, to account for the thickening of the sediment package towards the south within the Morondava Basin. In addition, this may allow for verification of model robustness between north and south transect.

In order to fully investigate the thermal history of the Morondava Basin from post-Pan-African orogeny cooling until present, a broad selection of ZHe dates spanning a modest range of eU values is required within a sample. Sample 41/1 does not satisfy this condition, with ZHe dates only between 400-500 Ma. Since these ZHe dates strongly reflect cooling before sedimentary deposition, this sample cannot be used to accurately produce a post-depositional thermal history, and has been excluded from the thermal history modelling methodology.

Four grains from each set of samples were used for modeling, selected to capture the widest range of ZHe dates and eU values within each sample. The model set-up also includes specific independent temperature-time (t-T) constraints that are relevant to the geology of the area, such as unconformities, and are described in detail below and summarized in the **Table SI2**. The model creates nodes within the user-defined constraints to construct a t-T path, and evaluates the fit of the modeled ages of each t-T path against the measured ZHe data. By leaving several degrees of freedom within the constraints, we allow for non-constant heating or cooling within each stage. Paths which have a minimum statistical value via Kolmogorov-Smirnov (K-S) test of 0.05 are termed "acceptable," whilst values above 0.5 are termed "good" (Ketcham et al., 2005). For our study, the inverse model was run until at least 100 "good" paths were found for each sample. Although, this does result in a variable number of total paths tested, and "acceptable" paths created between samples, this is the easiest method to guarantee sufficient "good" paths for each sample. The total number of paths tested range between 347,575 and 5,588,311 and the total number of "acceptable" paths ranged between 1120 and 32,870.

Partial resetting of all samples introduces some uncertainty regarding the time at which the zircon began to record a thermal history. Previous studies (e.g., Collins et al., 2012; Emmel et al., 2004, 2006), and zircon U-Pb data presented here suggest peak greenschist to amphibolite-grade metamorphic conditions in the basement terranes of Madagascar prior to 550 Ma associated with the assembly of Gondwana and amalgamation of Madagascar. These conditions are indicative of temperatures in excess of 300°C, sufficient to fully reset the zircon (U-Th/He) system as well as anneal radiation damage in zircon. Emmel et al. (2004, 2006) suggest initial cooling terminated at 500 Ma, followed by 150 Myr of protracted cooling. Cursory inspection of our ZHe data, with peak ZHe ages between 400 and 550 Ma, is consistent with this proposal. In our models, this is reflected by an initial t-T constraint of 280-300°C between 1000 Ma and 500 Ma. This temperature constraint is used to form the starting point for cooling prior to sediment deposition. A broad initial range was chosen for this constraint due to greater degree of uncertainty for the pre-depositional thermal history and account for overestimation/underestimation by the thermal history model.

For the Jurassic models, the next constraint is between 220 Ma and 180 Ma at near-surface temperatures (0-40°C), which is the depositional age of the formation. This is followed by a constraint allowing heating during burial at a rate no faster than 10°C/Myr. Sedimentation rates are poorly constrained in the Morondava Basin, but are estimated to be relatively low. Emmel et al. (2004) suggest relatively slow sedimentation rates of Jurassic sediments, accounting for no more than 2°C/Myr in their thermal models. In the coeval Mozambique Basin, located opposite to the Morondava Basin, Mesozoic and Paleogene sedimentation rates are estimated at 5-10 cm/kyr and 1-3 cm/kyr, respectively (Castelino et al., 2015). Maximum burial is constrained to 180°C over the succeeding 30 Myr based on maximum sediment thickness of 6 km established by seismic interpretations of the basin (**Fig. 4**). The presence of an unconformity in the Late Jurassic may have led to cooling subsequent to initial deposition, however the extent and significance of this unconformity is somewhat debated (Giese et al., 2012; Clark, 1998). In addition, overstepping of Early Cretaceous sediments overtop of the Jurassic sequences may have resulted in heating during later stages. This is taken into account by a constraint between 170 and 100 Ma, which allows for either heating or cooling. It is important to note that the magnitude of these events may not be sufficient to have an effect on the recorded thermal path.

For the Cretaceous models, the constraint following full-resetting prior to 500 Ma is between 145 and 110 Ma at near-surface temperatures (0-40°C), which is the approximate depositional age of the formation. The next constraint allows for heating up to 180°C based on burial of up to 6 km in depth as observed on seismic sections.

Both models then allow for heating or cooling into the Turonian between 90-70 Ma. The presence of Turonian basaltic dykes throughout the basin indicates tectonism at this time and likely a (local) higher geothermal gradient. Permitting the model to evaluate either heating and cooling allows flexibility in the impact of heating through magmatic activity as well as cooling through possible uplift. The penultimate constraint in both models between 70 Ma and 45 Ma allows for burial into the Late Cretaceous as sedimentation may have continued. Although the constraint allows for heating up to 180℃, the regional geology and seismic interpretation indicates burial up to 4 km. The model allows for heating up to 180℃ due to the possibility of a higher geothermal gradient up to 45℃/km (Emmel et al., 2004, 2008). The final constraint allows for heating or cooling into the Tertiary. Seismic interpretations indicate continued sedimentation into the Tertiary, which may have led to further heating of Cretaceous sediments depending on the extent of Tertiary sedimentation in the Morondava Basin.

**5.2 Modelling results**

In general inverse modelling produces a set of "acceptable" and "good" solutions that may be considered plausible thermal histories. From these paths, we have taken first-order observations from the best-fit and mean paths as well as patterns within the "good" paths to construct several forward models. It should be noted that there are an almost infinite set of unique solutions and testable forward models are used to evaluate different plausible thermal histories of the Morondava Basin. Additional inverse and forward models are available in the supplemental material (**Fig. SI2**), as well as inverse models which highlight inflections points instead of linear t-T paths (**Fig. SI3**).

With the exception of sample 41/1, zircon from the Jurassic samples have a wide range of eU values and therefore were suitable for resolving the thermal history from post-Pan-African orogenic cooling until present day. The best-fit path from the inverse model of the north transect shows relatively monotonic cooling until the time of deposition during the earliest Jurassic (**Fig.**

**8**). The strata was then rapidly heated to ~165°C during the Middle Jurassic followed by Late Jurassic and Early Cretaceous cooling to ~60°C in the Albian. The zircon (U-Th)/He data are not very sensitive to the relatively low temperatures in the final segments of the thermal history, which is more suited to apatite (U-Th)/He or fission track dating. It is important to note that the range of "good" time-temperature (t-T) paths is especially wide for the pre-depositional history. As mentioned above, difficulty in resolving the pre-depositional history within a partially reset thermochronology dataset is expected.

A series of forward models were tested for the northern Jurassic samples (**Fig. 8**). Path A is based on a simplified intepretation of the best-fit and mean paths produced by the inverse model. Path B evaluates the possibility of a second stage of heating from 100 to 50 Ma (**Fig. 8-IIIB**), with the final stage of cooling occurring in the Miocene. Although the thermal histories of the last 100 Myr are different between paths A and B, the date-eU envelopes are relatively similar and capture a comparable segment of the ZHe data. As noted, this is likely due to the lack of sensitivity of the zircon (U-Th)/He system at lower temperatures and the lack of ZHe dates younger than 100 Ma within the northern Jurassic samples. Path C is based on the general trend observed within the "good" solutions presented by the inverse model, whereby post-Pan-African cooling occurs more rapidly at ca. 450 Ma with the zircon being at near-surface temperatures from ca. 400 Ma until the time of deposition. The proposed path then follows a similar history to path B (**Fig. 8-IIIC**). The fit of each of these models is relatively strong, and each path produces a similar ZHe date-Eu curve. The major difference between these models is the inclusion or exclusion of the two zircon grains at ~800 ppm and ~1200 ppm eU. Paths A and B produce an envelope which includes the ~800 ppm grain. Assuming rapid pre-depositional cooling at ca. 450 Ma a curve is produced that excludes the ~800 ppm grain, but includes the ~1200 ppm grain.

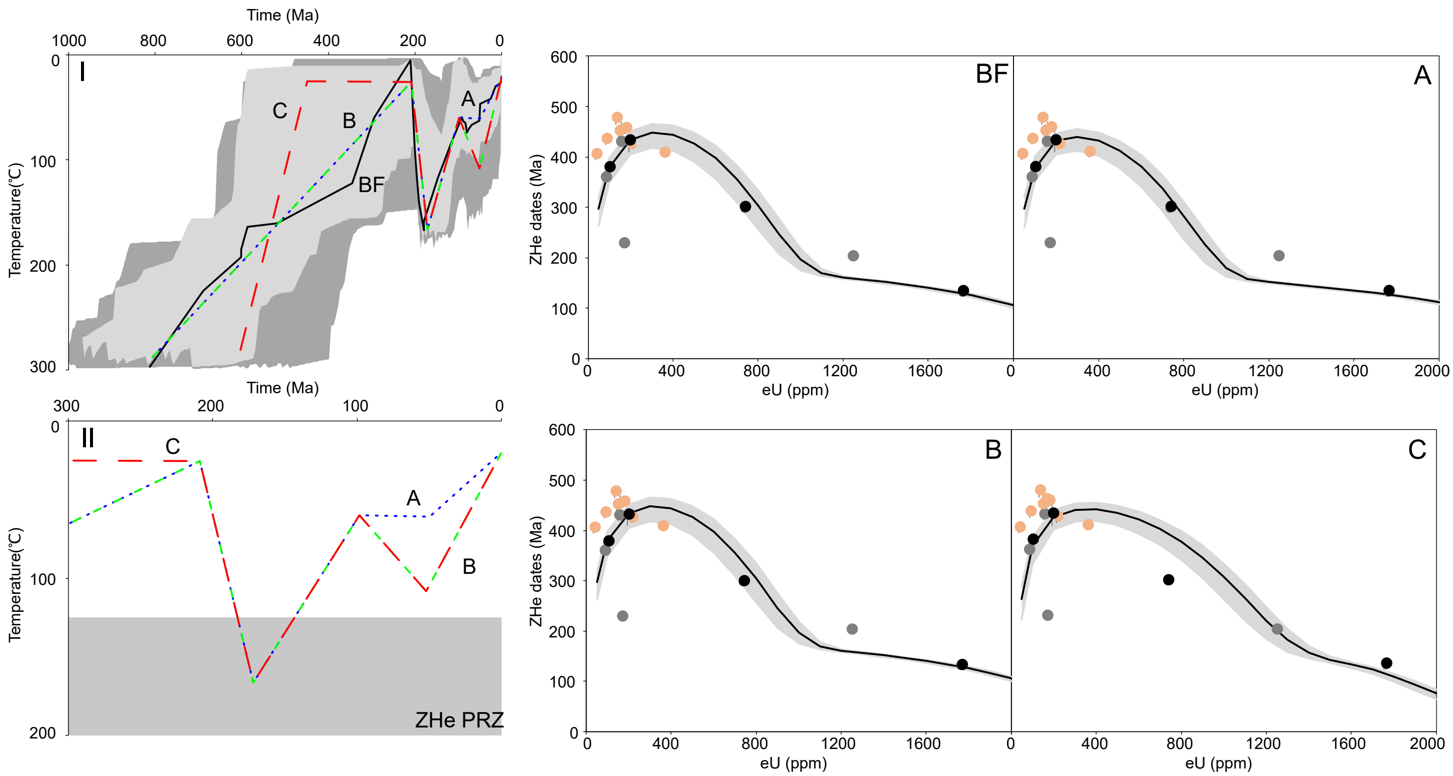


*Figure 8: North Transect – Jurassic samples: (I) inverse models with the range of “acceptable” path solutions in dark grey envelope, “good” path solutions in light grey and best-fit thermal history in black (BF). Selected forward models (A, B, C) based on best-fit path and observed trends in inverse paths. (II) Post-depositional t-T paths based on forward models A, B, C. Grey box represents the ZHe partial rentention zone. (III) Forward models of the expected ZHe date-eU response for (BF) best-fit thermal history, (A) simplified best-fit thermal history, (B) similar to A but with tertiary heating and rapid cooling, (C) similar to B but with rapid pre-depositional cooling at ca. 500 Ma. Black line represents the cooling path of the average (63 µm) grain-size within the sample, grey envelope represents the range of cooling paths between the maximum (73 µm) and minimum (51 µm) grain-size within the sample. Orange (41/1) and grey (01/2), bolded points represent grains used in inverse modelling.*

Compared to the results of the north transect, the best-fit paths produced by the inverse model for the south transect of the Jurassic samples reveal a broadly similar thermal history (**Fig. 9**). The best-fit path follows a somewhat more complex pre-depositional history, with cooling to 200℃ during the Cryogenian, followed by relatively static conditions and slow cooling prior to the time of deposition. The t-T paths then track with the thermal history of the northern part of the basin. Notable exceptions are slightly cooler conditions during the Albian and a more pronounced heating episode from 100 to 50 Ma, where temperatures in excess of 100℃ may have been attained. The final cooling is fairly continuous until the present. Forward model paths A, B, and C for the south transect (**Fig. 9**) are identical to those for the north, in part to test the validity of the forward models in this part of the basin. Unlike the inverse model best-fit path, Path A produces a t-T path with a linear pre-depositional cooling episode, and does not indicate any heating into the Cretaceous (100-50 Ma). Consequently, the date-eU curve indicates that this path does not capture higher eU and at younger ZHe dates (**Fig. 9-IIIA**). Path B is most similar to the best-fit path, with the major difference being the pre-depositional history. The resultant ZHe date-eU envelope is slightly less retentive than the modeled best-fit path (**Fig. 9-IIIB**). However, compared to path A, this path appears to accurately account for younger, less retentive zircon grains. Path C, as described above for the north transect, appears to overestimate the retentiveness of the zircon, and does not represent a strong fit to the Jurassic data for the south transect (**Fig. 9-IIIC**).

Zircon from the Cretaceous samples have approximately the same range of ZHe dates and eU values as the Jurassic samples. Similarly, this allows us to investigate the details of the thermal history of these samples. The lack of ZHe dates in the Triassic provides less certainty regarding the final stage of cooling and unroofing. The best-fit thermal path for the north transect cools slowly after cessation of the Pan-African orogeny prior to the time of Aptian sedimentation,

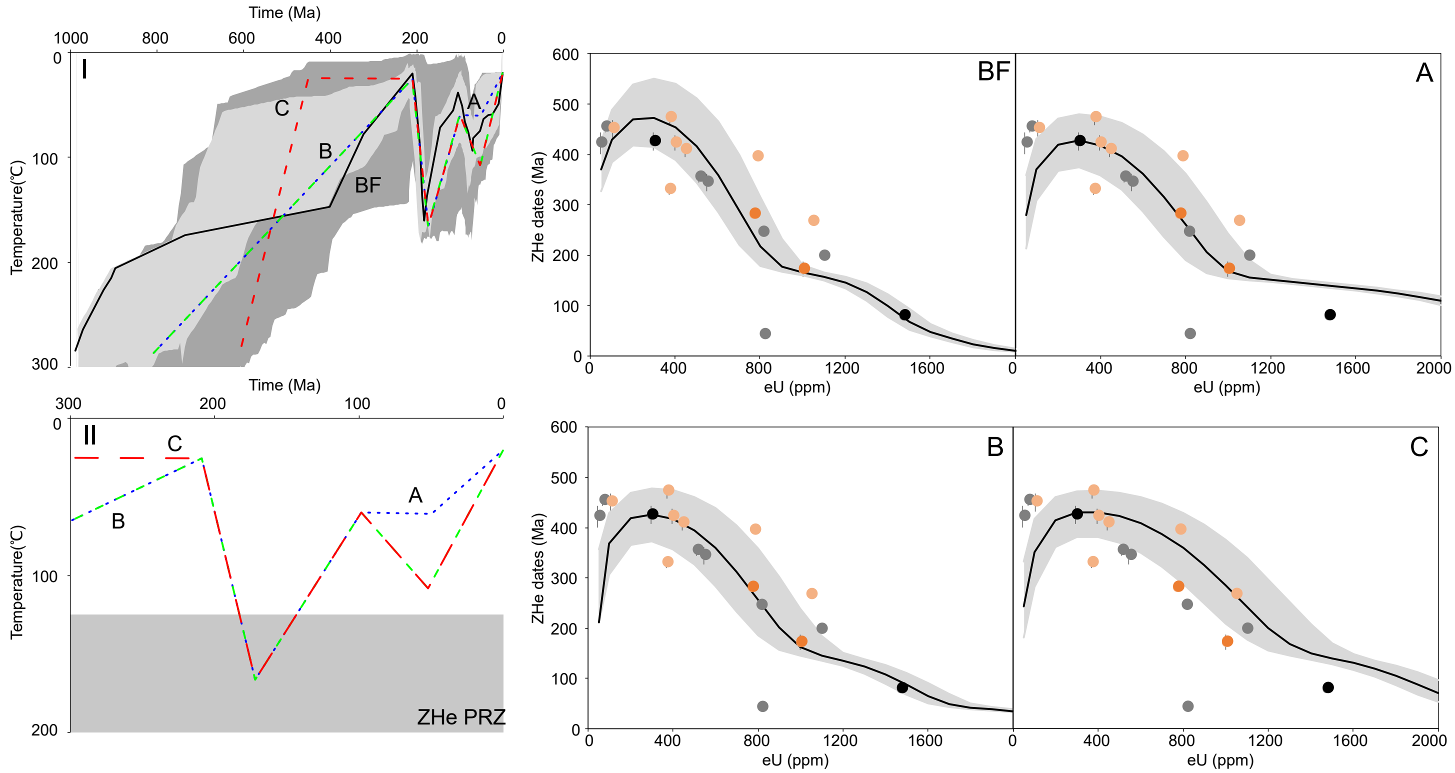


*Figure 9: South transect – Jurassic samples: (I) inverse models with the range of "acceptable" path solutions in dark grey envelope, "good" path solutions in light grey and best-fit thermal history in black (BF). Selected forward models (A, B, C) based on best-fit path and observed trends in inverse paths. (II) Post-depositional t-T paths based on forward models A, B, C. Grey box represents the ZHe partial rentention zone. (III) Forward models of the expected ZHe date-eU response for (BF) best-fit thermal history based on results for the north transect, (A) simplified best-fit thermal history, (B) simplified best-fit thermal history for south transect with Tertiary heating, (C) similar to B but with rapid pre-depositional cooling at ca. 500 Ma. Black line represents the cooling path of the average (57 µm) grain-size within the sample, grey envelope represents the range of cooling paths between the maximum (92 µm) and minimum (39 µm) grain-size within the sample. Orange points (40/3) and grey points (39/3), bolded points represent grains used in inverse modelling.*

possibly exhibiting moderately rapid cooling 50 Myr before deposition. Subsequently, the strata may have experienced slight, punctuated heating episodes during the Late Cretaceous and into the Tertiary. Because of the unreliability of the ZHe dates to record repeated, subtle details at such low (<100°C) temperatures, the paths are simplified in the forward models.

The forward model for path A presents a broad interpretation of the best-fit path (**Fig. 10**). It simplifies the pre-depositional cooling into three stages, and proposes slightly higher temperatures into the Middle Cretaceous compared to the best-fit path. Consequently, the date-eU envelope has a slightly more retentive response around 300-400 Ma relative to the response produced by the best-fit model, but achieves a reasonable fit with the data from both sample 09/2 and 17/1 (**Fig. 10-IIIA**). This forward model assumes that sediments remained buried and were exhumed only shortly before the time of deposition. Path B follows an alternative thermal history with monotonic pre-depositional cooling that is similar to the pre-depositional cooling histories observed for the Jurassic samples, reaching near-surface conditions by the latest Jurassic. This path was tested in order to evaluate the possible of sediment recycling, whereby sediments are deposited in Jurassic strata before being uplifted, eroded, and re-deposited in the Cretaceous strata. The path then infers near-surface temperatures until the time of deposition in the Albian. After deposition, the strata are then predicted to heat to ~170℃, slightly hotter than the range of “good paths” calculated by the inverse model, but still within the “acceptable” range. A single episode of cooling occurs in the Late Cretaceous, and assumes that no further heating occurred. Path B has a strong fit to the date-eU relationship, and produces an envelope similar to that produced by the best-fit model.

Finally, path C was modelled in order to reflect a cooling history in which pre-depositional cooling occurs gradually, followed by burial to temperatures up to ~170℃ followed by rapid final

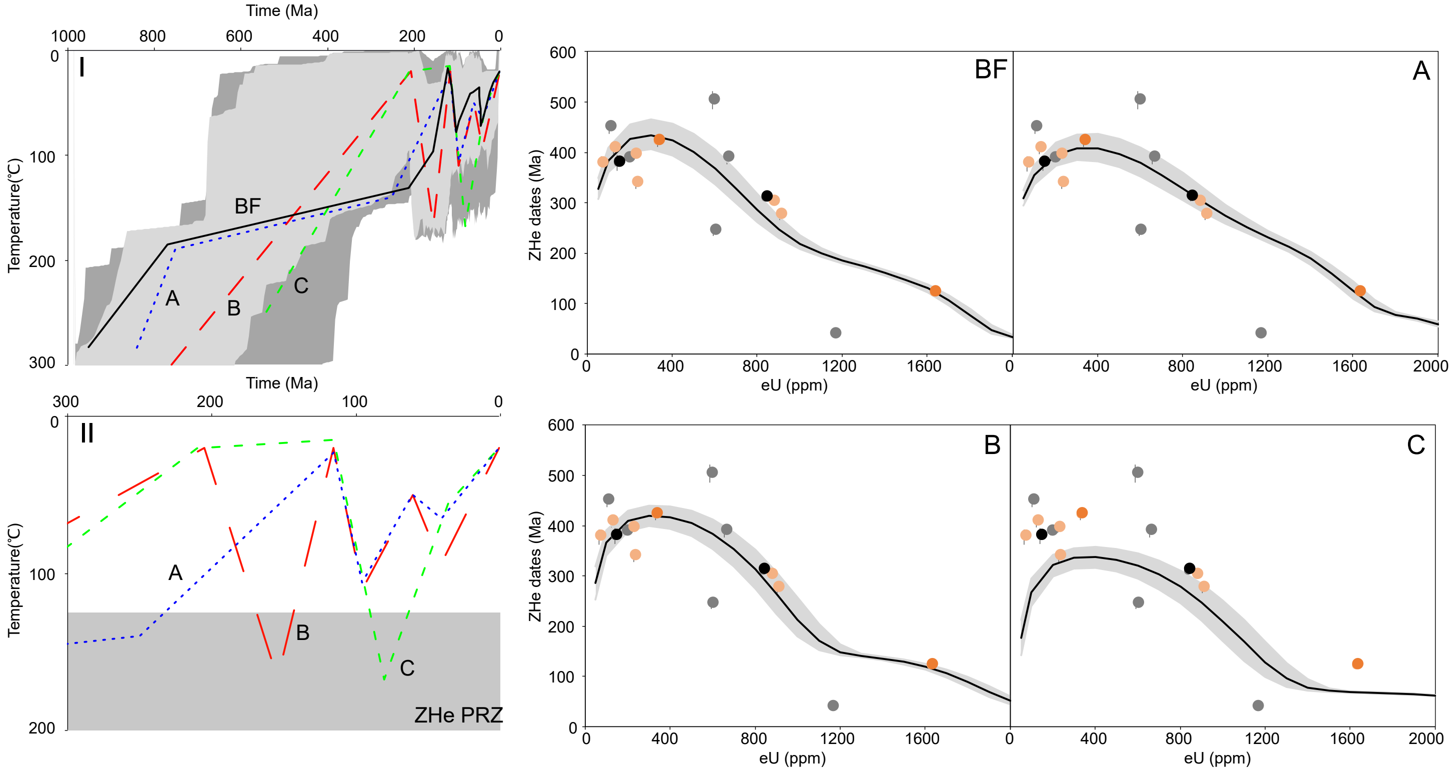


*Figure 10: North transect – Cretaceous samples: (I) inverse models with the range of "acceptable" path solutions in dark grey envelope, "good" path solutions in light grey and best-fit thermal history in black (BF). Selected forward models (A, B, C) based on best-fit path and observed trends in inverse paths. (II) Post-depositional t-T paths based on forward models A, B, C. Grey box represents the ZHe partial rentention zone. (III) Forward models of the expected ZHe date-eU response for (BF) best-fit thermal history, (A) simplified best-fit thermal history, (B) similar to A but with heating and cooling in the Middle Jurassic to test sediment recycling scenario, (C) similar to A but with higher temperature in Late Cretaceous and uninterrupted cooling in the Tertiary. Black line represents the cooling path of the average (59 µm) grain-size within the sample, grey envelope represents the range of cooling paths between the maximum (73 µm) and minimum (48 µm) grain-size within the sample. Orange points (17/1) and grey points (09/2), bolded points represent grains used in inverse modelling.*

cooling (**Fig. 10-IIIC**). This path is not based on observations from the inverse model produced by the sample, but is instead used to validate the forward models for the south transect. The model produces a date-eU curve that strongly underestimates the retentiveness of the zircon grains and does not produce a strong fit with the data. This t-T path is presented to note the differences in the thermal histories between the Cretaceous samples for the north and south transect, respectively.

Compared to the north transect, the two samples from the south transect display relatively poor agreement. Data from sample 31/1 (**grey points in Fig. 11**) have a relatively narrow range of ZHe dates and eU compared to the data from the other Cretaceous samples, 34/1. With no dates younger than Late Jurassic, the time of deposition, the data from this sample will poorly record the post-depositional thermal history of the strata. Therefore we have opted to base the inverse and forward modelling of the south transect on sample 34/1. The best-fit path produced by the inverse modelling highlights pre-depositional cooling similar to the Jurassic samples, relatively rapidly cooling until Early Triassic. The temperature then remains quite low (<40°C) until Cretaceous deposition. After this, the model suggests heating to 160°C in the Late Cretaceous and final cooling is relatively constant into the Tertiary. A second best-fit path is presented for the south transect (**Fig. 11**), also from sample 34/1, which reflects a possible scenario for recycling of sediment from Jurassic units, which is also visible in the Cretaceous data for the north transect, tested above. Here, the samples undergo heating in the earliest Jurassic as they are buried until reaching a temperature of ~150°C. The zircon then cool during exhumation until the time of middle Cretaceous (re)deposition, following a path similar to that presented in the first best-fit path discussed above. This path assumes slightly lower He retentivity as compared to best-fit path.

Path A of the forward model (**Fig. 11**) follows a simplified t-T path based on the first best-fit curve. As such, the ZHe date-eU envelope for path A is almost identical to that produced by the

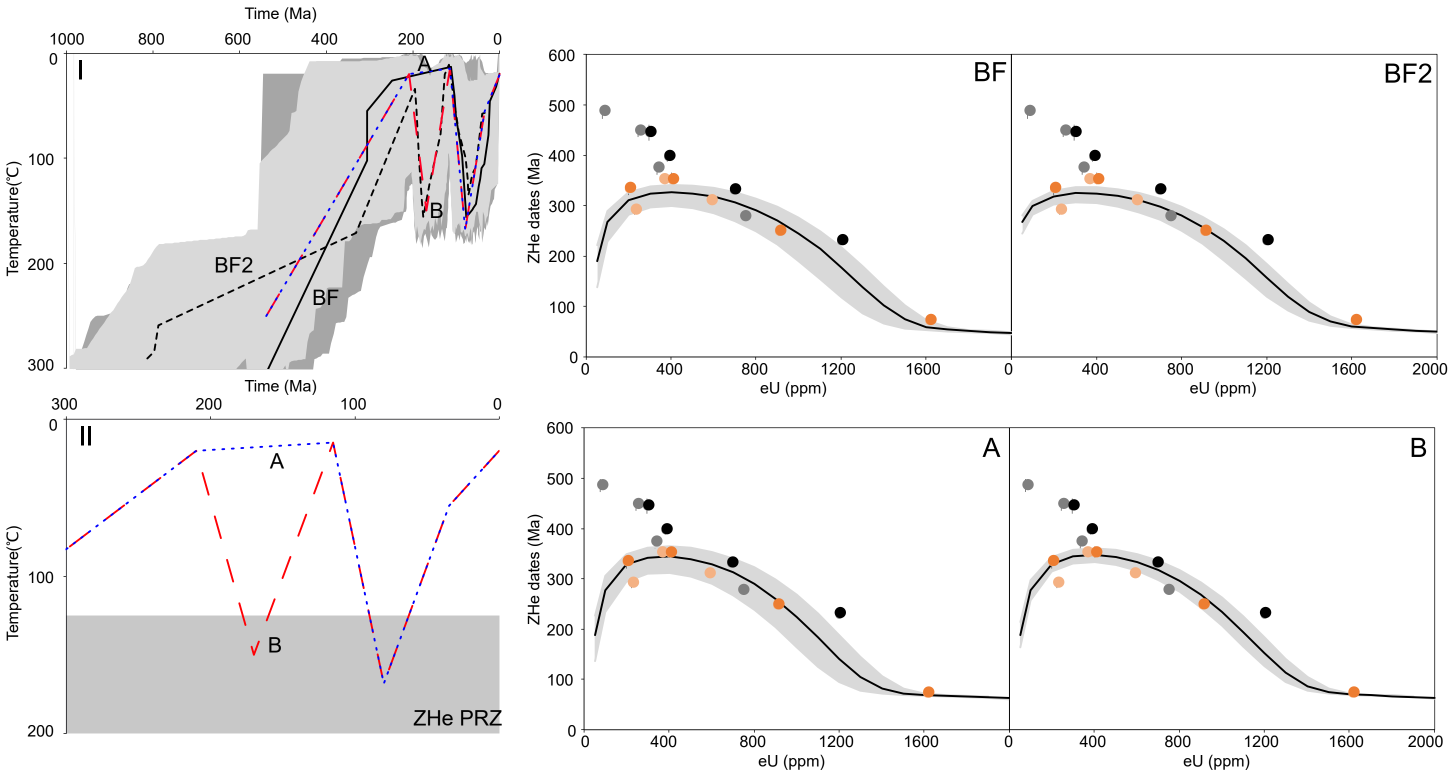


*Figure 11: South transect – Cretaceous samples: (I) inverse models with the range of "acceptable" path solutions in dark grey envelope, "good" path solutions in light grey and best-fit thermal history in black (BF). Selected forward models (A, B, C) based on best-fit path and observed trends in inverse paths. (II) Post-depositional t-T paths based on forward models A, B, C. Grey box represents the ZHe partial rentention zone. (III) Forward models of the expected ZHe date-eU response for (BF) best-fit thermal history, (BF2) best-fit thermal history testing sediment recycling scenario, (A) simplified best-fit thermal history, (B) simplified best-fit sediment recycling scenario thermal history. Black line represents the cooling path of the average (68 µm) grain-size within the sample, grey envelope represents the range of cooling paths between the maximum (80 µm) and minimum (59 µm) grain-size within the sample. Orange points (34/1) and grey points (31/1), bolded points represent the grains used in inverse modelling.*

best-fit path. Path A presented here is identical to Path B presented for the north transect (**Fig. 10**), and both have a good fit with their respective datasets. The date-eU envelope for path A fits the data for sample 34/1 (orange), however underestimates the He retentivity of sample 31/1 (grey), especially at ZHe ages older than ca. 350 Ma. Path B follows a possible path similar to the inverse model produced in the sediment recycling scenario. The major difference between these is the pre-depositional history, where path B follows a pre-depositional cooling history identical to path A. The thermal path in path B is identical to path B tested for the north transect described above. This path tests the possibility of cretaceous sediments having been recycled from older Jurassic strata, heating to a temperature of ~150°C before cooling to near-surface temperature during middle Cretaceous deposition. The post-depositional history for this path is identical to that of path A. The date-eU envelope for path B is similar to the results of path BF2 and provides a good estimation of the He retentivity of zircon (**Fig. 11-III, BF2, IIIB**).

Commonly workers using the ZRDAAM find that the diffusion model overestimates the amount of time required for zircon to accumulate radiation damage (e.g., Powell et al., 2016). Alternatively, the mechanisms that control alpha damage annealing in zircon is not sufficiently understood in order to predict annealing over geologic timescales at temperatures in excess of 300 °C (Guenthner et al., 2013). In our dataset, we find that the thermal models using ZRDAAM appropriately predict a fully reset system at the peak of the Pan-African orogeny, with onset of radiation damage accumulation shortly thereafter. We suggest that the temperatures experienced by zircon during the Pan-African orogeny were well in excess of 300°C, with high greenschist to amphibolite facies metamorphism throughout the majority of Madagascar. These temperatures are sufficient for full annealing of previous radiation damage, therefore resulting in an accurate prediction by the ZRDAAM. Additionally, the relatively short time between full resetting/annealing and deposition in the Morondava Basin may also contribute to the observed agreement between our data and predicted ZHe response by the ZRDAAM. A relatively uncomplicated cooling history prior to deposition, with a single episode of constant cooling as modeled in this study could also be a contributing factor. We therefore stipulate that studies wherein the predictions by the ZRDAAM are found to be overestimating the rate of zircon radiation damage accumulation is the result of more complex histories with annealing requiring higher temperatures over a longer period of time.

**6.0 Thermal evolution of the Morondava Basin**

Based on the inverse and forward thermal history models for the Jurassic and Cretaceous samples, we present a reconstruction of the Morondava Basin commencing in the Permian during which the rocks buried during amalgamation of Gondwana first began to exhume (**Fig. 12**). Several pre-depositional t-T paths were investigated (**Fig. 8-11**), with ZHe data recording primary cooling or becoming fully reset in the Cambrian (ca. 500 Ma). Notably, our zircon U-Pb geochronology possess a significant age population at 500-600 Ma, likely related to material derived from the western and central basement terranes of Madagascar, which experienced greenschist to amphibolite facies metamorphism during the Pan-African orogeny (Boger et al., 2019). Although these zircon crystallization dates are the youngest within the basin, they are still significantly older than the well-constrained depositional age of the Karoo sediments in the basin and are therefore not useful for the determination of a maximum depositional age. Detrital zircon ages of between 500-600 Ma in age, linked to the Pan-African orogeny, together with apparent ZHe ages ranging from 400-500 Ma in each sample are consistent throughout the entire basin. This leads us to conclude that sediments were sourced from rocks in proximity to the basin, having experienced

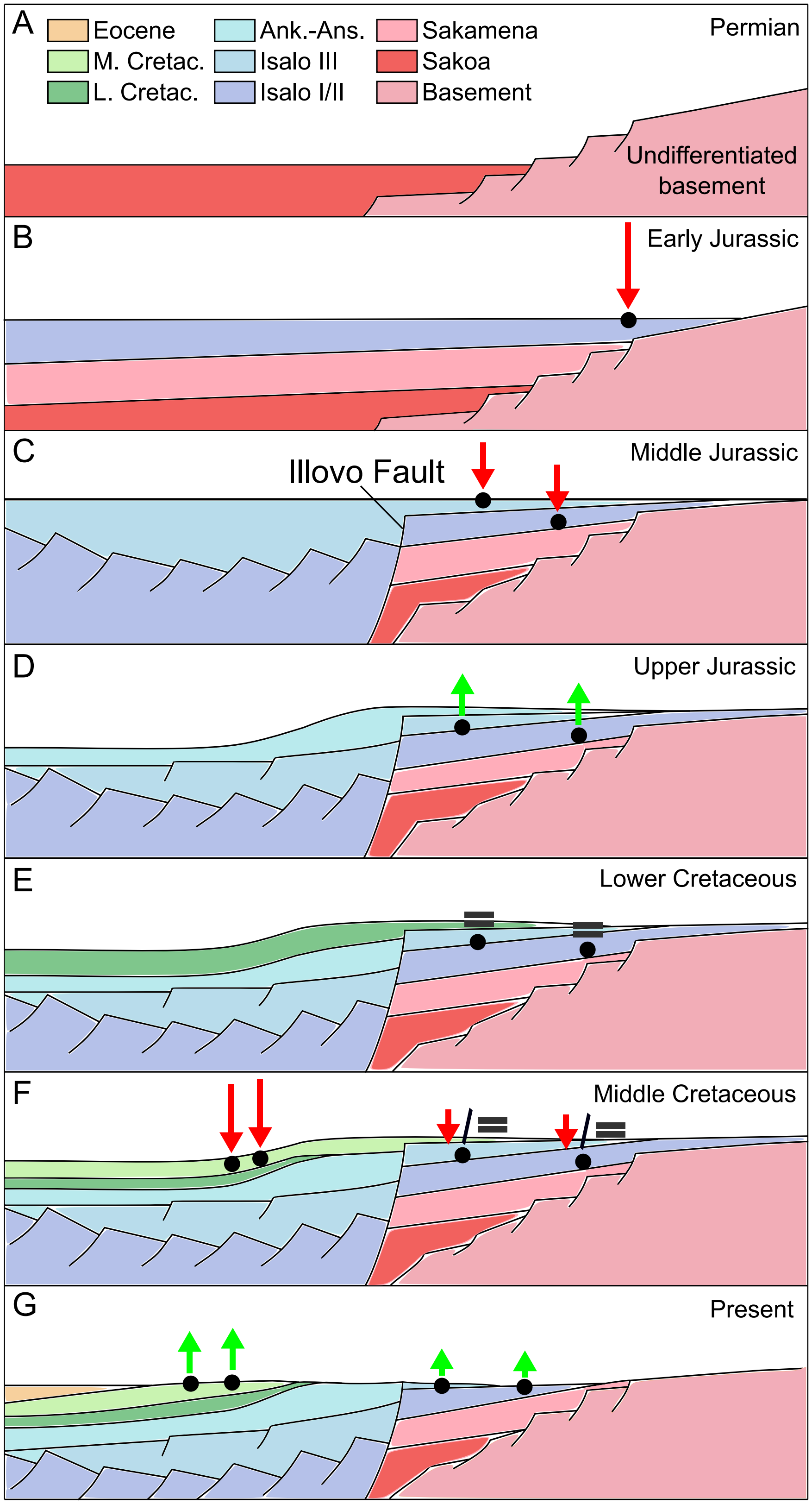


*Figure 12: Morondava Basin reconstruction based on detrital zircon (U-Th)/He thermochronology. Black circles mark approximate position of samples taken in this study. Cross-section based on the same transect examined in figure 4. Figure is not true to vertical scale. Red arrows indicate heating, green arrows indicate cooling with size indicating the relative magnitude of heating/cooling event. Equal sign denotes models show uncertainty or no significant thermal event occurring.*

metamorphism during the Pan-African orogeny and cooled at 500 Ma before being transport and deposited. This is consistent with the results of Emmel et al. (2006) where the authors found apatite grains to have experienced minimal transport. Sediments can directly be traced to individual basement terranes based on detrital zircon age distributions. Although sediment tracing in Madagascar is complicated by the large number of metasedimentary terranes which incorporate sediment from many proto-sources, we were able to identify two detrital zircon populations that can be linked to specific events or localities. In this study the Neoproterozoic to Cambrian (c. 500-600 Ma) zircon can directly be linked to the southern basement terranes having experienced metamorphism at this time, and a small population of Neoarchean to Mesoarchean zircon linked to zircon from the Antongil-Masora terranes and the Itremo Group. We suggest that these specific populations can be used in further detrital zircon studies in Madagascar for the purpose of sediment tracing. Differences in detrital zircon age distributions within the Jurassic samples allows us to identify an east-west sedimentation pattern consistent with direct sourcing of sediments from the basement. The northern samples were derived from the Antananarivo and Ikalamavony domains directly to the east of the basin, whilst the southern Jurassic samples were more likely to have been sourced from the southwestern basement terranes. However, such a differentiation could not be made in samples from the Cretaceous and Tertiary sedimentary rocks. We suggest that extensive mixing prior to deposition of these sediments, either due to a change of environment from fluvial to marine leading to sediments experiencing less direct transport or recycling of sediment within the basin from older stratigraphic units. The latter is consistent with previous investigations into sediment recycling within the Morondava Basin (Emmel et al., 2006).

The apparent ZHe ages indicate that the bulk of the sediment was produced during unroofing of the orogen, and the t-T models help inform the thermal history of the basin. Below we present a reconstruction of the Morondava Basin and the relevant discussions refer to the units and tectonic events illustrated in each panel (**Fig. 12A-G**).

A) During the Permian, the development of the Morondava Basin begins with the formation of a failed rift along the margin of eastern Gondwana due to crustal extension. This event is contemporaneous with the deposition of the Sakoa Group (ca. 300 Ma), which were not sampled as part of this study. Previous apatite FT dating by Emmel et al. (2006) indicates that sediments deposited in the Sakoa were later recycled into younger strata of the basin. None of our new data suggest that sediment was recycled from older Karoo strata, however the nature of partially reset thermochronometry systems make it difficult to investigate the pre-depositional history and evaluate the possibility of sediment recycling. Previous work by Jöns et al. (2009) in the northern Morondava Basin suggest the basement adjacent to the basin was at the near surface (or cooling) at the time of Karoo sedimentation, with maximum exhumation rates between the Permo-Triassic until Early Jurassic.

(B) The Sakamena Group and the Isalo Group are deposited on top of the Sakoa Group in the Early Jurassic, of which only the Isalo was sampled for this study. New detrital zircon U-Pb ages and ZHe ages suggest that these sediments are derived from metasedimentary basement terranes, proximal to the basin, that rapidly cooled during Cambro-Ordovician times. From our thermal history models it is unclear whether these sediments experienced a single continuous stage of cooling and exhumation (**Fig 8-IIIA**) or were more rapidly exhumed and then exposed to near-surface conditions for some time before being deposited (**Fig. 8-IIIC**). Stephenson et al. (2021) suggest an initial cooling episode between 275 and 200 Ma based on basement apatite FT and (U-Th)/He dates. Together with our results, this would suggest single-phase, monotonic basement uplift during the Permo-Triassic. Sediments within the basin have relatively immature composition, suggesting that sediments were deposited in low energy environments or not transported long distances. From our data, the thickness of the Isalo Group is difficult to determine due uncertainty with the geothermal gradient at the time of deposition, which is dependent on heat production/advection and topography-related isotherm distortions (Stüwe et al., 1994; Stüwe & Hintermüller, 2000). Whilst some researchers suggest a standard geothermal gradient of 20-25°C/km within in the Morondava Basin (Seward et al., 2004), other researchers suggest a steeper geothermal gradient of 30-45°C/km may have been possible (Emmel et al., 2004, 2008). Analogous examples of rifting such as the Red Sea record higher heat flow towards the centre of the structure quickly reverting to normal values towards the margins of the rifting system (Makris et al., 1991). A maximum temperature of ~180°C (Fig. 7, 8) for the Isalo Group from this study would yield a thickness between 4 km and 8 km. Reported thickness for the Isalo Group package varies throughout the basin, from a minimum of <2 km to a maximum of 6 km in the south of the basin (Coffin & Rabinowitz, 1988; Besairie, 1974).

C) In the Middle Jurassic, the development of a new rift separates the Isalo into large fault blocks that are subsequently tilted. The crustal-scale Illovo Fault, which is readily observed on seismic sections and geological maps, demarcates the margin between the Permo-Triassic failed rift and the newly formed rift. A thick package of organic-rich shales and limestones of the Andafia Formation is deposited. Thermal history models indicate that after this period, the sediments deposited to the east of the Illovo Fault began cooling, forming the shoulder to the new rift. This is marked by a period of monotonic cooling until ca. 100 Ma accounting for cooling of up to 70°C (**Fig. 8**). Assuming a similar thermal gradient as discussed above this would indicate the removal of between 2 and 3 km of material and the exhumation of the Jurassic samples in our study area to a depth of between 2.5 and 3.5 km. Similarities in detrital zircon U-Pb age populations between the samples to the west of the Illovo Fault show extensive mixing of sediment sources and may be suggestive of re-sedimentation. Consequently, rocks of the Permo-Triassic failed rift, as the new rift shoulder, supplied sediment to the newly-formed Jurassic rift.

D) Subsidence of the basin to the west of the Illovo Fault towards the end of the Jurassic led to the development of a carbonate platform on top of the half-grabens. The mudstones and limestones of the Bemaraha Formation, deposited in this environment, are more common in the northern Morondava Basin, however there are several exposures in the study area, mostly to the west of the Illovo Fault. Some small exposures to the west of the Illovo Fault do not exclude the possibility of overstepping onto the rift shoulder. Any heating associated with this subtle burial is not observed in our models, due to lack of sensitivity of the zircon (U-Th)/He chronometer at these conditions. Suitable accessory mineral-bearing horizons within the carbonate sequences on either side of the Illovo Fault would need to be targeted to resolve these issues with (U-Th)/He or FT dating.

E & F) Sedimentation continues into the Early and Middle Cretaceous with the deposition of several deep marine facies. Burial of these sediments continues into the Late Cretaceous reaching a maximum temperature of ~170℃. Assuming similar thermal gradients as the Jurassic samples, this would indicate burial up to a depth of 3.5 to 5.5 km. Forward models for the Jurassic samples at the time of Early to middle Cretaceous deposition also suggest heating of up to 40℃, may indicate that Cretaceous sediments overstepped onto the rift shoulder to the east of the Illovo Fault (**Fig. 8-IIIB, 9-IIIB**). These forward models would be consistent with deposition of up to 1.5 km of Cretaceous sediments on top of the basement shoulder. This observation holds for the south transect, where the forward models clearly suggest a period of heating during the Early to middle Cretaceous. Published t-T paths based on apatite FT basement samples taken along the eastern rift shoulder of the Morondava Basin show reheating up to 80°C in the Late Cretaceous or Neogene (Emmel et al., 2004). The authors propose heating is due to an elevated geothermal gradient as a result of rifting and the Marion hot spot related volcanism at the time of the opening of the Indian Ocean (Storey et al., 1995). Apatite within samples of proximity to the Androyen volcanic complex were possibly partially annealed due to this event (Emmel et al., 2004), though not fully reset, implying a maximum reheating to 80°C. However, work by the same authors on Jurassic sediments along the eastern margin of the basin do not suggest any significant thermal influence by a Late Cretaceous event (Emmel et al., 2006). The presence of several Turonian-age dykes and sills in our study area (e.g. Tari et al., 2018), especially in proximity to Cretaceous samples, indicate that there may have been some thermal influence from the shallow crustal volcanism. This may further explain heating to temperatures up to 160°C in the middle Cretaceous for the Cretaceous samples (**Fig. 10-IIIB, 11-IIIB**). With our current dataset and the understanding of regional geology, it is unclear whether the middle Cretaceous temperatures are reached through burial, heating due to Turonian magmatism, or a combination of both. In contrast, samples from Karoo strata on the rift shoulder show maximum heating of 110°C at this time, broadly consistent with published temperatures between 90-100°C (Giese et al., 2012). Heating in the Jurassic samples could also be attributed to either distal heating effects from Turonian dykes and sills, or overstepping of Cretaceous sediments onto the rift/basin shoulder resulting in burial-associated heating. Although it is difficult to fully reconcile the thermal influence of Turonian dykes on the entire Morondava Basin, we suggest that the more likely cause of widespread heating during the middle Cretaceous is burial as a result of sedimentation; our Jurassic samples preserve relatively long periods of heating (**Fig. 8-IIIB, 9-IIIB**).

G) Final cooling for the Cretaceous and Jurassic samples occurs sometime in the Late Cretaceous and the Tertiary (Oligocene), but is temporally poorly constrained by our data. The t-T paths that were evaluated in this study suggest that the latest cooling started at ca. 40-50 Ma. The Cretaceous samples in the Late Jurassic rift appear to be exhumed more rapidly compared to the Jurassic samples in the Permo-Triassic failed rift. This differential rate of exhumation would require re-activation of the Illovo Fault. There are several structural highs observed to the east of the Illovo and Bemaraha faults within the Morondava Basin that may support this theory, though no obvious structural high is observed to the east of the Illovo Fault in our study area (Montenat, 1993; Schandelmeier et al., 2004). Giese et al. (2012) suggest that cooling during the Late Cretaceous is related to movement along NNW-SSE trending faults, reactivated by thermal doming related to the Marion hot spot. Alternatively, they suggest an elevated geothermal gradient following the Late Cretaceous magmatic event responsible for the Turonian dykes. Published studies resolve the latest stage of cooling somewhat later at ca. 40 Ma using titanite and apatite FT dating (Jöns et al., 2009; Giese et al., 2012; Stephenson et al., 2021). Maybe somewhat unconvincingly, Emmel et al. (2008) suggest cooling and exhumation during the Eocene is related to isostatic compensation because of the Eocene carbonate platform in the southwestern Morondava Basin. Alternatively, Giese et al. (2012) discuss geodynamic changes in plate-motion could be the trigger for Eocene exhumation. Relative plate motion transitioned from NE-SW spreading between Madagascar and India to N-S spreading between Madagascar and Antarctica with a hiatus in plate motion at 43 Ma (Reeves, 2014). Giese et al. (2012) draw a connection between the change in stress regime, the formation of NNE-SSW trending faults in Eocene sediments along the western coast of Madagascar, and Eocene exhumation. Hereby, the reactivation of Eocene faults leads to relative subsidence in southern Madagascar compensated by relative exhumation in central and northern Madagascar. Our data does not suggest that further subsidence occurred in southern Madagascar, nor does displacement along NNE-SSW trending faults appear pervasive enough to accommodate final cooling across the entire basin. We suggest that this final stage of cooling was accommodated by reactivation of the larger Illovo Fault complex, though more investigation of the exact timing of fault required to come to a definitive conclusion. It should be considered that additional data using a lower closure temperature (apatite (U-Th)/He dating) or different systematics (apatite FT dating) would be required to fully resolve the last 40 Myr of tectonic evolution of the Morondava Basin.

## 7.0 Conclusions

New detrital zircon U-Pb geochronology data is used to investigate the sedimentation history along two transects in the Morondava Basin. The detrital ages from Jurassic sedimentary rocks in the north transect of the basin are characterized by age populations in the Neoproterozoic (800-900 Ma) and Paleoproterozoic-Archean (ca. 2500 Ma), and were likely derived from the Antananarivo terrane to the east of the basin. Detrital age populations from Tertiary, Cretaceous, and Jurassic units in the south transect, and Cretaceous units in the north transect were characterized by Cambrian (500 Ma), Mesoproterozoic (ca. 1000 Ma), and Meso-Paleoarchean (3000-3500 Ma) zircon. Sediment sources from these units likely lie in the Itremo Group (3000 Ma), and the Ikalamavony, Vohibory, and Androyen terranes, which experienced Cambrian to late Neoproterozoic metamorphism during amalgamation of Madagascar.

We also present new zircon (U-Th)/He data from these same sample unique to the western parts of the Morondava Basin. These datasets are partially reset and therefore record the pre-depositional history of the samples in addition to the post-depositional thermal history. Though this poses some challenges, through inverse and forward modelling much can be deduced regarding the thermal history of the basin system. Maximum ZHe dates range from 400 to 500 Ma within all samples, and eU values exhibit dispersion such that most sample possess a negative ZHe date-eU relationship. Inverse and forward models reveal the basin can be divided into different corridors, separated by the crustal scale Illovo Fault which splits the basin into a Permo-Triassic rift basin and a Middle Jurassic rift. Cooling of the failed Permo-Triassic rift contemporaneous with marine facies deposition in the Jurassic rift indicates the Permo-Triassic rift may have formed the rift flank of the newly developing rift. We propose two possible scenarios to heating in the Middle to Late Cretaceous on either side of the Illovo Fault: a) heating due to intrusion of Turonian dykes associated with the Marion hot spot and active rifting contemporaneous to the opening of the Indian Ocean or b) Cretaceous sedimentation overstepping onto the rift basin shoulder. The time of latest cooling is poorly constrained, but occurred in the last 40 Myr. Differential final cooling in the Tertiary on either side of the Illovo Fault may indicate re-activation of the fault and may offer an explanation for the presence of a structural high along the east flank of the fault. The temperatures observed within the basin indicate hydrocarbon potential within the basin is theoretically high. Complex structural and thermal history within the basin due to several stages of uplift and subsidence results in difficulties in identifying source-rocks and potential traps.

## References

Andersen, T., 2002. Correction of common lead in U-Pb analyses that do not report $^{204}$Pb. *Chemical Geology*, *192*, 59–79.

Andriampenomanana, F., Nyblade, A. A., Wysession, M. E., Durrheim, R. J., Tilmann, F., Julià, J., Pratt, M. J., Rambolamanana, G., Aleqabi, G., Shore, P. J., & Rakotondraibe, T. (2017). The structure of the crust and uppermost mantle beneath Madagascar. *Geophysical Journal International*, *210*(3), 1525–1544. https://doi.org/10.1093/gji/ggx243

Archibald, D. B., Collins, A. S., Foden, J. D., Payne, J. L., Taylor, R., Holden, P., Razakamanana, T., & Clark, C. (2015). Towards unravelling the Mozambique Ocean conundrum using a triumvirate of zircon isotopic proxies on the Ambatolampy Group, central Madagascar. *Tectonophysics*, *662*, 167–182. https://doi.org/10.1016/j.tecto.2015.02.018

Armistead, S. E., Collins, A. S., Schmitt, R. S., Costa, R. L., De Waele, B., Razakamanana, T., Payne, J. L., & Foden, J. D. (2021). Proterozoic basin evolution and tectonic geography of Madagascar: Implications for an East Africa connection during the Paleoproterozoic. *Tectonics*, *40*(3). https://doi.org/10.1029/2020TC006498

Ashwal, L. D., & Tucker, R. D. (1999). Geology of Madagascar: A brief outline. *Gondwana Research*, *2*(3), 335–339. https://doi.org/10.1016/S1342-937X(05)70270-7

Bauer, W., Walsh, G. J., de Waele, B., Thomas, R. J., Horstwood, M. S. A., Bracciali, L., Schofield, D. I., Wollenberg, U., Lidke, D. J., Rasaona, I. T., & Rabarimanana, M. H. (2011). Cover sequences at the northern margin of the Antongil Craton, NE Madagascar. *Precambrian Research*, *189*(3–4), 292–312. https://doi.org/10.1016/j.precamres.2011.07.018

Besairie, H. (1969). *Madagascar Carte Géologique 1:500 000 (8 sheets)* [Map]. Service Géologique de Madagascar, Direction des Mines et de l'Energie.

Boger, S. D., Hirdes, W., Ferreira, C. A. M., Jenett, T., Dallwig, R., & Fanning, C. M. (2015). The 580–520 Ma Gondwana suture of Madagascar and its continuation into Antarctica and Africa. *Gondwana Research*, *28*(3), 1048–1060. https://doi.org/10.1016/j.gr.2014.08.017

Boger, S. D., Hirdes, W., Ferreira, C. A. M., Schulte, B., Jenett, T., & Fanning, C. M. (2014). From passive margin to volcano–sedimentary forearc: The Tonian to Cryogenian evolution of the Anosyen Domain of southeastern Madagascar. *Precambrian Research*, *247*, 159–186. https://doi.org/10.1016/j.precamres.2014.04.004

Boger, S. D., Maas, R., Pastuhov, M., Macey, P. H., Hirdes, W., Schulte, B., Fanning, C. M., Ferreira, C. A. M., Jenett, T., & Dallwig, R. (2019). The tectonic domains of southern and western Madagascar. *Precambrian Research*, *327*, 144–175. https://doi.org/10.1016/j.precamres.2019.03.005

Castelino, J. A., Reichert, C., Klingelhoefer, F., Aslanian, D., & Jokat, W. (2015). Mesozoic and Early Cenozoic sediment influx and morphology of the Mozambique Basin. *Marine and Petroleum Geology*, *66*, 890–905. https://doi.org/10.1016/j.marpetgeo.2015.07.028

Clark, D. N. (1998). Review of the exploration potential of Madagascar. *Houston Geol. Soc. Bull.*, *40*, 23–29.

Coffin, M. F., & Rabinowitz, P. D. (1988). Evolution of the conjugate East African—Madagascan margins and the western Somali Basin. In M. F. Coffin & P. D. Rabinowitz (Eds.), *Evolution of the conjugate East African—Madagascan margins and the western*

*Somali Basin* (Vol. 226). Geological Society of America (Denver, USA). https://doi.org/10.1130/SPE226-p1

Collins, A. S., Kinny, P. D., & Razakamanana, T. (2012). Depositional age, provenance and metamorphic age of metasedimentary rocks from southern Madagascar. *Gondwana Research*, *21*(2–3), 353–361. https://doi.org/10.1016/j.gr.2010.12.006

Collins, A. S., Kröner, A., Fitzsimons, I. C. W., & Razakamanana, T. (2003). Detrital footprint of the Mozambique ocean: U–Pb SHRIMP and Pb evaporation zircon geochronology of metasedimentary gneisses in eastern Madagascar. *Tectonophysics*, *375*(1–4), 77–99. https://doi.org/10.1016/S0040-1951(03)00334-2

Cooperdock, E. H. G., Ketcham, R. A., & Stockli, D. F. (2019). Resolving the effects of 2-D versus 3-D grain measurements on apatite (U–Th)/He age data and reproducibility. *Geochronology*, *1*(1), 17–41. https://doi.org/10.5194/gchron-1-17-2019

Cox, R., Coleman, D. S., Chokel, C. B., DeOreo, S. B., Wooden, J. L., Collins, A. S., De Waele, B., & Kröner, A. (2004). Proterozoic tectonostratigraphy and paleogeography of central Madagascar derived from detrital zircon U-Pb age populations. *The Journal of Geology*, *112*(4), 379–399. https://doi.org/10.1086/421070

De Waele, B., Thomas, R. J., Macey, P. H., Horstwood, M. S. A., Tucker, R. D., Pitfield, P. E. J., Schofield, D. I., Goodenough, K. M., Bauer, W., Key, R. M., Potter, C. J., Armstrong, R. A., Miller, J. A., Randriamananjara, T., Ralison, V., Rafahatelo, J. M., Rabarimanana, M., & Bejoma, M. (2011). Provenance and tectonic significance of the Palaeoproterozoic metasedimentary successions of central and northern Madagascar. *Precambrian Research*, *189*(1–2), 18–42. https://doi.org/10.1016/j.precamres.2011.04.004

Delaunay, A. (2018). *Les mouvements verticaux de Madagascar (90 – 0 Ma): Une analyse couplée des formes du relief et de l'enregistrement sédimentaire des marges ouest malgaches* [PhD thesis]. Géosciences Rennes, 374 p.

Emmel, B., Geiger, M., & Jacobs, J. (2006). Detrital apatite fission-track ages in Middle Jurassic strata at the rifted margin of W Madagascar—Indicator for a protracted resedimentation history. *Sedimentary Geology*, *186*(1–2), 27–38. https://doi.org/10.1016/j.sedgeo.2005.09.022

Emmel, B., Jacobs, J., Kastowski, M., & Graser, G. (2006). Phanerozoic upper crustal tectono-thermal development of basement rocks from central Madagascar: An integrated fission-track and structural study. *Tectonophysics*, *412*(1–2), 61–86. https://doi.org/10.1016/j.tecto.2005.09.008

Emmel, B., Jacobs, J., & Razakamanana, T. (2004). Titanite and apatite fission track analyses on basement rocks of central-southern Madagascar: Constraints on exhumation and denudation rates along the eastern rift shoulder of the Morondava basin. *Journal of African Earth Sciences*, *38*(4), 343–361. https://doi.org/10.1016/j.jafrearsci.2003.10.009

Emmel, B., Jöns, N., Kröner, A., Jacobs, J., Wartho, J. -A., Schenk, V., Razakamanana, T., & Austegard, A. (2008). From closure of the Mozambique Ocean to Gondwana breakup: New evidence from geochronological data of the Vohibory Terrane, Southwest Madagascar. *The Journal of Geology*, *116*(1), 21–38. https://doi.org/10.1086/524121

Fitzsimons, I. C. W., & Hulscher, B. (2005). Out of Africa: Detrital zircon provenance of central Madagascar and Neoproterozoic terrane transfer across the Mozambique Ocean. *Terra Nova*, *17*(3), 224–235. https://doi.org/10.1111/j.1365-3121.2005.00595.x

Gehrels, G. (2011). Detrital Zircon U-Pb Geochronology: Current Methods and New Opportunities. In *Tectonics of Sedimentary Basins* (pp. 45–62). John Wiley & Sons, Ltd. https://doi.org/10.1002/9781444347166.ch2

Geiger, M., Clark, D. N., & Mette, W. (2004). Reappraisal of the timing of the breakup of Gondwana based on sedimentological and seismic evidence from the Morondava Basin, Madagascar. *Journal of African Earth Sciences*, *38*(4), 363–381. https://doi.org/10.1016/j.jafrearsci.2004.02.003

Geiger, M., & Schweigert, G. (2006). Toarcian–Kimmeridgian depositional cycles of the south-western Morondava Basin along the rifted continental margin of Madagascar. *Facies*, *52*(1), 85–112. https://doi.org/10.1007/s10347-005-0039-8

Giese, J., Seward, D., & Schreurs, G. (2012). Low-temperature evolution of the Morondava rift basin shoulder in western Madagascar: An apatite fission track study: evolution of the Morondava Basin. *Tectonics*, *31*(2). https://doi.org/10.1029/2011TC002921

Guenthner, W. R., Reiners, P. W., DeCelles, P. G., & Kendall, J. (2015). Sevier belt exhumation in central Utah constrained from complex zircon (U-Th)/He data sets: Radiation damage and He inheritance effects on partially reset detrital zircons. *Geological Society of America Bulletin*, *127*(3–4), 323–348. https://doi.org/10.1130/B31032.1

Guenthner, W. R., Reiners, P. W., Ketcham, R. A., Nasdala, L., & Giester, G. (2013). Helium diffusion in natural zircon: Radiation damage, anisotropy, and the interpretation of zircon (U-Th)/He thermochronology. *American Journal of Science*, *313*(3), 145–198. https://doi.org/10.2475/03.2013.01

Handke, M. J., Tucker, R. D., & Ashwal, L. D. (1999). Neoproterozoic continental arc magmatism in west-central Madagascar. *Geology*, *27*(4), 351. https://doi.org/10.1130/0091-7613(1999)027<0351:NCAMIW>2.3.CO;2

Ichiki, T., Ishikawa, M., Kimura, J., Senda, R., & Rakotondrazafy, R. (2015). Crustal assembly of the Antananarivo and Masora domains, central–eastern Madagascar: Constraints from U–Pb zircon geochronology and whole–rock geochemistry of meta–granitoids. *Journal of Mineralogical and Petrological Sciences*, *110*(3), 111–125. https://doi.org/10.2465/jmps.141225

Jöns, N., Emmel, B., Schenk, V., & Razakamanana, T. (2009). From orogenesis to passive margin—The cooling history of the Bemarivo Belt (N Madagascar), a multi-thermochronometer approach. *Gondwana Research*, *16*(1), 72–81. https://doi.org/10.1016/j.gr.2009.02.006

Kabete, J., Groves, D., McNaughton, N., & Dunphy, J. (2006). The geology, SHRIMP U–Pb geochronology and metallogenic significance of the Ankisatra-Besakay District, Andriamena belt, northern Madagascar. *Journal of African Earth Sciences*, *45*(1), 87–122. https://doi.org/10.1016/j.jafrearsci.2006.01.008

Ketcham, R. A. (2005). Forward and inverse modeling of low-temperature thermochronometry data. *Reviews in Mineralogy and Geochemistry*, *58*(1), 275–314. https://doi.org/10.2138/rmg.2005.58.11

Kroener, A. (2000). Age and magmatic history of the Antananarivo Block, central Madagascar, as derived from zircon geochronology and Nd isotopic systematics. *American Journal of Science*, *300*(4), 251–288. https://doi.org/10.2475/ajs.300.4.251

Luger, P., Gröschke, M., Bussmann, M., Dina, A., Mette, W., Uhmann, A., & Kallenbach, H. (1994). Comparison of the Jurassic and Cretaceous sedimentary cycles of Somalia and Madagascar: Implications for the Gondwana breakup. *Geologische Rundschau*, *83*(4), 711–727. https://doi.org/10.1007/BF00251070

McFarlane, C. R. M., & Luo, Y. (2012). U-Pb geochronology using 193 nm Excimer LA-ICP-MS optimized for in situ accessory mineral dating in thin sections. *Geoscience Canada* (39) 158–172.

Montenat, C. (1993). Tectonic-Sedimentary sequence of the western Malagasy margin during Jurassic times (Morondava Basin, Madagascar). *Comptes Rendus de l'Académie Des Sciences*, *317*(6), 811–818.

Moucha, R., & Forte, A. M. (2011). Changes in African topography driven by mantle convection. *Nature Geoscience*, *4*(10), 707–712. https://doi.org/10.1038/ngeo1235

Nemchin, A. A., & Cawood, P. A. (2005). Discordance of the U–Pb system in detrital zircons: Implication for provenance studies of sedimentary rocks. *Sedimentary Geology*, *182*(1–4), 143–162. https://doi.org/10.1016/j.sedgeo.2005.07.011

Paquette, J.-L., Nédélec, A., Moine, B., & Rakotondrazafy, M. (1994). U-Pb, single zircon Pb-evaporation, and Sm-Nd isotopic study of a granulite domain in SE Madagascar. *The Journal of Geology*, *102*(5), 523–538. https://doi.org/10.1086/629696

Pique, A. (1999). The geological evolution of Madagascar: An introduction. *Journal of African Earth Sciences*, *28*, 919–930. https://doi.org/10.1016/S0899-5362(99)00069-X

Powell, J., Schneider, D., Stockli, D., & Fallas, K. (2016). Zircon (U-Th)/He thermochronology of Neoproterozoic strata from the Mackenzie Mountains, Canada: Implications for the Phanerozoic exhumation and deformation history of the northern Canadian Cordillera:

Mackenzie Mountains thermochronology. *Tectonics*, *35*(3), 663–689. https://doi.org/10.1002/2015TC003989

Ramanampisoa, L., & Radke, M. (1992). Thermal maturity and hydrocarbon generation in rocks from the sedimentary basins of Madagascar. *Journal of Petroleum Geology*, *15*(4), 379–396. https://doi.org/10.1111/j.1747-5457.1992.tb01041.x

Razafimbelo, E. (1987). *Le bassin de Morondava (Madagascar). Synthèse géologique et structural* [PhD thesis]. University of Louis Pasteur, 189 p.

Reeves, C. (2014). The position of Madagascar within Gondwana and its movements during Gondwana dispersal. *Journal of African Earth Sciences*, *94*, 45–57. https://doi.org/10.1016/j.jafrearsci.2013.07.011

Reiners, P. W., Farley, K. A., & Hickes, H. J. (2002). He diffusion and (U–Th)/He thermochronometry of zircon: Initial results from Fish Canyon Tuff and Gold Butte. *Tectonophysics*, *349*(1–4), 297–308. https://doi.org/10.1016/S0040-1951(02)00058-6

Reiners, P. W., Spell, T. L., Nicolescu, S., & Zanetti, K. A. (2004). Zircon (U-Th)/He thermochronometry: He diffusion and comparisons with $^{40}Ar/^{39}Ar$ dating. *Geochimica et Cosmochimica Acta*, *68*(8), 1857–1887. https://doi.org/10.1016/j.gca.2003.10.021

Roig, J., Tucker, R. D., & Peters, L. (2012). *Carte geologique de la republique de Madagascar A 1/1000000* [Map]. Madagascar: Ministère des Mines, Geologie Programme de Gouvernance des Ressources Minerales.

Schandelmeier, H., Bremer, F., & Holl, H.-G. (2004). Kinematic evolution of the Morondava rift basin of SW Madagascar—from wrench tectonics to normal extension. *Journal of African Earth Sciences*, *38*(4), 321–330. https://doi.org/10.1016/j.jafrearsci.2003.11.002

Seward, D., Grujic, D., & Schreurs, G. (2004). An insight into the breakup of Gondwana: Identifying events through low-temperature thermochronology from the basement rocks of Madagascar: an insight into the breakup of Gondwana. *Tectonics*, *23*(3) https://doi.org/10.1029/2003TC001556

Sláma, J., Košler, J., Condon, D. J., Crowley, J. L., Gerdes, A., Hanchar, J. M., Horstwood, M. S. A., Morris, G. A., Nasdala, L., Norberg, N., Schaltegger, U., Schoene, B., Tubrett, M. N., & Whitehouse, M. J. (2008). Plešovice zircon—A new natural reference material for U–Pb and Hf isotopic microanalysis. *Chemical Geology*, *249*(1–2), 1–35. https://doi.org/10.1016/j.chemgeo.2007.11.005

Stephenson, S. N., White, N. J., Carter, A., Seward, D., Ball, P. W., & Klöcking, M. (2021). Cenozoic dynamic topography of Madagascar. *Geochemistry, Geophysics, Geosystems*, *22*(6). https://doi.org/10.1029/2020GC009624

Stüwe, K., & Hintermüller, M. (2000). Topography and isotherms revisited: The influence of laterally migrating drainage divides. *Earth and Planetary Science Letters*, *184*(1), 287–303. https://doi.org/10.1016/S0012-821X(00)00315-0

Stüwe, K., White, L., & Brown, R. (1994). The influence of eroding topography on steady-state isotherms. Application to fission track analysis. *Earth and Planetary Science Letters*, *124*(1–4), 63–74. https://doi.org/10.1016/0012-821X(94)00068-9

Tari, G., Hannke, K., Wilmot, G., Schretter, I., Bierbaumer, M., & Sattler, U. (2018). *Trap Formation by Turonian Sill Complexes in the Deepwater Morondava Basin, Madagascar* [AAPG Datapages/Search and Discovery Article #90332]. AAPG International Conference and Exhibition, Cape Town, South Africa.

Thomas, R. J., De Waele, B., Schofield, D. I., Goodenough, K. M., Horstwood, M., Tucker, R., Bauer, W., Annells, R., Howard, K., Walsh, G., Rabarimanana, M., Rafahatelo, J. M., Ralison, A. V., & Randriamananjara, T. (2009). Geological evolution of the Neoproterozoic Bemarivo Belt, northern Madagascar. *Precambrian Research*, *172*(3–4), 279–300. https://doi.org/10.1016/j.precamres.2009.04.008

Tian, Y., Qiu, N., Kohn, B. P., Zhu, C., Hu, S., Gleadow, A. J. W., & McInnes, B. I. A. (2012). Detrital zircon (U–Th)/He thermochronometry of the Mesozoic Daba Shan Foreland Basin, central China: Evidence for timing of post-orogenic denudation. *Tectonophysics*, *570–571*, 65–77. https://doi.org/10.1016/j.tecto.2012.08.010

Torsvik, T. H., Tucker, R. D., Ashwal, L. D., Eide, E. A., Rakotosolofo, N. A., & de Wit, M. J. (1998). Late Cretaceous magmatism in Madagascar: Palaeomagnetic evidence for a stationary Marion hotspot. *Earth and Planetary Science Letters*, *164*(1), 221–232. https://doi.org/10.1016/S0012-821X(98)00206-4

Tucker, R. D., Roig, J. Y., Macey, P. H., Delor, C., Amelin, Y., Armstrong, R. A., Rabarimanana, M. H., & Ralison, A. V. (2011). A new geological framework for south-central Madagascar, and its relevance to the “out-of-Africa” hypothesis. *Precambrian Research*, *185, 109–130*. https://doi.org/10.1016/j.precamres.2010.12.008

Vermeesch, P. (2013). Multi-sample comparison of detrital age distributions. *Chemical Geology*, *341*, 140–146. https://doi.org/10.1016/j.chemgeo.2013.01.010

Vermeesch, P. (2018). IsoplotR: A free and open toolbox for geochronology. *Geoscience Frontiers*, *9*(5), 1479–1493. https://doi.org/10.1016/j.gsf.2018.04.001

Wescott, W. A., & Diggens, J. N. (1998). Depositional history and stratigraphical evolution of the Sakamena group (Middle Karoo Supergroup) in the southern Morondava Basin, Madagascar. *Journal of African Earth Sciences*, *27*(3), 461–479. https://doi.org/10.1016/S0899-5362(98)00073-6

Wiedenbeck, M., Allé, P., Corfu, F., Griffin, W. L., Meier, M., Oberli, F., Quadt, A. V., Roddick, J. C., & Spiegel, W. (1995). Three natural zircon standards for U-Th-Pb, Lu-Hf, trace element and REE analyses. *Geostandards and Geoanalytical Research*, *19*(1), 1–23. https://doi.org/10.1111/j.1751-908X.1995.tb00147.x

Wolf, R. A., Farley, K. A., & Kass, D. M. (1998). Modeling of the temperature sensitivity of the apatite U–Th/He thermochronometer. *Chemical Geology*, 148(1–2), 105–114. https://doi.org/10.1016/S0009-2541(98)00024-2

**Supplemental Materials**

Table SI1. LA-ICP-MS U-Pb data for polished zircon from the Morondava Basin, Madagascar

Table SI2. Summary of model constraints used in HeFTy

Figure SI1. SEM images of zircon from Morondava Basin, Madagascar

Figure SI2. Detrital zircon U-Pb Cumulative Area Distribution (CAD) of <10% discordant U-Pb data. Colours for each sample correspond to lithological units as described in maps, cross-section, and stratigraphic column (Fig. 4).

Figure SI3. Alternative inverse thermal models for the Jurassic samples. A: North Transect (samples 01/2 and 41/1) B: South Transect (samples 39/3 and 40/1). The envelope for"acceptable"paths is shaded in green, the envelope for the "good" paths is shaded in purple.The mean path is shown by the blue line.

Figure SI4. Alternative inverse thermal models for the Cretaceous samples. A: North Transect (samples 09/2 and 17/1) B: South Transect (samples 31/1 and 34/1). The envelope for "acceptable"paths is shaded in green, the envelope for the "good" paths is shaded in purple. The mean path is shown by the blue line. Best path as determined by the model is shown in black.

Figure SI5. Alternative forward models for Cretaceous samples. A: North Transect (samples 09/2,17/1), B: South Transect (samples 31/1, 34/1). Black line represents the cooling path of the average grain size, grey lines represent the cooling path of the minimum and maximum grain sizes. Path tested are the mean paths for the inverse models from figure DR5.

Figure SI6. Alternative forward models for Jurassic samples. A: North Transect (samples 01/2,41/1), B: South Transect (samples 39/3, 40/1). Black line represents the cooling path of the average grain size, grey lines represent the cooling path of the minimum and maximum grain sizes.

Figure SI7. Constraint boxes and inflection points for the Jurassic inverse models. Constraint boxes are shown outlined in blue, based on the assumptions in table SI2. Green inflection points are “acceptable paths”, purple inflection points are “good paths”. Clustering within a constraint box indicates less uncertainty within the inverse model.

Figure SI8. Constraint boxes and inflection points for the Cretaceous inverse models. Constraint boxes are shown outlined in blue, based on the assumptions in table SI2. Green inflection points are “acceptable paths”, purple inflection points are “good paths”. Clustering within a constraint box indicates less uncertainty within the inverse model.

**Table SI1. LA-ICP-MS U-Pb data for polished zircon from the Morondava Basin, Madagascar**

| sample | $^{207}Pb^*/^{206}Pb^*$ | | $^{207}Pb^*/^{235}U$ | | $^{206}Pb^*/^{238}U$ | | $^{207}Pb/^{206}Pb$ | | $^{207}Pb/^{235}U$ | | $^{206}Pb/^{238}U$ | |
|---|---|---|---|---|---|---|---|---|---|---|---|---|
| | value | 1 s.e | value | 1 s.e | value | 1 s.e | age (Ma) | 1 s.e | age (Ma) | 1 s.e | age (Ma) | 1 s.e |
| 01_2 (19°42'10,2"S, 45°17'54,0"E) | | | | | | | | | | | | |
| WMS01_2_1 | 0.06791 | 0.00380 | 1.28594 | 0.06752 | 0.13343 | 0.00602 | 864.7 | 48.4 | 839.5 | 44.1 | 807.4 | 36.4 |
| WMS01_2_2 | 0.09456 | 0.00888 | 1.60990 | 0.14436 | 0.12257 | 0.00805 | 1518.5 | 142.6 | 974.1 | 87.3 | 745.3 | 49.0 |
| WMS01_2_3 | 0.15464 | 0.00849 | 10.32678 | 0.50057 | 0.48710 | 0.01768 | 2397.2 | 131.6 | 2464.5 | 119.5 | 2558.1 | 92.9 |
| WMS01_2_4 | 0.06339 | 0.00354 | 1.03210 | 0.05850 | 0.11809 | 0.00477 | 720.5 | 40.2 | 720.0 | 40.8 | 719.6 | 29.1 |
| WMS01_2_5 | 0.17857 | 0.00917 | 11.07617 | 0.93364 | 0.44519 | 0.05408 | 2638.9 | 135.5 | 2529.6 | 213.2 | 2373.8 | 288.4 |
| WMS01_2_6 | 0.05560 | 0.00265 | 0.67774 | 0.02967 | 0.08888 | 0.00277 | 435.5 | 20.8 | 525.4 | 23.0 | 548.9 | 17.1 |
| WMS01_2_7 | 0.18497 | 0.02825 | 3.36005 | 0.68083 | 0.13720 | 0.01331 | 2697.2 | 411.9 | 1495.1 | 303.0 | 828.8 | 80.4 |
| WMS01_2_8 | 0.06775 | 0.00260 | 1.43818 | 0.08879 | 0.15643 | 0.00834 | 859.9 | 32.9 | 905.0 | 55.9 | 936.9 | 50.0 |
| WMS01_2_9 | 0.06938 | 0.00469 | 1.17342 | 0.05338 | 0.12217 | 0.00589 | 909.2 | 61.4 | 788.2 | 35.9 | 743.0 | 35.8 |
| WMS01_2_10 | 0.08349 | 0.00790 | 1.35781 | 0.11400 | 0.11574 | 0.00824 | 1279.7 | 121.1 | 870.9 | 73.1 | 706.0 | 50.3 |
| WMS01_2_11 | 0.06163 | 0.00342 | 0.82816 | 0.05044 | 0.09802 | 0.00271 | 660.3 | 36.6 | 612.6 | 37.3 | 602.8 | 16.6 |
| WMS01_2_12 | 0.06536 | 0.00423 | 1.04977 | 0.05262 | 0.11820 | 0.00365 | 785.1 | 50.9 | 728.8 | 36.5 | 720.2 | 22.2 |
| WMS01_2_13 | 0.05572 | 0.00330 | 0.67973 | 0.04029 | 0.08859 | 0.00412 | 440.3 | 26.1 | 526.6 | 31.2 | 547.2 | 25.4 |
| WMS01_2_14 | 0.05734 | 0.00413 | 0.75313 | 0.07968 | 0.09535 | 0.00487 | 503.6 | 36.2 | 570.0 | 60.3 | 587.1 | 30.0 |
| WMS01_2_15 | 0.12005 | 0.00620 | 0.82005 | 0.04080 | 0.04966 | 0.00173 | 1956.2 | 101.1 | 608.1 | 30.3 | 312.4 | 10.9 |
| WMS01_2_16 | 0.14648 | 0.00616 | 10.12360 | 0.38923 | 0.50507 | 0.01795 | 2304.4 | 97.0 | 2446.1 | 94.0 | 2635.5 | 93.7 |
| WMS01_2_17 | 0.14656 | 0.00531 | 9.59892 | 0.39395 | 0.47637 | 0.01474 | 2305.4 | 83.5 | 2397.1 | 98.4 | 2511.4 | 77.7 |
| WMS01_2_18 | 0.06906 | 0.00237 | 1.15083 | 0.03755 | 0.12040 | 0.00364 | 899.7 | 30.9 | 777.6 | 25.4 | 732.9 | 22.2 |
| WMS01_2_19 | 0.06582 | 0.00302 | 1.19853 | 0.04839 | 0.13146 | 0.00450 | 799.9 | 36.7 | 799.9 | 32.3 | 796.2 | 27.2 |
| WMS01_2_20 | 0.05560 | 0.00321 | 0.68446 | 0.04293 | 0.08928 | 0.00206 | 435.5 | 25.2 | 529.5 | 33.2 | 551.3 | 12.7 |
| WMS01_2_21 | 0.16015 | 0.00725 | 4.69082 | 0.44289 | 0.21104 | 0.01656 | 2456.5 | 111.2 | 1765.6 | 166.7 | 1234.4 | 96.9 |
| WMS01_2_22 | 0.12211 | 0.00772 | 1.38810 | 0.10112 | 0.08229 | 0.00570 | 1986.5 | 125.6 | 883.9 | 64.4 | 509.8 | 35.3 |
| WMS01_2_23 | 0.15514 | 0.00467 | 10.17226 | 0.32537 | 0.46744 | 0.01192 | 2402.6 | 72.3 | 2450.6 | 78.4 | 2472.3 | 63.0 |
| WMS01_2_24 | 0.18464 | 0.00716 | 13.22693 | 0.81285 | 0.52024 | 0.02301 | 2694.3 | 104.5 | 2696.0 | 165.7 | 2700.2 | 119.4 |
| WMS01_2_25 | 0.17684 | 0.00802 | 11.82666 | 0.56198 | 0.48241 | 0.01453 | 2622.7 | 118.9 | 2590.8 | 123.1 | 2537.8 | 76.5 |
| WMS01_2_26 | 0.07852 | 0.00546 | 1.22112 | 0.08985 | 0.11312 | 0.00601 | 1159.2 | 80.6 | 810.3 | 59.6 | 690.8 | 36.7 |
| WMS01_2_27 | 0.17194 | 0.01294 | 9.08285 | 0.78180 | 0.38106 | 0.03122 | 2575.8 | 193.9 | 2346.4 | 202.0 | 2081.2 | 170.5 |
| WMS01_2_28 | 0.06751 | 0.00485 | 0.84950 | 0.07738 | 0.09014 | 0.00621 | 852.5 | 61.2 | 624.4 | 56.9 | 556.3 | 38.4 |
| WMS01_2_29 | 0.16788 | 0.01013 | 10.61663 | 0.78620 | 0.45214 | 0.04401 | 2535.8 | 153.1 | 2490.2 | 184.4 | 2404.8 | 234.1 |
| WMS01_2_30 | 0.15555 | 0.00768 | 9.96677 | 0.59246 | 0.45738 | 0.01508 | 2407.1 | 118.9 | 2431.7 | 144.5 | 2428.0 | 80.1 |
| WMS01_2_31 | 0.11023 | 0.03277 | 1.78413 | 0.54263 | 0.11584 | 0.00562 | 1802.4 | 535.8 | 1039.7 | 316.2 | 706.6 | 34.3 |
| WMS01_2_32 | 0.17676 | 0.00953 | 14.20591 | 0.73972 | 0.58218 | 0.03041 | 2621.9 | 141.4 | 2763.6 | 143.9 | 2957.6 | 154.5 |
| WMS01_2_33 | 0.06380 | 0.00318 | 1.08248 | 0.05817 | 0.12334 | 0.00372 | 733.9 | 36.6 | 744.8 | 40.0 | 749.7 | 22.6 |
| WMS01_2_34 | 0.06588 | 0.00375 | 1.18585 | 0.07830 | 0.13221 | 0.00806 | 801.7 | 45.6 | 794.0 | 52.4 | 800.5 | 48.8 |
| WMS01_2_35 | 0.07235 | 0.00500 | 1.16246 | 0.07302 | 0.11623 | 0.00507 | 994.8 | 68.7 | 783.1 | 49.2 | 708.8 | 30.9 |
| WMS01_2_36 | 0.06859 | 0.00388 | 1.19616 | 0.06422 | 0.12678 | 0.00444 | 885.4 | 50.1 | 798.8 | 42.9 | 769.4 | 26.9 |
| WMS01_2_37 | 0.07684 | 0.00395 | 0.86112 | 0.05028 | 0.08104 | 0.00579 | 1116.1 | 57.4 | 630.7 | 36.8 | 502.3 | 35.9 |
| WMS01_2_38 | 0.06397 | 0.00336 | 1.12592 | 0.06501 | 0.12783 | 0.00651 | 739.8 | 38.9 | 765.8 | 44.2 | 775.5 | 39.5 |
| WMS01_2_39 | 0.07131 | 0.00357 | 1.23555 | 0.06831 | 0.12403 | 0.00592 | 965.5 | 48.3 | 816.9 | 45.2 | 753.7 | 36.0 |
| WMS01_2_40 | 0.20441 | 0.00777 | 4.25440 | 0.24770 | 0.15213 | 0.00659 | 2861.0 | 108.7 | 1684.6 | 98.1 | 912.9 | 39.5 |
| WMS01_2_41 | 0.15189 | 0.02231 | 2.99656 | 0.55010 | 0.14099 | 0.00650 | 2366.5 | 347.6 | 1406.7 | 258.2 | 850.3 | 39.2 |
| WMS01_2_42 | 0.17609 | 0.00611 | 12.05188 | 0.50084 | 0.49682 | 0.02105 | 2615.6 | 90.7 | 2608.5 | 108.4 | 2600.1 | 110.2 |
| WMS01_2_43 | 0.06737 | 0.00374 | 1.22541 | 0.07222 | 0.12973 | 0.00831 | 848.4 | 47.1 | 812.2 | 47.9 | 786.3 | 50.3 |
| WMS01_2_44 | 0.05997 | 0.00401 | 0.74138 | 0.04734 | 0.08958 | 0.00325 | 601.5 | 40.2 | 563.2 | 36.0 | 553.1 | 20.1 |
| WMS01_2_45 | 0.16841 | 0.00573 | 10.78401 | 0.34914 | 0.46240 | 0.01433 | 2541.2 | 86.5 | 2504.7 | 81.1 | 2450.1 | 76.0 |
| WMS01_2_46 | 0.05593 | 0.00272 | 1.08222 | 0.05801 | 0.13846 | 0.00382 | 448.6 | 21.8 | 744.7 | 39.9 | 835.9 | 23.0 |
| WMS01_2_47 | 0.06798 | 0.00370 | 1.19517 | 0.07787 | 0.12704 | 0.00408 | 866.9 | 47.2 | 798.4 | 52.0 | 770.9 | 24.8 |
| WMS01_2_48 | 0.06642 | 0.00269 | 1.22432 | 0.04656 | 0.13318 | 0.00389 | 818.6 | 33.1 | 811.7 | 30.9 | 806.0 | 23.5 |
| WMS01_2_49 | 0.06599 | 0.00263 | 1.09810 | 0.04647 | 0.12090 | 0.00373 | 805.0 | 32.1 | 752.4 | 31.8 | 735.8 | 22.7 |
| WMS01_2_50 | 0.20805 | 0.00963 | 14.09544 | 0.59770 | 0.48603 | 0.01599 | 2889.7 | 133.7 | 2756.1 | 116.9 | 2553.5 | 84.0 |
| WMS01_2_51 | 0.16514 | 0.00614 | 8.63426 | 0.40638 | 0.38139 | 0.01742 | 2508.3 | 93.2 | 2300.2 | 108.3 | 2082.8 | 95.1 |
| WMS01_2_52 | 0.05700 | 0.00336 | 0.93073 | 0.05395 | 0.11688 | 0.00419 | 490.7 | 28.9 | 668.0 | 38.7 | 712.6 | 25.5 |
| WMS01_2_53 | 0.06477 | 0.00255 | 1.22132 | 0.05321 | 0.13645 | 0.00615 | 765.9 | 30.1 | 810.4 | 35.3 | 824.6 | 37.2 |
| WMS01_2_54 | 0.07196 | 0.00538 | 1.28377 | 0.07476 | 0.12692 | 0.00657 | 984.0 | 73.6 | 838.5 | 48.8 | 770.3 | 39.9 |
| WMS01_2_55 | 0.16559 | 0.00696 | 10.07540 | 0.41947 | 0.44307 | 0.01325 | 2512.8 | 105.7 | 2441.7 | 101.7 | 2364.4 | 70.7 |
| WMS01_2_56 | 0.13838 | 0.00697 | 9.04869 | 0.65840 | 0.47261 | 0.03100 | 2206.3 | 111.0 | 2342.9 | 170.5 | 2495.0 | 163.7 |
| WMS01_2_57 | 0.06372 | 0.00337 | 0.98951 | 0.04818 | 0.11166 | 0.00433 | 731.4 | 38.7 | 698.5 | 34.0 | 682.4 | 26.5 |
| WMS01_2_58 | 0.16678 | 0.00711 | 10.51106 | 0.42505 | 0.45508 | 0.01500 | 2524.8 | 107.6 | 2480.9 | 100.3 | 2417.8 | 79.7 |
| WMS01_2_59 | 0.15942 | 0.00594 | 10.53654 | 0.50068 | 0.47547 | 0.02023 | 2448.8 | 91.2 | 2483.1 | 118.0 | 2507.5 | 106.7 |
| WMS01_2_60 | 0.06747 | 0.00221 | 1.23964 | 0.05318 | 0.13251 | 0.00424 | 851.4 | 27.8 | 818.7 | 35.1 | 802.1 | 25.7 |
| WMS01_2_61 | 0.06436 | 0.00471 | 1.17242 | 0.08185 | 0.13137 | 0.00327 | 752.5 | 55.1 | 787.8 | 55.0 | 795.7 | 19.8 |
| WMS01_2_62 | 0.15806 | 0.00498 | 9.63625 | 0.36799 | 0.44166 | 0.01629 | 2434.3 | 76.7 | 2400.6 | 91.7 | 2358.1 | 87.0 |
| WMS01_2_63 | 0.06594 | 0.00295 | 1.22266 | 0.05596 | 0.13459 | 0.00383 | 803.4 | 36.0 | 811.0 | 37.1 | 814.0 | 23.2 |
| WMS01_2_64 | 0.06391 | 0.00308 | 0.89445 | 0.04152 | 0.10144 | 0.00630 | 737.6 | 35.5 | 648.8 | 30.1 | 622.9 | 38.7 |
| WMS01_2_65 | 0.06942 | 0.00309 | 1.27622 | 0.04483 | 0.13364 | 0.00364 | 910.2 | 40.5 | 835.2 | 29.3 | 808.6 | 22.0 |
| WMS01_2_66 | 0.15923 | 0.00657 | 10.48961 | 0.37511 | 0.47926 | 0.01515 | 2446.7 | 101.0 | 2479.0 | 88.6 | 2524.0 | 79.8 |
| WMS01_2_67 | 0.13731 | 0.00562 | 6.09699 | 0.39929 | 0.31648 | 0.01815 | 2192.8 | 89.7 | 1989.8 | 130.3 | 1772.5 | 101.6 |
| WMS01_2_68 | 0.06681 | 0.00320 | 1.04665 | 0.06039 | 0.11308 | 0.00691 | 830.9 | 39.8 | 727.2 | 42.0 | 690.6 | 42.2 |
| WMS01_2_69 | 0.16715 | 0.00668 | 11.13852 | 0.56599 | 0.48255 | 0.01913 | 2528.6 | 101.0 | 2534.8 | 128.8 | 2538.4 | 100.6 |
| WMS01_2_70 | 0.05523 | 0.00414 | 1.13457 | 0.07335 | 0.14641 | 0.00818 | 420.7 | 31.5 | 769.9 | 49.8 | 880.8 | 49.2 |
| WMS01_2_71 | 0.17636 | 0.00978 | 11.86677 | 0.59082 | 0.49061 | 0.02157 | 2618.2 | 145.3 | 2593.9 | 129.1 | 2573.3 | 113.1 |
| WMS01_2_72 | 0.06264 | 0.00272 | 1.00000 | 0.04040 | 0.11585 | 0.00339 | 695.2 | 30.2 | 703.8 | 28.4 | 706.6 | 20.7 |
| WMS01_2_73 | 0.06807 | 0.00432 | 1.16199 | 0.05523 | 0.12337 | 0.00626 | 869.7 | 55.1 | 782.9 | 37.2 | 749.9 | 38.0 |
| WMS01_2_74 | 0.06858 | 0.00444 | 1.41490 | 0.09223 | 0.14967 | 0.00636 | 885.1 | 57.3 | 895.2 | 58.4 | 899.1 | 38.2 |
| WMS01_2_75 | 0.06553 | 0.00402 | 1.13900 | 0.07973 | 0.12206 | 0.00606 | 790.6 | 48.5 | 772.0 | 54.0 | 742.4 | 36.9 |

| sample | $^{207}Pb^*/^{206}Pb^*$ | | $^{207}Pb^*/^{235}U$ | | $^{206}Pb^*/^{238}U$ | | $^{207}Pb/^{206}Pb$ | | $^{207}Pb/^{235}U$ | | $^{206}Pb/^{238}U$ | |
|---|---|---|---|---|---|---|---|---|---|---|---|---|
| | value | 1 s.e | value | 1 s.e | value | 1 s.e | age (Ma) | 1 s.e | age (Ma) | 1 s.e | age (Ma) | 1 s.e |
| WMS01_2_76 | 0.20786 | 0.00959 | 11.98228 | 0.99825 | 0.41625 | 0.03364 | 2888.2 | 133.3 | 2603.0 | 216.9 | 2243.4 | 181.3 |
| WMS01_2_77 | 0.13860 | 0.00590 | 5.89283 | 0.30543 | 0.30890 | 0.01442 | 2209.0 | 94.0 | 1960.2 | 101.6 | 1735.3 | 81.0 |
| WMS01_2_78 | 0.15083 | 0.00820 | 9.93243 | 0.63710 | 0.47385 | 0.02706 | 2354.6 | 128.0 | 2428.5 | 155.8 | 2500.4 | 142.8 |
| WMS01_2_79 | 0.17857 | 0.01225 | 11.56763 | 1.21680 | 0.46461 | 0.03676 | 2638.9 | 181.0 | 2570.1 | 270.3 | 2459.9 | 194.6 |
| WMS01_2_80 | 0.07332 | 0.00338 | 1.06015 | 0.05116 | 0.10529 | 0.00424 | 1022.0 | 47.1 | 733.9 | 35.4 | 645.3 | 26.0 |
| WMS01_2_81 | 0.07130 | 0.00402 | 1.32735 | 0.07877 | 0.13496 | 0.00447 | 965.2 | 54.5 | 857.7 | 50.9 | 816.1 | 27.0 |
| WMS01_2_82 | 0.16328 | 0.00761 | 10.78194 | 0.50647 | 0.47821 | 0.01930 | 2489.1 | 116.1 | 2504.5 | 117.6 | 2519.4 | 101.7 |
| WMS01_2_83 | 0.06456 | 0.00326 | 0.84405 | 0.04694 | 0.09504 | 0.00313 | 759.1 | 38.3 | 621.4 | 34.6 | 585.3 | 19.3 |
| WMS01_2_84 | 0.06872 | 0.00288 | 1.27479 | 0.05999 | 0.13460 | 0.00385 | 889.3 | 37.3 | 834.5 | 39.3 | 814.1 | 23.3 |
| WMS01_2_85 | 0.17697 | 0.00671 | 10.22822 | 0.37442 | 0.41988 | 0.01574 | 2623.9 | 99.5 | 2455.6 | 89.9 | 2259.9 | 84.7 |
| WMS01_2_86 | 0.06844 | 0.00324 | 1.22370 | 0.06525 | 0.12980 | 0.00625 | 881.0 | 41.6 | 811.5 | 43.3 | 786.7 | 37.9 |
| WMS01_2_87 | 0.06306 | 0.00320 | 0.80567 | 0.04443 | 0.09227 | 0.00423 | 709.5 | 36.0 | 600.0 | 33.1 | 569.0 | 26.1 |
| WMS01_2_88 | 0.06561 | 0.00375 | 1.18306 | 0.06526 | 0.13095 | 0.00494 | 792.9 | 45.3 | 792.7 | 43.7 | 793.3 | 29.9 |
| WMS01_2_89 | 0.17092 | 0.00578 | 7.67543 | 0.31921 | 0.32917 | 0.01262 | 2565.9 | 86.8 | 2193.7 | 91.2 | 1834.3 | 70.3 |
| WMS01_2_90 | 0.16897 | 0.00615 | 11.07962 | 0.45831 | 0.47742 | 0.01230 | 2546.7 | 92.7 | 2529.8 | 104.6 | 2516.0 | 64.8 |
| WMS01_2_91 | 0.15566 | 0.00609 | 10.59822 | 0.39626 | 0.49538 | 0.01142 | 2408.3 | 94.2 | 2488.6 | 93.0 | 2593.9 | 59.8 |
| WMS01_2_92 | 0.16223 | 0.00541 | 9.80896 | 0.30704 | 0.43677 | 0.01121 | 2478.3 | 82.7 | 2417.0 | 75.7 | 2336.1 | 59.9 |
| WMS01_2_93 | 0.16495 | 0.00489 | 10.08493 | 0.29340 | 0.43771 | 0.00970 | 2506.3 | 74.2 | 2442.6 | 71.1 | 2340.4 | 51.9 |
| WMS01_2_94 | 0.06342 | 0.00240 | 1.11913 | 0.04172 | 0.12908 | 0.00399 | 721.4 | 27.3 | 762.6 | 28.4 | 782.6 | 24.2 |
| WMS01_2_95 | 0.10744 | 0.00391 | 2.22915 | 0.14177 | 0.14919 | 0.00711 | 1755.7 | 63.8 | 1190.3 | 75.7 | 896.4 | 42.7 |
| WMS01_2_96 | 0.06490 | 0.00255 | 1.09855 | 0.04499 | 0.12257 | 0.00300 | 770.2 | 30.3 | 752.7 | 30.8 | 745.3 | 18.2 |
| WMS01_2_97 | 0.15249 | 0.00604 | 9.93225 | 0.40890 | 0.47238 | 0.01052 | 2373.2 | 94.0 | 2428.5 | 100.0 | 2494.0 | 55.5 |
| WMS01_2_98 | 0.07654 | 0.00306 | 1.28510 | 0.05942 | 0.12191 | 0.00446 | 1108.3 | 44.4 | 839.1 | 38.8 | 741.5 | 27.1 |
| WMS01_2_99 | 0.06679 | 0.00236 | 1.15886 | 0.03726 | 0.12612 | 0.00265 | 830.2 | 29.4 | 781.4 | 25.1 | 765.7 | 16.1 |
| WMS01_2_100 | 0.06622 | 0.00231 | 1.19269 | 0.03909 | 0.12873 | 0.00265 | 812.5 | 28.3 | 797.2 | 26.1 | 780.6 | 16.1 |
| WMS01_2_101 | 0.06367 | 0.00280 | 1.13541 | 0.04525 | 0.12909 | 0.00338 | 729.8 | 32.1 | 770.3 | 30.7 | 782.7 | 20.5 |
| WMS01_2_102 | 0.06619 | 0.00373 | 0.95850 | 0.05589 | 0.10516 | 0.00538 | 811.3 | 45.7 | 682.5 | 39.8 | 644.6 | 33.0 |
| WMS01_2_103 | 0.06304 | 0.00269 | 1.15768 | 0.06212 | 0.13264 | 0.00316 | 708.6 | 30.3 | 780.9 | 41.9 | 802.9 | 19.1 |
| WMS01_2_104 | 0.06579 | 0.00209 | 1.12657 | 0.03564 | 0.12387 | 0.00249 | 798.9 | 25.3 | 766.1 | 24.2 | 752.8 | 15.2 |
| WMS01_2_105 | 0.06565 | 0.00235 | 1.11864 | 0.03539 | 0.12395 | 0.00305 | 794.2 | 28.4 | 762.3 | 24.1 | 753.3 | 18.6 |
| WMS01_2_106 | 0.07316 | 0.00459 | 1.28262 | 0.06001 | 0.12701 | 0.00651 | 1017.5 | 63.8 | 838.0 | 39.2 | 770.8 | 39.5 |
| WMS01_2_107 | 0.06373 | 0.00284 | 0.99845 | 0.04270 | 0.11448 | 0.00290 | 731.9 | 32.6 | 703.0 | 30.1 | 698.7 | 17.7 |
| WMS01_2_108 | 0.15581 | 0.00522 | 8.57096 | 0.29159 | 0.39870 | 0.00722 | 2410.0 | 80.8 | 2293.5 | 78.0 | 2163.1 | 39.2 |
| WMS01_2_109 | 0.06862 | 0.00374 | 1.13971 | 0.05932 | 0.12088 | 0.00312 | 886.5 | 48.3 | 772.4 | 40.2 | 735.6 | 19.0 |
| WMS01_2_110 | 0.06431 | 0.00247 | 1.09158 | 0.03619 | 0.12361 | 0.00284 | 750.8 | 28.8 | 749.3 | 24.8 | 751.3 | 17.2 |
| WMS01_2_111 | 0.16990 | 0.00507 | 10.43940 | 0.30896 | 0.44528 | 0.00928 | 2555.9 | 76.3 | 2474.6 | 73.2 | 2374.2 | 49.5 |
| WMS01_2_112 | 0.06281 | 0.00357 | 0.88992 | 0.06116 | 0.10292 | 0.00362 | 700.9 | 39.8 | 646.3 | 44.4 | 631.5 | 22.2 |
| WMS01_2_113 | 0.06020 | 0.00303 | 1.07854 | 0.05511 | 0.13024 | 0.00326 | 609.9 | 30.6 | 742.9 | 38.0 | 789.2 | 19.7 |
| WMS01_2_114 | 0.06767 | 0.00333 | 1.28424 | 0.13349 | 0.13880 | 0.00703 | 857.6 | 42.3 | 838.7 | 87.2 | 837.9 | 42.4 |
| WMS01_2_115 | 0.11750 | 0.00435 | 2.30052 | 0.11090 | 0.14217 | 0.00518 | 1917.8 | 71.1 | 1212.4 | 58.4 | 856.9 | 31.2 |
| WMS01_2_116 | 0.16184 | 0.00519 | 10.86716 | 0.39708 | 0.48902 | 0.01200 | 2474.2 | 79.4 | 2511.8 | 91.8 | 2566.4 | 63.0 |
| WMS01_2_117 | 0.18302 | 0.00775 | 7.84780 | 0.45115 | 0.31102 | 0.01961 | 2679.7 | 113.5 | 2213.7 | 127.3 | 1745.7 | 110.1 |
| WMS01_2_118 | 0.06892 | 0.00212 | 1.21465 | 0.04007 | 0.12824 | 0.00309 | 895.3 | 27.5 | 807.3 | 26.6 | 777.8 | 18.8 |
| WMS01_2_119 | 0.14376 | 0.00577 | 5.39818 | 0.21529 | 0.27387 | 0.00942 | 2272.2 | 91.1 | 1884.6 | 75.2 | 1560.4 | 53.7 |
| WMS01_2_120 | 0.06878 | 0.00358 | 1.16653 | 0.06893 | 0.12306 | 0.00289 | 891.2 | 46.3 | 785.0 | 46.4 | 748.2 | 17.5 |
| WMS01_2_121 | 0.06412 | 0.00395 | 1.11029 | 0.06768 | 0.12711 | 0.00417 | 744.8 | 45.9 | 758.3 | 46.2 | 771.3 | 25.3 |
| WMS01_2_122 | 0.15965 | 0.00637 | 10.68165 | 0.42639 | 0.48689 | 0.01000 | 2451.2 | 97.8 | 2495.8 | 99.6 | 2557.2 | 52.5 |
| WMS01_2_123 | 0.06514 | 0.00251 | 1.15416 | 0.04299 | 0.12825 | 0.00228 | 777.8 | 30.0 | 779.2 | 29.0 | 777.8 | 13.9 |
| WMS01_2_124 | 0.16306 | 0.00561 | 10.37468 | 0.37759 | 0.46219 | 0.00914 | 2486.9 | 85.6 | 2468.8 | 89.9 | 2449.2 | 48.5 |
| WMS01_2_125 | 0.06589 | 0.00426 | 1.22468 | 0.09373 | 0.13437 | 0.00411 | 802.0 | 51.9 | 811.9 | 62.1 | 812.7 | 24.9 |
| WMS01_2_126 | 0.06639 | 0.00267 | 1.18944 | 0.04159 | 0.13001 | 0.00318 | 817.7 | 32.9 | 795.7 | 27.8 | 787.9 | 19.3 |
| WMS01_2_127 | 0.15794 | 0.00482 | 11.07452 | 0.41588 | 0.51239 | 0.01392 | 2433.0 | 74.2 | 2529.4 | 95.0 | 2666.8 | 72.5 |
| WMS01_2_128 | 0.06207 | 0.00225 | 1.01431 | 0.03958 | 0.11837 | 0.00278 | 675.6 | 24.5 | 711.0 | 27.7 | 721.2 | 17.0 |
| WMS01_2_129 | 0.17126 | 0.00686 | 10.37336 | 0.37922 | 0.44009 | 0.01565 | 2569.3 | 102.9 | 2468.7 | 90.2 | 2351.0 | 83.6 |
| WMS01_2_130 | 0.06855 | 0.00301 | 1.27289 | 0.06010 | 0.13362 | 0.00339 | 884.4 | 38.8 | 833.7 | 39.4 | 808.5 | 20.5 |
| WMS01_2_131 | 0.06232 | 0.00213 | 1.17047 | 0.03983 | 0.13666 | 0.00465 | 684.0 | 23.4 | 786.9 | 26.8 | 825.8 | 28.1 |
| WMS01_2_132 | 0.06164 | 0.00321 | 1.08640 | 0.05052 | 0.12763 | 0.00373 | 660.7 | 34.4 | 746.8 | 34.7 | 774.3 | 22.6 |
| WMS01_2_133 | 0.17072 | 0.00836 | 10.10581 | 0.60770 | 0.43052 | 0.02087 | 2564.0 | 125.5 | 2444.5 | 147.0 | 2308.1 | 111.9 |
| WMS01_2_134 | 0.06479 | 0.00326 | 1.20017 | 0.07188 | 0.13532 | 0.00748 | 766.7 | 38.6 | 800.7 | 48.0 | 818.2 | 45.2 |
| WMS01_2_134a | 0.14949 | 0.00669 | 9.93046 | 0.55133 | 0.47979 | 0.02231 | 2339.4 | 104.6 | 2428.3 | 134.8 | 2526.3 | 117.5 |
| WMS01_2_135 | 0.15123 | 0.01247 | 7.73887 | 0.50261 | 0.37202 | 0.02256 | 2359.1 | 194.6 | 2201.1 | 143.0 | 2038.9 | 123.7 |
| WMS01_2_136 | 0.06335 | 0.00251 | 1.13943 | 0.05643 | 0.12948 | 0.00420 | 719.0 | 28.5 | 772.2 | 38.2 | 784.9 | 25.5 |
| WMS01_2_137 | 0.17906 | 0.00867 | 12.34704 | 0.70131 | 0.49858 | 0.02455 | 2643.5 | 128.0 | 2631.2 | 149.4 | 2607.7 | 128.4 |
| WMS01_2_138 | 0.15481 | 0.00449 | 9.96358 | 0.31003 | 0.46642 | 0.00888 | 2399.0 | 69.6 | 2431.4 | 75.7 | 2467.8 | 47.0 |
| WMS01_2_139 | 0.06231 | 0.00318 | 1.13346 | 0.06044 | 0.13229 | 0.00317 | 683.7 | 34.8 | 769.4 | 41.0 | 800.9 | 19.2 |
| WMS01_2_140 | 0.15586 | 0.00610 | 10.36561 | 0.38285 | 0.48316 | 0.01251 | 2410.4 | 94.3 | 2468.0 | 91.2 | 2541.0 | 65.8 |
| WMS01_2_141 | 0.13324 | 0.01239 | 1.53631 | 0.09498 | 0.08435 | 0.00543 | 2140.3 | 199.0 | 945.0 | 58.4 | 522.1 | 33.6 |
| WMS01_2_142 | 0.16774 | 0.00485 | 9.20867 | 0.30400 | 0.39843 | 0.01080 | 2534.5 | 73.3 | 2359.0 | 77.9 | 2161.8 | 58.6 |
| WMS01_2_143 | 0.05368 | 0.00214 | 0.77323 | 0.03616 | 0.10405 | 0.00319 | 356.5 | 14.2 | 581.6 | 27.2 | 638.1 | 19.6 |
| WMS01_2_144 | 0.15465 | 0.00575 | 10.65365 | 0.42514 | 0.49702 | 0.01505 | 2397.2 | 89.1 | 2493.4 | 99.5 | 2601.0 | 78.8 |
| WMS01_2_145 | 0.08825 | 0.00633 | 1.60718 | 0.11755 | 0.13213 | 0.00786 | 1387.0 | 99.5 | 973.0 | 71.2 | 800.0 | 47.6 |
| 09_2 (19°43'32,53"S , 44°57'38,48"E) | | | | | | | | | | | | |
| WMS09_2_1 | 0.24725 | 0.00699 | 16.99658 | 0.75322 | 0.50559 | 0.02117 | 3166.6 | 89.6 | 2934.6 | 130.1 | 2637.8 | 110.4 |
| WMS09_2_2 | 0.07193 | 0.00405 | 1.20601 | 0.07716 | 0.12208 | 0.00518 | 983.2 | 55.4 | 803.4 | 51.4 | 742.5 | 31.5 |
| WMS09_2_3 | 0.06077 | 0.00283 | 0.81058 | 0.04074 | 0.09676 | 0.00258 | 630.1 | 29.4 | 602.8 | 30.3 | 595.4 | 15.9 |
| WMS09_2_4 | 0.06010 | 0.00379 | 0.77692 | 0.03170 | 0.09413 | 0.00340 | 606.2 | 38.2 | 583.7 | 23.8 | 579.9 | 20.9 |
| WMS09_2_5 | 0.06857 | 0.00227 | 1.36941 | 0.04694 | 0.14554 | 0.00507 | 884.8 | 29.3 | 875.9 | 30.0 | 875.9 | 30.5 |
| WMS09_2_6 | 0.09684 | 0.00435 | 2.57826 | 0.12404 | 0.19299 | 0.00554 | 1563.4 | 70.2 | 1294.5 | 62.3 | 1137.5 | 32.7 |

| sample | $^{207}Pb^*/^{206}Pb^*$ | | $^{207}Pb^*/^{235}U$ | | $^{206}Pb^*/^{238}U$ | | $^{207}Pb/^{206}Pb$ | | $^{207}Pb/^{235}U$ | | $^{206}Pb/^{238}U$ | |
|---|---|---|---|---|---|---|---|---|---|---|---|---|
| | value | 1 s.e | value | 1 s.e | value | 1 s.e | age (Ma) | 1 s.e | age (Ma) | 1 s.e | age (Ma) | 1 s.e |
| WMS09_2_7 | 0.05339 | 0.00319 | 0.76743 | 0.03766 | 0.10484 | 0.00355 | 344.5 | 20.6 | 578.3 | 28.4 | 642.7 | 21.8 |
| WMS09_2_8 | 0.25217 | 0.01193 | 11.60970 | 0.63185 | 0.33762 | 0.01678 | 3197.8 | 151.3 | 2573.5 | 140.1 | 1875.2 | 93.2 |
| WMS09_2_9 | 0.06499 | 0.00224 | 1.21483 | 0.04734 | 0.13574 | 0.00373 | 773.1 | 26.7 | 807.4 | 31.5 | 820.5 | 22.6 |
| WMS09_2_10 | 0.10565 | 0.00380 | 4.20755 | 0.22535 | 0.29001 | 0.01285 | 1724.8 | 62.0 | 1675.5 | 89.7 | 1641.6 | 72.8 |
| WMS09_2_11 | 0.06982 | 0.00332 | 1.20588 | 0.06352 | 0.12576 | 0.00539 | 922.0 | 43.9 | 803.3 | 42.3 | 763.6 | 32.7 |
| WMS09_2_12 | 0.26993 | 0.01064 | 24.53883 | 0.99472 | 0.66489 | 0.03052 | 3304.9 | 130.3 | 3290.0 | 133.4 | 3286.1 | 150.9 |
| WMS09_2_13 | 0.06667 | 0.00449 | 1.18560 | 0.07080 | 0.12907 | 0.00481 | 826.5 | 55.7 | 793.9 | 47.4 | 782.6 | 29.2 |
| WMS09_2_14 | 0.23931 | 0.00905 | 6.16890 | 0.36611 | 0.18963 | 0.01096 | 3114.7 | 117.8 | 2000.1 | 118.7 | 1119.3 | 64.7 |
| WMS09_2_15 | 0.05990 | 0.00219 | 0.81630 | 0.03041 | 0.09861 | 0.00304 | 598.9 | 21.9 | 606.0 | 22.6 | 606.3 | 18.7 |
| WMS09_2_16 | 0.06910 | 0.00351 | 0.57918 | 0.03518 | 0.06155 | 0.00403 | 900.7 | 45.8 | 463.9 | 28.2 | 385.0 | 25.2 |
| WMS09_2_17 | 0.05769 | 0.00205 | 0.76172 | 0.02705 | 0.09597 | 0.00182 | 517.2 | 18.4 | 575.0 | 20.4 | 590.7 | 11.2 |
| WMS09_2_18 | 0.05897 | 0.00286 | 0.75424 | 0.03260 | 0.09317 | 0.00216 | 564.9 | 27.4 | 570.7 | 24.7 | 574.3 | 13.3 |
| WMS09_2_19 | 0.12842 | 0.00400 | 5.86124 | 0.22686 | 0.32884 | 0.01029 | 2075.7 | 64.7 | 1955.5 | 75.7 | 1832.8 | 57.4 |
| WMS09_2_20 | 0.05964 | 0.00252 | 0.82341 | 0.03425 | 0.10020 | 0.00163 | 589.5 | 24.9 | 609.9 | 25.4 | 615.6 | 10.0 |
| WMS09_2_21 | 0.08237 | 0.00354 | 1.18775 | 0.07976 | 0.10499 | 0.00508 | 1253.6 | 53.9 | 794.9 | 53.4 | 643.6 | 31.2 |
| WMS09_2_22 | 0.06301 | 0.00201 | 1.06670 | 0.03851 | 0.12290 | 0.00314 | 707.6 | 22.6 | 737.1 | 26.6 | 747.2 | 19.1 |
| WMS09_2_23 | 0.28845 | 0.01009 | 18.30515 | 1.46319 | 0.46448 | 0.03106 | 3408.6 | 119.3 | 3005.9 | 240.3 | 2459.3 | 164.5 |
| WMS09_2_24 | 0.12566 | 0.00539 | 5.27199 | 0.27586 | 0.30471 | 0.01354 | 2037.4 | 87.4 | 1864.3 | 97.6 | 1714.6 | 76.2 |
| WMS09_2_25 | 0.05983 | 0.00263 | 0.75530 | 0.03362 | 0.09170 | 0.00211 | 596.4 | 26.2 | 571.3 | 25.4 | 565.6 | 13.0 |
| WMS09_2_26 | 0.06095 | 0.00351 | 0.83443 | 0.04639 | 0.09991 | 0.00431 | 636.4 | 36.6 | 616.1 | 34.2 | 613.9 | 26.5 |
| WMS09_2_27 | 0.12453 | 0.00380 | 5.16414 | 0.20973 | 0.30126 | 0.00969 | 2021.4 | 61.7 | 1846.7 | 75.0 | 1697.5 | 54.6 |
| WMS09_2_28 | 0.06120 | 0.00217 | 0.80986 | 0.02824 | 0.09600 | 0.00239 | 645.5 | 22.9 | 602.4 | 21.0 | 590.9 | 14.7 |
| WMS09_2_29 | 0.08060 | 0.00357 | 0.56128 | 0.02460 | 0.05110 | 0.00239 | 1210.8 | 53.6 | 452.4 | 19.8 | 321.3 | 15.0 |
| WMS09_2_30 | 0.06761 | 0.00427 | 0.81273 | 0.05027 | 0.08693 | 0.00228 | 855.6 | 54.0 | 604.0 | 37.4 | 537.3 | 14.1 |
| WMS09_2_31 | 0.16352 | 0.00590 | 10.45426 | 0.29514 | 0.46397 | 0.01022 | 2491.6 | 89.9 | 2475.9 | 69.9 | 2457.1 | 54.1 |
| WMS09_2_32 | 0.05675 | 0.00214 | 0.71028 | 0.02568 | 0.09093 | 0.00254 | 480.7 | 18.1 | 544.9 | 19.7 | 561.0 | 15.7 |
| WMS09_2_33 | 0.06577 | 0.00259 | 1.40900 | 0.04626 | 0.15566 | 0.00427 | 798.0 | 31.4 | 892.7 | 29.3 | 932.6 | 25.6 |
| WMS09_2_34 | 0.14080 | 0.00465 | 4.39220 | 0.16488 | 0.22538 | 0.00690 | 2236.3 | 73.8 | 1710.9 | 64.2 | 1310.2 | 40.1 |
| WMS09_2_35 | 0.05680 | 0.00276 | 0.73801 | 0.03369 | 0.09421 | 0.00327 | 482.9 | 23.4 | 561.2 | 25.6 | 580.4 | 20.1 |
| WMS09_2_36 | 0.15162 | 0.00604 | 6.85663 | 0.30052 | 0.32815 | 0.01393 | 2363.5 | 94.2 | 2093.1 | 91.7 | 1829.4 | 77.6 |
| WMS09_2_37 | 0.05816 | 0.00213 | 0.74169 | 0.02941 | 0.09206 | 0.00233 | 534.9 | 19.6 | 563.4 | 22.3 | 567.7 | 14.4 |
| WMS09_2_38 | 0.24844 | 0.01141 | 17.64093 | 0.79884 | 0.51365 | 0.02150 | 3174.1 | 145.7 | 2970.4 | 134.5 | 2672.2 | 111.8 |
| WMS09_2_39 | 0.06618 | 0.00297 | 0.77407 | 0.02942 | 0.08436 | 0.00322 | 811.1 | 36.4 | 582.1 | 22.1 | 522.1 | 19.9 |
| WMS09_2_40 | 0.24566 | 0.01318 | 19.22223 | 0.91410 | 0.56896 | 0.02540 | 3156.3 | 169.3 | 3053.0 | 145.2 | 2903.5 | 129.6 |
| WMS09_2_41 | 0.11218 | 0.00401 | 3.70663 | 0.13027 | 0.23945 | 0.00501 | 1834.3 | 65.5 | 1572.8 | 55.3 | 1383.8 | 28.9 |
| WMS09_2_42 | 0.06649 | 0.00359 | 1.16238 | 0.06090 | 0.12693 | 0.00280 | 820.9 | 44.3 | 783.1 | 41.0 | 770.3 | 17.0 |
| WMS09_2_43 | 0.06975 | 0.00302 | 1.09437 | 0.04444 | 0.11376 | 0.00484 | 920.0 | 39.8 | 750.6 | 30.5 | 694.5 | 29.5 |
| WMS09_2_44 | 0.06021 | 0.00240 | 0.75054 | 0.02790 | 0.09072 | 0.00263 | 610.2 | 24.4 | 568.5 | 21.1 | 559.8 | 16.2 |
| WMS09_2_45 | 0.09256 | 0.00448 | 0.57113 | 0.03074 | 0.04503 | 0.00238 | 1478.0 | 71.6 | 458.7 | 24.7 | 284.0 | 15.0 |
| WMS09_2_46 | 0.16146 | 0.00511 | 8.82581 | 0.30617 | 0.39668 | 0.00883 | 2470.2 | 78.2 | 2320.2 | 80.5 | 2153.7 | 48.0 |
| WMS09_2_47 | 0.11235 | 0.00438 | 4.19041 | 0.19889 | 0.27085 | 0.00937 | 1836.9 | 71.6 | 1672.1 | 79.4 | 1545.1 | 53.5 |
| WMS09_2_48 | 0.06064 | 0.00253 | 0.76336 | 0.03320 | 0.09122 | 0.00235 | 625.6 | 26.1 | 575.9 | 25.0 | 562.7 | 14.5 |
| WMS09_2_49 | 0.16842 | 0.00522 | 8.34118 | 0.32711 | 0.35885 | 0.01109 | 2541.2 | 78.7 | 2268.8 | 89.0 | 1976.7 | 61.1 |
| WMS09_2_50 | 0.06063 | 0.00243 | 0.74111 | 0.02599 | 0.08868 | 0.00240 | 625.1 | 25.1 | 563.1 | 19.7 | 547.7 | 14.8 |
| WMS09_2_51 | 0.06540 | 0.00281 | 0.82666 | 0.03466 | 0.09210 | 0.00291 | 786.3 | 33.8 | 611.8 | 25.7 | 567.9 | 18.0 |
| WMS09_2_52 | 0.11369 | 0.00383 | 5.08461 | 0.16123 | 0.32426 | 0.01010 | 1858.4 | 62.7 | 1833.5 | 58.1 | 1810.5 | 56.4 |
| WMS09_2_53 | 0.05454 | 0.00296 | 0.77722 | 0.03987 | 0.10266 | 0.00371 | 392.5 | 21.3 | 583.9 | 30.0 | 630.0 | 22.8 |
| WMS09_2_54 | 0.10129 | 0.00500 | 1.43366 | 0.07108 | 0.10322 | 0.00336 | 1647.1 | 81.2 | 903.1 | 44.8 | 633.2 | 20.6 |
| WMS09_2_55 | 0.06807 | 0.00262 | 1.20424 | 0.05035 | 0.12804 | 0.00259 | 869.8 | 33.5 | 802.5 | 33.6 | 776.7 | 15.7 |
| WMS09_2_56 | 0.06535 | 0.00512 | 1.07302 | 0.08373 | 0.11878 | 0.00469 | 784.6 | 61.5 | 740.2 | 57.8 | 723.5 | 28.6 |
| WMS09_2_57 | 0.12332 | 0.00554 | 5.12137 | 0.32398 | 0.30116 | 0.01478 | 2004.1 | 90.1 | 1839.7 | 116.4 | 1697.1 | 83.3 |
| WMS09_2_58 | 0.08910 | 0.00458 | 1.23477 | 0.06237 | 0.10042 | 0.00190 | 1405.4 | 72.3 | 816.5 | 41.2 | 616.9 | 11.7 |
| WMS09_2_59 | 0.06253 | 0.00271 | 0.80641 | 0.03494 | 0.09366 | 0.00189 | 691.2 | 30.0 | 600.4 | 26.0 | 577.1 | 11.6 |
| WMS09_2_60 | 0.06183 | 0.00236 | 0.80571 | 0.02943 | 0.09388 | 0.00311 | 667.2 | 25.5 | 600.0 | 21.9 | 578.5 | 19.2 |
| WMS09_2_61 | 0.06769 | 0.00353 | 0.92029 | 0.04505 | 0.09867 | 0.00274 | 858.2 | 44.8 | 662.5 | 32.4 | 606.6 | 16.9 |
| WMS09_2_62 | 0.08148 | 0.00320 | 1.98824 | 0.07436 | 0.17727 | 0.00417 | 1232.3 | 48.4 | 1111.5 | 41.6 | 1052.0 | 24.8 |
| WMS09_2_63 | 0.06252 | 0.00278 | 0.77336 | 0.03324 | 0.08976 | 0.00175 | 690.8 | 30.7 | 581.7 | 25.0 | 554.1 | 10.8 |
| WMS09_2_64 | 0.10188 | 0.00372 | 3.27659 | 0.13381 | 0.23321 | 0.00851 | 1657.8 | 60.6 | 1475.5 | 60.3 | 1351.3 | 49.3 |
| WMS09_2_65 | 0.06754 | 0.00252 | 1.17474 | 0.04453 | 0.12583 | 0.00313 | 853.6 | 31.8 | 788.9 | 29.9 | 764.0 | 19.0 |
| WMS09_2_66 | 0.06340 | 0.00298 | 1.23201 | 0.04336 | 0.14074 | 0.00543 | 720.6 | 33.9 | 815.3 | 28.7 | 848.8 | 32.8 |
| WMS09_2_67 | 0.17681 | 0.00482 | 12.51219 | 0.39637 | 0.51492 | 0.01158 | 2622.5 | 71.4 | 2643.6 | 83.7 | 2677.6 | 60.2 |
| WMS09_2_68 | 0.09620 | 0.00397 | 2.95342 | 0.16255 | 0.22139 | 0.00943 | 1550.8 | 64.0 | 1395.7 | 76.8 | 1289.2 | 54.9 |
| WMS09_2_69 | 0.10439 | 0.00406 | 4.07219 | 0.14865 | 0.28376 | 0.00845 | 1702.8 | 66.3 | 1648.8 | 60.2 | 1610.3 | 48.0 |
| WMS09_2_70 | 0.15491 | 0.00392 | 8.15178 | 0.23392 | 0.38193 | 0.00695 | 2400.1 | 60.7 | 2248.0 | 64.5 | 2085.3 | 37.9 |
| WMS09_2_71 | 0.06585 | 0.00186 | 1.14714 | 0.03430 | 0.12634 | 0.00182 | 800.8 | 22.6 | 775.9 | 23.2 | 767.0 | 11.1 |
| WMS09_2_72 | 0.05411 | 0.00237 | 0.61902 | 0.02641 | 0.08302 | 0.00190 | 374.6 | 16.4 | 489.2 | 20.9 | 514.1 | 11.7 |
| WMS09_2_73 | 0.06056 | 0.00272 | 0.84071 | 0.03828 | 0.10084 | 0.00298 | 622.8 | 28.0 | 619.5 | 28.2 | 619.4 | 18.3 |
| WMS09_2_74 | 0.10462 | 0.00296 | 4.27746 | 0.12955 | 0.29682 | 0.00606 | 1706.9 | 48.3 | 1689.0 | 51.2 | 1675.5 | 34.2 |
| WMS09_2_75 | 0.06502 | 0.00299 | 0.89190 | 0.04191 | 0.09974 | 0.00189 | 773.9 | 35.6 | 647.4 | 30.4 | 612.9 | 11.6 |
| WMS09_2_76 | 0.07112 | 0.00233 | 1.62259 | 0.05727 | 0.16567 | 0.00283 | 959.9 | 31.5 | 979.0 | 34.6 | 988.2 | 16.9 |
| WMS09_2_77 | 0.12670 | 0.00488 | 3.63652 | 0.29205 | 0.21112 | 0.01515 | 2052.0 | 79.1 | 1557.6 | 125.1 | 1234.8 | 88.6 |
| WMS09_2_78 | 0.05523 | 0.00259 | 0.64688 | 0.03491 | 0.08491 | 0.00178 | 420.6 | 19.7 | 506.6 | 27.3 | 525.4 | 11.0 |
| WMS09_2_79 | 0.06630 | 0.00219 | 1.17169 | 0.04281 | 0.12820 | 0.00264 | 815.0 | 26.9 | 787.4 | 28.8 | 777.6 | 16.0 |
| WMS09_2_80 | 0.26325 | 0.01018 | 17.68225 | 1.15514 | 0.48993 | 0.02682 | 3265.5 | 126.3 | 2972.6 | 194.2 | 2570.4 | 140.7 |
| WMS09_2_81 | 0.07815 | 0.00279 | 1.80581 | 0.07404 | 0.16803 | 0.00628 | 1149.7 | 41.0 | 1047.6 | 42.9 | 1001.2 | 37.4 |
| WMS09_2_82 | 0.11294 | 0.00467 | 2.53733 | 0.11287 | 0.16323 | 0.00467 | 1846.5 | 76.4 | 1282.8 | 57.1 | 974.7 | 27.9 |
| WMS09_2_83 | 0.05948 | 0.00206 | 0.73371 | 0.02660 | 0.08927 | 0.00173 | 583.7 | 20.3 | 558.7 | 20.3 | 551.2 | 10.7 |
| WMS09_2_84 | 0.07373 | 0.00229 | 1.46293 | 0.04710 | 0.14337 | 0.00373 | 1033.1 | 32.0 | 915.2 | 29.5 | 863.7 | 22.5 |
| WMS09_2_85 | 0.06038 | 0.00207 | 0.87173 | 0.03642 | 0.10451 | 0.00254 | 616.1 | 21.2 | 636.5 | 26.6 | 640.8 | 15.6 |
| WMS09_2_86 | 0.05787 | 0.00236 | 0.71298 | 0.03270 | 0.08939 | 0.00329 | 523.8 | 21.4 | 546.5 | 25.1 | 551.9 | 20.3 |
| WMS09_2_87 | 0.11137 | 0.00450 | 4.22303 | 0.20357 | 0.27571 | 0.01141 | 1821.0 | 73.7 | 1678.5 | 80.9 | 1569.7 | 65.0 |
| WMS09_2_88 | 0.07075 | 0.00347 | 0.57364 | 0.02917 | 0.05896 | 0.00201 | 949.3 | 46.6 | 460.4 | 23.4 | 369.3 | 12.6 |
| WMS09_2_89 | 0.11741 | 0.00416 | 4.10727 | 0.13991 | 0.25413 | 0.00573 | 1916.3 | 68.0 | 1655.7 | 56.4 | 1459.7 | 32.9 |
| WMS09_2_90 | 0.24948 | 0.00803 | 21.35534 | 0.81082 | 0.62209 | 0.01797 | 3180.8 | 102.4 | 3154.9 | 119.8 | 3118.2 | 90.1 |
| WMS09_2_91 | 0.19023 | 0.00704 | 12.24811 | 0.50409 | 0.46713 | 0.01412 | 2743.4 | 101.5 | 2623.6 | 108.0 | 2470.9 | 74.7 |
| WMS09_2_92 | 0.13075 | 0.00894 | 0.33684 | 0.01916 | 0.01859 | 0.00137 | 2107.3 | 144.0 | 294.8 | 16.8 | 118.7 | 8.8 |

| sample | $^{207}Pb^{*}/^{206}Pb^{*}$ | | $^{207}Pb^{*}/^{235}U$ | | $^{206}Pb^{*}/^{238}U$ | | $^{207}Pb/^{206}Pb$ | | $^{207}Pb/^{235}U$ | | $^{206}Pb/^{238}U$ | |
|---|---|---|---|---|---|---|---|---|---|---|---|---|
| | value | 1 s.e | value | 1 s.e | value | 1 s.e | age (Ma) | 1 s.e | age (Ma) | 1 s.e | age (Ma) | 1 s.e |
| WMS09_2_93 | 0.05866 | 0.00276 | 0.74615 | 0.03220 | 0.09252 | 0.00408 | 553.4 | 26.0 | 566.0 | 24.4 | 570.4 | 25.2 |
| WMS09_2_94 | 0.10775 | 0.00317 | 1.02067 | 0.04716 | 0.06884 | 0.00292 | 1761.0 | 51.8 | 714.3 | 33.0 | 429.1 | 18.2 |
| WMS09_2_95 | 0.08667 | 0.00433 | 0.56105 | 0.02647 | 0.04722 | 0.00337 | 1352.4 | 67.6 | 452.2 | 21.3 | 297.4 | 21.2 |
| WMS09_2_96 | 0.15496 | 0.00517 | 7.90675 | 0.34013 | 0.36728 | 0.01338 | 2400.7 | 80.1 | 2220.4 | 95.5 | 2016.6 | 73.4 |
| WMS09_2_97 | 0.06993 | 0.00392 | 1.47135 | 0.08069 | 0.15274 | 0.00365 | 925.3 | 51.9 | 918.7 | 50.4 | 916.3 | 21.9 |
| WMS09_2_98 | 0.16924 | 0.00504 | 9.96547 | 0.28167 | 0.42685 | 0.00957 | 2549.4 | 75.9 | 2431.6 | 68.7 | 2291.5 | 51.4 |
| WMS09_2_99 | 0.11319 | 0.00444 | 4.62781 | 0.16092 | 0.29660 | 0.01079 | 1850.4 | 72.6 | 1754.3 | 61.0 | 1674.4 | 60.9 |
| WMS09_2_100 | 0.05442 | 0.00305 | 0.63316 | 0.03708 | 0.08447 | 0.00315 | 387.3 | 21.7 | 498.1 | 29.2 | 522.8 | 19.5 |
| WMS09_2_101 | 0.05979 | 0.00250 | 0.70535 | 0.02533 | 0.08555 | 0.00249 | 595.1 | 24.9 | 542.0 | 19.5 | 529.2 | 15.4 |
| WMS09_2_102 | 0.06188 | 0.00206 | 0.79461 | 0.02727 | 0.09310 | 0.00125 | 668.9 | 22.2 | 593.8 | 20.4 | 573.8 | 7.7 |
| WMS09_2_103 | 0.06567 | 0.00300 | 0.95424 | 0.05072 | 0.10487 | 0.00279 | 795.0 | 36.3 | 680.3 | 36.2 | 642.9 | 17.1 |
| WMS09_2_104 | 0.11173 | 0.00284 | 4.36571 | 0.12373 | 0.28433 | 0.00461 | 1826.9 | 46.4 | 1705.9 | 48.3 | 1613.1 | 26.1 |
| WMS09_2_105 | 0.06947 | 0.00270 | 1.31128 | 0.05247 | 0.13723 | 0.00217 | 912.0 | 35.4 | 850.7 | 34.0 | 829.0 | 13.1 |
| WMS09_2_106 | 0.06000 | 0.00241 | 0.71513 | 0.02871 | 0.08650 | 0.00155 | 602.6 | 24.2 | 547.8 | 22.0 | 534.8 | 9.6 |
| WMS09_2_107 | 0.05794 | 0.00209 | 0.69991 | 0.02547 | 0.08755 | 0.00189 | 526.6 | 19.0 | 538.7 | 19.6 | 541.0 | 11.7 |
| WMS09_2_108 | 0.16715 | 0.00517 | 9.47447 | 0.31318 | 0.41041 | 0.01324 | 2528.6 | 78.2 | 2385.1 | 78.8 | 2216.8 | 71.5 |
| WMS09_2_109 | 0.06943 | 0.00259 | 1.37117 | 0.05031 | 0.14366 | 0.00357 | 910.5 | 34.0 | 876.7 | 32.2 | 865.3 | 21.5 |
| WMS09_2_110 | 0.48603 | 0.08421 | 11.20140 | 2.94900 | 0.16625 | 0.02526 | 4198.7 | 727.5 | 2540.0 | 668.7 | 991.4 | 150.6 |
| WMS09_2_111 | 0.09642 | 0.00360 | 2.20269 | 0.10456 | 0.16581 | 0.00498 | 1555.1 | 58.1 | 1181.9 | 56.1 | 989.0 | 29.7 |
| WMS09_2_112 | 0.12089 | 0.00591 | 2.65626 | 0.15739 | 0.15864 | 0.00820 | 1968.6 | 96.2 | 1316.4 | 78.0 | 949.2 | 49.1 |
| WMS09_2_113 | 0.06252 | 0.00307 | 0.79716 | 0.03667 | 0.09263 | 0.00342 | 691.1 | 33.9 | 595.2 | 27.4 | 571.1 | 21.1 |
| WMS09_2_114 | 0.24466 | 0.00770 | 22.85435 | 0.79755 | 0.67787 | 0.01473 | 3149.8 | 99.1 | 3220.8 | 112.4 | 3336.2 | 72.5 |
| WMS09_2_115 | 0.05771 | 0.00248 | 0.72861 | 0.03016 | 0.09140 | 0.00259 | 517.9 | 22.3 | 555.7 | 23.0 | 563.8 | 15.9 |
| WMS09_2_116 | 0.06202 | 0.00269 | 0.89761 | 0.04061 | 0.10512 | 0.00186 | 673.7 | 29.2 | 650.5 | 29.4 | 644.3 | 11.4 |
| WMS09_2_117 | 0.18565 | 0.00890 | 6.40482 | 0.31775 | 0.24955 | 0.00871 | 2703.3 | 129.6 | 2032.9 | 100.9 | 1436.2 | 50.1 |
| WMS09_2_118 | 0.10394 | 0.00426 | 4.99129 | 0.20285 | 0.34905 | 0.01036 | 1694.8 | 69.5 | 1817.8 | 73.9 | 1930.0 | 57.3 |
| WMS09_2_119 | 0.12618 | 0.00542 | 4.60087 | 0.21164 | 0.26300 | 0.01153 | 2044.6 | 87.8 | 1749.4 | 80.5 | 1505.2 | 66.0 |
| WMS09_2_120 | 0.05571 | 0.00252 | 0.66155 | 0.03013 | 0.08634 | 0.00220 | 439.8 | 19.9 | 515.6 | 23.5 | 533.9 | 13.6 |
| WMS09_2_121 | 0.10666 | 0.00633 | 2.37314 | 0.15693 | 0.16321 | 0.00823 | 1742.2 | 103.4 | 1234.5 | 81.6 | 974.6 | 49.1 |
| WMS09_2_122 | 0.12837 | 0.00454 | 6.21846 | 0.28869 | 0.35154 | 0.01170 | 2075.0 | 73.5 | 2007.0 | 93.2 | 1941.9 | 64.6 |
| WMS09_2_123 | 0.05669 | 0.00245 | 0.67302 | 0.03087 | 0.08634 | 0.00133 | 478.7 | 20.7 | 522.5 | 24.0 | 533.9 | 8.2 |
| WMS09_2_124 | 0.06235 | 0.00210 | 1.08510 | 0.03915 | 0.12642 | 0.00262 | 685.3 | 23.0 | 746.1 | 26.9 | 767.4 | 15.9 |
| WMS09_2_125 | 0.12296 | 0.00689 | 4.50660 | 0.26183 | 0.26578 | 0.01649 | 1998.8 | 112.1 | 1732.2 | 100.6 | 1519.3 | 94.2 |
| WMS09_2_126 | 0.14783 | 0.00773 | 8.59717 | 0.49579 | 0.42208 | 0.01991 | 2320.2 | 121.4 | 2296.3 | 132.4 | 2269.9 | 107.0 |
| WMS09_2_127 | 0.06257 | 0.00366 | 1.11260 | 0.05697 | 0.12883 | 0.00547 | 692.5 | 40.5 | 759.4 | 38.9 | 781.2 | 33.2 |
| WMS09_2_128 | 0.06185 | 0.00216 | 1.08318 | 0.04732 | 0.12690 | 0.00342 | 668.0 | 23.3 | 745.2 | 32.6 | 770.2 | 20.8 |
| WMS09_2_129 | 0.15980 | 0.00840 | 3.13510 | 0.18523 | 0.14251 | 0.00883 | 2452.8 | 128.9 | 1441.3 | 85.2 | 858.8 | 53.2 |
| WMS09_2_130 | 0.05665 | 0.00299 | 0.70866 | 0.04035 | 0.09110 | 0.00435 | 476.9 | 25.1 | 543.9 | 31.0 | 562.0 | 26.9 |
| WMS09_2_131 | 0.10172 | 0.00384 | 2.70226 | 0.12640 | 0.19188 | 0.00703 | 1655.0 | 62.5 | 1329.1 | 62.2 | 1131.6 | 41.5 |
| WMS09_2_132 | 0.08885 | 0.00332 | 0.87230 | 0.07875 | 0.07031 | 0.00503 | 1400.1 | 52.3 | 636.8 | 57.5 | 438.0 | 31.3 |
| WMS09_2_133 | 0.15178 | 0.00390 | 8.51883 | 0.23234 | 0.40745 | 0.00909 | 2365.3 | 60.9 | 2287.9 | 62.4 | 2203.3 | 49.2 |
| WMS09_2_134 | 0.05533 | 0.00216 | 0.63675 | 0.02503 | 0.08348 | 0.00147 | 424.5 | 16.6 | 500.3 | 19.7 | 516.8 | 9.1 |
| WMS09_2_135 | 0.05543 | 0.00256 | 0.67716 | 0.03060 | 0.08859 | 0.00115 | 428.4 | 19.8 | 525.1 | 23.7 | 547.2 | 7.1 |
| WMS09_2_136 | 0.05503 | 0.00261 | 0.65374 | 0.02918 | 0.08630 | 0.00127 | 412.3 | 19.5 | 510.8 | 22.8 | 533.6 | 7.8 |
| WMS09_2_137 | 0.06695 | 0.00245 | 1.08892 | 0.04192 | 0.11843 | 0.00194 | 835.3 | 30.5 | 748.0 | 28.8 | 721.5 | 11.8 |
| WMS09_2_138 | 0.10699 | 0.00292 | 4.90836 | 0.15978 | 0.33187 | 0.00721 | 1748.0 | 47.7 | 1803.7 | 58.7 | 1847.5 | 40.2 |
| WMS09_2_139 | 0.05762 | 0.00138 | 0.72560 | 0.01746 | 0.09129 | 0.00128 | 514.3 | 12.3 | 554.0 | 13.3 | 563.1 | 7.9 |
| WMS09_2_140 | 0.10704 | 0.00438 | 1.41114 | 0.06960 | 0.09582 | 0.00351 | 1748.7 | 71.6 | 893.6 | 44.1 | 589.9 | 21.6 |
| WMS09_2_141 | 0.05749 | 0.00221 | 0.73083 | 0.02704 | 0.09232 | 0.00167 | 509.5 | 19.5 | 557.0 | 20.6 | 569.3 | 10.3 |
| WMS09_2_142 | 0.05882 | 0.00224 | 0.71853 | 0.02689 | 0.08884 | 0.00107 | 559.3 | 21.3 | 549.8 | 20.6 | 548.7 | 6.6 |
| WMS09_2_143 | 0.16079 | 0.00389 | 9.78431 | 0.26605 | 0.44124 | 0.00697 | 2463.3 | 59.7 | 2414.7 | 65.7 | 2356.2 | 37.2 |
| WMS09_2_144 | 0.11283 | 0.00410 | 4.30609 | 0.20622 | 0.27774 | 0.01089 | 1844.7 | 67.0 | 1694.5 | 81.1 | 1579.9 | 61.9 |
| 17_1 (19°44'22,72"S , 44°55'14,56"E) | | | | | | | | | | | | |
| WMS17_1_1 | 0.05859 | 0.00268 | 0.75311 | 0.03444 | 0.09320 | 0.00290 | 551.1 | 25.2 | 570.0 | 26.1 | 574.4 | 17.9 |
| WMS17_1_2 | 0.11491 | 0.00824 | 4.40971 | 0.24359 | 0.28088 | 0.01670 | 1877.7 | 134.6 | 1714.2 | 94.7 | 1595.8 | 94.9 |
| WMS17_1_3 | 0.05844 | 0.00185 | 0.76032 | 0.02732 | 0.09488 | 0.00246 | 545.3 | 17.2 | 574.2 | 20.6 | 584.3 | 15.1 |
| WMS17_1_4 | 0.05857 | 0.00246 | 0.86107 | 0.04141 | 0.10706 | 0.00525 | 550.2 | 23.1 | 630.7 | 30.3 | 655.6 | 32.1 |
| WMS17_1_5 | 0.16365 | 0.00585 | 8.26170 | 0.31682 | 0.36699 | 0.00871 | 2493.0 | 89.2 | 2260.1 | 86.7 | 2015.2 | 47.8 |
| WMS17_1_6 | 0.05864 | 0.00309 | 0.69820 | 0.03631 | 0.08675 | 0.00196 | 552.8 | 29.2 | 537.7 | 28.0 | 536.3 | 12.1 |
| WMS17_1_7 | 0.06426 | 0.00311 | 0.83062 | 0.03954 | 0.09387 | 0.00362 | 749.3 | 36.3 | 614.0 | 29.2 | 578.4 | 22.3 |
| WMS17_1_8 | 0.05626 | 0.00222 | 0.85791 | 0.04403 | 0.11079 | 0.00492 | 461.5 | 18.2 | 629.0 | 32.3 | 677.4 | 30.1 |
| WMS17_1_9 | 0.10933 | 0.00402 | 4.35993 | 0.19631 | 0.28968 | 0.01128 | 1787.4 | 65.8 | 1704.8 | 76.8 | 1639.9 | 63.8 |
| WMS17_1_10 | 0.05569 | 0.00201 | 0.75451 | 0.02714 | 0.09850 | 0.00272 | 439.1 | 15.8 | 570.8 | 20.5 | 605.6 | 16.7 |
| WMS17_1_11 | 0.07189 | 0.00273 | 1.50567 | 0.05784 | 0.15246 | 0.00402 | 981.9 | 37.3 | 932.7 | 35.8 | 914.7 | 24.1 |
| WMS17_1_12 | 0.05637 | 0.00231 | 0.67019 | 0.02838 | 0.08639 | 0.00245 | 466.1 | 19.1 | 520.8 | 22.1 | 534.2 | 15.2 |
| WMS17_1_13 | 0.05895 | 0.00222 | 0.75050 | 0.02949 | 0.09257 | 0.00189 | 564.3 | 21.2 | 568.5 | 22.3 | 570.7 | 11.6 |
| WMS17_1_14 | 0.16112 | 0.00589 | 9.44516 | 0.34644 | 0.42698 | 0.01311 | 2466.7 | 90.2 | 2382.2 | 87.4 | 2292.1 | 70.4 |
| WMS17_1_15 | 0.12495 | 0.00422 | 5.66690 | 0.21102 | 0.32902 | 0.01127 | 2027.3 | 68.4 | 1926.3 | 71.7 | 1833.6 | 62.8 |
| WMS17_1_16 | 0.16641 | 0.00646 | 9.58415 | 0.35472 | 0.41849 | 0.01165 | 2521.1 | 97.8 | 2395.7 | 88.7 | 2253.6 | 62.7 |
| WMS17_1_17 | 0.05784 | 0.00235 | 0.69082 | 0.02878 | 0.08681 | 0.00272 | 522.6 | 21.2 | 533.3 | 22.2 | 536.7 | 16.8 |
| WMS17_1_18 | 0.06028 | 0.00236 | 0.71851 | 0.02843 | 0.08662 | 0.00230 | 612.7 | 24.0 | 549.8 | 21.8 | 535.5 | 14.2 |
| WMS17_1_19 | 0.06058 | 0.00359 | 0.73373 | 0.04688 | 0.08806 | 0.00220 | 623.5 | 36.9 | 558.7 | 35.7 | 544.1 | 13.6 |
| WMS17_1_20 | 0.06350 | 0.00326 | 1.18400 | 0.05680 | 0.13558 | 0.00576 | 724.1 | 37.1 | 793.2 | 38.0 | 819.6 | 34.8 |
| WMS17_1_21 | 0.05659 | 0.00268 | 0.78018 | 0.03074 | 0.10024 | 0.00428 | 474.4 | 22.5 | 585.6 | 23.1 | 615.8 | 26.3 |
| WMS17_1_22 | 0.11291 | 0.00421 | 3.69350 | 0.14922 | 0.23859 | 0.00861 | 1845.9 | 68.9 | 1570.0 | 63.4 | 1379.3 | 49.8 |
| WMS17_1_23 | 0.06120 | 0.00234 | 0.83129 | 0.02807 | 0.09895 | 0.00273 | 645.3 | 24.6 | 614.3 | 20.7 | 608.2 | 16.8 |
| WMS17_1_24 | 0.05886 | 0.00337 | 0.77207 | 0.04325 | 0.09566 | 0.00256 | 560.9 | 32.2 | 581.0 | 32.5 | 588.9 | 15.7 |
| WMS17_1_25 | 0.05950 | 0.00298 | 0.82633 | 0.03400 | 0.10071 | 0.00310 | 584.5 | 29.2 | 611.6 | 25.2 | 618.6 | 19.1 |
| WMS17_1_26 | 0.13562 | 0.00430 | 6.55584 | 0.19531 | 0.35165 | 0.00970 | 2171.2 | 68.9 | 2053.4 | 61.2 | 1942.5 | 53.6 |
| WMS17_1_27 | 0.06269 | 0.00299 | 1.35597 | 0.07078 | 0.15765 | 0.00568 | 696.9 | 33.2 | 870.1 | 45.4 | 943.7 | 34.0 |
| WMS17_1_28 | 0.16392 | 0.00734 | 12.14831 | 0.50567 | 0.53800 | 0.02293 | 2495.7 | 111.7 | 2615.9 | 108.9 | 2775.1 | 118.3 |
| WMS17_1_29 | 0.06475 | 0.00291 | 1.19612 | 0.05525 | 0.13450 | 0.00403 | 765.4 | 34.4 | 798.8 | 36.9 | 813.5 | 24.4 |
| WMS17_1_30 | 0.07869 | 0.00297 | 1.81427 | 0.07483 | 0.16761 | 0.00559 | 1163.4 | 44.0 | 1050.6 | 43.3 | 998.9 | 33.3 |
| WMS17_1_31 | 0.06188 | 0.00293 | 0.82374 | 0.03768 | 0.09668 | 0.00321 | 668.9 | 31.7 | 610.1 | 27.9 | 594.9 | 19.7 |
| WMS17_1_32 | 0.08154 | 0.00626 | 1.60940 | 0.12335 | 0.14382 | 0.00428 | 1233.6 | 94.8 | 973.9 | 74.6 | 866.2 | 25.8 |
| WMS17_1_33 | 0.17061 | 0.00856 | 10.11631 | 0.52632 | 0.43163 | 0.01385 | 2562.9 | 128.6 | 2445.5 | 127.2 | 2313.0 | 74.2 |

| sample | $^{207}Pb^*/^{206}Pb^*$ | | $^{207}Pb^*/^{235}U$ | | $^{206}Pb^*/^{238}U$ | | $^{207}Pb/^{206}Pb$ | | $^{207}Pb/^{235}U$ | | $^{206}Pb/^{238}U$ | |
|---|---|---|---|---|---|---|---|---|---|---|---|---|
| | value | 1 s.e | value | 1 s.e | value | 1 s.e | age (Ma) | 1 s.e | age (Ma) | 1 s.e | age (Ma) | 1 s.e |
| WMS17_1_34 | 0.12047 | 0.00447 | 3.16252 | 0.18603 | 0.19152 | 0.00866 | 1962.3 | 72.9 | 1448.1 | 85.2 | 1129.6 | 51.1 |
| WMS17_1_35 | 0.13471 | 0.00513 | 6.02552 | 0.21447 | 0.32538 | 0.00618 | 2159.4 | 82.3 | 1979.5 | 70.5 | 1815.9 | 34.5 |
| WMS17_1_36 | 0.05979 | 0.00213 | 0.68626 | 0.02310 | 0.08330 | 0.00161 | 595.1 | 21.2 | 530.6 | 17.9 | 515.8 | 10.0 |
| WMS17_1_37 | 0.06574 | 0.00377 | 1.13709 | 0.06139 | 0.12534 | 0.00446 | 797.2 | 45.7 | 771.1 | 41.6 | 761.2 | 27.1 |
| WMS17_1_38 | 0.06496 | 0.00250 | 1.23180 | 0.04746 | 0.13737 | 0.00447 | 772.1 | 29.7 | 815.2 | 31.4 | 829.8 | 27.0 |
| WMS17_1_39 | 0.06934 | 0.00282 | 0.93070 | 0.04038 | 0.09770 | 0.00284 | 907.9 | 36.9 | 668.0 | 29.0 | 600.9 | 17.5 |
| WMS17_1_40 | 0.06910 | 0.00345 | 1.08337 | 0.05004 | 0.11404 | 0.00376 | 900.8 | 44.9 | 745.3 | 34.4 | 696.1 | 22.9 |
| WMS17_1_41 | 0.06346 | 0.00276 | 1.19138 | 0.05652 | 0.13668 | 0.00408 | 722.9 | 31.5 | 796.6 | 37.8 | 825.9 | 24.7 |
| WMS17_1_42 | < DL | 0.00056 | < DL | 49.11403 | < DL | 0.06003 | < DL | 0.0 | < DL | 0.0 | < DL | 0.0 |
| WMS17_1_43 | 0.10768 | 0.01289 | 1.18536 | 0.31718 | 0.07998 | 0.00639 | 1759.8 | 210.6 | 793.8 | 212.4 | 496.0 | 39.6 |
| WMS17_1_44 | < DL | 0.00196 | < DL | 258.52561 | < DL | 0.14034 | < DL | 0.0 | < DL | 0.0 | < DL | 0.0 |
| WMS17_1_45 | 0.06488 | 0.00227 | 1.24679 | 0.04429 | 0.13952 | 0.00429 | 769.4 | 26.9 | 822.0 | 29.2 | 842.0 | 25.9 |
| WMS17_1_46 | 0.07841 | 0.00305 | 1.83517 | 0.07240 | 0.17011 | 0.00333 | 1156.3 | 44.9 | 1058.1 | 41.7 | 1012.7 | 19.8 |
| WMS17_1_47 | 0.06548 | 0.00278 | 1.24113 | 0.05836 | 0.13737 | 0.00351 | 789.0 | 33.5 | 819.4 | 38.5 | 829.8 | 21.2 |
| WMS17_1_48 | 0.15101 | 0.00464 | 10.75814 | 0.38989 | 0.51779 | 0.01467 | 2356.6 | 72.4 | 2502.5 | 90.7 | 2689.8 | 76.2 |
| WMS17_1_49 | 0.04941 | 0.00373 | 0.64110 | 0.04724 | 0.09384 | 0.00388 | 166.2 | 12.5 | 503.0 | 37.1 | 578.2 | 23.9 |
| WMS17_1_50 | 0.06332 | 0.00341 | 0.83859 | 0.04266 | 0.09617 | 0.00307 | 718.1 | 38.7 | 618.4 | 31.5 | 592.0 | 18.9 |
| WMS17_1_51 | 0.08382 | 0.00320 | 2.04293 | 0.07230 | 0.17748 | 0.00500 | 1287.5 | 49.1 | 1129.9 | 40.0 | 1053.2 | 29.7 |
| WMS17_1_52 | 0.06001 | 0.00275 | 0.79760 | 0.03625 | 0.09654 | 0.00274 | 603.1 | 27.7 | 595.5 | 27.1 | 594.1 | 16.9 |
| WMS17_1_53 | 0.06244 | 0.00367 | 0.79594 | 0.04583 | 0.09241 | 0.00276 | 688.3 | 40.5 | 594.5 | 34.2 | 569.8 | 17.0 |
| WMS17_1_54 | 0.09814 | 0.00404 | 2.40562 | 0.10527 | 0.17684 | 0.00733 | 1588.3 | 65.4 | 1244.3 | 54.5 | 1049.7 | 43.5 |
| WMS17_1_55 | 0.10448 | 0.00422 | 2.34286 | 0.19655 | 0.16311 | 0.01118 | 1704.4 | 68.8 | 1225.4 | 102.8 | 974.0 | 66.8 |
| WMS17_1_56 | 0.21245 | 0.00950 | 8.73665 | 0.38471 | 0.29884 | 0.01123 | 2923.6 | 130.7 | 2310.9 | 101.8 | 1685.5 | 63.3 |
| WMS17_1_57 | 0.05699 | 0.00265 | 0.74460 | 0.03438 | 0.09495 | 0.00252 | 490.2 | 22.8 | 565.1 | 26.1 | 584.7 | 15.5 |
| WMS17_1_58 | 0.05980 | 0.00246 | 0.96838 | 0.04250 | 0.11693 | 0.00395 | 595.3 | 24.4 | 687.6 | 30.2 | 712.9 | 24.1 |
| WMS17_1_59 | 0.10808 | 0.00329 | 3.77549 | 0.12956 | 0.25330 | 0.00636 | 1766.5 | 53.8 | 1587.5 | 54.5 | 1455.5 | 36.6 |
| WMS17_1_60 | 0.05972 | 0.00224 | 0.69515 | 0.02447 | 0.08466 | 0.00284 | 592.3 | 22.2 | 535.9 | 18.9 | 523.8 | 17.6 |
| WMS17_1_61 | 0.06481 | 0.00321 | 0.59029 | 0.02955 | 0.06652 | 0.00396 | 767.4 | 38.0 | 471.1 | 23.6 | 415.1 | 24.7 |
| WMS17_1_62 | 0.06868 | 0.00326 | 1.21178 | 0.05036 | 0.12796 | 0.00272 | 888.1 | 42.2 | 806.0 | 33.5 | 776.2 | 16.5 |
| WMS17_1_63 | 0.06102 | 0.00242 | 0.76068 | 0.02734 | 0.09029 | 0.00197 | 638.9 | 25.3 | 574.4 | 20.6 | 557.3 | 12.1 |
| WMS17_1_64 | 0.15640 | 0.00591 | 9.06255 | 0.38771 | 0.41832 | 0.01382 | 2416.4 | 91.4 | 2344.3 | 100.3 | 2252.8 | 74.4 |
| WMS17_1_65 | 0.06581 | 0.00267 | 0.91977 | 0.05021 | 0.10090 | 0.00282 | 799.5 | 32.5 | 662.2 | 36.2 | 619.7 | 17.3 |
| WMS17_1_66 | 0.06232 | 0.00262 | 1.11037 | 0.05832 | 0.12914 | 0.00563 | 684.3 | 28.8 | 758.4 | 39.8 | 782.9 | 34.1 |
| WMS17_1_67 | 0.05382 | 0.00251 | 0.73944 | 0.03691 | 0.09964 | 0.00352 | 362.4 | 16.9 | 562.1 | 28.1 | 612.3 | 21.6 |
| WMS17_1_68 | 0.05312 | 0.00296 | 0.70246 | 0.02996 | 0.09600 | 0.00413 | 333.1 | 18.6 | 540.3 | 23.0 | 590.9 | 25.4 |
| WMS17_1_69 | 0.06765 | 0.00330 | 1.11889 | 0.05323 | 0.11973 | 0.00341 | 856.8 | 41.8 | 762.4 | 36.3 | 729.0 | 20.8 |
| WMS17_1_70 | 0.06287 | 0.00268 | 1.14394 | 0.04404 | 0.13174 | 0.00437 | 702.7 | 29.9 | 774.4 | 29.8 | 797.8 | 26.5 |
| WMS17_1_71 | 0.06996 | 0.00522 | 1.23663 | 0.09588 | 0.12930 | 0.00542 | 926.2 | 69.1 | 817.4 | 63.4 | 783.9 | 32.9 |
| WMS17_1_72 | 0.05669 | 0.00245 | 0.68641 | 0.02880 | 0.08804 | 0.00185 | 478.7 | 20.7 | 530.6 | 22.3 | 543.9 | 11.4 |
| WMS17_1_73 | 0.10086 | 0.00543 | 2.97340 | 0.23659 | 0.21101 | 0.01305 | 1639.2 | 88.2 | 1400.8 | 111.5 | 1234.2 | 76.3 |
| WMS17_1_74 | 0.09623 | 0.00346 | 3.22472 | 0.16636 | 0.24389 | 0.01180 | 1551.5 | 55.8 | 1463.1 | 75.5 | 1406.9 | 68.1 |
| WMS17_1_75 | 0.09615 | 0.00362 | 2.69920 | 0.11904 | 0.20512 | 0.00758 | 1549.9 | 58.4 | 1328.2 | 58.6 | 1202.8 | 44.4 |
| WMS17_1_76 | 0.14493 | 0.02528 | 2.65562 | 0.76791 | 0.13326 | 0.01025 | 2286.1 | 398.8 | 1316.2 | 380.6 | 806.4 | 62.0 |
| WMS17_1_77 | 0.05776 | 0.00239 | 0.71922 | 0.03658 | 0.09065 | 0.00348 | 519.8 | 21.5 | 550.2 | 28.0 | 559.4 | 21.5 |
| WMS17_1_78 | 0.10967 | 0.00365 | 3.11373 | 0.13244 | 0.20760 | 0.00709 | 1793.0 | 59.8 | 1436.1 | 61.1 | 1216.0 | 41.6 |
| WMS17_1_79 | 0.15889 | 0.00668 | 9.88736 | 0.43437 | 0.45232 | 0.01188 | 2443.1 | 102.7 | 2424.3 | 106.5 | 2405.5 | 63.2 |
| WMS17_1_80 | 0.05901 | 0.00326 | 0.76862 | 0.03739 | 0.09459 | 0.00274 | 566.5 | 31.3 | 579.0 | 28.2 | 582.6 | 16.9 |
| WMS17_1_81 | 0.15735 | 0.00555 | 11.82178 | 0.43696 | 0.54528 | 0.01663 | 2426.6 | 85.7 | 2590.4 | 95.7 | 2805.5 | 85.5 |
| WMS17_1_82 | 0.17530 | 0.00671 | 10.25322 | 0.34317 | 0.42672 | 0.01946 | 2608.2 | 99.8 | 2457.9 | 82.3 | 2290.9 | 104.5 |
| WMS17_1_83 | 0.16386 | 0.00594 | 9.78296 | 0.35860 | 0.43507 | 0.01436 | 2495.1 | 90.5 | 2414.5 | 88.5 | 2328.5 | 76.9 |
| WMS17_1_84 | 0.06568 | 0.00276 | 1.20717 | 0.04414 | 0.13351 | 0.00443 | 795.2 | 33.4 | 803.9 | 29.4 | 807.9 | 26.8 |
| WMS17_1_85 | 0.06147 | 0.00276 | 0.79857 | 0.03511 | 0.09422 | 0.00350 | 654.6 | 29.3 | 596.0 | 26.2 | 580.4 | 21.5 |
| WMS17_1_86 | 0.06220 | 0.00269 | 0.92469 | 0.04263 | 0.10799 | 0.00365 | 680.0 | 29.4 | 664.8 | 30.7 | 661.1 | 22.4 |
| WMS17_1_87 | 0.06474 | 0.00309 | 1.21714 | 0.06577 | 0.13645 | 0.00510 | 765.0 | 36.6 | 808.5 | 43.7 | 824.5 | 30.8 |
| WMS17_1_88 | 0.12145 | 0.00427 | 5.99350 | 0.21461 | 0.35877 | 0.01182 | 1976.8 | 69.5 | 1974.9 | 70.7 | 1976.3 | 65.1 |
| WMS17_1_89 | 0.06357 | 0.00239 | 0.88230 | 0.03455 | 0.10075 | 0.00197 | 726.5 | 27.4 | 642.2 | 25.1 | 618.8 | 12.1 |
| WMS17_1_90 | 0.10734 | 0.00398 | 1.27430 | 0.08430 | 0.08684 | 0.00474 | 1753.9 | 65.0 | 834.3 | 55.2 | 536.8 | 29.3 |
| WMS17_1_91 | 0.06577 | 0.00351 | 0.72582 | 0.03839 | 0.08058 | 0.00275 | 798.0 | 42.6 | 554.1 | 29.3 | 499.6 | 17.1 |
| WMS17_1_92 | 0.11256 | 0.00408 | 4.96834 | 0.19887 | 0.32021 | 0.01439 | 1840.4 | 66.7 | 1813.9 | 72.6 | 1790.8 | 80.5 |
| WMS17_1_93 | 0.06641 | 0.00364 | 1.10298 | 0.05704 | 0.12100 | 0.00264 | 818.5 | 44.9 | 754.8 | 39.0 | 736.3 | 16.1 |
| WMS17_1_94 | 0.06477 | 0.00686 | 1.17372 | 0.12414 | 0.12869 | 0.00748 | 765.9 | 81.1 | 788.4 | 83.4 | 780.4 | 45.3 |
| WMS17_1_95 | < DL | 0.31646 | < DL | 40.66832 | < DL | 0.47507 | < DL | 2256.6 | < DL | 2189.8 | < DL | 2040.1 |
| WMS17_1_96 | 0.06118 | 0.00187 | 0.74056 | 0.02586 | 0.08789 | 0.00231 | 644.7 | 19.7 | 562.7 | 19.7 | 543.1 | 14.3 |
| WMS17_1_97 | 0.06099 | 0.00235 | 0.80227 | 0.02748 | 0.09534 | 0.00398 | 637.8 | 24.6 | 598.1 | 20.5 | 587.0 | 24.5 |
| WMS17_1_98 | 0.09706 | 0.00270 | 2.78038 | 0.07921 | 0.20783 | 0.00418 | 1567.6 | 43.6 | 1350.3 | 38.5 | 1217.3 | 24.5 |
| WMS17_1_99 | 0.11936 | 0.00354 | 3.50931 | 0.18613 | 0.21290 | 0.00772 | 1945.9 | 57.8 | 1529.3 | 81.1 | 1244.3 | 45.1 |
| WMS17_1_100 | 0.16293 | 0.00526 | 10.26233 | 0.31748 | 0.45684 | 0.01021 | 2485.5 | 80.2 | 2458.7 | 76.1 | 2425.6 | 54.2 |
| WMS17_1_101 | 0.05945 | 0.00200 | 0.83334 | 0.02819 | 0.10166 | 0.00167 | 582.5 | 19.6 | 615.5 | 20.8 | 624.1 | 10.3 |
| WMS17_1_102 | 0.05705 | 0.00187 | 0.72389 | 0.02425 | 0.09209 | 0.00166 | 492.4 | 16.1 | 553.0 | 18.5 | 567.9 | 10.2 |
| WMS17_1_103 | 0.06137 | 0.00267 | 0.72893 | 0.03391 | 0.08574 | 0.00305 | 651.2 | 28.4 | 555.9 | 25.9 | 530.3 | 18.8 |
| WMS17_1_104 | 0.05719 | 0.00281 | 0.80658 | 0.03923 | 0.10237 | 0.00186 | 497.9 | 24.5 | 600.5 | 29.2 | 628.3 | 11.4 |
| WMS17_1_105 | 0.67635 | 0.02860 | 45.49611 | 3.34822 | 0.48202 | 0.02890 | 4680.6 | 197.9 | 3898.4 | 286.9 | 2536.0 | 152.1 |
| WMS17_1_106 | 0.11679 | 0.00376 | 4.75955 | 0.17293 | 0.29632 | 0.00861 | 1906.8 | 61.4 | 1777.8 | 64.6 | 1673.0 | 48.6 |
| WMS17_1_107 | 0.06971 | 0.00213 | 1.61810 | 0.05437 | 0.16893 | 0.00295 | 919.0 | 28.1 | 977.3 | 32.8 | 1006.2 | 17.6 |
| WMS17_1_108 | 0.16416 | 0.00555 | 10.57036 | 0.54505 | 0.46824 | 0.02077 | 2498.2 | 84.5 | 2486.1 | 128.2 | 2475.8 | 109.8 |
| WMS17_1_109 | 0.05770 | 0.00209 | 0.74408 | 0.02585 | 0.09368 | 0.00347 | 517.3 | 18.8 | 564.8 | 19.6 | 577.3 | 21.4 |
| WMS17_1_110 | 0.11091 | 0.00415 | 4.15546 | 0.20712 | 0.27257 | 0.00913 | 1813.6 | 67.9 | 1665.3 | 83.0 | 1553.8 | 52.0 |
| WMS17_1_111 | 0.05816 | 0.00212 | 0.79475 | 0.02655 | 0.09936 | 0.00322 | 534.7 | 19.5 | 593.9 | 19.8 | 610.7 | 19.8 |
| WMS17_1_112 | 0.11413 | 0.00399 | 4.80774 | 0.17703 | 0.30631 | 0.00833 | 1865.4 | 65.2 | 1786.3 | 65.8 | 1722.5 | 46.8 |
| WMS17_1_113 | 0.10831 | 0.00329 | 4.58169 | 0.18000 | 0.30752 | 0.00962 | 1770.4 | 53.8 | 1745.9 | 68.6 | 1728.5 | 54.1 |
| WMS17_1_114 | 0.10651 | 0.00379 | 4.47285 | 0.18199 | 0.30538 | 0.01235 | 1739.7 | 61.9 | 1725.9 | 70.2 | 1717.9 | 69.5 |
| WMS17_1_115 | 0.06443 | 0.00373 | 0.88915 | 0.04660 | 0.10043 | 0.00251 | 754.9 | 43.7 | 645.9 | 33.9 | 616.9 | 15.4 |
| WMS17_1_116 | 0.05828 | 0.00201 | 0.77838 | 0.02881 | 0.09711 | 0.00286 | 539.3 | 18.6 | 584.6 | 21.6 | 597.5 | 17.6 |
| WMS17_1_117 | 0.07157 | 0.00365 | 1.21525 | 0.06348 | 0.12346 | 0.00301 | 972.8 | 49.6 | 807.6 | 42.2 | 750.4 | 18.3 |
| WMS17_1_118 | 0.07742 | 0.00560 | 1.19946 | 0.07763 | 0.11120 | 0.00373 | 1131.2 | 81.8 | 800.3 | 51.8 | 679.7 | 22.8 |
| WMS17_1_119 | 0.16683 | 0.00593 | 9.96796 | 0.35644 | 0.43181 | 0.01062 | 2525.3 | 89.8 | 2431.8 | 87.0 | 2313.9 | 56.9 |

| sample | $^{207}Pb^{*}/^{206}Pb^{*}$ | | $^{207}Pb^{*}/^{235}U$ | | $^{206}Pb^{*}/^{238}U$ | | $^{207}Pb/^{206}Pb$ | | $^{207}Pb/^{235}U$ | | $^{206}Pb/^{238}U$ | |
|---|---|---|---|---|---|---|---|---|---|---|---|---|
| | value | 1 s.e | value | 1 s.e | value | 1 s.e | age (Ma) | 1 s.e | age (Ma) | 1 s.e | age (Ma) | 1 s.e |
| WMS17_1_120 | 0.09818 | 0.00364 | 1.54249 | 0.08396 | 0.11469 | 0.00477 | 1589.0 | 58.9 | 947.5 | 51.6 | 699.9 | 29.1 |
| WMS17_1_121 | 0.06193 | 0.00297 | 1.18327 | 0.04513 | 0.13855 | 0.00438 | 670.6 | 32.2 | 792.8 | 30.2 | 836.5 | 26.5 |
| WMS17_1_122 | 0.06150 | 0.00261 | 0.78701 | 0.03491 | 0.09309 | 0.00257 | 656.0 | 27.8 | 589.5 | 26.1 | 573.8 | 15.8 |
| WMS17_1_123 | 0.06211 | 0.00246 | 1.03397 | 0.03718 | 0.12096 | 0.00394 | 677.0 | 26.8 | 720.9 | 25.9 | 736.1 | 24.0 |
| WMS17_1_124 | 0.05960 | 0.00300 | 0.70731 | 0.03371 | 0.08622 | 0.00251 | 588.2 | 29.6 | 543.2 | 25.9 | 533.1 | 15.5 |
| WMS17_1_125 | 0.05723 | 0.00221 | 0.68434 | 0.02914 | 0.08711 | 0.00234 | 499.4 | 19.3 | 529.4 | 22.5 | 538.4 | 14.5 |
| WMS17_1_126 | 0.06055 | 0.00261 | 0.74754 | 0.03087 | 0.08959 | 0.00318 | 622.2 | 26.9 | 566.8 | 23.4 | 553.1 | 19.7 |
| WMS17_1_127 | 0.05956 | 0.00285 | 0.75867 | 0.02983 | 0.09276 | 0.00364 | 586.8 | 28.1 | 573.2 | 22.5 | 571.9 | 22.5 |
| WMS17_1_128 | 0.06259 | 0.00370 | 0.78917 | 0.04009 | 0.09099 | 0.00313 | 693.4 | 41.0 | 590.7 | 30.0 | 561.4 | 19.3 |
| WMS17_1_129 | 0.06289 | 0.00335 | 0.75596 | 0.03855 | 0.08738 | 0.00198 | 703.5 | 37.5 | 571.7 | 29.2 | 540.0 | 12.2 |
| WMS17_1_130 | 0.07199 | 0.00262 | 1.63447 | 0.06044 | 0.16518 | 0.00308 | 984.7 | 35.8 | 983.6 | 36.4 | 985.5 | 18.4 |
| WMS17_1_131 | 0.15327 | 0.00537 | 9.33771 | 0.36446 | 0.44182 | 0.01191 | 2382.0 | 83.5 | 2371.7 | 92.6 | 2358.8 | 63.6 |
| WMS17_1_132 | 0.05700 | 0.00255 | 0.77273 | 0.03010 | 0.09846 | 0.00351 | 490.5 | 22.0 | 581.3 | 22.6 | 605.4 | 21.6 |
| WMS17_1_133 | 0.06476 | 0.00234 | 1.15079 | 0.04309 | 0.12923 | 0.00247 | 765.8 | 27.7 | 777.6 | 29.1 | 783.5 | 15.0 |
| WMS17_1_134 | 0.05704 | 0.00192 | 0.74852 | 0.02908 | 0.09540 | 0.00236 | 492.0 | 16.6 | 567.4 | 22.0 | 587.4 | 14.5 |
| WMS17_1_135 | 0.05776 | 0.00506 | 0.97378 | 0.08319 | 0.12282 | 0.00487 | 519.6 | 45.5 | 690.4 | 59.0 | 746.8 | 29.6 |
| WMS17_1_136 | 0.05810 | 0.00276 | 0.72200 | 0.03338 | 0.09028 | 0.00259 | 532.5 | 25.3 | 551.8 | 25.5 | 557.2 | 16.0 |
| WMS17_1_137 | 0.19449 | 0.00628 | 13.30009 | 0.39221 | 0.49550 | 0.01131 | 2779.8 | 89.7 | 2701.2 | 79.7 | 2594.4 | 59.2 |
| WMS17_1_138 | 0.10648 | 0.00271 | 3.86713 | 0.11620 | 0.26345 | 0.00772 | 1739.2 | 44.3 | 1606.8 | 48.3 | 1507.4 | 44.2 |
| WMS17_1_139 | 0.16161 | 0.00439 | 9.02844 | 0.29740 | 0.40630 | 0.00930 | 2471.8 | 67.1 | 2340.9 | 77.1 | 2198.0 | 50.3 |
| WMS17_1_140 | 0.06444 | 0.00247 | 1.14278 | 0.04640 | 0.12889 | 0.00307 | 755.1 | 28.9 | 773.8 | 31.4 | 781.6 | 18.6 |
| WMS17_1_141 | 0.10268 | 0.00626 | 1.75616 | 0.29955 | 0.12531 | 0.01456 | 1672.3 | 101.9 | 1029.4 | 175.6 | 761.0 | 88.4 |
| WMS17_1_142 | 0.06810 | 0.00219 | 1.47716 | 0.04750 | 0.15755 | 0.00352 | 870.6 | 28.0 | 921.1 | 29.6 | 943.2 | 21.1 |
| WMS17_1_143 | 0.05995 | 0.00399 | 0.92144 | 0.06527 | 0.11137 | 0.00403 | 600.9 | 39.9 | 663.1 | 47.0 | 680.7 | 24.7 |
| WMS17_1_144 | 0.05818 | 0.00228 | 0.76885 | 0.02922 | 0.09604 | 0.00212 | 535.5 | 21.0 | 579.1 | 22.0 | 591.2 | 13.1 |
| 27_1 (20°23'29,20"S , 44°45'41,33"E) | | | | | | | | | | | | |
| WMS27_1_1 | 0.05830 | 0.00321 | 0.73830 | 0.03560 | 0.09168 | 0.00320 | 540.2 | 29.7 | 561.4 | 27.1 | 565.5 | 19.8 |
| WMS27_1_2 | 0.06068 | 0.00274 | 0.86606 | 0.04028 | 0.10339 | 0.00408 | 627.0 | 28.3 | 633.4 | 29.5 | 634.2 | 25.0 |
| WMS27_1_3 | 0.05724 | 0.00271 | 0.84072 | 0.03498 | 0.10623 | 0.00380 | 499.7 | 23.6 | 619.5 | 25.8 | 650.8 | 23.3 |
| WMS27_1_4 | 0.06168 | 0.00344 | 0.72574 | 0.04093 | 0.08528 | 0.00290 | 662.0 | 36.9 | 554.0 | 31.2 | 527.6 | 18.0 |
| WMS27_1_5 | 0.06877 | 0.00284 | 1.36580 | 0.06025 | 0.14407 | 0.00538 | 891.0 | 36.7 | 874.4 | 38.6 | 867.6 | 32.4 |
| WMS27_1_6 | 0.05755 | 0.00214 | 0.75387 | 0.02967 | 0.09495 | 0.00278 | 511.8 | 19.0 | 570.5 | 22.5 | 584.8 | 17.1 |
| WMS27_1_7 | 0.11894 | 0.00609 | 5.13580 | 0.25937 | 0.31362 | 0.01214 | 1939.5 | 99.2 | 1842.0 | 93.0 | 1758.5 | 68.0 |
| WMS27_1_8 | 0.07021 | 0.00391 | 1.46276 | 0.07909 | 0.15108 | 0.00485 | 933.7 | 51.9 | 915.1 | 49.5 | 907.0 | 29.1 |
| WMS27_1_9 | 0.17770 | 0.00649 | 9.85108 | 0.33573 | 0.40209 | 0.01135 | 2630.8 | 96.1 | 2420.9 | 82.5 | 2178.7 | 61.5 |
| WMS27_1_10 | 0.15484 | 0.00638 | 6.58575 | 0.39060 | 0.30878 | 0.01485 | 2399.3 | 98.8 | 2057.4 | 122.0 | 1734.7 | 83.4 |
| WMS27_1_11 | 0.07699 | 0.00311 | 1.92233 | 0.09087 | 0.18121 | 0.00566 | 1119.9 | 45.3 | 1088.9 | 51.5 | 1073.6 | 33.5 |
| WMS27_1_12 | 0.16605 | 0.00628 | 10.61274 | 0.37333 | 0.46274 | 0.01101 | 2517.4 | 95.2 | 2489.8 | 87.6 | 2451.7 | 58.3 |
| WMS27_1_13 | 0.05874 | 0.00253 | 0.82604 | 0.02926 | 0.10232 | 0.00306 | 556.5 | 23.9 | 611.4 | 21.7 | 628.0 | 18.8 |
| WMS27_1_14 | 0.06625 | 0.00304 | 1.20238 | 0.05183 | 0.13170 | 0.00443 | 813.3 | 37.4 | 801.7 | 34.6 | 797.6 | 26.8 |
| WMS27_1_15 | 0.05911 | 0.00298 | 0.90251 | 0.04637 | 0.11058 | 0.00367 | 570.1 | 28.7 | 653.1 | 33.6 | 676.1 | 22.5 |
| WMS27_1_16 | 0.05794 | 0.00441 | 0.76278 | 0.04650 | 0.09530 | 0.00377 | 526.6 | 40.1 | 575.6 | 35.1 | 586.8 | 23.2 |
| WMS27_1_17 | 0.05877 | 0.00339 | 0.73465 | 0.04293 | 0.09122 | 0.00285 | 557.8 | 32.1 | 559.3 | 32.7 | 562.8 | 17.6 |
| WMS27_1_18 | 0.06013 | 0.00267 | 0.68159 | 0.02910 | 0.08257 | 0.00277 | 607.2 | 26.9 | 527.7 | 22.5 | 511.4 | 17.1 |
| WMS27_1_19 | 0.08206 | 0.00378 | 1.21753 | 0.07265 | 0.10778 | 0.00430 | 1246.1 | 57.4 | 808.6 | 48.3 | 659.8 | 26.3 |
| WMS27_1_20 | 0.06616 | 0.00291 | 0.82652 | 0.03563 | 0.09084 | 0.00283 | 810.7 | 35.6 | 611.7 | 26.4 | 560.5 | 17.4 |
| WMS27_1_21 | 0.15751 | 0.00552 | 9.62011 | 0.33764 | 0.44346 | 0.01457 | 2428.4 | 85.0 | 2399.1 | 84.2 | 2366.1 | 77.7 |
| WMS27_1_22 | 0.05739 | 0.00223 | 0.68826 | 0.02863 | 0.08695 | 0.00233 | 505.5 | 19.7 | 531.8 | 22.1 | 537.5 | 14.4 |
| WMS27_1_23 | 0.06839 | 0.00289 | 1.27588 | 0.05363 | 0.13524 | 0.00372 | 879.5 | 37.2 | 835.0 | 35.1 | 817.7 | 22.5 |
| WMS27_1_24 | 0.06308 | 0.00244 | 0.90862 | 0.03736 | 0.10461 | 0.00373 | 710.1 | 27.4 | 656.3 | 27.0 | 641.4 | 22.9 |
| WMS27_1_25 | 0.05751 | 0.00219 | 0.79857 | 0.03145 | 0.10038 | 0.00250 | 510.2 | 19.4 | 596.0 | 23.5 | 616.6 | 15.3 |
| WMS27_1_26 | 0.07387 | 0.00349 | 1.57822 | 0.07307 | 0.15496 | 0.00373 | 1036.9 | 49.0 | 961.7 | 44.5 | 928.7 | 22.4 |
| WMS27_1_27 | 0.06362 | 0.00254 | 1.19002 | 0.05944 | 0.13594 | 0.00415 | 728.2 | 29.0 | 796.0 | 39.8 | 821.7 | 25.1 |
| WMS27_1_28 | 0.06138 | 0.00309 | 0.73631 | 0.03101 | 0.08702 | 0.00280 | 651.7 | 32.8 | 560.2 | 23.6 | 537.9 | 17.3 |
| WMS27_1_29 | 0.06379 | 0.00326 | 0.92394 | 0.04988 | 0.10484 | 0.00295 | 733.9 | 37.5 | 664.4 | 35.9 | 642.7 | 18.1 |
| WMS27_1_30 | 0.06729 | 0.00295 | 1.24485 | 0.06521 | 0.13378 | 0.00421 | 845.8 | 37.1 | 821.1 | 43.0 | 809.4 | 25.5 |
| WMS27_1_31 | 0.05069 | 0.00458 | 0.63836 | 0.04746 | 0.09140 | 0.00435 | 225.7 | 20.4 | 501.3 | 37.3 | 563.8 | 26.9 |
| WMS27_1_32 | 0.07430 | 0.00338 | 1.63210 | 0.09464 | 0.15883 | 0.00500 | 1048.7 | 47.7 | 982.7 | 57.0 | 950.3 | 29.9 |
| WMS27_1_33 | 0.16271 | 0.00613 | 9.73455 | 0.41499 | 0.43327 | 0.01442 | 2483.3 | 93.6 | 2410.0 | 102.7 | 2320.4 | 77.2 |
| WMS27_1_34 | 0.06695 | 0.00302 | 1.20059 | 0.05732 | 0.13031 | 0.00441 | 835.2 | 37.7 | 800.9 | 38.2 | 789.7 | 26.7 |
| WMS27_1_35 | 0.05987 | 0.00298 | 1.09992 | 0.05514 | 0.13320 | 0.00392 | 597.9 | 29.7 | 753.3 | 37.8 | 806.1 | 23.7 |
| WMS27_1_36 | 0.06872 | 0.00302 | 1.78795 | 0.09430 | 0.18867 | 0.00568 | 889.5 | 39.0 | 1041.1 | 54.9 | 1114.1 | 33.5 |
| WMS27_1_37 | 0.05950 | 0.00236 | 0.75663 | 0.03902 | 0.09245 | 0.00334 | 584.3 | 23.1 | 572.1 | 29.5 | 570.0 | 20.6 |
| WMS27_1_38 | 0.06114 | 0.00403 | 0.81829 | 0.05393 | 0.09712 | 0.00348 | 643.2 | 42.4 | 607.1 | 40.0 | 597.5 | 21.4 |
| WMS27_1_39 | 0.06562 | 0.00327 | 1.08108 | 0.04619 | 0.11952 | 0.00371 | 793.4 | 39.6 | 744.2 | 31.8 | 727.8 | 22.6 |
| WMS27_1_40 | 0.06656 | 0.00277 | 1.28492 | 0.05641 | 0.13994 | 0.00511 | 823.2 | 34.2 | 839.0 | 36.8 | 844.3 | 30.8 |
| WMS27_1_41 | 0.07309 | 0.00289 | 1.67855 | 0.09240 | 0.16675 | 0.00693 | 1015.6 | 40.1 | 1000.4 | 55.1 | 994.2 | 41.3 |
| WMS27_1_42 | 0.24003 | 0.00886 | 23.26623 | 1.05559 | 0.70342 | 0.02567 | 3119.5 | 115.2 | 3238.1 | 146.9 | 3433.6 | 125.3 |
| WMS27_1_43 | 0.13667 | 0.00531 | 5.82931 | 0.29139 | 0.30966 | 0.01061 | 2184.7 | 84.8 | 1950.8 | 97.5 | 1739.0 | 59.6 |
| WMS27_1_44 | 0.15703 | 0.00604 | 9.35730 | 0.43934 | 0.43181 | 0.01868 | 2423.1 | 93.2 | 2373.7 | 111.4 | 2313.8 | 100.1 |
| WMS27_1_45 | 0.26059 | 0.01069 | 21.52068 | 0.77387 | 0.59997 | 0.01935 | 3249.6 | 133.2 | 3162.3 | 113.7 | 3029.7 | 97.7 |
| WMS27_1_46 | 0.07530 | 0.00254 | 1.91257 | 0.07634 | 0.18434 | 0.00700 | 1075.7 | 36.3 | 1085.5 | 43.3 | 1090.6 | 41.4 |
| WMS27_1_47 | 0.07134 | 0.00562 | 1.17758 | 0.09018 | 0.12036 | 0.00433 | 966.3 | 76.2 | 790.2 | 60.5 | 732.6 | 26.4 |
| WMS27_1_48 | 0.06148 | 0.00252 | 0.83924 | 0.04471 | 0.09882 | 0.00263 | 655.3 | 26.9 | 618.7 | 33.0 | 607.5 | 16.1 |
| WMS27_1_49 | 0.06280 | 0.00344 | 0.79701 | 0.04710 | 0.09252 | 0.00282 | 700.7 | 38.4 | 595.1 | 35.2 | 570.4 | 17.4 |
| WMS27_1_50 | 0.06070 | 0.00261 | 0.73925 | 0.03287 | 0.08842 | 0.00319 | 627.7 | 27.0 | 562.0 | 25.0 | 546.2 | 19.7 |
| WMS27_1_51 | 0.06621 | 0.00332 | 1.13434 | 0.05093 | 0.12467 | 0.00384 | 812.0 | 40.8 | 769.8 | 34.6 | 757.4 | 23.3 |
| WMS27_1_52 | 0.06205 | 0.00202 | 0.83080 | 0.02799 | 0.09737 | 0.00216 | 675.0 | 22.0 | 614.1 | 20.7 | 598.9 | 13.3 |
| WMS27_1_53 | 0.06847 | 0.00161 | 1.47572 | 0.03399 | 0.15602 | 0.00295 | 881.8 | 20.7 | 920.5 | 21.2 | 934.6 | 17.7 |
| WMS27_1_54 | 0.07235 | 0.00406 | 1.70710 | 0.08753 | 0.17117 | 0.00602 | 994.9 | 55.8 | 1011.2 | 51.8 | 1018.6 | 35.8 |
| WMS27_1_55 | 0.05967 | 0.00219 | 0.89902 | 0.03338 | 0.10942 | 0.00415 | 590.7 | 21.7 | 651.2 | 24.2 | 669.4 | 25.4 |
| WMS27_1_56 | 0.07558 | 0.00231 | 1.79052 | 0.05262 | 0.17183 | 0.00436 | 1083.2 | 33.1 | 1042.0 | 30.6 | 1022.2 | 25.9 |
| WMS27_1_57 | 0.07055 | 0.00274 | 1.32445 | 0.04627 | 0.13630 | 0.00344 | 943.4 | 36.6 | 856.5 | 29.9 | 823.7 | 20.8 |
| WMS27_1_58 | 0.06448 | 0.00202 | 1.14445 | 0.04182 | 0.12910 | 0.00418 | 756.6 | 23.7 | 774.6 | 28.3 | 782.7 | 25.3 |
| WMS27_1_59 | 0.06807 | 0.00242 | 1.66667 | 0.05549 | 0.17817 | 0.00545 | 869.7 | 30.9 | 995.9 | 33.2 | 1056.9 | 32.3 |
| WMS27_1_60 | 0.15729 | 0.00526 | 8.55947 | 0.25393 | 0.39456 | 0.01249 | 2425.9 | 81.2 | 2292.3 | 68.0 | 2143.9 | 67.9 |

| sample | $^{207}Pb^{*}/^{206}Pb^{*}$ | | $^{207}Pb^{*}/^{235}U$ | | $^{206}Pb^{*}/^{238}U$ | | $^{207}Pb/^{206}Pb$ | | $^{207}Pb/^{235}U$ | | $^{206}Pb/^{238}U$ | |
|---|---|---|---|---|---|---|---|---|---|---|---|---|
| | value | 1 s.e | value | 1 s.e | value | 1 s.e | age (Ma) | 1 s.e | age (Ma) | 1 s.e | age (Ma) | 1 s.e |
| WMS27_1_61 | 0.19572 | 0.01788 | 2.91463 | 0.44626 | 0.10799 | 0.00557 | 2790.1 | 254.9 | 1385.7 | 212.2 | 661.0 | 34.1 |
| WMS27_1_62 | 0.06945 | 0.00274 | 1.74593 | 0.07612 | 0.18299 | 0.00475 | 911.3 | 35.9 | 1025.7 | 44.7 | 1083.3 | 28.1 |
| WMS27_1_63 | 0.05760 | 0.00258 | 0.82071 | 0.03436 | 0.10345 | 0.00317 | 513.7 | 23.0 | 608.4 | 25.5 | 634.6 | 19.4 |
| WMS27_1_64 | 0.05806 | 0.00280 | 0.74555 | 0.03486 | 0.09326 | 0.00250 | 531.0 | 25.6 | 565.6 | 26.4 | 574.8 | 15.4 |
| WMS27_1_65 | 0.17209 | 0.00658 | 8.33869 | 0.32694 | 0.35249 | 0.01011 | 2577.3 | 98.5 | 2268.5 | 88.9 | 1946.5 | 55.8 |
| WMS27_1_66 | 0.05954 | 0.00306 | 0.87478 | 0.04232 | 0.10684 | 0.00320 | 586.1 | 30.1 | 638.2 | 30.9 | 654.4 | 19.6 |
| WMS27_1_67 | 0.06732 | 0.00293 | 1.06522 | 0.04728 | 0.11491 | 0.00251 | 846.8 | 36.9 | 736.4 | 32.7 | 701.2 | 15.3 |
| WMS27_1_68 | 0.07418 | 0.00356 | 1.81519 | 0.07909 | 0.17744 | 0.00593 | 1045.5 | 50.2 | 1051.0 | 45.8 | 1053.0 | 35.2 |
| WMS27_1_69 | 0.17572 | 0.00716 | 11.05274 | 0.38141 | 0.45666 | 0.01528 | 2612.1 | 106.4 | 2527.6 | 87.2 | 2424.8 | 81.1 |
| WMS27_1_70 | 0.06274 | 0.00250 | 0.77179 | 0.02839 | 0.08933 | 0.00272 | 698.5 | 27.8 | 580.8 | 21.4 | 551.6 | 16.8 |
| WMS27_1_71 | 0.06559 | 0.00309 | 0.94567 | 0.04507 | 0.10377 | 0.00316 | 792.4 | 37.3 | 675.8 | 32.2 | 636.5 | 19.4 |
| WMS27_1_72 | 0.07806 | 0.00298 | 1.85431 | 0.07465 | 0.17238 | 0.00398 | 1147.5 | 43.8 | 1065.0 | 42.9 | 1025.2 | 23.7 |
| WMS27_1_73 | 0.05980 | 0.00237 | 0.71929 | 0.02731 | 0.08723 | 0.00284 | 595.4 | 23.6 | 550.2 | 20.9 | 539.1 | 17.5 |
| WMS27_1_74 | 0.05880 | 0.00234 | 0.73903 | 0.02815 | 0.09137 | 0.00223 | 558.6 | 22.2 | 561.8 | 21.4 | 563.6 | 13.8 |
| WMS27_1_75 | 0.25683 | 0.00854 | 22.70623 | 0.83707 | 0.64140 | 0.01484 | 3226.7 | 107.3 | 3214.4 | 118.5 | 3194.5 | 73.9 |
| WMS27_1_76 | 0.06874 | 0.00501 | 0.96942 | 0.05987 | 0.10222 | 0.00292 | 890.1 | 64.9 | 688.2 | 42.5 | 627.4 | 17.9 |
| WMS27_1_77 | 0.07612 | 0.00280 | 1.78550 | 0.06692 | 0.17038 | 0.00475 | 1097.2 | 40.3 | 1040.2 | 39.0 | 1014.2 | 28.3 |
| WMS27_1_78 | 0.12272 | 0.00510 | 5.00616 | 0.22917 | 0.29653 | 0.01044 | 1995.3 | 83.0 | 1820.4 | 83.3 | 1674.1 | 59.0 |
| WMS27_1_79 | 0.06461 | 0.00248 | 0.83754 | 0.03354 | 0.09404 | 0.00210 | 760.8 | 29.2 | 617.8 | 24.7 | 579.4 | 12.9 |
| WMS27_1_80 | 0.06854 | 0.00319 | 1.39288 | 0.06066 | 0.14737 | 0.00420 | 883.9 | 41.2 | 885.9 | 38.6 | 886.2 | 25.3 |
| WMS27_1_81 | 0.07191 | 0.00321 | 1.24393 | 0.04888 | 0.12548 | 0.00374 | 982.3 | 43.8 | 820.7 | 32.3 | 762.0 | 22.7 |
| WMS27_1_82 | 0.07819 | 0.00370 | 1.76160 | 0.08280 | 0.16336 | 0.00292 | 1150.7 | 54.5 | 1031.4 | 48.5 | 975.4 | 17.5 |
| WMS27_1_83 | 0.06928 | 0.00421 | 1.22355 | 0.08541 | 0.12803 | 0.00353 | 906.2 | 55.1 | 811.4 | 56.6 | 776.6 | 21.4 |
| WMS27_1_84 | 0.07186 | 0.00404 | 1.59007 | 0.08710 | 0.16046 | 0.00429 | 981.1 | 55.2 | 966.3 | 52.9 | 959.3 | 25.7 |
| WMS27_1_85 | 0.06688 | 0.00255 | 1.18893 | 0.04845 | 0.12943 | 0.00308 | 833.2 | 31.8 | 795.5 | 32.4 | 784.6 | 18.7 |
| WMS27_1_86 | 0.06190 | 0.00326 | 1.09501 | 0.05788 | 0.12833 | 0.00274 | 669.7 | 35.3 | 750.9 | 39.7 | 778.3 | 16.6 |
| WMS27_1_87 | 0.16835 | 0.00770 | 11.39013 | 0.53171 | 0.49251 | 0.01903 | 2540.5 | 116.2 | 2555.6 | 119.3 | 2581.5 | 99.7 |
| WMS27_1_88 | 0.25622 | 0.01074 | 11.47142 | 0.47799 | 0.32554 | 0.01024 | 3222.9 | 135.1 | 2562.3 | 106.8 | 1816.7 | 57.2 |
| WMS27_1_89 | 0.16444 | 0.00595 | 10.43686 | 0.35591 | 0.46089 | 0.01306 | 2501.1 | 90.5 | 2474.3 | 84.4 | 2443.5 | 69.2 |
| WMS27_1_90 | 0.07379 | 0.00264 | 1.65503 | 0.05919 | 0.16282 | 0.00362 | 1034.8 | 37.1 | 991.5 | 35.5 | 972.4 | 21.6 |
| WMS27_1_91 | 0.05592 | 0.00272 | 0.67866 | 0.03099 | 0.08804 | 0.00258 | 448.3 | 21.8 | 526.0 | 24.0 | 544.0 | 15.9 |
| WMS27_1_92 | 0.07590 | 0.00365 | 1.46305 | 0.06104 | 0.14016 | 0.00382 | 1091.5 | 52.5 | 915.3 | 38.2 | 845.5 | 23.0 |
| WMS27_1_93 | 0.06492 | 0.00485 | 0.87392 | 0.06480 | 0.09766 | 0.00294 | 770.8 | 57.5 | 637.7 | 47.3 | 600.7 | 18.1 |
| WMS27_1_94 | 0.05956 | 0.00294 | 0.73246 | 0.02395 | 0.08911 | 0.00304 | 586.5 | 28.9 | 558.0 | 18.2 | 550.3 | 18.8 |
| WMS27_1_95 | 0.15766 | 0.00599 | 9.85162 | 0.36787 | 0.45147 | 0.01408 | 2430.0 | 92.3 | 2421.0 | 90.4 | 2401.8 | 74.9 |
| WMS27_1_96 | 0.06410 | 0.00226 | 1.05040 | 0.04028 | 0.11915 | 0.00295 | 743.8 | 26.2 | 729.1 | 28.0 | 725.6 | 18.0 |
| WMS27_1_97 | 0.05831 | 0.00238 | 0.76353 | 0.03611 | 0.09483 | 0.00299 | 540.6 | 22.0 | 576.0 | 27.2 | 584.0 | 18.4 |
| WMS27_1_98 | 0.05671 | 0.00247 | 0.84909 | 0.03433 | 0.10842 | 0.00297 | 479.2 | 20.9 | 624.1 | 25.2 | 663.6 | 18.2 |
| WMS27_1_99 | 0.05878 | 0.00211 | 0.81300 | 0.03069 | 0.10021 | 0.00283 | 558.1 | 20.0 | 604.1 | 22.8 | 615.7 | 17.4 |
| WMS27_1_100 | 0.06334 | 0.00250 | 1.18928 | 0.04070 | 0.13603 | 0.00364 | 718.7 | 28.4 | 795.6 | 27.2 | 822.2 | 22.0 |
| WMS27_1_101 | 0.05899 | 0.00279 | 0.91546 | 0.03804 | 0.11254 | 0.00532 | 565.8 | 26.7 | 660.0 | 27.4 | 687.5 | 32.5 |
| WMS27_1_102 | 0.06452 | 0.00273 | 1.18794 | 0.04180 | 0.13364 | 0.00293 | 757.7 | 32.1 | 795.0 | 28.0 | 808.6 | 17.7 |
| WMS27_1_103 | 0.10541 | 0.00357 | 4.88268 | 0.16310 | 0.33557 | 0.00902 | 1720.7 | 58.2 | 1799.3 | 60.1 | 1865.3 | 50.1 |
| WMS27_1_104 | 0.05909 | 0.00217 | 0.92420 | 0.03395 | 0.11324 | 0.00235 | 569.3 | 20.9 | 664.6 | 24.4 | 691.5 | 14.4 |
| WMS27_1_105 | 0.15986 | 0.00532 | 9.71796 | 0.32501 | 0.44021 | 0.01175 | 2453.4 | 81.6 | 2408.4 | 80.5 | 2351.6 | 62.8 |
| WMS27_1_106 | 0.13522 | 0.00546 | 6.50982 | 0.28049 | 0.34775 | 0.00978 | 2166.1 | 87.4 | 2047.2 | 88.2 | 1923.8 | 54.1 |
| WMS27_1_107 | 0.05788 | 0.00234 | 0.78795 | 0.03453 | 0.09845 | 0.00233 | 524.4 | 21.2 | 590.0 | 25.9 | 605.3 | 14.3 |
| WMS27_1_108 | 0.15443 | 0.00529 | 10.32498 | 0.31742 | 0.48484 | 0.01192 | 2394.9 | 82.0 | 2464.3 | 75.8 | 2548.3 | 62.7 |
| WMS27_1_109 | 0.05620 | 0.00289 | 0.79233 | 0.04362 | 0.10225 | 0.00356 | 459.2 | 23.6 | 592.5 | 32.6 | 627.6 | 21.9 |
| WMS27_1_110 | 0.15935 | 0.00582 | 10.09605 | 0.34710 | 0.46019 | 0.00840 | 2448.0 | 89.5 | 2443.6 | 84.0 | 2440.4 | 44.6 |
| WMS27_1_111 | 0.05702 | 0.00234 | 0.70736 | 0.02464 | 0.09011 | 0.00258 | 491.2 | 20.2 | 543.2 | 18.9 | 556.2 | 16.0 |
| WMS27_1_112 | 0.23798 | 0.00758 | 19.99182 | 0.60275 | 0.60870 | 0.01568 | 3105.8 | 99.0 | 3091.0 | 93.2 | 3064.8 | 79.0 |
| WMS27_1_113 | 0.06290 | 0.00312 | 1.44730 | 0.06988 | 0.16678 | 0.00471 | 704.0 | 34.9 | 908.8 | 43.9 | 994.3 | 28.1 |
| WMS27_1_114 | 0.05979 | 0.00253 | 0.92904 | 0.03529 | 0.11277 | 0.00371 | 595.1 | 25.2 | 667.1 | 25.3 | 688.8 | 22.7 |
| WMS27_1_115 | 0.05774 | 0.00376 | 0.66495 | 0.03823 | 0.08369 | 0.00256 | 519.0 | 33.8 | 517.6 | 29.8 | 518.1 | 15.8 |
| WMS27_1_116 | 0.05853 | 0.00296 | 0.92687 | 0.05011 | 0.11472 | 0.00259 | 548.6 | 27.7 | 666.0 | 36.0 | 700.1 | 15.8 |
| WMS27_1_117 | 0.16708 | 0.00551 | 10.34025 | 0.32714 | 0.44913 | 0.01179 | 2527.9 | 83.3 | 2465.7 | 78.0 | 2391.4 | 62.8 |
| WMS27_1_118 | 0.27428 | 0.01060 | 18.70863 | 0.79597 | 0.49568 | 0.01617 | 3330.0 | 128.7 | 3026.9 | 128.8 | 2595.2 | 84.7 |
| WMS27_1_119 | 0.23791 | 0.00813 | 19.91667 | 0.65143 | 0.60882 | 0.01627 | 3105.3 | 106.2 | 3087.3 | 101.0 | 3065.3 | 81.9 |
| WMS27_1_120 | 0.05647 | 0.00232 | 0.74751 | 0.03143 | 0.09617 | 0.00217 | 469.9 | 19.3 | 566.8 | 23.8 | 591.9 | 13.4 |
| WMS27_1_121 | 0.15693 | 0.00511 | 10.09169 | 0.38541 | 0.46660 | 0.01176 | 2422.1 | 78.8 | 2443.2 | 93.3 | 2468.6 | 62.2 |
| WMS27_1_122 | 0.05646 | 0.00245 | 0.74697 | 0.03270 | 0.09604 | 0.00230 | 469.4 | 20.4 | 566.5 | 24.8 | 591.2 | 14.1 |
| WMS27_1_123 | 0.10531 | 0.00366 | 4.01102 | 0.15879 | 0.27535 | 0.00779 | 1718.9 | 59.7 | 1636.4 | 64.8 | 1567.9 | 44.3 |
| WMS27_1_124 | 0.07527 | 0.00336 | 1.55998 | 0.06845 | 0.15091 | 0.00443 | 1074.8 | 48.0 | 954.5 | 41.9 | 906.0 | 26.6 |
| WMS27_1_125 | 0.07270 | 0.00271 | 1.67099 | 0.06370 | 0.16627 | 0.00380 | 1004.7 | 37.5 | 997.6 | 38.0 | 991.5 | 22.7 |
| WMS27_1_126 | 0.07353 | 0.00281 | 1.75308 | 0.06410 | 0.17325 | 0.00464 | 1027.7 | 39.3 | 1028.3 | 37.6 | 1030.0 | 27.6 |
| WMS27_1_127 | 0.15588 | 0.00573 | 9.24311 | 0.32656 | 0.42957 | 0.01045 | 2410.7 | 88.6 | 2362.4 | 83.5 | 2303.8 | 56.0 |
| WMS27_1_128 | 0.17111 | 0.00603 | 11.68641 | 0.41756 | 0.49405 | 0.00871 | 2567.8 | 90.5 | 2579.6 | 92.2 | 2588.2 | 45.6 |
| WMS27_1_129 | 0.07631 | 0.00398 | 1.73422 | 0.09029 | 0.16472 | 0.00317 | 1102.3 | 57.5 | 1021.3 | 53.2 | 982.9 | 18.9 |
| WMS27_1_130 | 0.21935 | 0.01000 | 17.01004 | 1.02763 | 0.56174 | 0.02301 | 2975.2 | 135.6 | 2935.4 | 177.3 | 2873.8 | 117.7 |
| WMS27_1_131 | 0.06499 | 0.00279 | 1.13502 | 0.05404 | 0.12751 | 0.00284 | 773.1 | 33.2 | 770.1 | 36.7 | 773.6 | 17.3 |
| WMS27_1_132 | 0.06423 | 0.00264 | 0.83986 | 0.06026 | 0.09479 | 0.00360 | 748.2 | 30.7 | 619.1 | 44.4 | 583.8 | 22.2 |
| WMS27_1_133 | 0.06648 | 0.00297 | 1.14492 | 0.05492 | 0.12460 | 0.00252 | 820.6 | 36.7 | 774.8 | 37.2 | 757.0 | 15.3 |
| WMS27_1_134 | 0.07386 | 0.00294 | 1.65454 | 0.06322 | 0.16264 | 0.00335 | 1036.8 | 41.2 | 991.3 | 37.9 | 971.4 | 20.0 |
| WMS27_1_135 | 0.11365 | 0.00442 | 5.15375 | 0.19492 | 0.32963 | 0.00725 | 1857.8 | 72.3 | 1845.0 | 69.8 | 1836.6 | 40.4 |
| WMS27_1_136 | 0.30330 | 0.01168 | 30.54648 | 1.26460 | 0.73009 | 0.01788 | 3486.5 | 134.3 | 3504.6 | 145.1 | 3533.7 | 86.5 |
| WMS27_1_137 | 0.20915 | 0.00796 | 12.50840 | 0.45153 | 0.43435 | 0.00882 | 2898.2 | 110.3 | 2643.4 | 95.4 | 2325.3 | 47.2 |
| WMS27_1_138 | 0.06338 | 0.00260 | 0.75619 | 0.03143 | 0.08649 | 0.00182 | 719.9 | 29.5 | 571.8 | 23.8 | 534.8 | 11.2 |
| WMS27_1_139 | 0.07382 | 0.00358 | 1.68595 | 0.09259 | 0.16556 | 0.00311 | 1035.7 | 50.3 | 1003.2 | 55.1 | 987.6 | 18.5 |
| WMS27_1_140 | 0.07569 | 0.00394 | 1.78020 | 0.10549 | 0.17097 | 0.00688 | 1086.0 | 56.5 | 1038.3 | 61.5 | 1017.4 | 41.0 |
| WMS27_1_141 | 0.07361 | 0.00405 | 1.59532 | 0.07800 | 0.15736 | 0.00406 | 1029.8 | 56.7 | 968.4 | 47.3 | 942.1 | 24.3 |
| WMS27_1_142 | 0.06889 | 0.00283 | 1.23073 | 0.04884 | 0.12932 | 0.00360 | 894.5 | 36.8 | 814.7 | 32.3 | 784.0 | 21.8 |
| WMS27_1_143 | 0.07500 | 0.00356 | 1.75107 | 0.08199 | 0.16930 | 0.00383 | 1067.7 | 50.7 | 1027.6 | 48.1 | 1008.2 | 22.8 |
| WMS27_1_144 | 0.06330 | 0.00296 | 1.00464 | 0.04610 | 0.11490 | 0.00288 | 717.5 | 33.6 | 706.2 | 32.4 | 701.1 | 17.6 |
| 31_1 (20°23'45,17"S , 44°54'29,72"E) | | | | | | | | | | | | |
| WMS31_1_1 | 0.06892 | 0.00194 | 1.46048 | 0.03862 | 0.15401 | 0.00270 | 895.4 | 25.2 | 914.2 | 24.2 | 923.4 | 16.2 |

| sample | $^{207}Pb^{*}/^{206}Pb^{*}$ | | $^{207}Pb^{*}/^{235}U$ | | $^{206}Pb^{*}/^{238}U$ | | $^{207}Pb/^{206}Pb$ | | $^{207}Pb/^{235}U$ | | $^{206}Pb/^{238}U$ | |
|---|---|---|---|---|---|---|---|---|---|---|---|---|
| | value | 1 s.e | value | 1 s.e | value | 1 s.e | age (Ma) | 1 s.e | age (Ma) | 1 s.e | age (Ma) | 1 s.e |
| WMS31_1_2 | 0.16673 | 0.00457 | 7.82015 | 0.30557 | 0.33985 | 0.00931 | 2524.4 | 69.2 | 2210.5 | 86.4 | 1886.0 | 51.7 |
| WMS31_1_3 | 0.10534 | 0.00421 | 3.25889 | 0.14761 | 0.22410 | 0.00631 | 1719.5 | 68.7 | 1471.3 | 66.6 | 1303.5 | 36.7 |
| WMS31_1_4 | 0.05987 | 0.00161 | 0.77377 | 0.02664 | 0.09394 | 0.00213 | 597.8 | 16.0 | 581.9 | 20.0 | 578.8 | 13.1 |
| WMS31_1_5 | 0.16920 | 0.00466 | 10.98588 | 0.33442 | 0.47175 | 0.01194 | 2549.0 | 70.2 | 2521.9 | 76.8 | 2491.2 | 63.0 |
| WMS31_1_6 | 0.14747 | 0.00475 | 8.68689 | 0.27555 | 0.42853 | 0.00963 | 2316.1 | 74.5 | 2305.7 | 73.1 | 2299.1 | 51.7 |
| WMS31_1_7 | 0.05599 | 0.00199 | 0.65355 | 0.02379 | 0.08474 | 0.00144 | 451.1 | 16.0 | 510.7 | 18.6 | 524.4 | 8.9 |
| WMS31_1_8 | 0.07623 | 0.00499 | 0.83558 | 0.06288 | 0.07978 | 0.00194 | 1100.3 | 72.0 | 616.7 | 46.4 | 494.8 | 12.1 |
| WMS31_1_9 | 0.16687 | 0.00488 | 10.40560 | 0.32782 | 0.45491 | 0.01096 | 2525.8 | 73.8 | 2471.5 | 77.9 | 2417.0 | 58.2 |
| WMS31_1_10 | 0.06396 | 0.00262 | 1.06948 | 0.04213 | 0.12148 | 0.00271 | 739.4 | 30.3 | 738.5 | 29.1 | 739.1 | 16.5 |
| WMS31_1_11 | 0.06118 | 0.00213 | 0.79655 | 0.02827 | 0.09459 | 0.00207 | 644.6 | 22.5 | 594.9 | 21.1 | 582.6 | 12.7 |
| WMS31_1_12 | 0.06777 | 0.00265 | 1.27181 | 0.04992 | 0.13632 | 0.00308 | 860.6 | 33.7 | 833.2 | 32.7 | 823.8 | 18.6 |
| WMS31_1_13 | 0.06961 | 0.00345 | 1.25150 | 0.05926 | 0.12994 | 0.00422 | 916.1 | 45.4 | 824.1 | 39.0 | 787.5 | 25.6 |
| WMS31_1_14 | 0.11250 | 0.00403 | 3.11546 | 0.15682 | 0.19820 | 0.00654 | 1839.4 | 65.9 | 1436.5 | 72.3 | 1165.6 | 38.5 |
| WMS31_1_15 | 0.11186 | 0.00346 | 3.15887 | 0.11248 | 0.20553 | 0.00554 | 1829.0 | 56.6 | 1447.2 | 51.5 | 1205.0 | 32.5 |
| WMS31_1_16 | 0.05860 | 0.00249 | 0.79762 | 0.03282 | 0.09888 | 0.00132 | 551.4 | 23.4 | 595.5 | 24.5 | 607.9 | 8.1 |
| WMS31_1_17 | 0.08088 | 0.00329 | 0.25475 | 0.01142 | 0.02286 | 0.00068 | 1217.6 | 49.6 | 230.4 | 10.3 | 145.7 | 4.4 |
| WMS31_1_18 | 0.10193 | 0.00421 | 3.63546 | 0.25006 | 0.25924 | 0.01420 | 1658.8 | 68.6 | 1557.3 | 107.1 | 1486.0 | 81.4 |
| WMS31_1_19 | 0.06452 | 0.00327 | 1.13494 | 0.05655 | 0.12804 | 0.00359 | 757.9 | 38.4 | 770.1 | 38.4 | 776.7 | 21.8 |
| WMS31_1_20 | 0.05629 | 0.00213 | 0.63909 | 0.02871 | 0.08265 | 0.00371 | 462.9 | 17.5 | 501.7 | 22.5 | 511.9 | 23.0 |
| WMS31_1_21 | 0.06052 | 0.00185 | 0.71873 | 0.02243 | 0.08635 | 0.00176 | 621.1 | 18.9 | 549.9 | 17.2 | 533.9 | 10.9 |
| WMS31_1_22 | 0.07343 | 0.00252 | 1.65995 | 0.06355 | 0.16403 | 0.00386 | 1025.0 | 35.1 | 993.4 | 38.0 | 979.1 | 23.0 |
| WMS31_1_23 | 0.06127 | 0.00242 | 0.80667 | 0.03243 | 0.09571 | 0.00182 | 647.7 | 25.6 | 600.6 | 24.1 | 589.2 | 11.2 |
| WMS31_1_24 | 0.16856 | 0.00550 | 11.68166 | 0.36939 | 0.50375 | 0.01072 | 2542.6 | 83.0 | 2579.2 | 81.6 | 2629.9 | 56.0 |
| WMS31_1_25 | 0.10812 | 0.00337 | 3.40182 | 0.16089 | 0.23011 | 0.00843 | 1767.1 | 55.1 | 1504.8 | 71.2 | 1335.1 | 48.9 |
| WMS31_1_26 | 0.16820 | 0.00507 | 10.47376 | 0.29956 | 0.45270 | 0.01043 | 2539.1 | 76.5 | 2477.6 | 70.9 | 2407.2 | 55.5 |
| WMS31_1_27 | 0.06480 | 0.00227 | 1.07809 | 0.03754 | 0.12085 | 0.00247 | 767.1 | 26.9 | 742.7 | 25.9 | 735.4 | 15.0 |
| WMS31_1_28 | 0.10797 | 0.00371 | 3.60176 | 0.15654 | 0.24295 | 0.00719 | 1764.6 | 60.7 | 1549.9 | 67.4 | 1402.0 | 41.5 |
| WMS31_1_29 | 0.11561 | 0.00476 | 5.23654 | 0.18700 | 0.32955 | 0.00982 | 1888.6 | 77.8 | 1858.6 | 66.4 | 1836.2 | 54.7 |
| WMS31_1_30 | 0.12346 | 0.00396 | 5.63400 | 0.19557 | 0.33183 | 0.00707 | 2006.0 | 64.4 | 1921.3 | 66.7 | 1847.2 | 39.3 |
| WMS31_1_31 | 0.05687 | 0.00268 | 0.74331 | 0.03055 | 0.09514 | 0.00273 | 485.7 | 22.9 | 564.3 | 23.2 | 585.9 | 16.8 |
| WMS31_1_32 | 0.09974 | 0.00373 | 2.92178 | 0.14959 | 0.21305 | 0.00846 | 1618.5 | 60.6 | 1387.6 | 71.0 | 1245.0 | 49.5 |
| WMS31_1_33 | 0.05855 | 0.00226 | 0.86039 | 0.03393 | 0.10672 | 0.00225 | 549.4 | 21.3 | 630.3 | 24.9 | 653.7 | 13.8 |
| WMS31_1_34 | 0.15088 | 0.00519 | 6.32930 | 0.24537 | 0.30522 | 0.00857 | 2355.1 | 81.0 | 2022.5 | 78.4 | 1717.1 | 48.2 |
| WMS31_1_35 | 0.06453 | 0.00379 | 1.18287 | 0.06780 | 0.13359 | 0.00442 | 758.0 | 44.5 | 792.6 | 45.4 | 808.3 | 26.8 |
| WMS31_1_36 | 0.15108 | 0.00503 | 8.44052 | 0.35205 | 0.40777 | 0.01178 | 2357.4 | 78.4 | 2279.5 | 95.1 | 2204.7 | 63.7 |
| WMS31_1_37 | 0.05836 | 0.00238 | 0.83629 | 0.03182 | 0.10439 | 0.00302 | 542.3 | 22.1 | 617.1 | 23.5 | 640.1 | 18.5 |
| WMS31_1_38 | 0.06968 | 0.00251 | 1.73977 | 0.06446 | 0.18188 | 0.00494 | 918.0 | 33.0 | 1023.4 | 37.9 | 1077.2 | 29.3 |
| WMS31_1_39 | 0.05901 | 0.00279 | 0.81799 | 0.04132 | 0.10057 | 0.00239 | 566.6 | 26.8 | 606.9 | 30.7 | 617.7 | 14.7 |
| WMS31_1_40 | 0.11774 | 0.00351 | 4.09421 | 0.15983 | 0.25343 | 0.00661 | 1921.4 | 57.3 | 1653.1 | 64.5 | 1456.1 | 38.0 |
| WMS31_1_41 | 0.14134 | 0.00512 | 5.82996 | 0.35294 | 0.29934 | 0.01474 | 2243.0 | 81.2 | 1950.9 | 118.1 | 1688.0 | 83.1 |
| WMS31_1_42 | 0.12428 | 0.00495 | 3.89890 | 0.18986 | 0.22847 | 0.00828 | 2017.7 | 80.3 | 1613.5 | 78.6 | 1326.5 | 48.1 |
| WMS31_1_43 | 0.05952 | 0.00457 | 0.71754 | 0.06131 | 0.08754 | 0.00358 | 585.3 | 44.9 | 549.2 | 46.9 | 541.0 | 22.1 |
| WMS31_1_44 | 0.06033 | 0.00320 | 0.68490 | 0.03380 | 0.08265 | 0.00325 | 614.5 | 32.6 | 529.7 | 26.1 | 511.9 | 20.1 |
| WMS31_1_45 | 0.13688 | 0.00410 | 6.71283 | 0.21061 | 0.35484 | 0.00729 | 2187.4 | 65.6 | 2074.3 | 65.1 | 1957.7 | 40.2 |
| WMS31_1_46 | 0.10890 | 0.00655 | 4.50158 | 0.31797 | 0.29987 | 0.01712 | 1780.3 | 107.1 | 1731.3 | 122.3 | 1690.7 | 96.5 |
| WMS31_1_47 | 0.17601 | 0.00945 | 7.92491 | 0.41977 | 0.32919 | 0.01452 | 2614.9 | 140.3 | 2222.5 | 117.7 | 1834.4 | 80.9 |
| WMS31_1_48 | 0.06223 | 0.00234 | 0.80191 | 0.02844 | 0.09356 | 0.00229 | 680.9 | 25.6 | 597.9 | 21.2 | 576.6 | 14.1 |
| WMS31_1_49 | 0.06714 | 0.00316 | 0.94386 | 0.06126 | 0.10211 | 0.00311 | 841.0 | 39.6 | 674.9 | 43.8 | 626.8 | 19.1 |
| WMS31_1_50 | 0.05683 | 0.00372 | 0.65187 | 0.04056 | 0.08320 | 0.00192 | 483.9 | 31.7 | 509.6 | 31.7 | 515.2 | 11.9 |
| WMS31_1_51 | 0.05839 | 0.00251 | 0.75018 | 0.02954 | 0.09315 | 0.00241 | 543.3 | 23.4 | 568.3 | 22.4 | 574.2 | 14.8 |
| WMS31_1_52 | 0.10797 | 0.00324 | 3.18402 | 0.13048 | 0.21441 | 0.00594 | 1764.6 | 52.9 | 1453.3 | 59.6 | 1252.3 | 34.7 |
| WMS31_1_53 | 0.05822 | 0.00314 | 0.68857 | 0.03612 | 0.08629 | 0.00344 | 537.2 | 29.0 | 531.9 | 27.9 | 533.6 | 21.3 |
| WMS31_1_54 | 0.10093 | 0.00372 | 4.29196 | 0.18394 | 0.30802 | 0.00834 | 1640.4 | 60.4 | 1691.8 | 72.5 | 1730.9 | 46.9 |
| WMS31_1_55 | 0.06691 | 0.00433 | 1.12988 | 0.07470 | 0.12293 | 0.00304 | 834.0 | 54.0 | 767.7 | 50.8 | 747.4 | 18.5 |
| WMS31_1_56 | 0.15382 | 0.00560 | 7.31503 | 0.36920 | 0.34667 | 0.01271 | 2388.1 | 86.9 | 2150.6 | 108.5 | 1918.7 | 70.4 |
| WMS31_1_57 | 0.08829 | 0.00343 | 1.72756 | 0.07919 | 0.14230 | 0.00383 | 1388.0 | 53.9 | 1018.8 | 46.7 | 857.7 | 23.1 |
| WMS31_1_58 | 0.07124 | 0.00336 | 0.84413 | 0.04238 | 0.08637 | 0.00324 | 963.3 | 45.5 | 621.4 | 31.2 | 534.0 | 20.0 |
| WMS31_1_59 | 0.15434 | 0.00534 | 7.92118 | 0.30144 | 0.37240 | 0.00961 | 2393.8 | 82.8 | 2222.1 | 84.6 | 2040.7 | 52.7 |
| WMS31_1_60 | 0.15554 | 0.00554 | 10.80758 | 0.35492 | 0.50491 | 0.01337 | 2407.0 | 85.7 | 2506.7 | 82.3 | 2634.8 | 69.8 |
| WMS31_1_61 | 0.06592 | 0.00272 | 1.13737 | 0.05215 | 0.12540 | 0.00382 | 802.9 | 33.1 | 771.3 | 35.4 | 761.6 | 23.2 |
| WMS31_1_62 | 0.19678 | 0.00711 | 11.12146 | 0.49377 | 0.41211 | 0.01368 | 2798.9 | 101.1 | 2533.4 | 112.5 | 2224.6 | 73.8 |
| WMS31_1_63 | 0.15263 | 0.00543 | 9.09418 | 0.38174 | 0.43135 | 0.01209 | 2374.9 | 84.5 | 2347.5 | 98.5 | 2311.8 | 64.8 |
| WMS31_1_64 | 0.05701 | 0.00244 | 0.69013 | 0.02766 | 0.08826 | 0.00291 | 491.0 | 21.0 | 532.9 | 21.4 | 545.2 | 18.0 |
| WMS31_1_65 | 0.10972 | 0.00433 | 4.87570 | 0.21234 | 0.32291 | 0.00785 | 1793.9 | 70.7 | 1798.1 | 78.3 | 1803.9 | 43.9 |
| WMS31_1_66 | 0.11094 | 0.00391 | 5.14688 | 0.22540 | 0.33744 | 0.01265 | 1814.1 | 63.9 | 1843.9 | 80.7 | 1874.4 | 70.3 |
| WMS31_1_67 | 0.05933 | 0.00315 | 0.70140 | 0.03970 | 0.08584 | 0.00244 | 578.1 | 30.7 | 539.6 | 30.5 | 530.9 | 15.1 |
| WMS31_1_68 | 0.05958 | 0.00317 | 0.70472 | 0.03858 | 0.08601 | 0.00238 | 587.3 | 31.3 | 541.6 | 29.7 | 531.9 | 14.7 |
| WMS31_1_69 | 0.05716 | 0.00426 | 1.00801 | 0.07330 | 0.12800 | 0.00390 | 496.7 | 37.0 | 707.9 | 51.5 | 776.5 | 23.7 |
| WMS31_1_70 | 0.05734 | 0.00198 | 0.75144 | 0.02409 | 0.09517 | 0.00257 | 503.7 | 17.4 | 569.1 | 18.2 | 586.1 | 15.8 |
| WMS31_1_71 | 0.13052 | 0.00519 | 6.84230 | 0.33455 | 0.38118 | 0.01218 | 2104.2 | 83.7 | 2091.2 | 102.2 | 2081.8 | 66.5 |
| WMS31_1_72 | 0.16029 | 0.00556 | 11.21321 | 0.42787 | 0.50935 | 0.01213 | 2458.0 | 85.3 | 2541.0 | 97.0 | 2653.8 | 63.2 |
| WMS31_1_73 | 0.05258 | 0.00241 | 0.62797 | 0.02625 | 0.08673 | 0.00293 | 309.5 | 14.2 | 494.8 | 20.7 | 536.2 | 18.1 |
| WMS31_1_74 | 0.12060 | 0.00389 | 4.32424 | 0.15408 | 0.26063 | 0.00559 | 1964.3 | 63.4 | 1698.0 | 60.5 | 1493.1 | 32.0 |
| WMS31_1_75 | 0.09149 | 0.00374 | 2.37625 | 0.09553 | 0.18763 | 0.00505 | 1455.9 | 59.4 | 1235.5 | 49.7 | 1108.5 | 29.9 |
| WMS31_1_76 | 0.06153 | 0.00253 | 1.13100 | 0.04516 | 0.13381 | 0.00384 | 656.8 | 27.0 | 768.2 | 30.7 | 809.6 | 23.3 |
| WMS31_1_77 | 0.16612 | 0.00607 | 9.87596 | 0.54599 | 0.43356 | 0.02067 | 2518.2 | 92.0 | 2423.3 | 134.0 | 2321.7 | 110.7 |
| WMS31_1_78 | 0.06243 | 0.00482 | 0.64316 | 0.05044 | 0.07492 | 0.00265 | 687.9 | 53.1 | 504.3 | 39.5 | 465.7 | 16.5 |
| WMS31_1_79 | 0.11603 | 0.00380 | 4.39125 | 0.20060 | 0.27426 | 0.01282 | 1895.2 | 62.1 | 1710.7 | 78.1 | 1562.4 | 73.0 |
| WMS31_1_80 | 0.11380 | 0.00427 | 4.65432 | 0.19407 | 0.29723 | 0.00885 | 1860.2 | 69.8 | 1759.1 | 73.3 | 1677.6 | 50.0 |
| WMS31_1_81 | 0.05805 | 0.00172 | 0.72591 | 0.02471 | 0.09074 | 0.00310 | 530.8 | 15.7 | 554.2 | 18.9 | 559.9 | 19.1 |
| WMS31_1_82 | 0.08887 | 0.00325 | 1.71228 | 0.06693 | 0.14005 | 0.00515 | 1400.5 | 51.3 | 1013.1 | 39.6 | 845.0 | 31.1 |
| WMS31_1_83 | 0.14958 | 0.00579 | 5.99674 | 0.38579 | 0.29269 | 0.01129 | 2340.3 | 90.6 | 1975.4 | 127.1 | 1654.9 | 63.9 |
| WMS31_1_84 | 0.18944 | 0.00704 | 2.69904 | 0.09988 | 0.10363 | 0.00324 | 2736.5 | 101.7 | 1328.2 | 49.1 | 635.6 | 19.9 |
| WMS31_1_85 | 0.06038 | 0.00256 | 0.77243 | 0.03317 | 0.09303 | 0.00348 | 616.4 | 26.2 | 581.2 | 25.0 | 573.4 | 21.4 |
| WMS31_1_86 | 0.05868 | 0.00271 | 0.73831 | 0.03282 | 0.09105 | 0.00316 | 554.2 | 25.6 | 561.4 | 25.0 | 561.7 | 19.5 |
| WMS31_1_87 | 0.17919 | 0.00604 | 11.17238 | 0.31059 | 0.45377 | 0.00978 | 2644.7 | 89.1 | 2537.6 | 70.5 | 2412.0 | 52.0 |

| sample | $^{207}Pb^*/^{206}Pb^*$ | | $^{207}Pb^*/^{235}U$ | | $^{206}Pb^*/^{238}U$ | | $^{207}Pb/^{206}Pb$ | | $^{207}Pb/^{235}U$ | | $^{206}Pb/^{238}U$ | |
|---|---|---|---|---|---|---|---|---|---|---|---|---|
| | value | 1 s.e | value | 1 s.e | value | 1 s.e | age (Ma) | 1 s.e | age (Ma) | 1 s.e | age (Ma) | 1 s.e |
| WMS31_1_88 | 0.12865 | 0.00588 | 3.62397 | 0.19891 | 0.20354 | 0.00831 | 2078.8 | 95.0 | 1554.8 | 85.3 | 1194.3 | 48.8 |
| WMS31_1_89 | 0.06661 | 0.00223 | 1.11428 | 0.03665 | 0.12154 | 0.00473 | 824.7 | 27.6 | 760.2 | 25.0 | 739.4 | 28.8 |
| WMS31_1_90 | 0.08331 | 0.00393 | 0.30356 | 0.01494 | 0.02653 | 0.00093 | 1275.6 | 60.2 | 269.2 | 13.2 | 168.8 | 5.9 |
| WMS31_1_91 | 0.15747 | 0.00605 | 8.19402 | 0.34411 | 0.37611 | 0.01156 | 2427.9 | 93.3 | 2252.7 | 94.6 | 2058.1 | 63.3 |
| WMS31_1_92 | 0.06208 | 0.00220 | 0.73700 | 0.02455 | 0.08637 | 0.00223 | 675.8 | 23.9 | 560.7 | 18.7 | 534.0 | 13.8 |
| WMS31_1_93 | 0.07005 | 0.00297 | 1.17695 | 0.04809 | 0.12241 | 0.00335 | 929.0 | 39.3 | 789.9 | 32.3 | 744.4 | 20.3 |
| WMS31_1_94 | 0.06821 | 0.00355 | 1.17626 | 0.05890 | 0.12448 | 0.00345 | 874.1 | 45.4 | 789.6 | 39.5 | 756.3 | 20.9 |
| WMS31_1_95 | 0.05790 | 0.00293 | 0.77503 | 0.03708 | 0.09707 | 0.00335 | 525.0 | 26.5 | 582.6 | 27.9 | 597.2 | 20.6 |
| WMS31_1_96 | 0.06083 | 0.00283 | 0.73064 | 0.02719 | 0.08743 | 0.00262 | 632.3 | 29.4 | 556.9 | 20.7 | 540.3 | 16.2 |
| WMS31_1_97 | 0.06333 | 0.00314 | 0.90225 | 0.04062 | 0.10304 | 0.00418 | 718.5 | 35.6 | 652.9 | 29.4 | 632.2 | 25.7 |
| WMS31_1_98 | 0.16978 | 0.00678 | 8.70594 | 0.35265 | 0.37387 | 0.01220 | 2554.7 | 102.1 | 2307.7 | 93.5 | 2047.6 | 66.8 |
| WMS31_1_99 | 0.07082 | 0.00253 | 1.51706 | 0.05012 | 0.15540 | 0.00258 | 951.5 | 33.9 | 937.3 | 31.0 | 931.2 | 15.5 |
| WMS31_1_100 | 0.18003 | 0.00609 | 11.73503 | 0.40252 | 0.47152 | 0.01143 | 2652.4 | 89.8 | 2583.5 | 88.6 | 2490.2 | 60.3 |
| WMS31_1_101 | 0.14782 | 0.00479 | 7.59130 | 0.29178 | 0.37250 | 0.00875 | 2320.0 | 75.1 | 2183.8 | 83.9 | 2041.1 | 48.0 |
| WMS31_1_102 | 0.15978 | 0.00552 | 9.86394 | 0.36939 | 0.45060 | 0.01288 | 2452.6 | 84.7 | 2422.1 | 90.7 | 2397.9 | 68.5 |
| WMS31_1_103 | 0.15678 | 0.00487 | 8.62852 | 0.30764 | 0.40089 | 0.01163 | 2420.4 | 75.2 | 2299.6 | 82.0 | 2173.1 | 63.1 |
| WMS31_1_104 | 0.06106 | 0.00198 | 1.07046 | 0.03439 | 0.12734 | 0.00546 | 640.3 | 20.8 | 739.0 | 23.7 | 772.6 | 33.2 |
| WMS31_1_105 | 0.06725 | 0.00380 | 1.17909 | 0.05861 | 0.12670 | 0.00276 | 844.6 | 47.7 | 790.9 | 39.3 | 769.0 | 16.8 |
| WMS31_1_106 | 0.05698 | 0.00210 | 0.70327 | 0.02879 | 0.08953 | 0.00249 | 489.8 | 18.1 | 540.7 | 22.1 | 552.8 | 15.4 |
| WMS31_1_107 | 0.06703 | 0.00234 | 1.25107 | 0.04492 | 0.13542 | 0.00277 | 837.7 | 29.3 | 823.9 | 29.6 | 818.7 | 16.7 |
| WMS31_1_108 | 0.06209 | 0.00420 | 0.75935 | 0.07006 | 0.08903 | 0.00242 | 676.3 | 45.7 | 573.6 | 52.9 | 549.8 | 15.0 |
| WMS31_1_109 | 0.06384 | 0.00333 | 1.24750 | 0.06327 | 0.14136 | 0.00634 | 735.3 | 38.4 | 822.3 | 41.7 | 852.4 | 38.2 |
| WMS31_1_110 | 0.08726 | 0.00365 | 1.94591 | 0.12185 | 0.16314 | 0.00701 | 1365.3 | 57.1 | 1097.0 | 68.7 | 974.2 | 41.8 |
| WMS31_1_111 | 0.05377 | 0.00277 | 0.61093 | 0.03148 | 0.08251 | 0.00208 | 360.4 | 18.6 | 484.1 | 24.9 | 511.1 | 12.9 |
| WMS31_1_112 | 0.10165 | 0.00352 | 3.28755 | 0.16848 | 0.23538 | 0.00784 | 1653.7 | 57.2 | 1478.1 | 75.7 | 1362.7 | 45.4 |
| WMS31_1_113 | 0.07004 | 0.00360 | 1.31798 | 0.14008 | 0.13593 | 0.00616 | 928.7 | 47.7 | 853.6 | 90.7 | 821.6 | 37.3 |
| WMS31_1_114 | 0.09464 | 0.00393 | 2.35956 | 0.10003 | 0.18140 | 0.00407 | 1520.2 | 63.1 | 1230.5 | 52.2 | 1074.6 | 24.1 |
| WMS31_1_115 | 0.07614 | 0.00515 | 1.01431 | 0.07707 | 0.09685 | 0.00434 | 1097.8 | 74.3 | 711.1 | 54.0 | 595.9 | 26.7 |
| WMS31_1_116 | 0.06042 | 0.00286 | 0.75006 | 0.03277 | 0.09002 | 0.00372 | 617.5 | 29.3 | 568.3 | 24.8 | 555.6 | 22.9 |
| WMS31_1_117 | 0.06012 | 0.00224 | 0.68506 | 0.03798 | 0.08310 | 0.00399 | 606.9 | 22.6 | 529.8 | 29.4 | 514.6 | 24.7 |
| WMS31_1_118 | 0.06541 | 0.00340 | 1.20978 | 0.06116 | 0.13442 | 0.00331 | 786.8 | 40.9 | 805.1 | 40.7 | 813.0 | 20.0 |
| WMS31_1_119 | 0.10148 | 0.00416 | 3.04939 | 0.13775 | 0.21907 | 0.00883 | 1650.6 | 67.7 | 1420.1 | 64.2 | 1277.0 | 51.5 |
| WMS31_1_120 | 0.05830 | 0.00207 | 0.67997 | 0.02469 | 0.08478 | 0.00140 | 540.1 | 19.2 | 526.8 | 19.1 | 524.6 | 8.7 |
| WMS31_1_121 | 0.10580 | 0.00394 | 4.59186 | 0.17686 | 0.31504 | 0.00762 | 1727.4 | 64.3 | 1747.8 | 67.3 | 1765.5 | 42.7 |
| WMS31_1_122 | 0.06760 | 0.00281 | 1.35770 | 0.07250 | 0.14544 | 0.00476 | 855.5 | 35.6 | 870.9 | 46.5 | 875.3 | 28.7 |
| WMS31_1_123 | 0.06519 | 0.00286 | 1.21401 | 0.05289 | 0.13515 | 0.00299 | 779.5 | 34.2 | 807.0 | 35.2 | 817.2 | 18.1 |
| WMS31_1_124 | 0.15787 | 0.00688 | 9.20931 | 0.36781 | 0.42399 | 0.01146 | 2432.2 | 106.0 | 2359.0 | 94.2 | 2278.6 | 61.6 |
| WMS31_1_125 | 0.14831 | 0.00594 | 6.14989 | 0.23627 | 0.30002 | 0.00843 | 2325.8 | 93.2 | 1997.4 | 76.7 | 1691.4 | 47.5 |
| WMS31_1_126 | 0.06182 | 0.00272 | 0.68177 | 0.03433 | 0.07998 | 0.00213 | 667.0 | 29.3 | 527.8 | 26.6 | 496.0 | 13.2 |
| WMS31_1_127 | 0.06539 | 0.00231 | 1.08257 | 0.04102 | 0.12006 | 0.00263 | 786.0 | 27.8 | 744.9 | 28.2 | 730.9 | 16.0 |
| WMS31_1_128 | 0.06804 | 0.00230 | 1.18534 | 0.04240 | 0.12644 | 0.00315 | 868.7 | 29.3 | 793.8 | 28.4 | 767.5 | 19.1 |
| WMS31_1_129 | 0.06185 | 0.00256 | 0.70920 | 0.02763 | 0.08316 | 0.00141 | 667.9 | 27.7 | 544.3 | 21.2 | 514.9 | 8.7 |
| WMS31_1_130 | 0.11151 | 0.00340 | 4.87219 | 0.17383 | 0.31781 | 0.00814 | 1823.4 | 55.6 | 1797.5 | 64.1 | 1779.0 | 45.5 |
| WMS31_1_131 | 0.06706 | 0.00411 | 0.96653 | 0.05788 | 0.10495 | 0.00279 | 838.8 | 51.4 | 686.7 | 41.1 | 643.4 | 17.1 |
| WMS31_1_132 | 0.06008 | 0.00320 | 0.68105 | 0.03565 | 0.08276 | 0.00201 | 605.3 | 32.3 | 527.4 | 27.6 | 512.6 | 12.4 |
| WMS31_1_133 | 0.17617 | 0.00574 | 9.90672 | 0.36519 | 0.40789 | 0.01040 | 2616.4 | 85.3 | 2426.1 | 89.4 | 2205.2 | 56.2 |
| WMS31_1_134 | 0.05959 | 0.00204 | 0.70079 | 0.02387 | 0.08536 | 0.00132 | 587.6 | 20.1 | 539.3 | 18.4 | 528.0 | 8.1 |
| WMS31_1_135 | 0.14544 | 0.00560 | 7.17394 | 0.29398 | 0.35772 | 0.01046 | 2292.2 | 88.3 | 2133.3 | 87.4 | 1971.3 | 57.6 |
| WMS31_1_136 | 0.06049 | 0.00243 | 0.69811 | 0.02764 | 0.08363 | 0.00128 | 620.2 | 24.9 | 537.7 | 21.3 | 517.7 | 7.9 |
| WMS31_1_137 | 0.06213 | 0.00267 | 0.83013 | 0.03949 | 0.09693 | 0.00298 | 677.6 | 29.1 | 613.7 | 29.2 | 596.4 | 18.3 |
| WMS31_1_138 | 0.05867 | 0.00341 | 0.68775 | 0.03884 | 0.08514 | 0.00230 | 553.7 | 32.2 | 531.4 | 30.0 | 526.7 | 14.2 |
| WMS31_1_139 | 0.07473 | 0.00241 | 1.69337 | 0.05687 | 0.16492 | 0.00334 | 1060.3 | 34.2 | 1006.0 | 33.8 | 984.1 | 19.9 |
| WMS31_1_140 | 0.17689 | 0.00694 | 11.57573 | 0.42542 | 0.47540 | 0.01590 | 2623.1 | 102.9 | 2570.7 | 94.5 | 2507.2 | 83.9 |
| WMS31_1_141 | 0.10135 | 0.00408 | 2.59591 | 0.13528 | 0.18581 | 0.00681 | 1648.1 | 66.3 | 1299.5 | 67.7 | 1098.6 | 40.3 |
| WMS31_1_142 | 0.07159 | 0.00232 | 1.45543 | 0.05192 | 0.14752 | 0.00327 | 973.3 | 31.6 | 912.1 | 32.5 | 887.0 | 19.7 |
| WMS31_1_143 | 0.13834 | 0.00419 | 7.16073 | 0.24440 | 0.37649 | 0.00705 | 2205.7 | 66.8 | 2131.6 | 72.8 | 2059.8 | 38.6 |
| WMS31_1_144 | 0.27771 | 0.00917 | 26.86391 | 0.97828 | 0.70343 | 0.01773 | 3349.4 | 110.6 | 3378.5 | 123.0 | 3433.6 | 86.5 |
| 34_1 (20°22'31,89"S , 44°59'24,26"E) | | | | | | | | | | | | |
| WMS34_1_1 | 0.09276 | 0.00440 | 2.09245 | 0.11487 | 0.16400 | 0.00712 | 1482.1 | 70.3 | 1146.3 | 62.9 | 978.9 | 42.5 |
| WMS34_1_2 | 0.16762 | 0.00755 | 10.60457 | 0.68406 | 0.46204 | 0.02907 | 2533.3 | 114.1 | 2489.1 | 160.6 | 2448.6 | 154.1 |
| WMS34_1_3 | 0.07338 | 0.00278 | 1.84290 | 0.06474 | 0.18179 | 0.00513 | 1023.6 | 38.8 | 1060.9 | 37.3 | 1076.7 | 30.4 |
| WMS34_1_4 | 0.17645 | 0.00758 | 10.30961 | 0.42171 | 0.42332 | 0.01682 | 2619.1 | 112.5 | 2463.0 | 100.7 | 2275.5 | 90.4 |
| WMS34_1_5 | 0.16886 | 0.00928 | 3.97518 | 0.19208 | 0.17238 | 0.00917 | 2545.7 | 139.8 | 1629.1 | 78.7 | 1025.2 | 54.5 |
| WMS34_1_6 | 0.05495 | 0.00331 | 0.68777 | 0.03746 | 0.09076 | 0.00341 | 409.1 | 24.7 | 531.5 | 28.9 | 560.0 | 21.1 |
| WMS34_1_7 | 0.06083 | 0.00266 | 0.81181 | 0.02982 | 0.09518 | 0.00292 | 632.2 | 27.7 | 603.5 | 22.2 | 586.1 | 18.0 |
| WMS34_1_8 | 0.06525 | 0.00307 | 0.90684 | 0.04532 | 0.10071 | 0.00449 | 781.3 | 36.7 | 655.4 | 32.8 | 618.6 | 27.6 |
| WMS34_1_9 | 0.15177 | 0.00541 | 7.46632 | 0.29344 | 0.35823 | 0.01036 | 2365.2 | 84.3 | 2169.0 | 85.2 | 1973.8 | 57.1 |
| WMS34_1_10 | 0.07879 | 0.00394 | 1.07543 | 0.06423 | 0.09977 | 0.00651 | 1166.0 | 58.2 | 741.4 | 44.3 | 613.0 | 40.0 |
| WMS34_1_11 | 0.18902 | 0.00845 | 11.55836 | 0.58398 | 0.44277 | 0.01663 | 2732.9 | 122.2 | 2569.3 | 129.8 | 2363.0 | 88.7 |
| WMS34_1_12 | 0.15125 | 0.00564 | 4.64822 | 0.29729 | 0.22210 | 0.01222 | 2359.3 | 87.9 | 1758.0 | 112.4 | 1293.0 | 71.1 |
| WMS34_1_13 | 0.16458 | 0.00782 | 12.32511 | 0.59430 | 0.54361 | 0.02261 | 2502.5 | 118.8 | 2629.5 | 126.8 | 2798.5 | 116.4 |
| WMS34_1_14 | 0.15645 | 0.00795 | 9.16286 | 0.45556 | 0.42197 | 0.02091 | 2416.8 | 122.8 | 2354.4 | 117.1 | 2269.4 | 112.4 |
| WMS34_1_15 | 0.11087 | 0.00358 | 4.26745 | 0.18731 | 0.27953 | 0.01131 | 1812.9 | 58.6 | 1687.1 | 74.1 | 1589.0 | 64.3 |
| WMS34_1_16 | 0.11722 | 0.00583 | 4.78531 | 0.25918 | 0.29396 | 0.01787 | 1913.5 | 95.2 | 1782.3 | 96.5 | 1661.3 | 101.0 |
| WMS34_1_17 | 0.05526 | 0.00175 | 0.68342 | 0.02287 | 0.08970 | 0.00257 | 421.9 | 13.4 | 528.8 | 17.7 | 553.8 | 15.9 |
| WMS34_1_18 | 0.06157 | 0.00277 | 0.80822 | 0.03659 | 0.09474 | 0.00447 | 658.1 | 29.6 | 601.5 | 27.2 | 583.5 | 27.5 |
| WMS34_1_19 | 0.05960 | 0.00232 | 0.78006 | 0.03266 | 0.09492 | 0.00187 | 588.0 | 22.9 | 585.5 | 24.5 | 584.6 | 11.5 |
| WMS34_1_20 | 0.21559 | 0.00741 | 15.78052 | 0.72891 | 0.52969 | 0.02183 | 2947.3 | 101.3 | 2863.6 | 132.3 | 2740.2 | 112.9 |
| WMS34_1_21 | 0.06291 | 0.00298 | 0.94979 | 0.05566 | 0.10824 | 0.00472 | 704.2 | 33.3 | 678.0 | 39.7 | 662.5 | 28.9 |
| WMS34_1_22 | 0.15074 | 0.00485 | 8.13717 | 0.27542 | 0.39099 | 0.01024 | 2353.5 | 75.7 | 2246.4 | 76.0 | 2127.4 | 55.7 |
| WMS34_1_23 | 0.06672 | 0.00288 | 1.19242 | 0.05778 | 0.12986 | 0.00564 | 828.2 | 35.7 | 797.1 | 38.6 | 787.1 | 34.2 |
| WMS34_1_24 | 0.06389 | 0.00246 | 1.09063 | 0.04976 | 0.12380 | 0.00445 | 736.9 | 28.4 | 748.8 | 34.2 | 752.4 | 27.0 |
| WMS34_1_25 | 0.10701 | 0.00485 | 4.19295 | 0.18740 | 0.28489 | 0.00956 | 1748.4 | 79.3 | 1672.6 | 74.8 | 1615.9 | 54.3 |
| WMS34_1_26 | 0.12186 | 0.00912 | 1.50107 | 0.11408 | 0.08845 | 0.00695 | 1982.8 | 148.3 | 930.8 | 70.7 | 546.3 | 42.9 |
| WMS34_1_27 | 0.15383 | 0.00614 | 9.73867 | 0.41989 | 0.45934 | 0.01608 | 2388.2 | 95.3 | 2410.4 | 103.9 | 2436.6 | 85.3 |
| WMS34_1_28 | 0.10293 | 0.00451 | 3.26815 | 0.12161 | 0.23019 | 0.00889 | 1676.8 | 73.5 | 1473.5 | 54.8 | 1335.5 | 51.6 |

| sample | $^{207}Pb^{*}/^{206}Pb^{*}$ | | $^{207}Pb^{*}/^{235}U$ | | $^{206}Pb^{*}/^{238}U$ | | $^{207}Pb/^{206}Pb$ | | $^{207}Pb/^{235}U$ | | $^{206}Pb/^{238}U$ | |
|---|---|---|---|---|---|---|---|---|---|---|---|---|
| | value | 1 s.e | value | 1 s.e | value | 1 s.e | age (Ma) | 1 s.e | age (Ma) | 1 s.e | age (Ma) | 1 s.e |
| WMS34_1_29 | 0.06112 | 0.00245 | 0.75605 | 0.02874 | 0.08964 | 0.00297 | 642.6 | 25.7 | 571.7 | 21.7 | 553.4 | 18.3 |
| WMS34_1_30 | 0.06372 | 0.00361 | 0.84332 | 0.05844 | 0.09700 | 0.00615 | 731.4 | 41.4 | 621.0 | 43.0 | 596.8 | 37.8 |
| WMS34_1_31 | 0.09556 | 0.00527 | 2.51374 | 0.22030 | 0.18800 | 0.01261 | 1538.3 | 84.9 | 1276.0 | 111.8 | 1110.5 | 74.5 |
| WMS34_1_32 | 0.05857 | 0.00241 | 0.77041 | 0.03271 | 0.09533 | 0.00236 | 550.3 | 22.6 | 580.0 | 24.6 | 587.0 | 14.6 |
| WMS34_1_33 | 0.05993 | 0.00210 | 1.00314 | 0.04229 | 0.12045 | 0.00400 | 600.0 | 21.0 | 705.4 | 29.7 | 733.1 | 24.4 |
| WMS34_1_34 | 0.05709 | 0.00303 | 0.70021 | 0.03553 | 0.08894 | 0.00385 | 494.2 | 26.3 | 538.9 | 27.3 | 549.2 | 23.8 |
| WMS34_1_35 | 0.05838 | 0.00300 | 0.70016 | 0.02726 | 0.08665 | 0.00297 | 543.1 | 27.9 | 538.9 | 21.0 | 535.7 | 18.3 |
| WMS34_1_36 | 0.09832 | 0.00399 | 3.04780 | 0.10957 | 0.22471 | 0.00713 | 1591.6 | 64.6 | 1419.7 | 51.0 | 1306.7 | 41.5 |
| WMS34_1_37 | 0.10791 | 0.00567 | 3.25438 | 0.26562 | 0.20641 | 0.01698 | 1763.6 | 92.7 | 1470.2 | 120.0 | 1209.7 | 99.5 |
| WMS34_1_38 | 0.07089 | 0.00535 | 1.16061 | 0.10193 | 0.11898 | 0.00410 | 953.4 | 72.0 | 782.2 | 68.7 | 724.7 | 24.9 |
| WMS34_1_39 | 0.06042 | 0.00257 | 0.71312 | 0.02898 | 0.08574 | 0.00194 | 617.8 | 26.3 | 546.6 | 22.2 | 530.3 | 12.0 |
| WMS34_1_40 | 0.11825 | 0.00399 | 5.19727 | 0.18662 | 0.31933 | 0.00817 | 1929.1 | 65.1 | 1852.2 | 66.5 | 1786.5 | 45.7 |
| WMS34_1_41 | 0.08496 | 0.00408 | 1.66661 | 0.14922 | 0.14138 | 0.00888 | 1313.8 | 63.0 | 995.9 | 89.2 | 852.5 | 53.5 |
| WMS34_1_42 | 0.12687 | 0.00433 | 4.60036 | 0.18345 | 0.26319 | 0.00630 | 2054.2 | 70.1 | 1749.3 | 69.8 | 1506.1 | 36.0 |
| WMS34_1_43 | 0.11856 | 0.00585 | 4.26188 | 0.16746 | 0.26149 | 0.01002 | 1933.9 | 95.4 | 1686.0 | 66.2 | 1497.4 | 57.4 |
| WMS34_1_44 | 0.11962 | 0.00636 | 5.28296 | 0.19977 | 0.31789 | 0.01806 | 1949.7 | 103.7 | 1866.1 | 70.6 | 1779.4 | 101.1 |
| WMS34_1_45 | 0.18615 | 0.00803 | 12.51248 | 0.45554 | 0.49166 | 0.01881 | 2707.7 | 116.8 | 2643.7 | 96.2 | 2577.9 | 98.6 |
| WMS34_1_46 | 0.17137 | 0.00972 | 10.00001 | 0.64349 | 0.42008 | 0.01846 | 2570.3 | 145.9 | 2434.8 | 156.7 | 2260.8 | 99.3 |
| WMS34_1_47 | 0.05714 | 0.00249 | 0.69472 | 0.02784 | 0.08774 | 0.00215 | 495.9 | 21.6 | 535.6 | 21.5 | 542.1 | 13.3 |
| WMS34_1_48 | 0.16241 | 0.00647 | 7.91920 | 0.33878 | 0.35646 | 0.01150 | 2480.2 | 98.9 | 2221.9 | 95.0 | 1965.4 | 63.4 |
| WMS34_1_49 | 0.05612 | 0.00248 | 0.68792 | 0.03014 | 0.08905 | 0.00208 | 456.1 | 20.1 | 531.5 | 23.3 | 549.9 | 12.8 |
| WMS34_1_50 | 0.06473 | 0.00268 | 1.15572 | 0.04844 | 0.12974 | 0.00504 | 764.8 | 31.7 | 779.9 | 32.7 | 786.4 | 30.6 |
| WMS34_1_51 | 0.11160 | 0.00447 | 4.22978 | 0.15992 | 0.27881 | 0.01035 | 1824.9 | 73.1 | 1679.8 | 63.5 | 1585.4 | 58.9 |
| WMS34_1_52 | 0.05836 | 0.00243 | 0.75159 | 0.03192 | 0.09345 | 0.00279 | 542.3 | 22.6 | 569.1 | 24.2 | 575.9 | 17.2 |
| WMS34_1_53 | 0.05445 | 0.00220 | 0.68466 | 0.02443 | 0.09128 | 0.00272 | 388.8 | 15.7 | 529.6 | 18.9 | 563.1 | 16.8 |
| WMS34_1_54 | 0.10830 | 0.00406 | 4.40106 | 0.14097 | 0.29419 | 0.00928 | 1770.2 | 66.4 | 1712.5 | 54.9 | 1662.4 | 52.4 |
| WMS34_1_55 | 0.06811 | 0.00220 | 1.22978 | 0.04395 | 0.13064 | 0.00277 | 871.1 | 28.1 | 814.2 | 29.1 | 791.5 | 16.8 |
| WMS34_1_56 | 0.05865 | 0.00209 | 0.67319 | 0.02634 | 0.08298 | 0.00174 | 553.1 | 19.7 | 522.6 | 20.4 | 513.9 | 10.8 |
| WMS34_1_57 | 0.09489 | 0.00286 | 3.46118 | 0.14124 | 0.25933 | 0.00980 | 1525.1 | 45.9 | 1518.4 | 62.0 | 1486.4 | 56.2 |
| WMS34_1_58 | 0.06226 | 0.00282 | 1.10836 | 0.05110 | 0.12858 | 0.00631 | 682.1 | 30.8 | 757.4 | 34.9 | 779.8 | 38.3 |
| WMS34_1_59 | 0.11613 | 0.00433 | 5.34660 | 0.17223 | 0.33303 | 0.00951 | 1896.6 | 70.8 | 1876.3 | 60.4 | 1853.0 | 52.9 |
| WMS34_1_60 | 0.06202 | 0.00273 | 0.79945 | 0.02667 | 0.09328 | 0.00335 | 673.9 | 29.7 | 596.5 | 19.9 | 574.9 | 20.7 |
| WMS34_1_61 | 0.10516 | 0.00403 | 4.76101 | 0.16988 | 0.32628 | 0.01001 | 1716.4 | 65.9 | 1778.1 | 63.4 | 1820.3 | 55.9 |
| WMS34_1_62 | 0.10466 | 0.00329 | 4.54681 | 0.20404 | 0.31476 | 0.01176 | 1707.5 | 53.7 | 1739.6 | 78.1 | 1764.1 | 65.9 |
| WMS34_1_63 | 0.11070 | 0.00443 | 2.04656 | 0.09191 | 0.13424 | 0.00523 | 1810.1 | 72.5 | 1131.2 | 50.8 | 812.0 | 31.6 |
| WMS34_1_64 | 0.06705 | 0.00323 | 1.21958 | 0.06006 | 0.13338 | 0.00518 | 838.3 | 40.4 | 809.6 | 39.9 | 807.1 | 31.4 |
| WMS34_1_65 | 0.07238 | 0.00363 | 0.67907 | 0.03069 | 0.06834 | 0.00288 | 995.6 | 49.9 | 526.2 | 23.8 | 426.1 | 18.0 |
| WMS34_1_66 | 0.10326 | 0.00327 | 3.53510 | 0.16441 | 0.24710 | 0.00972 | 1682.7 | 53.3 | 1535.1 | 71.4 | 1423.5 | 56.0 |
| WMS34_1_67 | 0.05913 | 0.00343 | 0.75252 | 0.04551 | 0.09187 | 0.00388 | 570.9 | 33.1 | 569.7 | 34.5 | 566.6 | 23.9 |
| WMS34_1_68 | 0.15927 | 0.00638 | 7.79557 | 0.40548 | 0.34924 | 0.01455 | 2447.1 | 98.0 | 2207.7 | 114.8 | 1931.0 | 80.4 |
| WMS34_1_69 | 0.05840 | 0.00284 | 0.73917 | 0.03372 | 0.09173 | 0.00238 | 543.8 | 26.4 | 561.9 | 25.6 | 565.8 | 14.7 |
| WMS34_1_70 | 0.05619 | 0.00261 | 0.73075 | 0.03052 | 0.09428 | 0.00359 | 458.8 | 21.4 | 557.0 | 23.3 | 580.8 | 22.1 |
| WMS34_1_71 | 0.15958 | 0.00697 | 9.17779 | 0.33139 | 0.41811 | 0.01275 | 2450.4 | 107.1 | 2355.9 | 85.1 | 2251.9 | 68.7 |
| WMS34_1_72 | 0.05968 | 0.00210 | 0.74166 | 0.02567 | 0.09014 | 0.00168 | 591.1 | 20.8 | 563.4 | 19.5 | 556.4 | 10.4 |
| WMS34_1_73 | 0.17945 | 0.00673 | 12.11607 | 0.48543 | 0.48902 | 0.01523 | 2647.1 | 99.3 | 2613.4 | 104.7 | 2566.4 | 79.9 |
| WMS34_1_74 | 0.10827 | 0.00543 | 4.23572 | 0.26261 | 0.28420 | 0.01556 | 1769.7 | 88.8 | 1681.0 | 104.2 | 1612.5 | 88.3 |
| WMS34_1_75 | 0.06721 | 0.00258 | 1.18285 | 0.04220 | 0.12782 | 0.00407 | 843.5 | 32.4 | 792.6 | 28.3 | 775.4 | 24.7 |
| WMS34_1_76 | 0.06623 | 0.00225 | 0.99575 | 0.03618 | 0.10900 | 0.00245 | 812.7 | 27.6 | 701.6 | 25.5 | 666.9 | 15.0 |
| WMS34_1_77 | 0.10979 | 0.00381 | 4.73806 | 0.14325 | 0.31397 | 0.00841 | 1795.1 | 62.2 | 1774.0 | 53.6 | 1760.2 | 47.1 |
| WMS34_1_78 | 0.08940 | 0.00447 | 0.79163 | 0.04316 | 0.06438 | 0.00328 | 1411.8 | 70.5 | 592.1 | 32.3 | 402.2 | 20.5 |
| WMS34_1_79 | 0.16705 | 0.00739 | 9.24572 | 0.39434 | 0.40045 | 0.01349 | 2527.6 | 111.7 | 2362.7 | 100.8 | 2171.1 | 73.1 |
| WMS34_1_80 | 0.16846 | 0.00749 | 8.80995 | 0.43104 | 0.37938 | 0.01540 | 2541.7 | 113.0 | 2318.5 | 113.4 | 2073.4 | 84.2 |
| WMS34_1_81 | 0.16154 | 0.00694 | 9.31180 | 0.34306 | 0.42202 | 0.01682 | 2471.1 | 106.2 | 2369.2 | 87.3 | 2269.7 | 90.5 |
| WMS34_1_82 | 0.06358 | 0.00345 | 0.80583 | 0.04119 | 0.09190 | 0.00252 | 726.8 | 39.4 | 600.1 | 30.7 | 566.8 | 15.5 |
| WMS34_1_83 | 0.05503 | 0.00212 | 0.75478 | 0.02679 | 0.09949 | 0.00282 | 412.3 | 15.9 | 571.0 | 20.3 | 611.4 | 17.3 |
| WMS34_1_84 | 0.17015 | 0.00793 | 8.12850 | 0.31910 | 0.34702 | 0.01600 | 2558.4 | 119.3 | 2245.4 | 88.1 | 1920.4 | 88.6 |
| WMS34_1_85 | 0.06430 | 0.00292 | 1.01785 | 0.03729 | 0.11509 | 0.00351 | 750.5 | 34.0 | 712.8 | 26.1 | 702.2 | 21.4 |
| WMS34_1_86 | 0.05363 | 0.00319 | 0.68391 | 0.03947 | 0.09385 | 0.00389 | 354.7 | 21.1 | 529.1 | 30.5 | 578.3 | 24.0 |
| WMS34_1_87 | 0.08055 | 0.00327 | 0.85612 | 0.06990 | 0.07763 | 0.00564 | 1209.5 | 49.2 | 628.0 | 51.3 | 482.0 | 35.0 |
| WMS34_1_88 | 0.06041 | 0.00236 | 0.99924 | 0.04109 | 0.12048 | 0.00428 | 617.4 | 24.1 | 703.4 | 28.9 | 733.3 | 26.1 |
| WMS34_1_89 | 0.16608 | 0.00460 | 10.43380 | 0.31900 | 0.45665 | 0.01014 | 2517.7 | 69.7 | 2474.1 | 75.6 | 2424.7 | 53.8 |
| WMS34_1_90 | 0.10507 | 0.00297 | 3.75183 | 0.11910 | 0.25909 | 0.00620 | 1714.7 | 48.5 | 1582.5 | 50.2 | 1485.2 | 35.5 |
| WMS34_1_91 | 0.10659 | 0.00371 | 4.15074 | 0.14290 | 0.28224 | 0.00809 | 1741.1 | 60.5 | 1664.4 | 57.3 | 1602.6 | 45.9 |
| WMS34_1_92 | 0.05287 | 0.00172 | 0.63626 | 0.02048 | 0.08747 | 0.00166 | 322.4 | 10.5 | 500.0 | 16.1 | 540.6 | 10.3 |
| WMS34_1_93 | 0.09975 | 0.00445 | 3.28225 | 0.21156 | 0.23620 | 0.01092 | 1618.6 | 72.2 | 1476.9 | 95.2 | 1366.9 | 63.2 |
| WMS34_1_94 | 0.07785 | 0.00316 | 1.30508 | 0.05015 | 0.12154 | 0.00470 | 1142.2 | 46.3 | 848.0 | 32.6 | 739.4 | 28.6 |
| WMS34_1_95 | 0.05851 | 0.00195 | 0.76398 | 0.02593 | 0.09458 | 0.00219 | 547.9 | 18.3 | 576.3 | 19.6 | 582.6 | 13.5 |
| WMS34_1_96 | 0.16186 | 0.00477 | 10.68697 | 0.33278 | 0.47858 | 0.00905 | 2474.4 | 73.0 | 2496.3 | 77.7 | 2521.1 | 47.7 |
| WMS34_1_97 | 0.06352 | 0.00302 | 1.17282 | 0.04735 | 0.13393 | 0.00426 | 724.8 | 34.4 | 788.0 | 31.8 | 810.3 | 25.8 |
| WMS34_1_98 | 0.06205 | 0.00217 | 0.85963 | 0.03026 | 0.10046 | 0.00221 | 675.0 | 23.7 | 629.9 | 22.2 | 617.1 | 13.6 |
| WMS34_1_99 | 0.12073 | 0.00440 | 5.54411 | 0.19849 | 0.33344 | 0.00980 | 1966.2 | 71.6 | 1907.5 | 68.3 | 1855.0 | 54.5 |
| WMS34_1_100 | 0.05617 | 0.00202 | 0.66203 | 0.02431 | 0.08541 | 0.00203 | 458.2 | 16.4 | 515.9 | 18.9 | 528.3 | 12.5 |
| WMS34_1_101 | 0.11347 | 0.00416 | 2.98079 | 0.18426 | 0.19164 | 0.00828 | 1854.9 | 68.0 | 1402.7 | 86.7 | 1130.3 | 48.8 |
| WMS34_1_102 | 0.10166 | 0.00498 | 3.85394 | 0.21583 | 0.27604 | 0.01544 | 1653.9 | 81.1 | 1604.1 | 89.8 | 1571.4 | 87.9 |
| WMS34_1_103 | 0.10012 | 0.00347 | 2.39324 | 0.07976 | 0.17320 | 0.00515 | 1625.5 | 56.4 | 1240.6 | 41.3 | 1029.7 | 30.6 |
| WMS34_1_104 | 0.06731 | 0.00300 | 0.64677 | 0.03090 | 0.06937 | 0.00226 | 846.4 | 37.7 | 506.5 | 24.2 | 432.4 | 14.1 |
| WMS34_1_105 | 0.07311 | 0.00307 | 1.45694 | 0.05585 | 0.14480 | 0.00403 | 1016.0 | 42.6 | 912.7 | 35.0 | 871.8 | 24.3 |
| WMS34_1_106 | 0.16220 | 0.00859 | 7.48121 | 0.49885 | 0.33394 | 0.01593 | 2478.0 | 131.2 | 2170.7 | 144.7 | 1857.5 | 88.6 |
| WMS34_1_107 | 0.05984 | 0.00292 | 0.75885 | 0.03129 | 0.09190 | 0.00412 | 596.7 | 29.1 | 573.3 | 23.6 | 566.8 | 25.4 |
| WMS34_1_108 | 0.18516 | 0.00716 | 12.84243 | 0.46415 | 0.50309 | 0.01517 | 2698.9 | 104.4 | 2668.2 | 96.4 | 2627.0 | 79.2 |
| WMS34_1_109 | 0.06552 | 0.00324 | 0.86544 | 0.04669 | 0.09565 | 0.00358 | 790.3 | 39.0 | 633.1 | 34.2 | 588.9 | 22.0 |
| WMS34_1_110 | 0.09911 | 0.00494 | 1.37704 | 0.12285 | 0.09930 | 0.00757 | 1606.7 | 80.0 | 879.2 | 78.4 | 610.3 | 46.5 |
| WMS34_1_111 | 0.16717 | 0.00786 | 8.95588 | 0.54337 | 0.38444 | 0.01987 | 2528.8 | 118.9 | 2333.5 | 141.6 | 2097.0 | 108.4 |
| WMS34_1_112 | 0.06542 | 0.00329 | 0.97545 | 0.05579 | 0.10731 | 0.00424 | 787.1 | 39.5 | 691.3 | 39.5 | 657.1 | 25.9 |
| WMS34_1_113 | 0.09090 | 0.00688 | 0.51254 | 0.03341 | 0.04089 | 0.00299 | 1443.7 | 109.3 | 420.2 | 27.4 | 258.3 | 18.9 |
| WMS34_1_114 | 0.07616 | 0.00787 | 0.90207 | 0.08535 | 0.08652 | 0.00549 | 1098.5 | 113.5 | 652.8 | 61.8 | 534.9 | 34.0 |

| sample | $^{207}Pb^{*}/^{206}Pb^{*}$ | | $^{207}Pb^{*}/^{235}U$ | | $^{206}Pb^{*}/^{238}U$ | | $^{207}Pb/^{206}Pb$ | | $^{207}Pb/^{235}U$ | | $^{206}Pb/^{238}U$ | |
|---|---|---|---|---|---|---|---|---|---|---|---|---|
| | value | 1 s.e | value | 1 s.e | value | 1 s.e | age (Ma) | 1 s.e | age (Ma) | 1 s.e | age (Ma) | 1 s.e |
| WMS34_1_115 | 0.06529 | 0.00316 | 0.84436 | 0.03391 | 0.09355 | 0.00362 | 782.8 | 37.9 | 621.5 | 25.0 | 576.5 | 22.3 |
| WMS34_1_116 | 0.05955 | 0.00237 | 0.86861 | 0.03287 | 0.10593 | 0.00269 | 586.2 | 23.4 | 634.8 | 24.0 | 649.0 | 16.5 |
| WMS34_1_117 | 0.09748 | 0.00415 | 2.50909 | 0.12646 | 0.18585 | 0.00567 | 1575.7 | 67.1 | 1274.7 | 64.2 | 1098.9 | 33.5 |
| WMS34_1_118 | 0.11352 | 0.00567 | 3.50332 | 0.16759 | 0.22528 | 0.01140 | 1855.6 | 92.6 | 1528.0 | 73.1 | 1309.7 | 66.3 |
| WMS34_1_119 | 0.16385 | 0.00689 | 9.04230 | 0.45607 | 0.40225 | 0.01844 | 2495.0 | 104.9 | 2342.3 | 118.1 | 2179.4 | 99.9 |
| WMS34_1_120 | 0.11865 | 0.00582 | 4.07010 | 0.20357 | 0.24816 | 0.01143 | 1935.3 | 94.9 | 1648.3 | 82.4 | 1429.0 | 65.8 |
| WMS34_1_121 | < DL | 0.00157 | < DL | 0.02403 | 0.11771 | 0.00674 | < DL | 0.0 | < DL | 0.0 | 717.4 | 41.1 |
| WMS34_1_121 | 0.05221 | 0.00417 | 1.07752 | 0.08405 | 0.14833 | 0.00585 | 293.8 | 23.5 | 742.4 | 57.9 | 891.6 | 35.2 |
| WMS34_1_122 | 0.06464 | 0.00230 | 1.16273 | 0.03944 | 0.13029 | 0.00323 | 761.7 | 27.1 | 783.2 | 26.6 | 789.5 | 19.6 |
| WMS34_1_123 | 0.06010 | 0.00309 | 0.73564 | 0.03514 | 0.08876 | 0.00280 | 606.2 | 31.2 | 559.9 | 26.7 | 548.2 | 17.3 |
| WMS34_1_124 | 0.15628 | 0.00640 | 8.74738 | 0.43329 | 0.40766 | 0.01717 | 2415.0 | 99.0 | 2312.0 | 114.5 | 2204.2 | 92.9 |
| WMS34_1_125 | 0.06740 | 0.00313 | 0.97417 | 0.07240 | 0.10403 | 0.00420 | 849.4 | 39.4 | 690.6 | 51.3 | 638.0 | 25.8 |
| WMS34_1_126 | 0.05407 | 0.00247 | 0.65836 | 0.02955 | 0.08850 | 0.00229 | 373.2 | 17.1 | 513.6 | 23.0 | 546.6 | 14.1 |
| WMS34_1_127 | 0.06500 | 0.00254 | 0.77918 | 0.02596 | 0.08680 | 0.00308 | 773.4 | 30.3 | 585.0 | 19.5 | 536.6 | 19.0 |
| WMS34_1_128 | 0.06862 | 0.00269 | 1.31065 | 0.05043 | 0.13853 | 0.00356 | 886.5 | 34.8 | 850.4 | 32.7 | 836.4 | 21.5 |
| WMS34_1_129 | 0.14005 | 0.00470 | 4.88775 | 0.30858 | 0.25141 | 0.01194 | 2227.0 | 74.7 | 1800.1 | 113.6 | 1445.7 | 68.7 |
| WMS34_1_130 | 0.17031 | 0.00544 | 10.00270 | 0.28085 | 0.42505 | 0.00899 | 2559.9 | 81.7 | 2435.0 | 68.4 | 2283.3 | 48.3 |
| WMS34_1_131 | 0.14238 | 0.00633 | 4.63481 | 0.25833 | 0.23639 | 0.01154 | 2255.5 | 100.2 | 1755.6 | 97.8 | 1367.9 | 66.8 |
| WMS34_1_132 | 0.07888 | 0.00517 | 2.00181 | 0.14852 | 0.18245 | 0.00830 | 1168.3 | 76.5 | 1116.1 | 82.8 | 1080.4 | 49.1 |
| WMS34_1_133 | 0.09651 | 0.00495 | 2.27952 | 0.17328 | 0.17036 | 0.01117 | 1557.0 | 79.8 | 1206.0 | 91.7 | 1014.1 | 66.5 |
| WMS34_1_134 | 0.08928 | 0.00520 | 1.40695 | 0.10349 | 0.11516 | 0.00724 | 1409.4 | 82.1 | 891.9 | 65.6 | 702.6 | 44.2 |
| WMS34_1_135 | 0.07461 | 0.00275 | 1.78824 | 0.06938 | 0.17357 | 0.00438 | 1057.0 | 38.9 | 1041.2 | 40.4 | 1031.7 | 26.0 |
| WMS34_1_136 | 0.11173 | 0.00400 | 4.66865 | 0.16282 | 0.30420 | 0.00909 | 1826.9 | 65.5 | 1761.6 | 61.4 | 1712.1 | 51.2 |
| WMS34_1_137 | 0.17137 | 0.00744 | 9.78080 | 0.42231 | 0.41394 | 0.01057 | 2570.3 | 111.6 | 2414.3 | 104.2 | 2232.9 | 57.0 |
| WMS34_1_138 | 0.05803 | 0.00254 | 0.69694 | 0.03202 | 0.08656 | 0.00418 | 529.8 | 23.2 | 537.0 | 24.7 | 535.1 | 25.8 |
| WMS34_1_139 | 0.16390 | 0.00630 | 7.49209 | 0.27165 | 0.33215 | 0.01552 | 2495.6 | 95.9 | 2172.0 | 78.8 | 1848.8 | 86.4 |
| WMS34_1_140 | 0.05813 | 0.00341 | 0.78582 | 0.04261 | 0.09798 | 0.00180 | 533.6 | 31.3 | 588.8 | 31.9 | 602.5 | 11.1 |
| WMS34_1_141 | 0.10745 | 0.00402 | 5.24230 | 0.21192 | 0.35342 | 0.01789 | 1755.8 | 65.7 | 1859.5 | 75.2 | 1950.9 | 98.8 |
| WMS34_1_142 | 0.05490 | 0.00259 | 0.70138 | 0.03681 | 0.09310 | 0.00387 | 407.3 | 19.2 | 539.6 | 28.3 | 573.8 | 23.8 |
| WMS34_1_143 | 0.13258 | 0.00575 | 0.29800 | 0.01349 | 0.01638 | 0.00053 | 2131.7 | 92.5 | 264.8 | 12.0 | 104.7 | 3.4 |
| WMS34_1_144 | 0.10350 | 0.00430 | 4.96939 | 0.19963 | 0.35003 | 0.01235 | 1687.0 | 70.0 | 1814.1 | 72.9 | 1934.7 | 68.3 |
| 39_3 (20°27'30,3"S , 45°13'36,8"E) | | | | | | | | | | | | |
| WMS39_3_1 | 0.05519 | 0.00458 | 0.99359 | 0.08330 | 0.13095 | 0.00928 | 419.1 | 34.8 | 700.5 | 58.7 | 793.3 | 56.2 |
| WMS39_3_2 | 0.06198 | 0.00449 | 0.82964 | 0.06427 | 0.09635 | 0.00623 | 672.5 | 48.7 | 613.4 | 47.5 | 593.0 | 38.3 |
| WMS39_3_3 | 0.05913 | 0.00209 | 0.78679 | 0.03041 | 0.09632 | 0.00305 | 571.0 | 20.2 | 589.4 | 22.8 | 592.8 | 18.8 |
| WMS39_3_4 | 0.38608 | 0.02498 | 7.27823 | 0.42860 | 0.13676 | 0.00649 | 3855.0 | 249.4 | 2146.1 | 126.4 | 826.3 | 39.2 |
| WMS39_3_5 | 0.07022 | 0.00410 | 1.49301 | 0.08133 | 0.15368 | 0.00627 | 933.9 | 54.5 | 927.5 | 50.5 | 921.6 | 37.6 |
| WMS39_3_6 | 0.06266 | 0.00278 | 0.86827 | 0.03535 | 0.10083 | 0.00225 | 695.7 | 30.8 | 634.6 | 25.8 | 619.2 | 13.8 |
| WMS39_3_7 | 0.12946 | 0.00796 | 2.68386 | 0.18184 | 0.14844 | 0.00975 | 2089.9 | 128.6 | 1324.0 | 89.7 | 892.2 | 58.6 |
| WMS39_3_8 | 0.15873 | 0.00570 | 8.79624 | 0.28769 | 0.40162 | 0.01050 | 2441.5 | 87.7 | 2317.1 | 75.8 | 2176.5 | 56.9 |
| WMS39_3_9 | 0.42840 | 0.04099 | 27.41737 | 1.73324 | 0.46577 | 0.02778 | 4011.2 | 383.8 | 3398.5 | 214.8 | 2465.0 | 147.0 |
| WMS39_3_10 | 0.06010 | 0.00281 | 1.09197 | 0.05973 | 0.13213 | 0.00428 | 606.2 | 28.3 | 749.5 | 41.0 | 800.0 | 25.9 |
| WMS39_3_11 | 0.07721 | 0.00420 | 1.72705 | 0.10646 | 0.16167 | 0.00561 | 1125.8 | 61.2 | 1018.7 | 62.8 | 966.1 | 33.5 |
| WMS39_3_12 | 0.15637 | 0.00679 | 9.86363 | 0.46632 | 0.45747 | 0.01838 | 2416.0 | 105.0 | 2422.1 | 114.5 | 2428.4 | 97.6 |
| WMS39_3_13 | 0.05821 | 0.00353 | 0.76756 | 0.04773 | 0.09572 | 0.00493 | 536.6 | 32.5 | 578.4 | 36.0 | 589.3 | 30.3 |
| WMS39_3_14 | 0.06590 | 0.00663 | 0.87097 | 0.11211 | 0.09698 | 0.00720 | 802.3 | 80.7 | 636.1 | 81.9 | 596.7 | 44.3 |
| WMS39_3_15 | 0.06018 | 0.00368 | 0.83920 | 0.04330 | 0.10146 | 0.00420 | 609.3 | 37.3 | 618.7 | 31.9 | 622.9 | 25.8 |
| WMS39_3_16 | 0.11362 | 0.01263 | 2.19614 | 0.17076 | 0.13959 | 0.00703 | 1857.2 | 206.5 | 1179.8 | 91.7 | 842.4 | 42.4 |
| WMS39_3_17 | 0.04817 | 0.00328 | 0.60591 | 0.04799 | 0.09237 | 0.00368 | 106.5 | 7.3 | 481.0 | 38.1 | 569.5 | 22.7 |
| WMS39_3_18 | 0.07014 | 0.00371 | 1.49678 | 0.07329 | 0.15546 | 0.00531 | 931.7 | 49.2 | 929.1 | 45.5 | 931.5 | 31.8 |
| WMS39_3_19 | 0.05915 | 0.00420 | 1.12021 | 0.08362 | 0.13731 | 0.00435 | 571.7 | 40.6 | 763.1 | 57.0 | 829.5 | 26.3 |
| WMS39_3_20 | 0.07454 | 0.00322 | 1.81618 | 0.08068 | 0.17669 | 0.00483 | 1055.3 | 45.6 | 1051.3 | 46.7 | 1048.8 | 28.7 |
| WMS39_3_21 | 0.14568 | 0.00505 | 6.50001 | 0.23889 | 0.32347 | 0.00827 | 2295.1 | 79.6 | 2045.9 | 75.2 | 1806.6 | 46.2 |
| WMS39_3_22 | 0.21976 | 0.01349 | 11.40668 | 0.76220 | 0.37865 | 0.02736 | 2978.2 | 182.8 | 2557.0 | 170.9 | 2070.0 | 149.5 |
| WMS39_3_23 | 0.09508 | 0.00374 | 1.30452 | 0.07440 | 0.09972 | 0.00405 | 1528.9 | 60.1 | 847.7 | 48.4 | 612.8 | 24.9 |
| WMS39_3_24 | 0.06192 | 0.00367 | 0.78696 | 0.04913 | 0.09209 | 0.00269 | 670.5 | 39.7 | 589.4 | 36.8 | 567.9 | 16.6 |
| WMS39_3_25 | 0.08909 | 0.00386 | 2.69816 | 0.11473 | 0.22035 | 0.00751 | 1405.1 | 60.8 | 1328.0 | 56.5 | 1283.7 | 43.8 |
| WMS39_3_26 | 0.17214 | 0.00978 | 8.84824 | 0.41725 | 0.37365 | 0.02174 | 2577.8 | 146.4 | 2322.5 | 109.5 | 2046.6 | 119.1 |
| WMS39_3_27 | 0.07304 | 0.00488 | 1.58545 | 0.11057 | 0.15745 | 0.00364 | 1014.2 | 67.7 | 964.5 | 67.3 | 942.6 | 21.8 |
| WMS39_3_28 | 0.07784 | 0.00312 | 1.65839 | 0.06884 | 0.15502 | 0.00485 | 1141.8 | 45.7 | 992.8 | 41.2 | 929.1 | 29.1 |
| WMS39_3_29 | 0.06266 | 0.00246 | 0.79527 | 0.03224 | 0.09217 | 0.00212 | 695.8 | 27.3 | 594.2 | 24.1 | 568.4 | 13.1 |
| WMS39_3_30 | 0.15421 | 0.00671 | 4.88881 | 0.31721 | 0.23044 | 0.01190 | 2392.4 | 104.1 | 1800.3 | 116.8 | 1336.8 | 69.0 |
| WMS39_3_31 | 0.07432 | 0.00633 | 2.04183 | 0.10640 | 0.20001 | 0.01202 | 1049.2 | 89.4 | 1129.6 | 58.9 | 1175.4 | 70.6 |
| WMS39_3_32 | 0.26093 | 0.00921 | 22.89377 | 0.94301 | 0.63463 | 0.02058 | 3251.7 | 114.7 | 3222.4 | 132.7 | 3167.9 | 102.7 |
| WMS39_3_33 | 0.08408 | 0.00561 | 0.95398 | 0.06277 | 0.08327 | 0.00601 | 1293.5 | 86.3 | 680.2 | 44.8 | 515.6 | 37.2 |
| WMS39_3_34 | 0.19391 | 0.01120 | 3.88464 | 0.21065 | 0.14669 | 0.00672 | 2774.9 | 160.3 | 1610.5 | 87.3 | 882.4 | 40.4 |
| WMS39_3_35 | 0.11147 | 0.00419 | 4.00872 | 0.23377 | 0.26156 | 0.01130 | 1822.7 | 68.4 | 1636.0 | 95.4 | 1497.8 | 64.7 |
| WMS39_3_36 | 0.06868 | 0.00341 | 1.03194 | 0.05844 | 0.10908 | 0.00388 | 888.3 | 44.1 | 719.9 | 40.8 | 667.4 | 23.8 |
| WMS39_3_37 | 0.11293 | 0.00730 | 2.37690 | 0.12535 | 0.15329 | 0.00897 | 1846.3 | 119.4 | 1235.7 | 65.2 | 919.4 | 53.8 |
| WMS39_3_38 | 0.09434 | 0.00835 | 1.99020 | 0.11733 | 0.15377 | 0.00775 | 1514.2 | 134.1 | 1112.2 | 65.6 | 922.1 | 46.5 |
| WMS39_3_39 | 0.22087 | 0.00923 | 19.91232 | 0.73623 | 0.65165 | 0.01893 | 2986.4 | 124.8 | 3087.1 | 114.1 | 3234.6 | 94.0 |
| WMS39_3_40 | 0.05713 | 0.00285 | 0.86890 | 0.04133 | 0.11083 | 0.00550 | 495.7 | 24.7 | 635.0 | 30.2 | 677.6 | 33.6 |
| WMS39_3_41 | 0.21663 | 0.01591 | 14.10097 | 1.09250 | 0.47211 | 0.02639 | 2955.1 | 217.0 | 2756.5 | 213.6 | 2492.8 | 139.3 |
| WMS39_3_42 | 0.07803 | 0.00378 | 1.37074 | 0.06436 | 0.12729 | 0.00524 | 1146.9 | 55.5 | 876.5 | 41.2 | 772.4 | 31.8 |
| WMS39_3_43 | 0.09912 | 0.00751 | 0.83791 | 0.04271 | 0.06135 | 0.00318 | 1606.8 | 121.8 | 618.0 | 31.5 | 383.8 | 19.9 |
| WMS39_3_44 | 0.17828 | 0.00722 | 12.46852 | 0.51101 | 0.50490 | 0.01862 | 2636.2 | 106.8 | 2640.4 | 108.2 | 2634.8 | 97.2 |
| WMS39_3_45 | 0.06733 | 0.00358 | 1.16322 | 0.05118 | 0.12510 | 0.00480 | 847.0 | 45.0 | 783.5 | 34.5 | 759.8 | 29.2 |
| WMS39_3_46 | 0.05416 | 0.00373 | 0.64104 | 0.04661 | 0.08583 | 0.00341 | 376.5 | 25.9 | 503.0 | 36.6 | 530.8 | 21.1 |
| WMS39_3_47 | 0.17089 | 0.00705 | 10.70394 | 0.48593 | 0.45512 | 0.01306 | 2565.6 | 105.9 | 2497.8 | 113.4 | 2418.0 | 69.4 |
| WMS39_3_48 | 0.06452 | 0.00233 | 1.23099 | 0.05124 | 0.13856 | 0.00418 | 757.8 | 27.4 | 814.8 | 33.9 | 836.5 | 25.2 |
| WMS39_3_49 | 0.05922 | 0.00273 | 0.86228 | 0.03766 | 0.10579 | 0.00322 | 574.1 | 26.5 | 631.4 | 27.6 | 648.3 | 19.7 |
| WMS39_3_50 | 0.06549 | 0.00451 | 0.80830 | 0.05724 | 0.08935 | 0.00216 | 789.2 | 54.3 | 601.5 | 42.6 | 551.7 | 13.3 |
| WMS39_3_51 | 0.06167 | 0.00339 | 0.88114 | 0.04864 | 0.10389 | 0.00469 | 661.8 | 36.4 | 641.6 | 35.4 | 637.2 | 28.7 |
| WMS39_3_52 | 0.29697 | 0.01972 | 26.08633 | 1.62071 | 0.64329 | 0.05285 | 3453.8 | 229.4 | 3349.8 | 208.1 | 3201.9 | 263.0 |
| WMS39_3_53 | 0.16171 | 0.00636 | 8.16267 | 0.31401 | 0.36625 | 0.01151 | 2472.9 | 97.2 | 2249.2 | 86.5 | 2011.7 | 63.2 |
| WMS39_3_54 | 0.19594 | 0.00958 | 13.02895 | 0.78939 | 0.48491 | 0.01984 | 2791.9 | 136.5 | 2681.8 | 162.5 | 2548.6 | 104.3 |

| sample | $^{207}Pb^*/^{206}Pb^*$ | | $^{207}Pb^*/^{235}U$ | | $^{206}Pb^*/^{238}U$ | | $^{207}Pb/^{206}Pb$ | | $^{207}Pb/^{235}U$ | | $^{206}Pb/^{238}U$ | |
|---|---|---|---|---|---|---|---|---|---|---|---|---|
| | value | 1 s.e | value | 1 s.e | value | 1 s.e | age (Ma) | 1 s.e | age (Ma) | 1 s.e | age (Ma) | 1 s.e |
| WMS39_3_55 | 0.07070 | 0.00313 | 1.79541 | 0.09317 | 0.18488 | 0.01120 | 947.7 | 42.0 | 1043.8 | 54.2 | 1093.6 | 66.3 |
| WMS39_3_56 | 0.06126 | 0.00370 | 0.82666 | 0.04890 | 0.09818 | 0.00436 | 647.3 | 39.1 | 611.8 | 36.2 | 603.7 | 26.8 |
| WMS39_3_57 | 0.06741 | 0.00336 | 1.33812 | 0.08428 | 0.14326 | 0.00815 | 849.5 | 42.4 | 862.4 | 54.3 | 863.0 | 49.1 |
| WMS39_3_58 | 0.10407 | 0.00558 | 2.84353 | 0.18259 | 0.19871 | 0.00833 | 1697.2 | 91.0 | 1367.1 | 87.8 | 1168.4 | 49.0 |
| WMS39_3_59 | 0.07401 | 0.00367 | 1.71991 | 0.10262 | 0.16806 | 0.00876 | 1041.0 | 51.6 | 1016.0 | 60.6 | 1001.4 | 52.2 |
| WMS39_3_60 | 0.06408 | 0.00401 | 1.38276 | 0.09078 | 0.15498 | 0.00674 | 743.3 | 46.6 | 881.6 | 57.9 | 928.8 | 40.4 |
| WMS39_3_61 | 0.06571 | 0.00288 | 1.24345 | 0.06384 | 0.13734 | 0.00470 | 796.2 | 34.9 | 820.4 | 42.1 | 829.6 | 28.4 |
| WMS39_3_62 | 0.07664 | 0.00329 | 1.90547 | 0.07798 | 0.17998 | 0.00634 | 1110.9 | 47.7 | 1083.0 | 44.3 | 1066.8 | 37.6 |
| WMS39_3_63 | 0.26799 | 0.01478 | 7.66039 | 0.48430 | 0.20554 | 0.01011 | 3293.6 | 181.6 | 2192.0 | 138.6 | 1205.0 | 59.3 |
| WMS39_3_64 | 0.06719 | 0.00471 | 0.85256 | 0.05942 | 0.09210 | 0.00521 | 842.9 | 59.0 | 626.1 | 43.6 | 567.9 | 32.1 |
| WMS39_3_65 | 0.06775 | 0.00305 | 1.30207 | 0.07469 | 0.13911 | 0.00586 | 860.1 | 38.8 | 846.6 | 48.6 | 839.6 | 35.4 |
| WMS39_3_66 | 0.06840 | 0.00260 | 1.27553 | 0.05389 | 0.13570 | 0.00430 | 879.7 | 33.4 | 834.9 | 35.3 | 820.3 | 26.0 |
| WMS39_3_67 | 0.06328 | 0.00452 | 0.95811 | 0.05050 | 0.10990 | 0.00511 | 716.8 | 51.2 | 682.3 | 36.0 | 672.2 | 31.3 |
| WMS39_3_68 | 0.18914 | 0.00666 | 12.96224 | 0.52669 | 0.49855 | 0.01573 | 2733.9 | 96.3 | 2676.9 | 108.8 | 2607.6 | 82.3 |
| WMS39_3_69 | 0.16275 | 0.00669 | 10.35237 | 0.37541 | 0.46214 | 0.01093 | 2483.7 | 102.1 | 2466.8 | 89.5 | 2449.0 | 57.9 |
| WMS39_3_70 | 0.07698 | 0.00394 | 1.24989 | 0.06702 | 0.11729 | 0.00342 | 1119.9 | 57.4 | 823.4 | 44.1 | 714.9 | 20.9 |
| WMS39_3_71 | 0.27262 | 0.01908 | 12.99761 | 0.86795 | 0.34534 | 0.02129 | 3320.5 | 232.4 | 2679.5 | 178.9 | 1912.3 | 117.9 |
| WMS39_3_72 | 0.11165 | 0.00569 | 4.22279 | 0.20995 | 0.27325 | 0.01072 | 1825.6 | 93.1 | 1678.5 | 83.4 | 1557.3 | 61.1 |
| WMS39_3_73 | 0.06072 | 0.00399 | 0.77543 | 0.04620 | 0.09286 | 0.00394 | 628.3 | 41.3 | 582.9 | 34.7 | 572.5 | 24.3 |
| WMS39_3_73a | 0.06097 | 0.00356 | 0.73026 | 0.04372 | 0.08735 | 0.00393 | 637.3 | 37.2 | 556.7 | 33.3 | 539.8 | 24.3 |
| WMS39_3_74 | 0.16256 | 0.00682 | 10.30714 | 0.39805 | 0.45850 | 0.02126 | 2481.7 | 104.2 | 2462.7 | 95.1 | 2432.9 | 112.8 |
| WMS39_3_75 | 0.12765 | 0.00634 | 3.36447 | 0.15012 | 0.19234 | 0.00999 | 2065.0 | 102.6 | 1496.2 | 66.8 | 1134.0 | 58.9 |
| WMS39_3_76 | 0.06375 | 0.00402 | 1.01951 | 0.06350 | 0.11596 | 0.00598 | 732.5 | 46.2 | 713.7 | 44.5 | 707.3 | 36.5 |
| WMS39_3_77 | 0.08984 | 0.00548 | 1.66622 | 0.08686 | 0.13324 | 0.00744 | 1421.3 | 86.6 | 995.7 | 51.9 | 806.3 | 45.0 |
| WMS39_3_78 | 0.18685 | 0.00990 | 8.57837 | 0.50972 | 0.33448 | 0.02358 | 2713.9 | 143.8 | 2294.3 | 136.3 | 1860.1 | 131.1 |
| WMS39_3_79 | 0.17205 | 0.00703 | 11.30584 | 0.58121 | 0.47796 | 0.01463 | 2577.0 | 105.3 | 2548.7 | 131.0 | 2518.3 | 77.1 |
| WMS39_3_80 | 0.06582 | 0.00270 | 1.18744 | 0.05060 | 0.13107 | 0.00327 | 799.8 | 32.8 | 794.8 | 33.9 | 794.0 | 19.8 |
| WMS39_3_81 | 0.20734 | 0.00992 | 19.37367 | 1.27516 | 0.67790 | 0.03418 | 2884.2 | 138.1 | 3060.6 | 201.4 | 3336.3 | 168.2 |
| WMS39_3_82 | 0.15507 | 0.00702 | 7.68460 | 0.30874 | 0.36056 | 0.01449 | 2401.9 | 108.7 | 2194.8 | 88.2 | 1984.8 | 79.8 |
| WMS39_3_83 | 0.06935 | 0.00379 | 1.72321 | 0.09972 | 0.18039 | 0.00779 | 908.2 | 49.6 | 1017.2 | 58.9 | 1069.1 | 46.2 |
| WMS39_3_84 | 0.07802 | 0.00418 | 1.02137 | 0.06489 | 0.09503 | 0.00310 | 1146.6 | 61.5 | 714.6 | 45.4 | 585.2 | 19.1 |
| WMS39_3_85 | 0.08105 | 0.00521 | 1.06492 | 0.06313 | 0.09521 | 0.00332 | 1221.8 | 78.6 | 736.2 | 43.6 | 586.3 | 20.4 |
| WMS39_3_86 | 0.07137 | 0.00290 | 1.50107 | 0.06028 | 0.15265 | 0.00457 | 967.2 | 39.3 | 930.8 | 37.4 | 915.8 | 27.4 |
| WMS39_3_87 | 0.16452 | 0.00822 | 10.33793 | 0.39207 | 0.45702 | 0.01790 | 2501.9 | 125.0 | 2465.5 | 93.5 | 2426.4 | 95.1 |
| WMS39_3_88 | 0.05864 | 0.00339 | 0.69402 | 0.04136 | 0.08588 | 0.00252 | 552.7 | 32.0 | 535.2 | 31.9 | 531.1 | 15.6 |
| WMS39_3_89 | 0.25540 | 0.01367 | 5.33710 | 0.35217 | 0.15302 | 0.00911 | 3217.8 | 172.2 | 1874.8 | 123.7 | 917.9 | 54.6 |
| WMS39_3_90 | 0.05711 | 0.00320 | 0.70410 | 0.04199 | 0.08933 | 0.00362 | 494.9 | 27.7 | 541.2 | 32.3 | 551.6 | 22.3 |
| WMS39_3_91 | 0.16701 | 0.00657 | 7.00596 | 0.43354 | 0.30728 | 0.01535 | 2527.1 | 99.5 | 2112.2 | 130.7 | 1727.3 | 86.3 |
| WMS39_3_92 | 0.05974 | 0.00268 | 0.80287 | 0.03414 | 0.09802 | 0.00303 | 593.1 | 26.6 | 598.4 | 25.4 | 602.8 | 18.6 |
| WMS39_3_93 | 0.14822 | 0.00730 | 6.80572 | 0.28371 | 0.33206 | 0.01316 | 2324.7 | 114.5 | 2086.5 | 87.0 | 1848.4 | 73.3 |
| WMS39_3_94 | 0.06107 | 0.00241 | 0.80668 | 0.03927 | 0.09654 | 0.00352 | 640.9 | 25.3 | 600.6 | 29.2 | 594.1 | 21.7 |
| WMS39_3_95 | 0.17930 | 0.01038 | 9.23128 | 0.45240 | 0.37086 | 0.02031 | 2645.7 | 153.2 | 2361.2 | 115.7 | 2033.5 | 111.4 |
| WMS39_3_96 | 0.17035 | 0.00880 | 8.70044 | 0.49616 | 0.37035 | 0.01819 | 2560.3 | 132.2 | 2307.1 | 131.6 | 2031.0 | 99.8 |
| WMS39_3_97 | 0.12045 | 0.00541 | 4.20060 | 0.21972 | 0.25257 | 0.00861 | 1962.0 | 88.2 | 1674.1 | 87.6 | 1451.7 | 49.5 |
| WMS39_3_98 | 0.06492 | 0.00312 | 1.15100 | 0.05028 | 0.12869 | 0.00342 | 770.9 | 37.0 | 777.7 | 34.0 | 780.4 | 20.7 |
| WMS39_3_99 | 0.16814 | 0.00640 | 10.96695 | 0.36352 | 0.47390 | 0.01378 | 2538.4 | 96.6 | 2520.3 | 83.5 | 2500.6 | 72.7 |
| WMS39_3_100 | 0.06425 | 0.00407 | 1.06743 | 0.06433 | 0.12052 | 0.00302 | 749.0 | 47.4 | 737.5 | 44.4 | 733.6 | 18.4 |
| WMS39_3_101 | 0.16673 | 0.00648 | 10.69740 | 0.37811 | 0.46654 | 0.01492 | 2524.4 | 98.1 | 2497.2 | 88.3 | 2468.3 | 78.9 |
| WMS39_3_102 | 0.16251 | 0.00661 | 8.68179 | 0.53173 | 0.39447 | 0.02606 | 2481.2 | 100.9 | 2305.2 | 141.2 | 2143.5 | 141.6 |
| WMS39_3_103 | 0.06517 | 0.00286 | 0.90972 | 0.03635 | 0.10191 | 0.00297 | 778.8 | 34.2 | 656.9 | 26.2 | 625.6 | 18.3 |
| WMS39_3_104 | 0.18324 | 0.00924 | 8.47719 | 0.49895 | 0.33797 | 0.01205 | 2681.7 | 135.3 | 2283.5 | 134.4 | 1876.9 | 66.9 |
| WMS39_3_105 | 0.21251 | 0.01162 | 2.21983 | 0.11511 | 0.07623 | 0.00344 | 2924.1 | 159.9 | 1187.3 | 61.6 | 473.6 | 21.4 |
| WMS39_3_106 | 0.06986 | 0.00457 | 0.92066 | 0.05555 | 0.09661 | 0.00411 | 923.3 | 60.4 | 662.7 | 40.0 | 594.5 | 25.3 |
| WMS39_3_107 | 0.07635 | 0.00299 | 1.61813 | 0.06785 | 0.15532 | 0.00427 | 1103.4 | 43.3 | 977.3 | 41.0 | 930.7 | 25.6 |
| 40_3 (20°25'43,3"S , 45°22'57,3"E) | | | | | | | | | | | | |
| WMS_40_3_1 | 0.05755 | 0.00275 | 0.78911 | 0.03005 | 0.09915 | 0.00359 | 511.8 | 24.4 | 590.7 | 22.5 | 609.4 | 22.1 |
| WMS_40_3_2 | 0.06572 | 0.00336 | 1.21269 | 0.06223 | 0.13398 | 0.00372 | 796.5 | 40.7 | 806.4 | 41.4 | 810.5 | 22.5 |
| WMS_40_3_3 | 0.06260 | 0.00202 | 1.12667 | 0.03933 | 0.13136 | 0.00250 | 693.8 | 22.4 | 766.2 | 26.7 | 795.6 | 15.1 |
| WMS_40_3_4 | 0.07297 | 0.00416 | 1.67853 | 0.06996 | 0.16752 | 0.00910 | 1012.1 | 57.7 | 1000.4 | 41.7 | 998.4 | 54.2 |
| WMS_40_3_5 | 0.06897 | 0.00695 | 1.15251 | 0.10874 | 0.12129 | 0.00953 | 896.8 | 90.4 | 778.4 | 73.4 | 738.0 | 58.0 |
| WMS_40_3_6 | 0.11862 | 0.00391 | 1.66492 | 0.11958 | 0.10093 | 0.00778 | 1934.8 | 63.7 | 995.3 | 71.5 | 619.8 | 47.8 |
| WMS_40_3_7 | 0.16252 | 0.00605 | 9.38036 | 0.32493 | 0.41628 | 0.01451 | 2481.3 | 92.3 | 2375.9 | 82.3 | 2243.6 | 78.2 |
| WMS_40_3_8 | 0.07805 | 0.00273 | 1.82689 | 0.06214 | 0.17025 | 0.00332 | 1147.3 | 40.2 | 1055.2 | 35.9 | 1013.5 | 19.7 |
| WMS_40_3_9 | 0.27334 | 0.01544 | 4.40528 | 0.30254 | 0.11657 | 0.00333 | 3324.6 | 187.8 | 1713.3 | 117.7 | 710.8 | 20.3 |
| WMS_40_3_10 | 0.17810 | 0.00426 | 10.81759 | 0.38917 | 0.44064 | 0.01227 | 2634.5 | 63.0 | 2507.6 | 90.2 | 2353.5 | 65.6 |
| WMS_40_3_11 | 0.21366 | 0.00498 | 17.63175 | 0.40511 | 0.59812 | 0.00629 | 2932.8 | 68.4 | 2969.9 | 68.2 | 3022.2 | 31.8 |
| WMS_40_3_12 | 0.05963 | 0.00270 | 0.74604 | 0.03300 | 0.09086 | 0.00148 | 589.1 | 26.7 | 565.9 | 25.0 | 560.6 | 9.1 |
| WMS_40_3_13 | 0.06760 | 0.00269 | 1.34943 | 0.04833 | 0.14438 | 0.00324 | 855.5 | 34.1 | 867.3 | 31.1 | 869.4 | 19.5 |
| WMS_40_3_14 | 0.06659 | 0.01039 | 0.87122 | 0.12603 | 0.09494 | 0.00280 | 824.2 | 128.6 | 636.2 | 92.0 | 584.7 | 17.3 |
| WMS_40_3_15 | 0.06460 | 0.00250 | 1.20487 | 0.04833 | 0.13501 | 0.00318 | 760.5 | 29.4 | 802.8 | 32.2 | 816.4 | 19.2 |
| WMS_40_3_16 | 0.05318 | 0.00435 | 0.67041 | 0.05042 | 0.09169 | 0.00343 | 335.4 | 27.4 | 521.0 | 39.2 | 565.5 | 21.2 |
| WMS_40_3_17 | 0.11489 | 0.01297 | 1.69677 | 0.17723 | 0.10751 | 0.00357 | 1877.3 | 211.9 | 1007.3 | 105.2 | 658.3 | 21.9 |
| WMS_40_3_18 | 0.06151 | 0.00271 | 0.74167 | 0.03225 | 0.08724 | 0.00285 | 656.2 | 28.9 | 563.4 | 24.5 | 539.2 | 17.6 |
| WMS_40_3_19 | 0.10568 | 0.00327 | 4.19766 | 0.19279 | 0.28691 | 0.01084 | 1725.3 | 53.4 | 1673.6 | 76.9 | 1626.1 | 61.5 |
| WMS_40_3_20 | 0.06040 | 0.00317 | 1.12694 | 0.06014 | 0.13530 | 0.00258 | 617.0 | 32.4 | 766.3 | 40.9 | 818.0 | 15.6 |
| WMS_40_3_21 | 0.25992 | 0.00830 | 5.39240 | 0.24799 | 0.15157 | 0.00514 | 3245.5 | 103.7 | 1883.6 | 86.6 | 909.7 | 30.8 |
| WMS_40_3_22 | 0.06342 | 0.00227 | 0.69968 | 0.02268 | 0.07964 | 0.00206 | 721.5 | 25.8 | 538.6 | 17.5 | 494.0 | 12.8 |
| WMS_40_3_23 | 0.10483 | 0.00293 | 3.48221 | 0.11329 | 0.24004 | 0.00589 | 1710.5 | 47.8 | 1523.2 | 49.6 | 1386.9 | 34.0 |
| WMS_40_3_24 | 0.06068 | 0.00200 | 0.83158 | 0.02807 | 0.09932 | 0.00143 | 627.1 | 20.6 | 614.5 | 20.7 | 610.4 | 8.8 |
| WMS_40_3_25 | 0.06173 | 0.00235 | 1.01989 | 0.03783 | 0.11979 | 0.00407 | 664.0 | 25.2 | 713.9 | 26.5 | 729.3 | 24.8 |
| WMS_40_3_26 | 0.06058 | 0.00208 | 0.93083 | 0.03279 | 0.11103 | 0.00313 | 623.3 | 21.4 | 668.1 | 23.5 | 678.7 | 19.1 |
| WMS_40_3_27 | 0.05191 | 0.00255 | 0.62520 | 0.03160 | 0.08717 | 0.00216 | 280.4 | 13.8 | 493.1 | 24.9 | 538.8 | 13.3 |
| WMS_40_3_28 | 0.15714 | 0.00568 | 10.58261 | 0.36712 | 0.48649 | 0.01098 | 2424.4 | 87.6 | 2487.2 | 86.3 | 2555.5 | 57.7 |

| sample | $^{207}Pb^*/^{206}Pb^*$ | | $^{207}Pb^*/^{235}U$ | | $^{206}Pb^*/^{238}U$ | | $^{207}Pb/^{206}Pb$ | | $^{207}Pb/^{235}U$ | | $^{206}Pb/^{238}U$ | |
|---|---|---|---|---|---|---|---|---|---|---|---|---|
| | value | 1 s.e | value | 1 s.e | value | 1 s.e | age (Ma) | 1 s.e | age (Ma) | 1 s.e | age (Ma) | 1 s.e |
| WMS_40_3_29 | 0.06309 | 0.00234 | 1.10432 | 0.04083 | 0.12476 | 0.00266 | 710.3 | 26.3 | 755.4 | 27.9 | 757.9 | 16.2 |
| WMS_40_3_30 | 0.14889 | 0.00413 | 6.70090 | 0.22912 | 0.32656 | 0.00798 | 2332.4 | 64.7 | 2072.7 | 70.9 | 1821.7 | 44.5 |
| WMS_40_3_31 | 0.25418 | 0.01265 | 5.10311 | 0.48757 | 0.14723 | 0.01477 | 3210.3 | 159.7 | 1836.6 | 175.5 | 885.4 | 88.8 |
| WMS_40_3_32 | 0.05703 | 0.00420 | 0.66950 | 0.05183 | 0.08505 | 0.00215 | 491.8 | 36.3 | 520.4 | 40.3 | 526.2 | 13.3 |
| WMS_40_3_33 | 0.06081 | 0.00250 | 0.82359 | 0.03095 | 0.09862 | 0.00258 | 631.5 | 26.0 | 610.0 | 22.9 | 606.3 | 15.9 |
| WMS_40_3_34 | 0.05900 | 0.00239 | 0.72810 | 0.03026 | 0.08922 | 0.00177 | 566.2 | 22.9 | 555.4 | 23.1 | 550.9 | 10.9 |
| WMS_40_3_35 | 0.05944 | 0.00229 | 0.74146 | 0.02824 | 0.09026 | 0.00213 | 582.2 | 22.4 | 563.3 | 21.5 | 557.1 | 13.2 |
| WMS_40_3_36 | 0.06128 | 0.00281 | 0.70473 | 0.03094 | 0.08340 | 0.00110 | 648.2 | 29.7 | 541.6 | 23.8 | 516.4 | 6.8 |
| WMS_40_3_37 | 0.16518 | 0.00578 | 8.19638 | 0.30728 | 0.36158 | 0.00905 | 2508.6 | 87.7 | 2252.9 | 84.5 | 1989.7 | 49.8 |
| WMS_40_3_38 | 0.27572 | 0.01177 | 14.85288 | 0.97802 | 0.39504 | 0.02861 | 3338.1 | 142.5 | 2805.9 | 184.8 | 2146.1 | 155.5 |
| WMS_40_3_39 | 0.05998 | 0.00485 | 0.82852 | 0.06502 | 0.09961 | 0.00370 | 601.8 | 48.7 | 612.8 | 48.1 | 612.1 | 22.7 |
| WMS_40_3_40 | 0.07114 | 0.00342 | 1.51009 | 0.06316 | 0.15364 | 0.00570 | 960.4 | 46.2 | 934.5 | 39.1 | 921.4 | 34.2 |
| WMS_40_3_41 | 0.05778 | 0.00292 | 0.70738 | 0.03693 | 0.08865 | 0.00273 | 520.5 | 26.3 | 543.2 | 28.4 | 547.5 | 16.9 |
| WMS_40_3_42 | 0.05855 | 0.00245 | 0.75163 | 0.02915 | 0.09269 | 0.00297 | 549.6 | 23.0 | 569.2 | 22.1 | 571.4 | 18.3 |
| WMS_40_3_44 | 0.05724 | 0.00193 | 0.74663 | 0.02497 | 0.09463 | 0.00162 | 499.9 | 16.8 | 566.3 | 18.9 | 582.9 | 9.9 |
| WMS_40_3_45 | 0.23503 | 0.01135 | 21.15183 | 0.88049 | 0.65095 | 0.02330 | 3085.9 | 149.1 | 3145.6 | 130.9 | 3231.9 | 115.7 |
| WMS_40_3_46 | 0.14344 | 0.00409 | 6.34682 | 0.20298 | 0.32189 | 0.00786 | 2268.4 | 64.7 | 2024.9 | 64.8 | 1799.0 | 43.9 |
| WMS_40_3_47 | 0.05950 | 0.00211 | 0.85712 | 0.03160 | 0.10422 | 0.00175 | 584.5 | 20.8 | 628.5 | 23.2 | 639.1 | 10.7 |
| WMS_40_3_48 | 0.06561 | 0.00311 | 1.15884 | 0.05642 | 0.12464 | 0.00527 | 792.9 | 37.6 | 781.4 | 38.0 | 757.2 | 32.0 |
| WMS_40_3_49 | 0.05872 | 0.00259 | 0.74421 | 0.03519 | 0.09074 | 0.00235 | 555.9 | 24.5 | 564.9 | 26.7 | 559.9 | 14.5 |
| WMS_40_3_50 | 0.16366 | 0.00704 | 9.89377 | 0.41996 | 0.43542 | 0.01765 | 2493.1 | 107.3 | 2424.9 | 102.9 | 2330.1 | 94.5 |
| WMS_40_3_51 | 0.12002 | 0.00445 | 3.02643 | 0.22404 | 0.18150 | 0.00925 | 1955.7 | 72.5 | 1414.3 | 104.7 | 1075.2 | 54.8 |
| WMS_40_3_52 | 0.15456 | 0.00572 | 10.11291 | 0.37181 | 0.47272 | 0.01131 | 2396.2 | 88.7 | 2445.2 | 89.9 | 2495.5 | 59.7 |
| WMS_40_3_53 | 0.14315 | 0.00637 | 7.84103 | 0.33700 | 0.38995 | 0.01346 | 2264.9 | 100.7 | 2212.9 | 95.1 | 2122.6 | 73.3 |
| WMS_40_3_54 | 0.06197 | 0.00287 | 0.99545 | 0.04674 | 0.11640 | 0.00471 | 672.2 | 31.1 | 701.5 | 32.9 | 709.8 | 28.7 |
| WMS_40_3_55 | 0.05731 | 0.00219 | 0.69652 | 0.02781 | 0.08809 | 0.00119 | 502.5 | 19.2 | 536.7 | 21.4 | 544.2 | 7.3 |
| WMS_40_3_56 | 0.05846 | 0.00357 | 0.79258 | 0.05005 | 0.09724 | 0.00273 | 546.0 | 33.3 | 592.6 | 37.4 | 598.2 | 16.8 |
| WMS_40_3_57 | 0.06775 | 0.00223 | 1.23735 | 0.06318 | 0.13209 | 0.00444 | 860.1 | 28.3 | 817.7 | 41.8 | 799.8 | 26.9 |
| WMS_40_3_58 | 0.05743 | 0.00203 | 0.68803 | 0.02398 | 0.08672 | 0.00203 | 507.0 | 17.9 | 531.6 | 18.5 | 536.1 | 12.5 |
| WMS_40_3_59 | 0.17823 | 0.00567 | 12.38182 | 0.38958 | 0.50064 | 0.01109 | 2635.8 | 83.9 | 2633.8 | 82.9 | 2616.5 | 58.0 |
| WMS_40_3_60 | 0.07423 | 0.00287 | 1.83577 | 0.06801 | 0.17689 | 0.00342 | 1046.9 | 40.5 | 1058.3 | 39.2 | 1050.0 | 20.3 |
| WMS_40_3_61 | 0.05835 | 0.00191 | 0.70140 | 0.02335 | 0.08708 | 0.00176 | 541.9 | 17.7 | 539.6 | 18.0 | 538.2 | 10.9 |
| WMS_40_3_62 | 0.06309 | 0.00231 | 0.91460 | 0.03661 | 0.10318 | 0.00252 | 710.2 | 26.0 | 659.5 | 26.4 | 633.0 | 15.5 |
| WMS_40_3_63 | 0.06351 | 0.00255 | 1.17127 | 0.04080 | 0.13370 | 0.00364 | 724.4 | 29.1 | 787.2 | 27.4 | 809.0 | 22.0 |
| WMS_40_3_64 | 0.06591 | 0.00326 | 1.03382 | 0.05554 | 0.11275 | 0.00417 | 802.5 | 39.7 | 720.8 | 38.7 | 688.7 | 25.5 |
| WMS_40_3_65 | 0.06177 | 0.00382 | 1.26115 | 0.07400 | 0.14534 | 0.00445 | 665.1 | 41.2 | 828.4 | 48.6 | 874.8 | 26.8 |
| WMS_40_3_66 | 0.05645 | 0.00305 | 0.75787 | 0.03359 | 0.09770 | 0.00395 | 468.9 | 25.4 | 572.8 | 25.4 | 600.9 | 24.3 |
| WMS_40_3_67 | 0.05422 | 0.00302 | 0.74615 | 0.03739 | 0.09809 | 0.00352 | 379.1 | 21.1 | 566.0 | 28.4 | 603.2 | 21.6 |
| WMS_40_3_68 | 0.16198 | 0.00798 | 7.62715 | 0.32754 | 0.34225 | 0.01079 | 2475.7 | 122.0 | 2188.1 | 94.0 | 1897.5 | 59.8 |
| WMS_40_3_69 | 0.16736 | 0.00709 | 7.48853 | 0.32149 | 0.32128 | 0.01307 | 2530.7 | 107.2 | 2171.6 | 93.2 | 1796.0 | 73.1 |
| WMS_40_3_70 | 0.05896 | 0.00228 | 0.77678 | 0.02972 | 0.09536 | 0.00162 | 564.6 | 21.8 | 583.6 | 22.3 | 587.1 | 10.0 |
| WMS_40_3_71 | 0.06820 | 0.00213 | 1.24164 | 0.03491 | 0.13187 | 0.00195 | 873.6 | 27.2 | 819.6 | 23.0 | 798.5 | 11.8 |
| WMS_40_3_72 | 0.12142 | 0.00844 | 3.65076 | 0.33507 | 0.21726 | 0.01066 | 1976.4 | 137.3 | 1560.7 | 143.2 | 1267.4 | 62.2 |
| WMS_40_3_73 | 0.06329 | 0.00242 | 1.08684 | 0.03993 | 0.12470 | 0.00288 | 717.0 | 27.5 | 747.0 | 27.4 | 757.5 | 17.5 |
| WMS_40_3_74 | 0.06136 | 0.00250 | 0.88178 | 0.03049 | 0.10415 | 0.00352 | 651.0 | 26.5 | 641.9 | 22.2 | 638.7 | 21.6 |
| WMS_40_3_75 | 0.08201 | 0.00621 | 1.54191 | 0.12979 | 0.13706 | 0.00350 | 1245.0 | 94.3 | 947.3 | 79.7 | 828.0 | 21.1 |
| WMS_40_3_76 | 0.20725 | 0.02041 | 7.20900 | 0.90869 | 0.25209 | 0.01426 | 2883.4 | 284.0 | 2137.6 | 269.4 | 1449.2 | 82.0 |
| WMS_40_3_77 | 0.06956 | 0.00249 | 1.41328 | 0.04952 | 0.14768 | 0.00470 | 914.3 | 32.7 | 894.5 | 31.3 | 887.9 | 28.3 |
| WMS_40_3_78 | 0.15441 | 0.00628 | 8.79742 | 0.37749 | 0.40884 | 0.01142 | 2394.6 | 97.4 | 2317.2 | 99.4 | 2209.6 | 61.7 |
| WMS_40_3_79 | 0.06094 | 0.00261 | 0.76166 | 0.03344 | 0.09104 | 0.00190 | 636.1 | 27.2 | 575.0 | 25.2 | 561.7 | 11.7 |
| WMS_40_3_80 | 0.07364 | 0.00247 | 1.94105 | 0.06046 | 0.19191 | 0.00342 | 1030.8 | 34.6 | 1095.4 | 34.1 | 1131.7 | 20.2 |
| WMS_40_3_81 | 0.06696 | 0.00263 | 1.15971 | 0.04525 | 0.12523 | 0.00272 | 835.6 | 32.8 | 781.8 | 30.5 | 760.6 | 16.5 |
| WMS_40_3_82 | 0.06847 | 0.00268 | 1.62480 | 0.06867 | 0.17269 | 0.00494 | 882.0 | 34.5 | 979.9 | 41.4 | 1026.9 | 29.4 |
| WMS_40_3_83 | 0.17090 | 0.00791 | 7.91559 | 0.42252 | 0.33723 | 0.01512 | 2565.7 | 118.7 | 2221.5 | 118.6 | 1873.3 | 84.0 |
| WMS_40_3_84 | 0.05913 | 0.00213 | 0.70320 | 0.02578 | 0.08648 | 0.00212 | 570.9 | 20.6 | 540.7 | 19.8 | 534.7 | 13.1 |
| WMS_40_3_85 | 0.06073 | 0.00260 | 0.78286 | 0.03485 | 0.09371 | 0.00271 | 628.7 | 26.9 | 587.1 | 26.1 | 577.4 | 16.7 |
| WMS_40_3_86 | 0.06258 | 0.00319 | 0.94712 | 0.04751 | 0.11202 | 0.00400 | 693.2 | 35.4 | 676.6 | 33.9 | 684.5 | 24.4 |
| WMS_40_3_87 | 0.06577 | 0.00353 | 1.29053 | 0.07474 | 0.14212 | 0.00505 | 798.2 | 42.8 | 841.5 | 48.7 | 856.6 | 30.5 |
| WMS_40_3_88 | 0.07169 | 0.00289 | 1.32748 | 0.05698 | 0.13447 | 0.00300 | 976.2 | 39.3 | 857.8 | 36.8 | 813.3 | 18.1 |
| WMS_40_3_89 | 0.06471 | 0.00447 | 1.16780 | 0.08200 | 0.13060 | 0.00318 | 763.9 | 52.8 | 785.6 | 55.2 | 791.3 | 19.3 |
| WMS_40_3_90 | 0.07321 | 0.00448 | 1.06173 | 0.07703 | 0.10480 | 0.00472 | 1018.9 | 62.3 | 734.7 | 53.3 | 642.4 | 28.9 |
| WMS_40_3_91 | 0.06737 | 0.00354 | 1.31429 | 0.06559 | 0.14157 | 0.00389 | 848.3 | 44.6 | 852.0 | 42.5 | 853.5 | 23.5 |
| WMS_40_3_92 | 0.06676 | 0.00414 | 1.09884 | 0.07458 | 0.11866 | 0.00418 | 829.3 | 51.5 | 752.8 | 51.1 | 722.8 | 25.5 |
| WMS_40_3_93 | 0.07417 | 0.00804 | 0.95180 | 0.06732 | 0.09191 | 0.00553 | 1045.2 | 113.3 | 679.0 | 48.0 | 566.8 | 34.1 |
| WMS_40_3_94 | 0.07572 | 0.00352 | 1.28803 | 0.06117 | 0.12265 | 0.00237 | 1086.8 | 50.6 | 840.4 | 39.9 | 745.8 | 14.4 |
| WMS_40_3_95 | 0.26628 | 0.01119 | 23.60121 | 1.19153 | 0.63565 | 0.02992 | 3283.5 | 137.9 | 3252.1 | 164.2 | 3171.9 | 149.3 |
| WMS_40_3_96 | 0.16853 | 0.00640 | 9.75419 | 0.39533 | 0.42011 | 0.01353 | 2542.3 | 96.6 | 2411.8 | 97.8 | 2261.0 | 72.8 |
| WMS_40_3_97 | 0.15442 | 0.01176 | 9.74607 | 0.69761 | 0.46060 | 0.03303 | 2394.7 | 182.4 | 2411.1 | 172.6 | 2442.2 | 175.1 |
| WMS_40_3_98 | 0.07909 | 0.00418 | 1.76722 | 0.10800 | 0.16139 | 0.00646 | 1173.6 | 62.0 | 1033.5 | 63.2 | 964.5 | 38.6 |
| WMS_40_3_99 | 0.05825 | 0.00267 | 0.75850 | 0.03082 | 0.09394 | 0.00280 | 538.0 | 24.6 | 573.1 | 23.3 | 578.8 | 17.3 |
| WMS_40_3_100 | 0.06806 | 0.00330 | 1.10537 | 0.05036 | 0.11778 | 0.00312 | 869.5 | 42.2 | 755.9 | 34.4 | 717.8 | 19.0 |
| WMS_40_3_101 | 0.06303 | 0.00422 | 0.98162 | 0.06886 | 0.11200 | 0.00310 | 708.3 | 47.4 | 694.4 | 48.7 | 684.3 | 18.9 |
| WMS_40_3_102 | 0.06046 | 0.00429 | 0.79141 | 0.05610 | 0.09489 | 0.00292 | 619.2 | 44.0 | 592.0 | 42.0 | 584.4 | 18.0 |
| WMS_40_3_103 | 0.25510 | 0.01096 | 18.50987 | 1.30879 | 0.52508 | 0.03584 | 3216.0 | 138.1 | 3016.6 | 213.3 | 2720.7 | 185.7 |
| WMS_40_3_104 | 0.06269 | 0.00267 | 0.88495 | 0.03514 | 0.10271 | 0.00219 | 696.7 | 29.7 | 643.7 | 25.6 | 630.3 | 13.4 |
| WMS_40_3_105 | 0.06661 | 0.00433 | 0.91202 | 0.05795 | 0.09946 | 0.00281 | 824.8 | 53.6 | 658.1 | 41.8 | 611.3 | 17.3 |
| WMS_40_3_106 | 0.07740 | 0.00541 | 1.47228 | 0.09151 | 0.13827 | 0.00512 | 1130.6 | 79.0 | 919.1 | 57.1 | 834.8 | 30.9 |
| WMS_40_3_107 | 0.07229 | 0.00334 | 1.54803 | 0.07520 | 0.15302 | 0.00622 | 993.3 | 45.9 | 949.7 | 46.1 | 917.9 | 37.3 |

| sample | $^{207}Pb^*/^{206}Pb^*$ | | $^{207}Pb^*/^{235}U$ | | $^{206}Pb^*/^{238}U$ | | $^{207}Pb/^{206}Pb$ | | $^{207}Pb/^{235}U$ | | $^{206}Pb/^{238}U$ | |
|---|---|---|---|---|---|---|---|---|---|---|---|---|
| | value | 1 s.e | value | 1 s.e | value | 1 s.e | age (Ma) | 1 s.e | age (Ma) | 1 s.e | age (Ma) | 1 s.e |
| WMS_40_3_108 | 0.20062 | 0.01037 | 11.61545 | 0.80084 | 0.42102 | 0.02075 | 2830.5 | 146.3 | 2573.9 | 177.5 | 2265.1 | 111.7 |
| WMS_40_3_109 | 0.07166 | 0.00600 | 1.29842 | 0.09948 | 0.13017 | 0.00989 | 975.5 | 81.7 | 845.0 | 64.7 | 788.8 | 59.9 |
| WMS_40_3_110 | 0.06526 | 0.00279 | 1.03609 | 0.04492 | 0.11517 | 0.00543 | 781.6 | 33.4 | 722.0 | 31.3 | 702.7 | 33.1 |
| WMS_40_3_111 | 0.14659 | 0.00797 | 5.01026 | 0.44624 | 0.24389 | 0.01984 | 2305.8 | 125.3 | 1821.1 | 162.2 | 1406.9 | 114.4 |
| WMS_40_3_112 | 0.16107 | 0.00561 | 3.02274 | 0.16979 | 0.13379 | 0.00737 | 2466.1 | 85.8 | 1413.4 | 79.4 | 809.4 | 44.6 |
| WMS_40_3_113 | 0.06284 | 0.00337 | 1.12983 | 0.06841 | 0.13116 | 0.00579 | 701.8 | 37.6 | 767.7 | 46.5 | 794.5 | 35.1 |
| WMS_40_3_114 | 0.06189 | 0.00344 | 1.21052 | 0.07771 | 0.14138 | 0.00615 | 669.3 | 37.2 | 805.4 | 51.7 | 852.5 | 37.1 |
| WMS_40_3_115 | 0.17842 | 0.00788 | 1.22573 | 0.08266 | 0.04985 | 0.00373 | 2637.5 | 116.4 | 812.4 | 54.8 | 313.6 | 23.4 |
| WMS_40_3_116 | 0.06236 | 0.00359 | 1.20566 | 0.06691 | 0.13784 | 0.00526 | 685.4 | 39.4 | 803.2 | 44.6 | 832.4 | 31.8 |
| WMS_40_3_117 | 0.11759 | 0.00505 | 2.63053 | 0.12318 | 0.16116 | 0.00640 | 1919.1 | 82.3 | 1309.2 | 61.3 | 963.2 | 38.3 |
| WMS_40_3_118 | 0.23469 | 0.00843 | 20.38508 | 0.78118 | 0.63035 | 0.01274 | 3083.6 | 110.7 | 3109.8 | 119.2 | 3151.0 | 63.7 |
| WMS_40_3_119 | 0.06038 | 0.00248 | 0.74355 | 0.03458 | 0.08999 | 0.00336 | 616.2 | 25.3 | 564.5 | 26.3 | 555.5 | 20.8 |
| WMS_40_3_120 | 0.06232 | 0.00535 | 1.07100 | 0.08786 | 0.12527 | 0.00453 | 684.1 | 58.7 | 739.2 | 60.6 | 760.8 | 27.5 |
| WMS_40_3_121 | 0.10749 | 0.00832 | 3.14419 | 0.50141 | 0.20932 | 0.02548 | 1756.5 | 136.0 | 1443.6 | 230.2 | 1225.2 | 149.1 |
| WMS_40_3_122 | 0.06143 | 0.00320 | 0.70466 | 0.03597 | 0.08265 | 0.00410 | 653.3 | 34.0 | 541.6 | 27.6 | 511.9 | 25.4 |
| WMS_40_3_123 | 0.05910 | 0.00261 | 0.73977 | 0.03170 | 0.09130 | 0.00284 | 569.7 | 25.2 | 562.3 | 24.1 | 563.2 | 17.5 |
| WMS_40_3_124 | 0.06662 | 0.00284 | 1.49167 | 0.06447 | 0.16239 | 0.00439 | 825.0 | 35.2 | 927.0 | 40.1 | 970.0 | 26.2 |
| WMS_40_3_125 | 0.05435 | 0.00552 | 0.70622 | 0.06641 | 0.09472 | 0.00326 | 384.6 | 39.1 | 542.5 | 51.0 | 583.4 | 20.1 |
| WMS_40_3_126 | 0.06893 | 0.00330 | 1.05044 | 0.04820 | 0.11068 | 0.00442 | 895.7 | 42.9 | 729.1 | 33.5 | 676.7 | 27.0 |
| WMS_40_3_127 | 0.05660 | 0.00423 | 0.83252 | 0.05763 | 0.10653 | 0.00495 | 475.2 | 35.5 | 615.0 | 42.6 | 652.5 | 30.3 |
| WMS_40_3_128 | 0.05222 | 0.00370 | 0.65993 | 0.04326 | 0.09147 | 0.00688 | 294.2 | 20.8 | 514.6 | 33.7 | 564.2 | 42.4 |
| WMS_40_3_129 | 0.15753 | 0.00680 | 9.10813 | 0.42176 | 0.41372 | 0.01445 | 2428.5 | 104.8 | 2348.9 | 108.8 | 2231.9 | 77.9 |
| WMS_40_3_130 | 0.07337 | 0.00430 | 1.73245 | 0.11888 | 0.16878 | 0.00803 | 1023.4 | 59.9 | 1020.7 | 70.0 | 1005.4 | 47.9 |
| WMS_40_3_131 | 0.25764 | 0.00869 | 24.20106 | 0.96525 | 0.68160 | 0.01627 | 3231.6 | 109.0 | 3276.5 | 130.7 | 3350.5 | 80.0 |
| WMS_40_3_132 | 0.15907 | 0.00652 | 8.14044 | 0.41406 | 0.37284 | 0.01427 | 2445.1 | 100.2 | 2246.7 | 114.3 | 2042.7 | 78.2 |
| WMS_40_3_133 | 0.15359 | 0.00581 | 9.63866 | 0.36861 | 0.45090 | 0.01099 | 2385.6 | 90.3 | 2400.9 | 91.8 | 2399.2 | 58.5 |
| WMS_40_3_134 | 0.07189 | 0.00385 | 1.52373 | 0.06613 | 0.15398 | 0.00724 | 981.8 | 52.5 | 940.0 | 40.8 | 923.3 | 43.4 |
| WMS_40_3_135 | 0.17678 | 0.00553 | 12.54667 | 0.54235 | 0.51687 | 0.01952 | 2622.2 | 82.1 | 2646.2 | 114.4 | 2685.9 | 101.4 |
| WMS_40_3_136 | 0.24795 | 0.00948 | 19.06314 | 0.71504 | 0.56014 | 0.01665 | 3171.0 | 121.2 | 3045.0 | 114.2 | 2867.2 | 85.2 |
| WMS_40_3_137 | 0.14163 | 0.01022 | 4.73141 | 0.64989 | 0.24736 | 0.02243 | 2246.4 | 162.1 | 1772.8 | 243.5 | 1424.9 | 129.2 |
| WMS_40_3_138 | 0.05836 | 0.00222 | 0.73202 | 0.03130 | 0.09072 | 0.00316 | 542.4 | 20.6 | 557.7 | 23.8 | 559.8 | 19.5 |
| WMS_40_3_139 | 0.10822 | 0.00448 | 4.28285 | 0.18372 | 0.28310 | 0.00737 | 1768.9 | 73.2 | 1690.1 | 72.5 | 1607.0 | 41.8 |
| WMS_40_3_140 | 0.16347 | 0.00534 | 8.95857 | 0.36198 | 0.39888 | 0.01298 | 2491.1 | 81.3 | 2333.8 | 94.3 | 2163.9 | 70.4 |
| WMS_40_3_141 | 0.05719 | 0.00318 | 0.77540 | 0.04212 | 0.09851 | 0.00445 | 498.0 | 27.7 | 582.9 | 31.7 | 605.7 | 27.4 |
| WMS_40_3_142 | 0.06076 | 0.00311 | 0.80987 | 0.04815 | 0.09806 | 0.00447 | 629.7 | 32.3 | 602.4 | 35.8 | 603.0 | 27.5 |
| WMS_40_3_143 | 0.06783 | 0.00389 | 1.09730 | 0.05971 | 0.11783 | 0.00476 | 862.3 | 49.5 | 752.0 | 40.9 | 718.1 | 29.0 |
| WMS_40_3_144 | 0.06637 | 0.00317 | 1.30171 | 0.07615 | 0.14197 | 0.00556 | 817.2 | 39.0 | 846.5 | 49.5 | 855.8 | 33.5 |
| 1_1 ( 19°45'05,7"S , 45°29'48,6"E) | | | | | | | | | | | | |
| WMS_41_1_1 | 0.06807 | 0.00404 | 1.20209 | 0.08507 | 0.13058 | 0.00621 | 869.7 | 51.6 | 801.6 | 56.7 | 791.2 | 37.6 |
| WMS_41_1_2 | 0.07904 | 0.00786 | 1.53525 | 0.15373 | 0.14087 | 0.00652 | 1172.1 | 116.6 | 944.6 | 94.6 | 849.6 | 39.3 |
| WMS_41_1_3 | 0.05737 | 0.00272 | 1.08310 | 0.05850 | 0.13673 | 0.00775 | 505.0 | 24.0 | 745.1 | 40.2 | 826.1 | 46.8 |
| WMS_41_1_4 | 0.07201 | 0.00383 | 1.38632 | 0.08016 | 0.13891 | 0.00494 | 985.3 | 52.4 | 883.1 | 51.1 | 838.5 | 29.8 |
| WMS_41_1_5 | 0.05649 | 0.00245 | 0.84663 | 0.04225 | 0.10863 | 0.00438 | 470.8 | 20.4 | 622.8 | 31.1 | 664.8 | 26.8 |
| WMS_41_1_6 | 0.06145 | 0.00233 | 1.12323 | 0.04184 | 0.13112 | 0.00473 | 654.1 | 24.8 | 764.5 | 28.5 | 794.3 | 28.6 |
| WMS_41_1_7 | 0.07105 | 0.00391 | 1.28437 | 0.08833 | 0.13218 | 0.00489 | 957.8 | 52.7 | 838.8 | 57.7 | 800.3 | 29.6 |
| WMS_41_1_8 | 0.06186 | 0.00332 | 1.15367 | 0.06976 | 0.13608 | 0.00570 | 668.2 | 35.9 | 779.0 | 47.1 | 822.5 | 34.5 |
| WMS_41_1_9 | 0.06315 | 0.00566 | 1.05732 | 0.10348 | 0.12236 | 0.00813 | 712.4 | 63.9 | 732.5 | 71.7 | 744.1 | 49.5 |
| WMS_41_1_10 | 0.06012 | 0.00350 | 0.90015 | 0.05832 | 0.10811 | 0.00624 | 607.0 | 35.4 | 651.8 | 42.2 | 661.8 | 38.2 |
| WMS_41_1_11 | 0.06560 | 0.00396 | 1.23901 | 0.05891 | 0.13708 | 0.00479 | 792.8 | 47.8 | 818.4 | 38.9 | 828.2 | 28.9 |
| WMS_41_1_12 | 0.07140 | 0.00662 | 1.24244 | 0.09161 | 0.12626 | 0.01012 | 968.1 | 89.8 | 820.0 | 60.5 | 766.5 | 61.5 |
| WMS_41_1_13 | 0.14904 | 0.01152 | 7.78285 | 0.67080 | 0.38127 | 0.03135 | 2334.2 | 180.4 | 2206.2 | 190.2 | 2082.2 | 171.2 |
| WMS_41_1_14 | 0.05845 | 0.00353 | 1.03412 | 0.06001 | 0.12735 | 0.00532 | 545.5 | 33.0 | 721.0 | 41.8 | 772.8 | 32.3 |
| WMS_41_1_15 | 0.06786 | 0.00470 | 1.17699 | 0.07085 | 0.12612 | 0.00425 | 863.3 | 59.8 | 789.9 | 47.5 | 765.7 | 25.8 |
| WMS_41_1_16 | 0.05748 | 0.00745 | 1.11194 | 0.13708 | 0.14276 | 0.00702 | 508.8 | 66.0 | 759.1 | 93.6 | 860.2 | 42.3 |
| WMS_41_1_17 | 0.16064 | 0.00673 | 10.78840 | 0.41913 | 0.48823 | 0.01844 | 2461.7 | 103.1 | 2505.1 | 97.3 | 2563.0 | 96.8 |
| WMS_41_1_18 | 0.06013 | 0.00630 | 1.08438 | 0.09989 | 0.13140 | 0.01085 | 607.2 | 63.7 | 745.8 | 68.7 | 795.8 | 65.7 |
| WMS_41_1_19 | 0.06035 | 0.00387 | 1.15392 | 0.09505 | 0.13839 | 0.00812 | 615.2 | 39.5 | 779.1 | 64.2 | 835.5 | 49.0 |
| WMS_41_1_20 | 0.06298 | 0.00366 | 1.22595 | 0.08108 | 0.14132 | 0.00594 | 706.5 | 41.1 | 812.5 | 53.7 | 852.1 | 35.8 |
| WMS_41_1_21 | 0.10023 | 0.00817 | 2.50115 | 0.31006 | 0.17919 | 0.01129 | 1627.6 | 132.7 | 1272.4 | 157.7 | 1062.6 | 66.9 |
| WMS_41_1_22 | 0.07012 | 0.00320 | 1.29253 | 0.05894 | 0.13358 | 0.00422 | 931.1 | 42.5 | 842.4 | 38.4 | 808.2 | 25.6 |
| WMS_41_1_23 | 0.06648 | 0.00382 | 1.33019 | 0.09783 | 0.14496 | 0.01008 | 820.5 | 47.1 | 859.0 | 63.2 | 872.6 | 60.7 |
| WMS_41_1_24 | 0.06339 | 0.00319 | 1.11430 | 0.05758 | 0.12655 | 0.00386 | 720.3 | 36.2 | 760.2 | 39.3 | 768.1 | 23.4 |
| WMS_41_1_25 | 0.06639 | 0.00678 | 1.22746 | 0.11502 | 0.13476 | 0.00365 | 817.8 | 83.5 | 813.2 | 76.2 | 815.0 | 22.1 |
| WMS_41_1_26 | 0.06695 | 0.00443 | 1.26055 | 0.08450 | 0.13867 | 0.00673 | 835.3 | 55.2 | 828.2 | 55.5 | 837.1 | 40.6 |
| WMS_41_1_27 | 0.17624 | 0.00669 | 11.71941 | 0.52298 | 0.47782 | 0.01313 | 2617.0 | 99.3 | 2582.3 | 115.2 | 2517.8 | 69.2 |
| WMS_41_1_28 | 0.05947 | 0.00430 | 0.92689 | 0.07133 | 0.11302 | 0.00277 | 583.4 | 42.1 | 666.0 | 51.3 | 690.3 | 16.9 |
| WMS_41_1_29 | 0.06657 | 0.00386 | 1.13001 | 0.06761 | 0.12291 | 0.00293 | 823.4 | 47.8 | 767.8 | 45.9 | 747.3 | 17.8 |
| WMS_41_1_30 | 0.16034 | 0.00466 | 11.02362 | 0.34819 | 0.50132 | 0.01054 | 2458.5 | 71.5 | 2525.1 | 79.8 | 2619.4 | 55.1 |
| WMS_41_1_31 | 0.06262 | 0.00349 | 1.10573 | 0.07326 | 0.12793 | 0.00541 | 694.5 | 38.7 | 756.1 | 50.1 | 776.0 | 32.8 |
| WMS_41_1_32 | 0.10677 | 0.01670 | 1.91452 | 0.34264 | 0.12787 | 0.00367 | 1744.2 | 272.8 | 1086.2 | 194.4 | 775.7 | 22.3 |
| WMS_41_1_33 | 0.06190 | 0.00264 | 1.10773 | 0.04802 | 0.12991 | 0.00427 | 669.5 | 28.6 | 757.1 | 32.8 | 787.3 | 25.9 |
| WMS_41_1_34 | 0.06576 | 0.00320 | 1.08254 | 0.05451 | 0.11942 | 0.00345 | 797.8 | 38.8 | 744.9 | 37.5 | 727.2 | 21.0 |
| WMS_41_1_35 | 0.06942 | 0.00511 | 1.30621 | 0.09646 | 0.13628 | 0.00882 | 910.5 | 67.0 | 848.5 | 62.7 | 823.6 | 53.3 |
| WMS_41_1_36 | 0.05853 | 0.00324 | 1.13482 | 0.06622 | 0.13889 | 0.00612 | 548.8 | 30.4 | 770.0 | 44.9 | 838.4 | 36.9 |
| WMS_41_1_47 | 0.19620 | 0.00689 | 13.88182 | 0.49348 | 0.51256 | 0.01369 | 2794.1 | 98.2 | 2741.7 | 97.5 | 2667.6 | 71.3 |
| WMS_41_1_37 | 0.06360 | 0.00260 | 1.07542 | 0.04210 | 0.12422 | 0.00451 | 727.5 | 29.8 | 741.4 | 29.0 | 754.8 | 27.4 |
| WMS_41_1_38 | 0.06993 | 0.00309 | 1.18550 | 0.05910 | 0.12366 | 0.00398 | 925.4 | 40.8 | 793.9 | 39.6 | 751.6 | 24.2 |
| WMS_41_1_39 | 0.06757 | 0.00275 | 1.13561 | 0.05842 | 0.12259 | 0.00538 | 854.3 | 34.8 | 770.4 | 39.6 | 745.5 | 32.7 |

| sample | $^{207}Pb^*/^{206}Pb^*$ | | $^{207}Pb^*/^{235}U$ | | $^{206}Pb^*/^{238}U$ | | $^{207}Pb/^{206}Pb$ | | $^{207}Pb/^{235}U$ | | $^{206}Pb/^{238}U$ | |
|---|---|---|---|---|---|---|---|---|---|---|---|---|
| | value | 1 s.e | value | 1 s.e | value | 1 s.e | age (Ma) | 1 s.e | age (Ma) | 1 s.e | age (Ma) | 1 s.e |
| WMS_41_1_40 | 0.06368 | 0.00352 | 1.11403 | 0.06796 | 0.12629 | 0.00638 | 730.1 | 40.4 | 760.1 | 46.4 | 766.6 | 38.7 |
| WMS_41_1_41 | 0.06865 | 0.00533 | 1.20336 | 0.07742 | 0.12693 | 0.00488 | 887.5 | 68.9 | 802.1 | 51.6 | 770.3 | 29.6 |
| WMS_41_1_42 | 0.06706 | 0.00260 | 1.17569 | 0.04595 | 0.12620 | 0.00443 | 838.7 | 32.5 | 789.3 | 30.9 | 766.2 | 26.9 |
| WMS_41_1_43 | 0.06402 | 0.00241 | 1.14993 | 0.04385 | 0.13067 | 0.00330 | 741.5 | 28.0 | 777.2 | 29.6 | 791.7 | 20.0 |
| WMS_41_1_44 | 0.08316 | 0.02218 | 1.54505 | 0.52192 | 0.13532 | 0.00570 | 1272.0 | 339.3 | 948.5 | 320.4 | 818.1 | 34.5 |
| WMS_41_1_45 | 0.06240 | 0.00294 | 1.11611 | 0.05149 | 0.12936 | 0.00421 | 686.9 | 32.4 | 761.1 | 35.1 | 784.2 | 25.5 |
| WMS_41_1_46 | 0.06461 | 0.00289 | 1.29588 | 0.06448 | 0.14665 | 0.00638 | 760.6 | 34.1 | 843.9 | 42.0 | 882.2 | 38.4 |
| WMS_41_1_48 | 0.06057 | 0.00402 | 1.03983 | 0.07049 | 0.12553 | 0.00630 | 623.2 | 41.4 | 723.8 | 49.1 | 762.3 | 38.3 |
| WMS_41_1_49 | 0.12531 | 0.01032 | 2.14620 | 0.19853 | 0.12307 | 0.00725 | 2032.4 | 167.4 | 1163.8 | 107.7 | 748.2 | 44.1 |
| WMS_41_1_50 | 0.07001 | 0.00603 | 1.12525 | 0.09716 | 0.11800 | 0.00622 | 927.8 | 79.9 | 765.5 | 66.1 | 719.0 | 37.9 |
| WMS_41_1_51 | 0.41909 | 0.07425 | 10.38902 | 2.92167 | 0.18195 | 0.01964 | 3978.4 | 704.8 | 2470.1 | 694.7 | 1077.6 | 116.3 |
| WMS_41_1_52 | 0.07638 | 0.00440 | 0.58564 | 0.06410 | 0.05536 | 0.00669 | 1104.2 | 63.7 | 468.1 | 51.2 | 347.3 | 42.0 |
| WMS_41_1_53 | 0.06235 | 0.00398 | 1.02003 | 0.06384 | 0.11890 | 0.00534 | 685.3 | 43.8 | 713.9 | 44.7 | 724.2 | 32.5 |
| WMS_41_1_54 | 0.13762 | 0.00896 | 7.90287 | 0.54257 | 0.42730 | 0.01536 | 2196.7 | 143.1 | 2220.0 | 152.4 | 2293.5 | 82.4 |
| WMS_41_1_55 | 0.11770 | 0.01983 | 2.39299 | 1.12691 | 0.14943 | 0.02262 | 1920.8 | 323.6 | 1240.5 | 584.2 | 897.8 | 135.9 |
| WMS_41_1_56 | 0.05784 | 0.00402 | 1.07988 | 0.07589 | 0.13301 | 0.00848 | 522.8 | 36.3 | 743.6 | 52.3 | 805.0 | 51.3 |
| WMS_41_1_57 | 0.05663 | 0.00374 | 0.93522 | 0.06012 | 0.11854 | 0.00515 | 476.2 | 31.4 | 670.4 | 43.1 | 722.2 | 31.4 |
| WMS_41_1_58 | 0.05036 | 0.00367 | 0.72574 | 0.05580 | 0.10392 | 0.00543 | 210.5 | 15.3 | 554.0 | 42.6 | 637.3 | 33.3 |
| WMS_41_1_59 | 0.05136 | 0.00329 | 0.88647 | 0.05728 | 0.12554 | 0.00451 | 256.2 | 16.4 | 644.5 | 41.6 | 762.4 | 27.4 |
| WMS_41_1_93 | 0.09440 | 0.01186 | 1.50399 | 0.19420 | 0.11786 | 0.00424 | 1515.2 | 190.4 | 932.0 | 120.3 | 718.2 | 25.8 |
| WMS_41_1_60 | 0.05074 | 0.00272 | 0.90499 | 0.06320 | 0.13063 | 0.00639 | 227.8 | 12.2 | 654.4 | 45.7 | 791.5 | 38.7 |
| WMS_41_1_61 | 0.04933 | 0.00451 | 0.88349 | 0.09282 | 0.13118 | 0.00675 | 162.3 | 14.8 | 642.9 | 67.5 | 794.6 | 40.9 |
| WMS_41_1_62 | 0.06298 | 0.00465 | 1.09861 | 0.09431 | 0.12727 | 0.00441 | 706.5 | 52.2 | 752.7 | 64.6 | 772.3 | 26.7 |
| WMS_41_1_63 | 0.12459 | 0.00566 | 2.29236 | 0.11494 | 0.13335 | 0.00721 | 2022.2 | 91.9 | 1209.9 | 60.7 | 807.0 | 43.7 |
| WMS_41_1_64 | 0.14520 | 0.00625 | 8.99759 | 0.42177 | 0.45609 | 0.01289 | 2289.4 | 98.6 | 2337.8 | 109.6 | 2422.3 | 68.4 |
| WMS_41_1_65 | 0.05836 | 0.00268 | 1.05120 | 0.05089 | 0.13232 | 0.00418 | 542.3 | 24.9 | 729.5 | 35.3 | 801.1 | 25.3 |
| WMS_41_1_66 | 0.05891 | 0.00392 | 1.10459 | 0.07364 | 0.13459 | 0.00595 | 562.8 | 37.5 | 755.6 | 50.4 | 814.0 | 36.0 |
| WMS_41_1_67 | 0.06771 | 0.00421 | 1.24115 | 0.09174 | 0.13389 | 0.00403 | 858.7 | 53.4 | 819.4 | 60.6 | 810.0 | 24.4 |
| WMS_41_1_68 | 0.05181 | 0.00332 | 0.91536 | 0.06150 | 0.12998 | 0.00471 | 276.1 | 17.7 | 659.9 | 44.3 | 787.8 | 28.5 |
| WMS_41_1_69 | 0.06083 | 0.00318 | 1.10373 | 0.06553 | 0.13358 | 0.00635 | 632.1 | 33.0 | 755.2 | 44.8 | 808.3 | 38.4 |
| WMS_41_1_70 | 0.07225 | 0.00404 | 1.18734 | 0.06616 | 0.12111 | 0.00511 | 992.1 | 55.5 | 794.7 | 44.3 | 737.0 | 31.1 |
| WMS_41_1_71 | 0.06687 | 0.00307 | 1.14944 | 0.05562 | 0.12687 | 0.00518 | 832.8 | 38.3 | 777.0 | 37.6 | 770.0 | 31.5 |
| WMS_41_1_72 | 0.11087 | 0.01164 | 1.97544 | 0.22917 | 0.13136 | 0.00725 | 1812.9 | 190.3 | 1107.2 | 128.4 | 795.6 | 43.9 |
| WMS_41_1_73 | 0.18654 | 0.01473 | 13.71989 | 1.08746 | 0.54092 | 0.05083 | 2711.2 | 214.1 | 2730.6 | 216.4 | 2787.3 | 261.9 |
| WMS_41_1_74 | 0.07095 | 0.00319 | 1.09602 | 0.04965 | 0.11192 | 0.00383 | 955.2 | 43.0 | 751.4 | 34.0 | 683.9 | 23.4 |
| WMS_41_1_75 | 0.06122 | 0.00340 | 1.29242 | 0.07403 | 0.15463 | 0.00539 | 646.1 | 35.8 | 842.4 | 48.3 | 926.9 | 32.3 |
| WMS_41_1_76 | 0.06688 | 0.00369 | 1.27313 | 0.07546 | 0.13834 | 0.00717 | 833.1 | 46.0 | 833.8 | 49.4 | 835.3 | 43.3 |
| WMS_41_1_77 | 0.06594 | 0.00300 | 1.26507 | 0.06294 | 0.13972 | 0.00447 | 803.7 | 36.6 | 830.2 | 41.3 | 843.1 | 26.9 |
| WMS_41_1_78 | 0.06219 | 0.00369 | 1.16654 | 0.06488 | 0.13562 | 0.00830 | 679.6 | 40.3 | 785.0 | 43.7 | 819.8 | 50.2 |
| WMS_41_1_79 | 0.05886 | 0.00392 | 1.21537 | 0.08026 | 0.14887 | 0.00900 | 560.8 | 37.3 | 807.7 | 53.3 | 894.6 | 54.1 |
| WMS_41_1_80 | 0.16143 | 0.00654 | 11.03085 | 0.47942 | 0.49604 | 0.01539 | 2469.9 | 100.0 | 2525.7 | 109.8 | 2596.7 | 80.6 |
| WMS_41_1_81 | 0.06197 | 0.00284 | 1.07724 | 0.06217 | 0.12610 | 0.00576 | 672.2 | 30.8 | 742.3 | 42.8 | 765.6 | 35.0 |
| WMS_41_1_82 | 0.06474 | 0.00339 | 1.19947 | 0.07493 | 0.13395 | 0.00540 | 765.0 | 40.0 | 800.3 | 50.0 | 810.4 | 32.7 |
| WMS_41_1_83 | 0.17769 | 0.00628 | 10.78151 | 0.38241 | 0.43929 | 0.01207 | 2630.7 | 92.9 | 2504.5 | 88.8 | 2347.5 | 64.5 |
| WMS_41_1_84 | 0.06257 | 0.00519 | 1.04796 | 0.08525 | 0.12168 | 0.00526 | 692.5 | 57.4 | 727.9 | 59.2 | 740.2 | 32.0 |
| WMS_41_1_85 | 0.07502 | 0.00612 | 1.37390 | 0.11592 | 0.13283 | 0.00953 | 1068.2 | 87.1 | 877.8 | 74.1 | 804.0 | 57.7 |
| WMS_41_1_86 | 0.12018 | 0.01539 | 2.24818 | 0.34322 | 0.13574 | 0.00339 | 1958.2 | 250.7 | 1196.2 | 182.6 | 820.5 | 20.5 |
| WMS_41_1_87 | 0.06667 | 0.00272 | 1.09666 | 0.04951 | 0.11786 | 0.00311 | 826.6 | 33.8 | 751.7 | 33.9 | 718.2 | 19.0 |
| WMS_41_1_88 | 0.06553 | 0.00433 | 1.19602 | 0.08400 | 0.13261 | 0.00420 | 790.4 | 52.2 | 798.7 | 56.1 | 802.8 | 25.4 |
| WMS_41_1_89 | 0.06939 | 0.00372 | 1.55141 | 0.19365 | 0.15951 | 0.01265 | 909.4 | 48.8 | 951.1 | 118.7 | 954.0 | 75.6 |
| WMS_41_1_90 | 0.06933 | 0.00372 | 1.27617 | 0.07423 | 0.13567 | 0.00430 | 907.8 | 48.7 | 835.1 | 48.6 | 820.1 | 26.0 |
| WMS_41_1_91 | 0.06991 | 0.00458 | 1.20523 | 0.08208 | 0.12517 | 0.00445 | 924.8 | 60.6 | 803.0 | 54.7 | 760.2 | 27.0 |
| WMS_41_1_92 | 0.06829 | 0.00490 | 1.25422 | 0.08351 | 0.13396 | 0.00612 | 876.5 | 62.9 | 825.3 | 55.0 | 810.4 | 37.0 |
| WMS_41_1_94 | 0.07807 | 0.00518 | 1.32165 | 0.09142 | 0.12236 | 0.00473 | 1147.7 | 76.2 | 855.2 | 59.2 | 744.1 | 28.7 |
| WMS_41_1_95 | 0.06989 | 0.00351 | 1.21029 | 0.07398 | 0.12547 | 0.00527 | 924.3 | 46.4 | 805.3 | 49.2 | 762.0 | 32.0 |
| WMS_41_1_96 | 0.07068 | 0.00363 | 1.11831 | 0.07573 | 0.11613 | 0.00753 | 947.4 | 48.6 | 762.2 | 51.6 | 708.3 | 45.9 |
| WMS_41_1_97 | 0.06508 | 0.00375 | 1.18366 | 0.07720 | 0.13235 | 0.00753 | 776.0 | 44.8 | 793.0 | 51.7 | 801.2 | 45.6 |
| WMS_41_1_98 | 0.06911 | 0.00275 | 1.21805 | 0.05103 | 0.12722 | 0.00365 | 901.2 | 35.8 | 808.9 | 33.9 | 772.0 | 22.2 |
| WMS_41_1_99 | 0.17372 | 0.00806 | 11.81227 | 0.70916 | 0.49502 | 0.02562 | 2593.1 | 120.4 | 2589.6 | 155.5 | 2592.3 | 134.2 |
| WMS_41_1_100 | 0.06768 | 0.00563 | 1.41671 | 0.20831 | 0.15472 | 0.01676 | 857.7 | 71.3 | 896.0 | 131.7 | 927.4 | 100.4 |
| WMS_41_1_101 | 0.06179 | 0.00232 | 1.17753 | 0.04944 | 0.13815 | 0.00405 | 665.8 | 25.0 | 790.2 | 33.2 | 834.2 | 24.5 |
| WMS_41_1_102 | 0.16384 | 0.00578 | 8.34655 | 0.41300 | 0.37238 | 0.01776 | 2494.9 | 88.0 | 2269.4 | 112.3 | 2040.6 | 97.3 |
| WMS_41_1_103 | 0.06551 | 0.00460 | 1.22960 | 0.09059 | 0.13466 | 0.00690 | 789.9 | 55.5 | 814.2 | 60.0 | 814.4 | 41.8 |
| WMS_41_1_104 | 0.07210 | 0.00264 | 1.19906 | 0.04917 | 0.12129 | 0.00312 | 987.7 | 36.1 | 800.2 | 32.8 | 738.0 | 19.0 |
| WMS_41_1_105 | 0.08164 | 0.00525 | 1.52741 | 0.10489 | 0.13363 | 0.00553 | 1235.9 | 79.5 | 941.5 | 64.7 | 808.5 | 33.4 |
| WMS_41_1_106 | 0.06858 | 0.00644 | 1.26371 | 0.12880 | 0.13431 | 0.00817 | 885.2 | 83.1 | 829.6 | 84.6 | 812.4 | 49.4 |
| WMS_41_1_107 | 0.06689 | 0.00318 | 1.19096 | 0.05604 | 0.12916 | 0.00307 | 833.5 | 39.7 | 796.4 | 37.5 | 783.1 | 18.6 |
| WMS_41_1_108 | 0.07216 | 0.00432 | 1.33399 | 0.07214 | 0.13553 | 0.00386 | 989.4 | 59.3 | 860.6 | 46.5 | 819.4 | 23.3 |
| WMS_41_1_109 | 0.08400 | 0.00434 | 2.01153 | 0.14166 | 0.16988 | 0.00728 | 1291.7 | 66.7 | 1119.4 | 78.8 | 1011.5 | 43.4 |
| WMS_41_1_110 | 0.06405 | 0.00327 | 0.95874 | 0.05390 | 0.10853 | 0.00571 | 742.4 | 37.9 | 682.6 | 38.4 | 664.2 | 35.0 |
| WMS_41_1_111 | 0.06801 | 0.00606 | 1.35332 | 0.13433 | 0.14429 | 0.00819 | 868.0 | 77.4 | 869.0 | 86.3 | 868.8 | 49.3 |
| WMS_41_1_112 | 0.06630 | 0.00292 | 1.15355 | 0.05276 | 0.12665 | 0.00433 | 815.1 | 35.9 | 778.9 | 35.6 | 768.7 | 26.3 |
| WMS_41_1_113 | 0.06772 | 0.00249 | 1.24341 | 0.04320 | 0.13366 | 0.00292 | 858.9 | 31.6 | 820.4 | 28.5 | 808.7 | 17.7 |
| WMS_41_1_114 | 0.15308 | 0.00753 | 8.61002 | 0.45051 | 0.41234 | 0.01784 | 2379.9 | 117.1 | 2297.6 | 120.2 | 2225.6 | 96.3 |
| WMS_41_1_115 | 0.06956 | 0.00342 | 1.04848 | 0.07020 | 0.10909 | 0.00723 | 914.3 | 45.0 | 728.1 | 48.8 | 667.5 | 44.3 |
| WMS_41_1_116 | 0.06514 | 0.00303 | 1.13470 | 0.05207 | 0.12691 | 0.00326 | 777.8 | 36.2 | 770.0 | 35.3 | 770.2 | 19.8 |
| WMS_41_1_117 | 0.07012 | 0.00388 | 1.25077 | 0.07943 | 0.12916 | 0.00710 | 931.0 | 51.5 | 823.8 | 52.3 | 783.1 | 43.1 |
| WMS_41_1_118 | 0.06175 | 0.00287 | 1.11571 | 0.05426 | 0.13244 | 0.00427 | 664.5 | 30.8 | 760.9 | 37.0 | 801.8 | 25.8 |

| sample | $^{207}Pb^*/^{206}Pb^*$ | | $^{207}Pb^*/^{235}U$ | | $^{206}Pb^*/^{238}U$ | | $^{207}Pb/^{206}Pb$ | | $^{207}Pb/^{235}U$ | | $^{206}Pb/^{238}U$ | |
|---|---|---|---|---|---|---|---|---|---|---|---|---|
| | value | 1 s.e | value | 1 s.e | value | 1 s.e | age (Ma) | 1 s.e | age (Ma) | 1 s.e | age (Ma) | 1 s.e |
| WMS_41_1_119 | 0.16376 | 0.00612 | 10.35347 | 0.38820 | 0.45404 | 0.01255 | 2494.1 | 93.1 | 2466.9 | 92.5 | 2413.2 | 66.7 |
| WMS_41_1_120 | 0.06397 | 0.00383 | 0.77311 | 0.04577 | 0.08836 | 0.00404 | 739.8 | 44.3 | 581.5 | 34.4 | 545.8 | 25.0 |
| WMS_41_1_121 | 0.06692 | 0.00256 | 1.12019 | 0.04660 | 0.12244 | 0.00349 | 834.3 | 31.9 | 763.1 | 31.7 | 744.6 | 21.2 |
| WMS_41_1_122 | 0.07087 | 0.00225 | 1.19305 | 0.03988 | 0.12236 | 0.00266 | 952.9 | 30.3 | 797.4 | 26.7 | 744.2 | 16.2 |
| WMS_41_1_123 | 0.06982 | 0.00342 | 1.28724 | 0.06356 | 0.13375 | 0.00493 | 922.0 | 45.2 | 840.1 | 41.5 | 809.2 | 29.8 |
| WMS_41_1_124 | 0.07138 | 0.00317 | 1.38661 | 0.06347 | 0.14189 | 0.00489 | 967.3 | 42.9 | 883.3 | 40.4 | 855.3 | 29.5 |
| WMS_41_1_125 | 0.09472 | 0.00859 | 1.70949 | 0.13937 | 0.13224 | 0.00597 | 1521.7 | 138.0 | 1012.1 | 82.5 | 800.6 | 36.1 |
| WMS_41_1_126 | 0.05731 | 0.00252 | 0.75406 | 0.03234 | 0.09394 | 0.00589 | 502.4 | 22.1 | 570.6 | 24.5 | 578.8 | 36.3 |
| WMS_41_1_127 | 0.07110 | 0.00418 | 1.36209 | 0.07836 | 0.13823 | 0.00488 | 959.5 | 56.4 | 872.8 | 50.2 | 834.7 | 29.5 |
| WMS_41_1_128 | 0.07312 | 0.00418 | 1.32680 | 0.08263 | 0.13275 | 0.00774 | 1016.4 | 58.1 | 857.5 | 53.4 | 803.5 | 46.8 |
| WMS_41_1_129 | 0.15249 | 0.00645 | 7.66850 | 0.63813 | 0.36608 | 0.02306 | 2373.2 | 100.4 | 2192.9 | 182.5 | 2010.9 | 126.7 |
| WMS_41_1_130 | 0.06092 | 0.00403 | 1.03710 | 0.10282 | 0.12113 | 0.00881 | 635.6 | 42.0 | 722.5 | 71.6 | 737.0 | 53.6 |
| WMS_41_1_131 | 0.05621 | 0.00695 | 1.03652 | 0.15855 | 0.13154 | 0.01148 | 459.7 | 56.8 | 722.2 | 110.5 | 796.6 | 69.5 |
| WMS_41_1_132 | 0.06246 | 0.00400 | 1.28685 | 0.10377 | 0.14867 | 0.00896 | 688.9 | 44.2 | 839.9 | 67.7 | 893.5 | 53.9 |
| WMS_41_1_133 | 0.07187 | 0.00268 | 1.66905 | 0.07473 | 0.16848 | 0.00658 | 981.4 | 36.6 | 996.8 | 44.6 | 1003.8 | 39.2 |
| WMS_41_1_134 | 0.06317 | 0.00454 | 1.23752 | 0.10673 | 0.14237 | 0.00836 | 713.0 | 51.2 | 817.8 | 70.5 | 858.0 | 50.4 |
| WMS_41_1_135 | 0.06067 | 0.00275 | 1.11854 | 0.06274 | 0.13340 | 0.00581 | 626.5 | 28.4 | 762.3 | 42.8 | 807.2 | 35.1 |
| WMS_41_1_136 | 0.06688 | 0.00320 | 1.21344 | 0.06294 | 0.13107 | 0.00386 | 833.2 | 39.9 | 806.8 | 41.8 | 794.0 | 23.4 |
| WMS_41_1_137 | 0.06674 | 0.00333 | 1.27787 | 0.06787 | 0.13784 | 0.00486 | 828.6 | 41.3 | 835.9 | 44.4 | 832.4 | 29.4 |
| WMS_41_1_138 | 0.06307 | 0.00598 | 1.13293 | 0.11029 | 0.13108 | 0.01375 | 709.7 | 67.3 | 769.1 | 74.9 | 794.0 | 83.3 |
| WMS_41_1_139 | 0.16283 | 0.00819 | 10.50944 | 0.59247 | 0.46812 | 0.01830 | 2484.6 | 124.9 | 2480.8 | 139.9 | 2475.3 | 96.8 |
| WMS_41_1_140 | 0.06054 | 0.00374 | 1.03857 | 0.06547 | 0.12409 | 0.00370 | 622.1 | 38.4 | 723.2 | 45.6 | 754.1 | 22.5 |
| WMS_41_1_141 | 0.06860 | 0.00354 | 1.22008 | 0.06737 | 0.12867 | 0.00367 | 885.9 | 45.8 | 809.8 | 44.7 | 780.2 | 22.3 |
| WMS_41_1_142 | 0.05598 | 0.00315 | 0.67344 | 0.03753 | 0.08679 | 0.00386 | 450.7 | 25.3 | 522.8 | 29.1 | 536.5 | 23.9 |
| WMS_41_1_143 | 0.06510 | 0.00287 | 1.08592 | 0.05008 | 0.12094 | 0.00391 | 776.6 | 34.2 | 746.5 | 34.4 | 736.0 | 23.8 |
| WMS_41_1_144 | 0.06138 | 0.00416 | 0.83795 | 0.09803 | 0.10031 | 0.00798 | 651.5 | 44.2 | 618.0 | 72.3 | 616.2 | 49.0 |
| WMS_41_1_145 | 0.15739 | 0.00719 | 10.40801 | 0.70046 | 0.47846 | 0.02806 | 2427.0 | 110.9 | 2471.8 | 166.3 | 2520.5 | 147.8 |

**Table SI2. Summary of model constraints used in HeFTy**

**1. Thermochronologic data**

Samples and data used in simulation

| North Transect - Jurassic | | South Transect - Jurassic |
|---|---|---|
| Samples used in final modelling | | Samples used in final modelling |
| 01/2-z03 | | 39/3-z03 |
| 01/2-z04 | | 39/3-z08 |
| 01/2-z06 | | 40/3-z08 |
| 01/2-z07 | | South Transect - Cretaceous |
| North Transect - Cretaceous | | Samples used in final modelling |
| Samples used in final modelling | | 09/2-z01 |
| Trial #1 | Trial #2 | 09/2-z08 |
| 31/1-z01 | 34/1-z02 | 17/1-z04 |
| 31/1-z03 | 34/1-z03 | 17/1-z07 |
| 31/1-z06 | 34/1-z06 | |
| 31/1-z07 | 34/1z08 | |

Data Treatment:
He dates (Ma): Mean uncorrected He date of each sample
Error (Ma) applied in modelling: 2 sigma sample standard deviation was applied
Stopping distances: Ketcham et al. (2011)
Alpha calculation: Redistribution
Mean equivalent spherical radius: Calculated as the average of each grain within the sample

**2. Additional Geologic information**

| Time-frame | Assumption | |
|---|---|---|
| Pre-deposition | | |
| | Fully reset to temperatures >300℃ during Gondwana amalgamation | High greenschist to amphibolite facies metamorphism of Madagascar (Boger et al., 2019) |
| | Cooling following peak Gondwana temperatures | Partial resetting of samples (fig. 7), previous results by e.g. Emmel et al. (2006), Giese et al (2012), Stephenson et al. (2021) |
| Jurassic | | |
| | Deposition of Jurassic sediments at ~200 Ma, to maximum depths of 4-6 km between 180 and 160 Ma | Stratigraphy of basin showing Jurassic deposition into Callovian (Fig. 4), descriptions and analysis in Geiger et al. (2004) and Clark (1998) |
| | Uplift of Jurassic sediments following maximum burial depth, prior to deposition of Cretaceous sediments (not restricted) | Models not forced to assume cooling prior to Cretaceous deposition, observed trend during initial Jurassic trials |
| Cretaceous | | |
| | Deposition of Cretaceous sediments at ~100 Ma, to maximum depths of 2.5-4 km at ~80 Ma | Stratigraphy of basin showing Jurassic deposition into Callovian (Fig. 4), descriptions and analysis in Geiger et al. (2004) and Clark (1998) |
| Final Uplift | | |
| | At surface temperature of 25℃ by 0 Ma | 25℃ as approximate annual average temperature |

**3. System and model-specific parameters**

He kinetic model: ZRDAAM
Statistical fitting criteria: Merit value for "good" fit = 0.5, merit value for "acceptable fit = 0.05
Number of tT paths attempted: 100 good paths for all, varying # of acceptable and tested paths
tT path characteristics: Gradual with maximum rates of 10℃/Ma during burial, unrestricted episodic during cooling

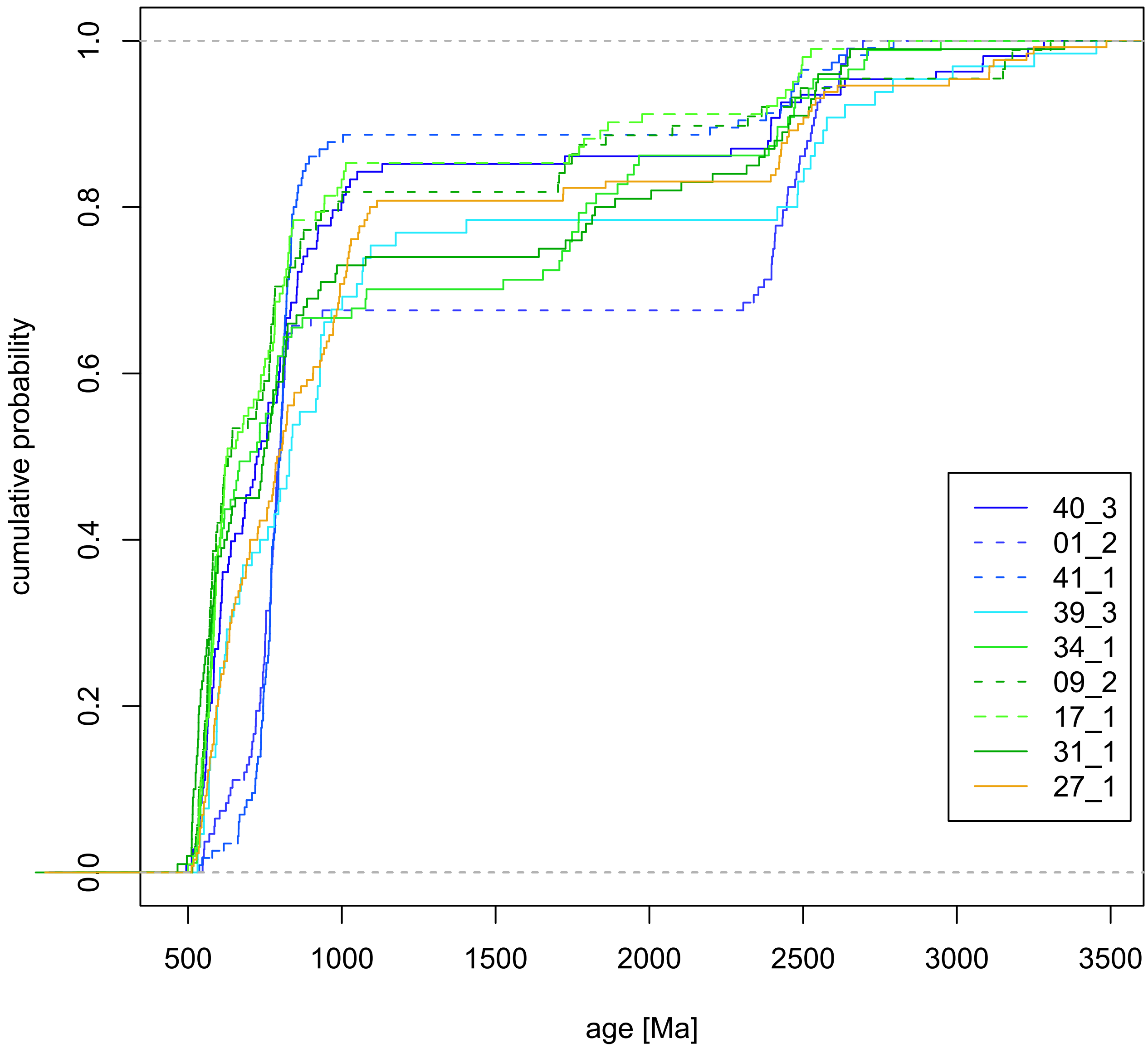


*Figure SI1: Detrital zircon U-Pb Cumulative Area Distribution (CAD) of <10% discordant U-Pb data. Colours for each sample correspond to lithological units as described in maps, cross-section, and stratigraphic column (Fig. 4) .*

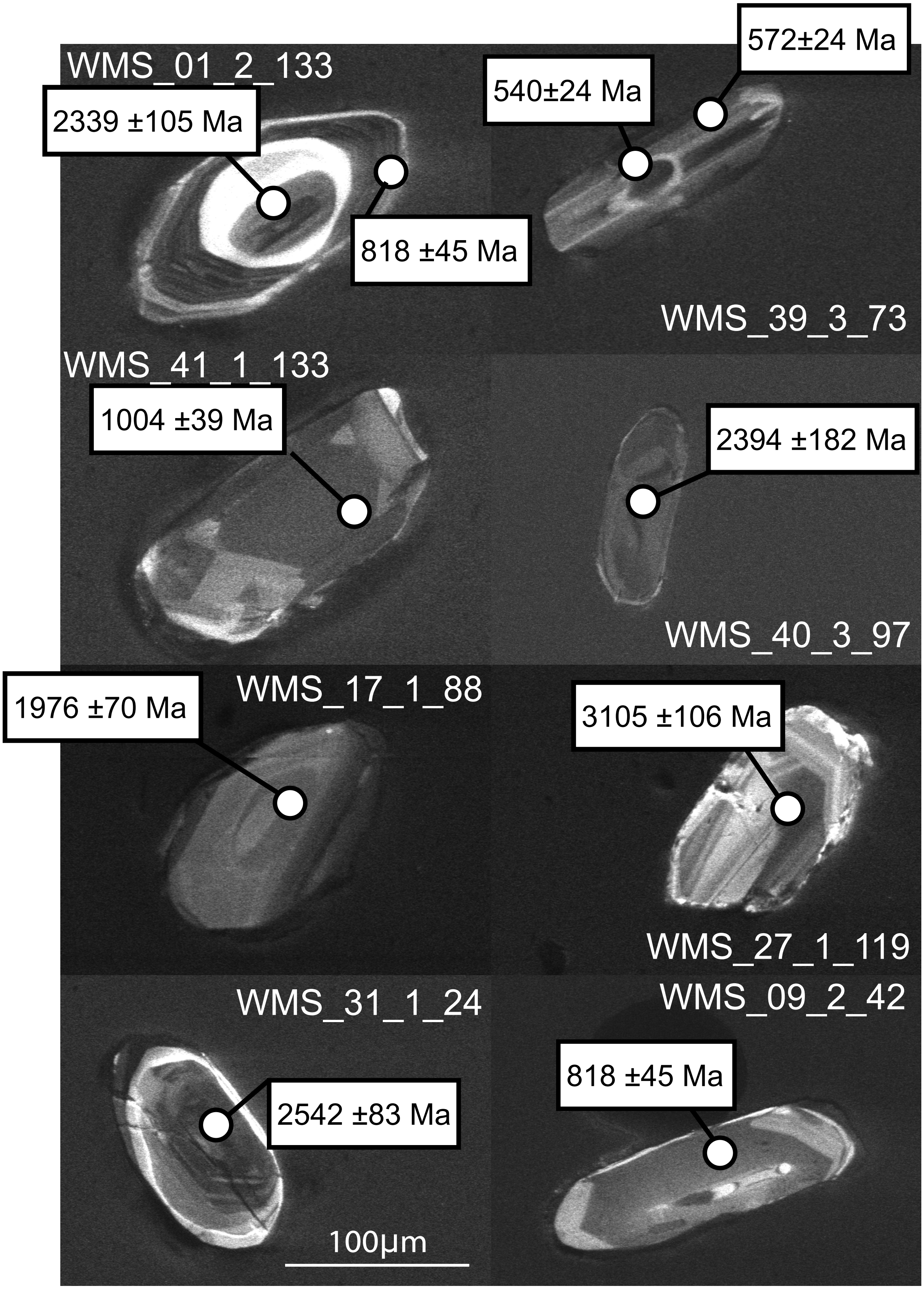


*Figure SI2: SEM images of zircon from Morondava Basin, Madagascar.*

A

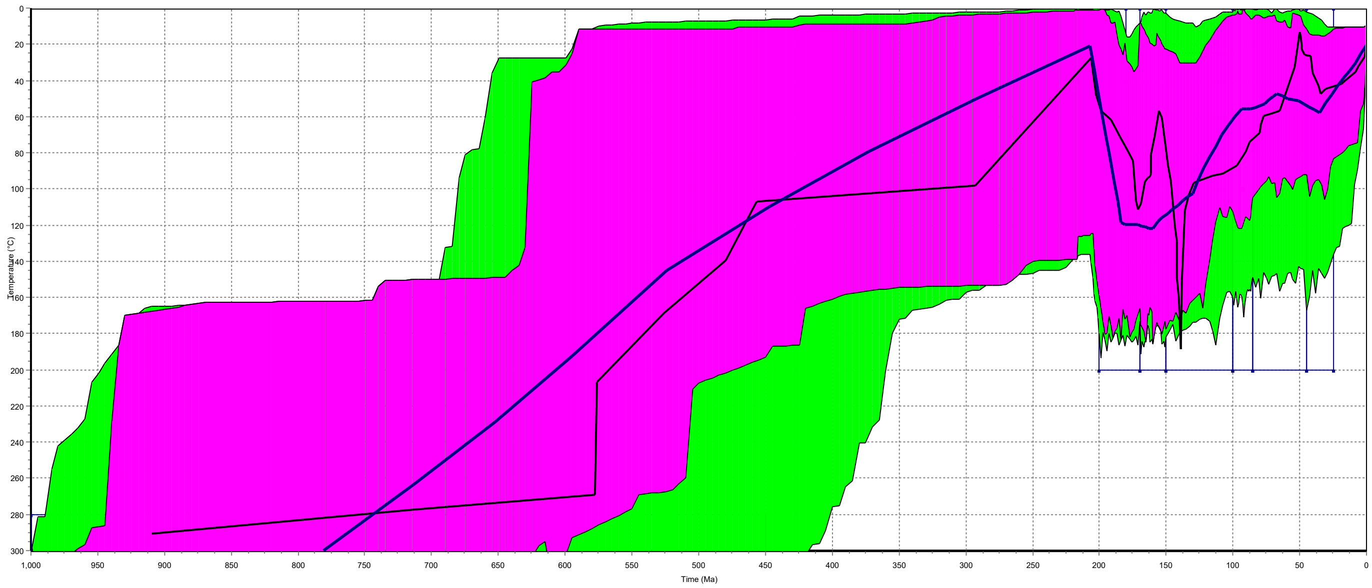


B

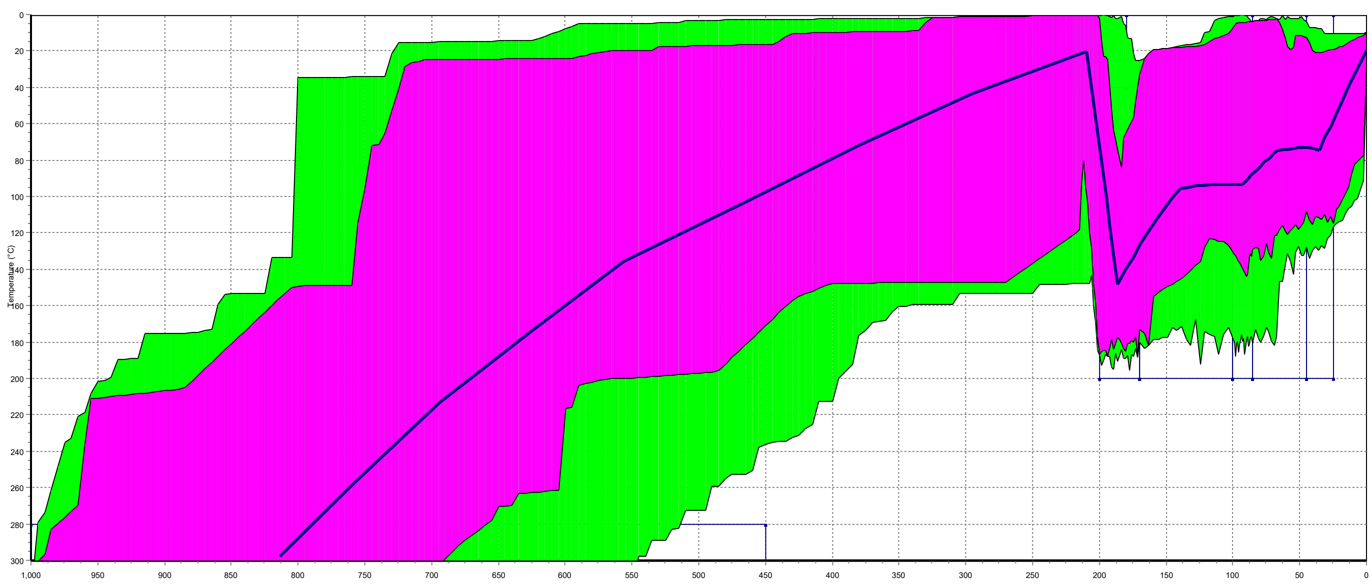


*Figure SI3: Alternative inverse thermal models for the Jurassic samples. A: North Transect (samples 01/2 and 41/1) B: South Transect (samples 39/3 and 40/1). The envelope for "acceptable"paths is shaded in green, the envelope for the "good" paths is shaded in purple. The mean path is shown by the blue line.*

A

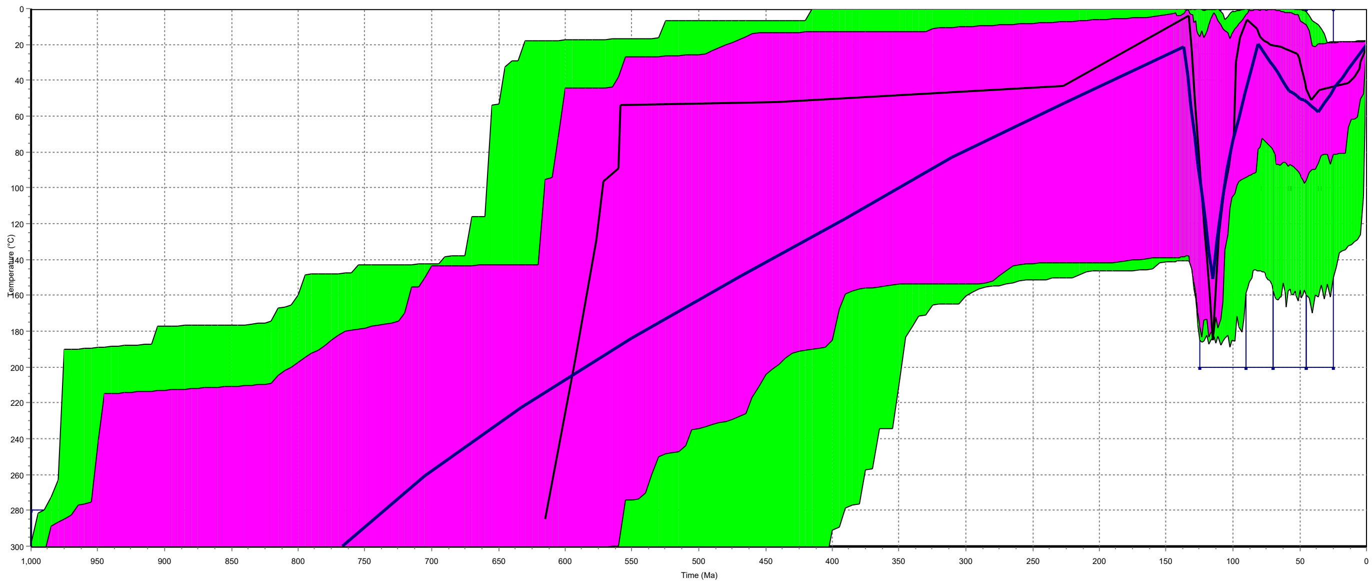


B

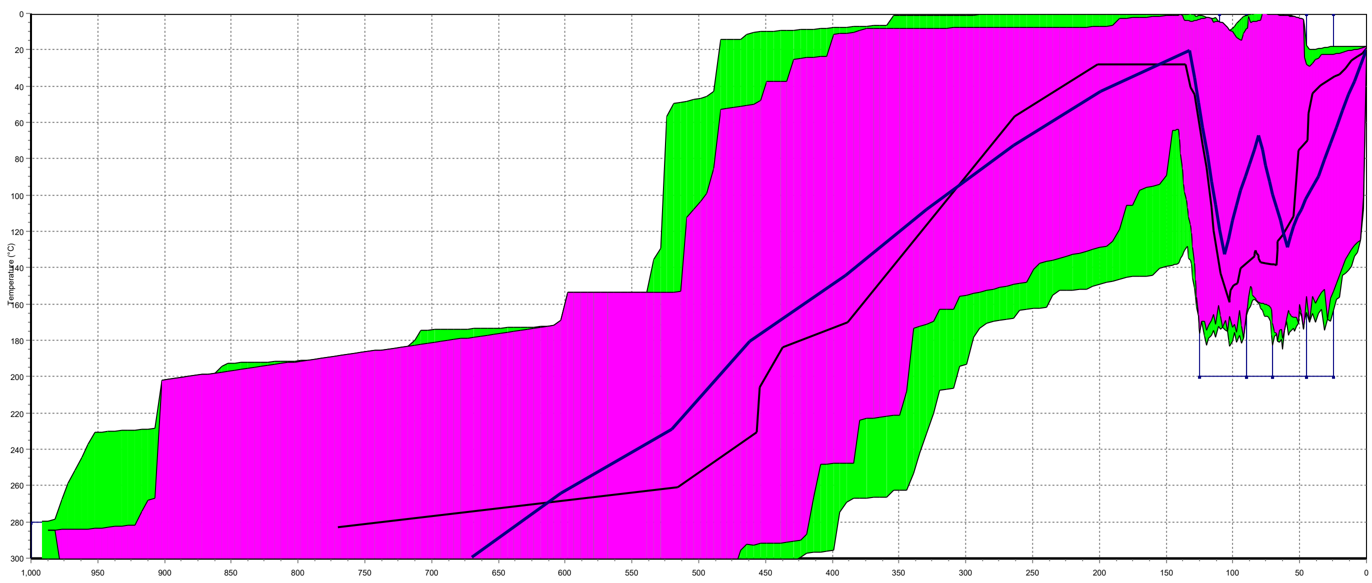


*Figure SI4: Alternative inverse thermal models for the Cretaceous samples. A: North Transect (samples 09/2 and 17/1) B: South Transect (samples 31/1 and 34/1). The envelope for "acceptable"paths is shaded in green, the envelope for the "good" paths is shaded in purple. The mean path is shown by the blue line. Best path as determined by the model is shown in black.*

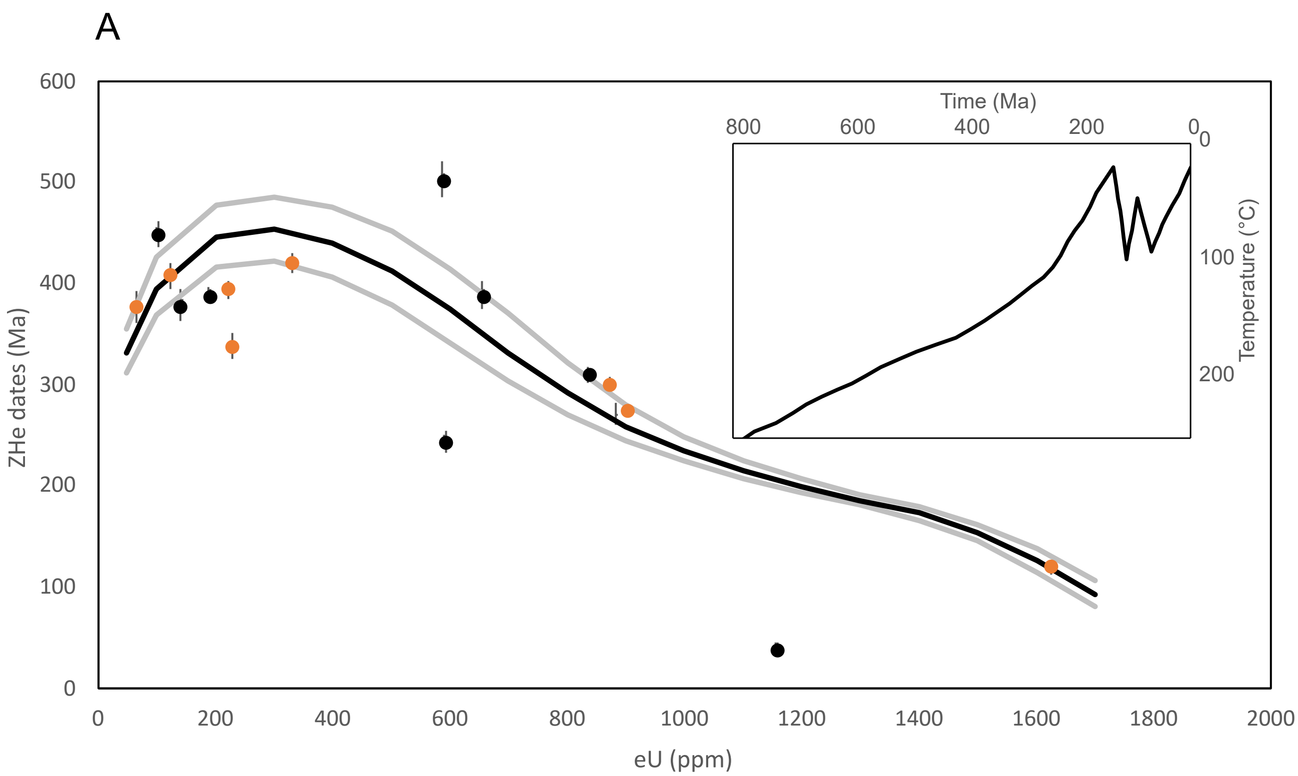


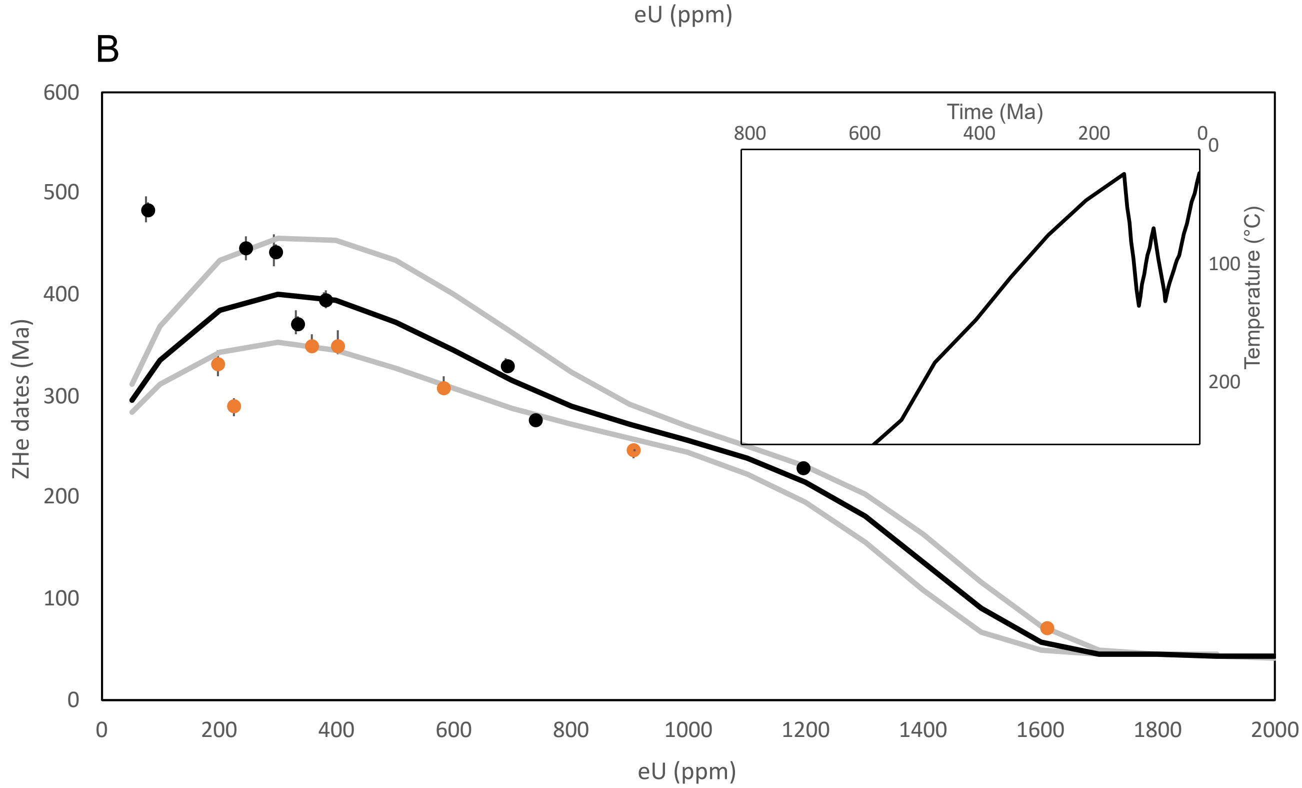


*Figure SI5: Alternative forward models for Cretaceous samples. A: North Transect (samples 09/2, 17/1), B: South Transect (samples 31/1, 34/1). Black line represents the cooling path of the average grain size, grey lines represent the cooling path of the minimum and maximum grain sizes. Path tested are the mean paths for the inverse models from figure DR5.*

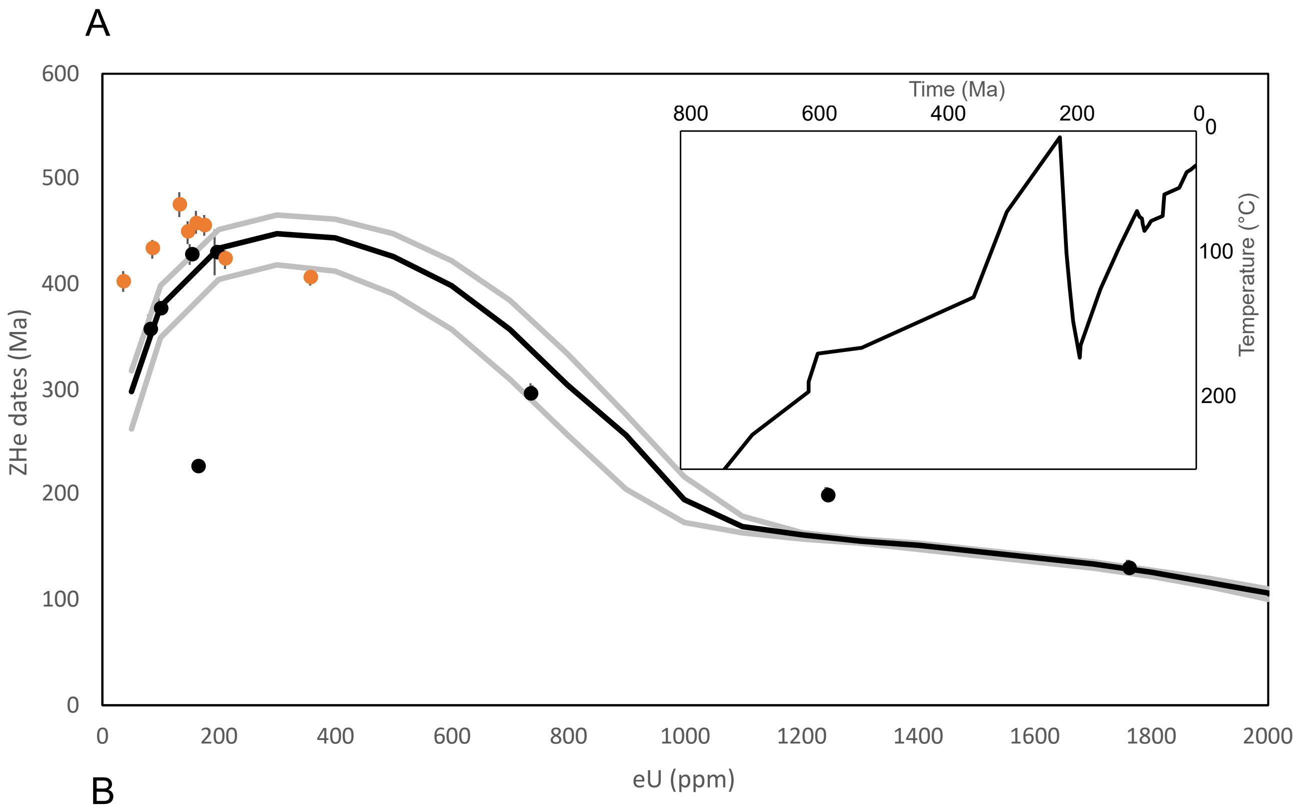


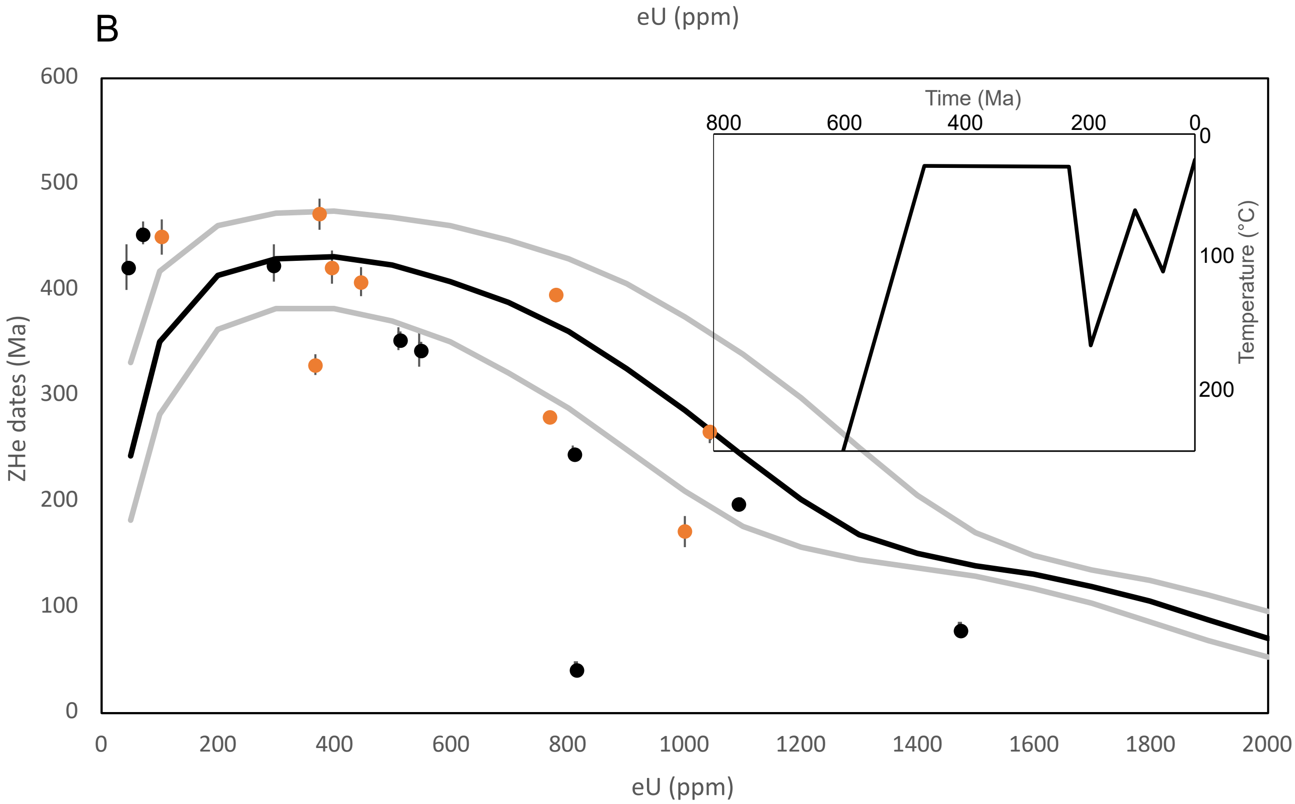


*Figure SI6: Alternative forward models for Jurassic samples. A: North Transect (samples 01/2, 41/1), B: South Transect (samples 39/3, 40/1). Black line represents the cooling path of the average grain size, grey lines represent the cooling path of the minimum and maximum grain sizes.*

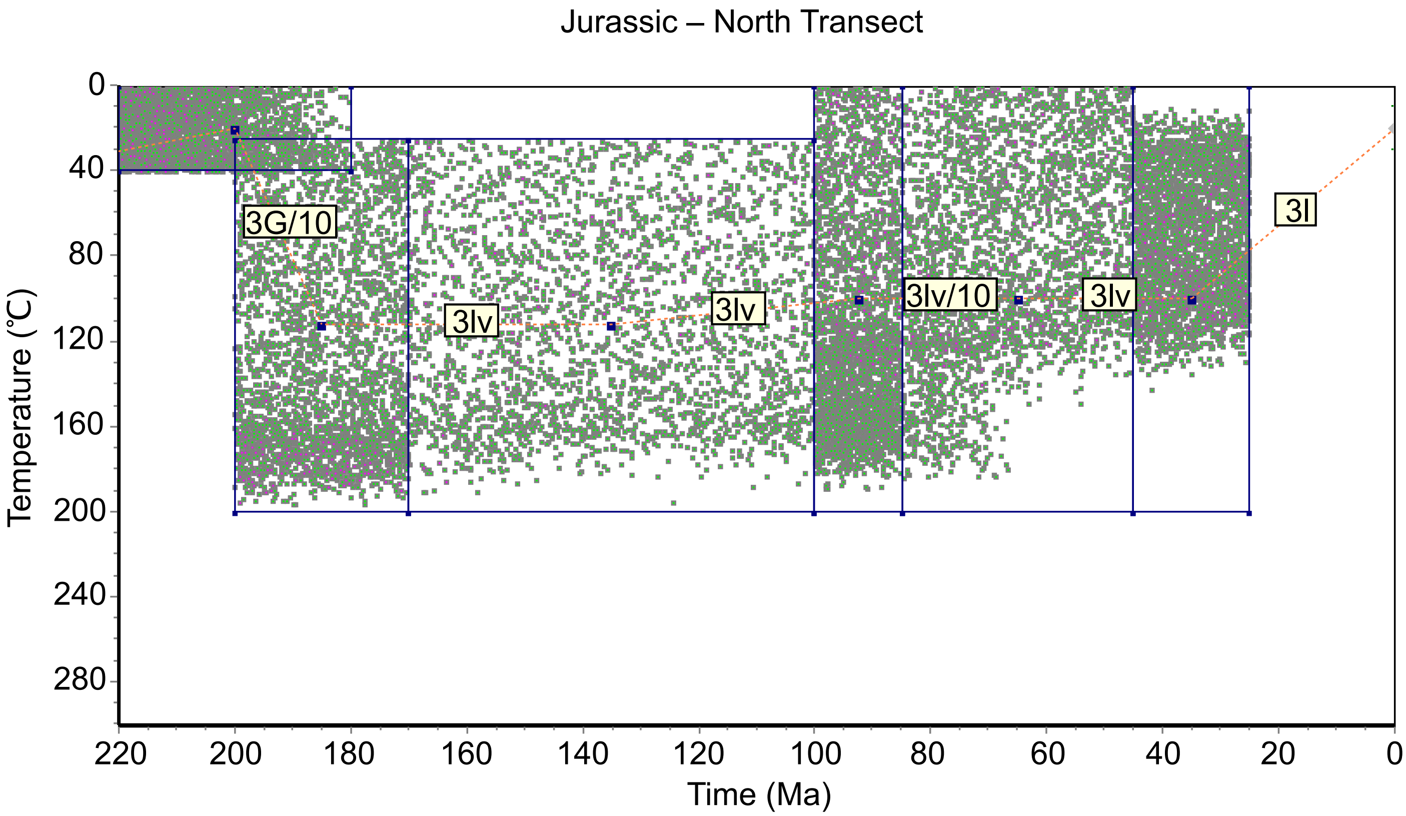


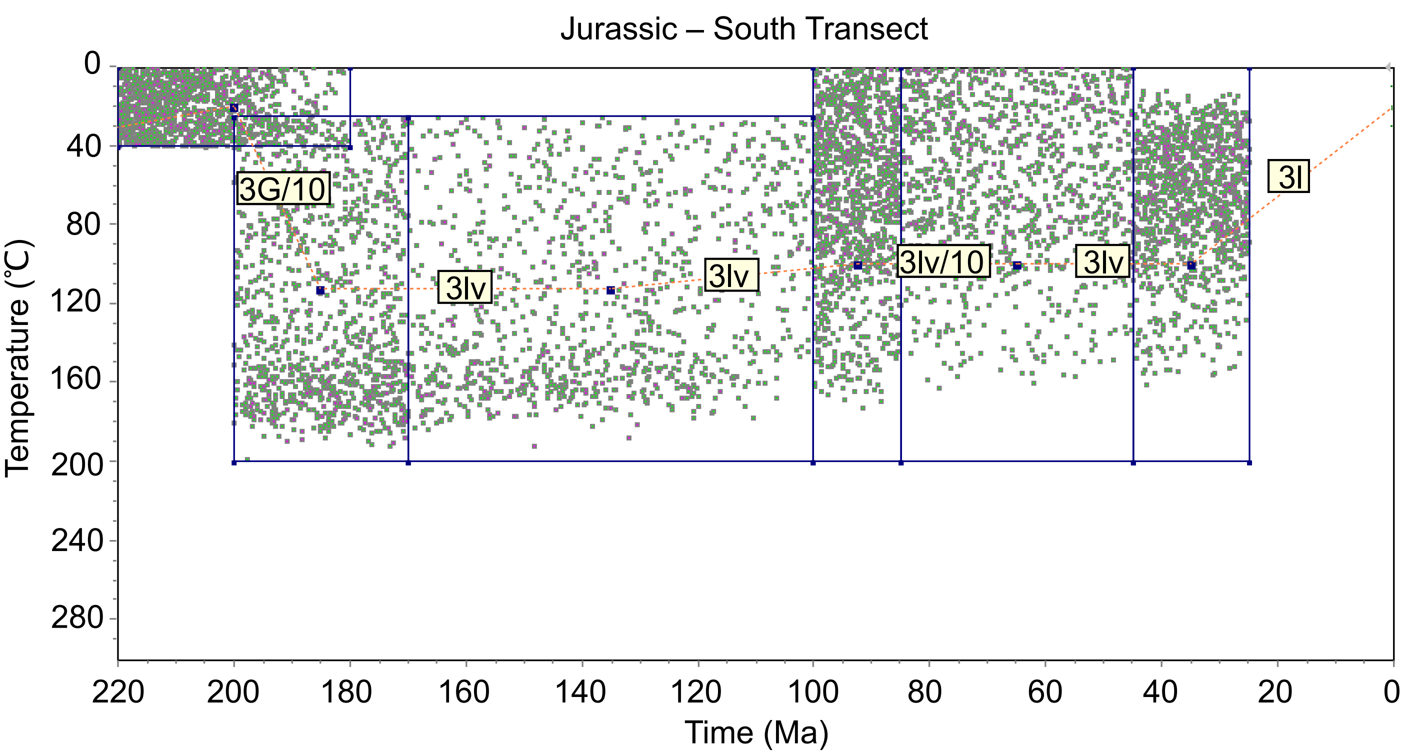


Figure SI8: Constraint boxes and inflection points for the Jurassic inverse models. Constraint boxes are shown outlined in blue, based on the assumptions in table SI2. Green inflection points are "acceptable paths", purple inflection points are "good paths". Clustering within a constraint box indicates less uncertainty within the inverse model.

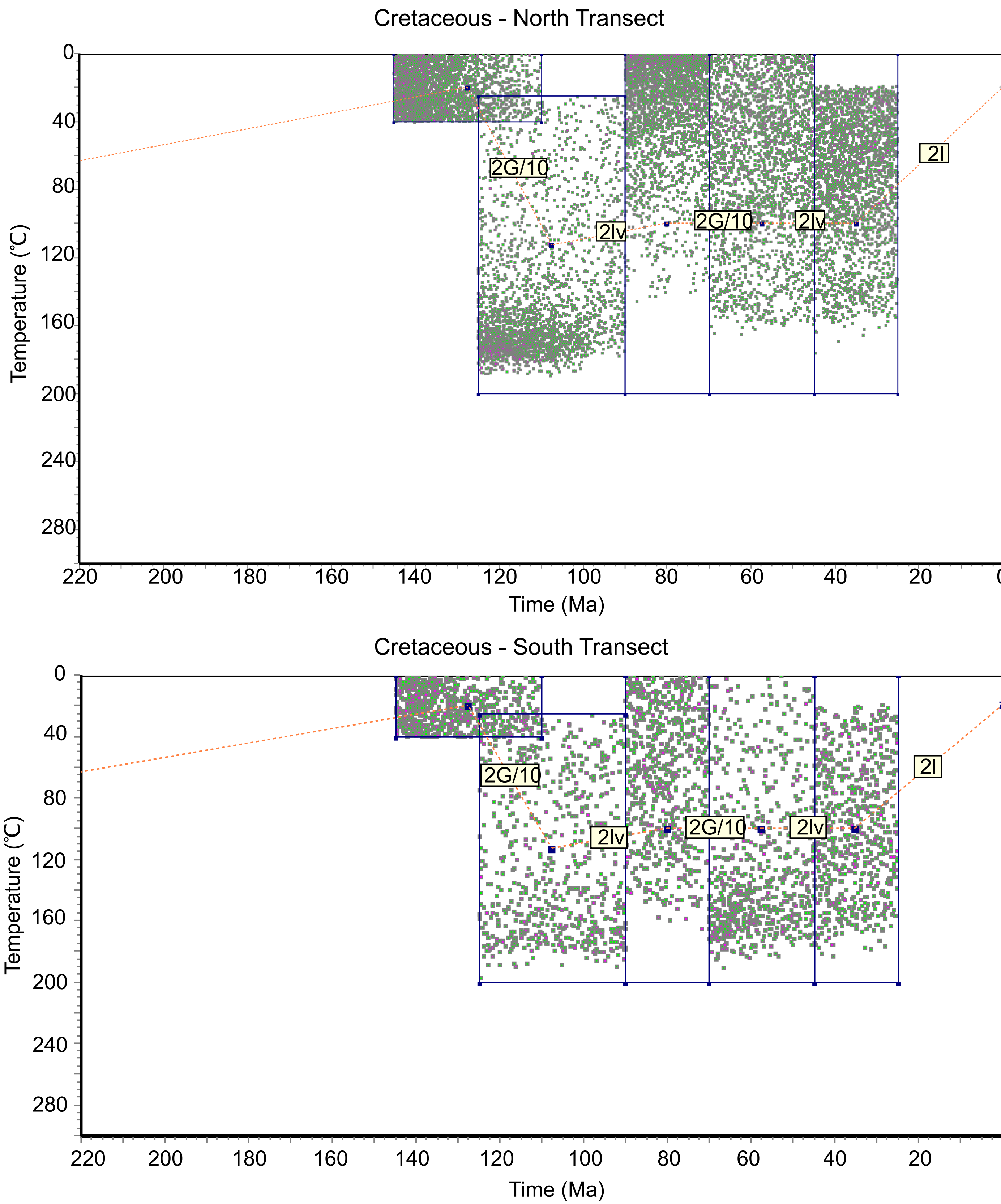


Figure SI8: Constraint boxes and inflection points for the Cretaceous inverse models. Constraint boxes are shown outlined in blue, based on the assumptions in table SI2. Green inflection points are "acceptable paths", purple inflection points are "good paths". Clustering within a constraint box indicates less uncertainty within the inverse model.